

Environmental
Studies
Research
Funds

091 Evaluation of Two Search
Radar Systems for
Detection of Ice Masses

The Environmental Studies Research Funds are financed from special levies on the oil and gas industry and administered by the Canada Oil and Gas Lands Administration for the Minister of Energy, Mines and Resources, and by the Northern Affairs Program for the Minister of Indian Affairs and Northern Development.

The Environmental Studies Research Funds and any person acting on their behalf assume no liability arising from the use of the information contained in this document. The opinions expressed are those of the authors and do not necessarily reflect those of the Environmental Studies Research Funds agencies. The use of trade names or identification of specific products does not constitute an endorsement or recommendation for use.

Environmental Studies Research Funds

Report No. 091

January 1988

EVALUATION OF TWO SEARCH RADAR SYSTEMS
FOR DETECTION OF ICE MASSES

Kenneth Klein

Centre for Cold Ocean Resources Engineering
Bartlett Building
Memorial University of Newfoundland
St. John's, Newfoundland
A1B 3X5 CANADA

Joseph P. Ryan
Marlowe House

Sigma Engineering Limited
P.O. Box 5414
St. John's, Newfoundland
A1C 5W2 CANADA

Scientific Advisors: F.J. Eley
B. Currie

The correct citation for this report is:

Klein, K., J.P. Ryan, and M. House. 1987. Evaluation of two search radar systems for detection of ice masses. Environmental Studies Research Funds Report No.091, Ottawa. 240 p.

Published under the auspices
of the Environmental Science
Research Funds

ISBN 0-920783-90-2

©1987 - Husky/Bow Valley East Coast Project

Acknowledgements

The authors wish to thank Husky/Bow Valley and Petro-Canada Inc. for providing the use of their ice reconnaissance aircraft (chartered from Atlantic Airways Limited of St. John's) to conduct this lengthy study. The authors also wish to thank Atlantic Airways Ltd who operated the aircraft and radar system. Their staff collected data for the program while flying iceberg surveillance missions in support of drilling operations and during flights dedicated to data collection. Special thanks are due Ken Ludlow, and Philip Rudkin, both of Atlantic Airways Ltd. Mr. Ludlow operated the radar, and supplied the audio documentation track for post-flight analysis. Mr. Rudkin provided the aerial photography of icebergs, made visual estimates of iceberg type and class, and calculated their dimensions.

Duncan Finlayson, of NORDCO Limited, provided the environmental hindcasts. Litton Systems Canada Limited made available a working description of the APS 504 (V)3 radar system. Dobrocky Seatech Ltd. mounted the calibrated radar reflectors on buoys and deployed them offshore under contract to Husky/Bow Valley. Environmental information (offshore) was made available by Husky/Bow Valley. Special thanks are due Mobil Oil Canada, Ltd. for the use of their Waverider buoy. Thanks to Glyn Snow of Fenco Newfoundland Limited for advice on the interpretation of environmental conditions. Mr. F.J. Eley, with Atmospheric Environment Service who was the scientific advisor for the program, provided many useful comments throughout the program. Mr. Brian Currie, of Communications Research Laboratory, McMaster University, acted as technical advisor, and also provided many useful comments.

The digital data collection and analysis for the APS 504(V)3 was conducted by Viatic Resource Systems Inc. Sigma Engineering Limited

undertook this component of the program for the (V)5 evaluation utilizing the same personnel and equipment.

A very special thank you is due Mr. Greg Warbanski, Husky/Bow Valley East Coast project, who managed the overall project from start to finish, and Mr. L.R. Prather, East Coast Manager of the Husky/Bow Valley East Coast Project who provided very strong support to the program throughout its two year life.

The authors wish to thank Ms. Norma Matthews and Ms. Gail Greenslade for the preparation of this manuscript and Ms. Desiree King for the illustrations.

CONTENTS

	Page
Acknowledgements	iii
Summary	1
Résumé	7
Introduction	13
Iceberg detection	15
System description	16
Study objective	19
Study program	19
Study modifications	21
Report format	23
Part I: APS 504 (V)3	25
Methodology	25
Documentation and data base	27
The radar system	28
Radar signal recording	28
Modelling and performance prediction	29
Environmental Conditions for Each Flight	31
Calibration and Digital Analysis	33
System description	33
System calibration	35
Target analysis	45
Sea clutter statistics	52

Model Used for APS 504 (V)3	59
General description	59
Limitations of the model	63
Apparent required signal-to-noise ratio as a function of threshold	65
Calibrated radar buoys	70
Relationship between blip-to-scan ratios and cross-sections	70
Comparison of modelled results and surface data ...	73
 Distributions of Modelled Radar Free-Space Cross- Sections	85
Calculated cross-sections	85
Statistical distribution of modelled iceberg free-space cross-sections	91
Modelled performance predictions	99
Performance predictions for six sea states	99
Detrimental effect of increasing altitude	109
Modelled iceberg detection	112
Effect on operational surveillance	118
 Sea Clutter Analysis	121
 Part II: APS 504 (V)5	127
Methodology	127
System parameters	128
Surface verification	129
Radar signal data acquisition	131
Observed performance data collection	137
 Summary of Data Collected	141

Hindcast environmental conditions	141
Iceberg population	141
Example of flight lines	141
Radar signal data	145
Observations and Performance	149
Initial observations and conclusions	150
Measure of performance	156
Data reduction	158
Matrix of results and analysis	169
Conclusions	197
Radar Signal Analysis	199
Radar system calibration	199
Iceberg radar cross-sections	205
Sea clutter statistics	211
A detection example	218
Operational Considerations	221
Line spacing and observed performance	221
Noise-limited detection	222
Transition to clutter-limited detection	222
Clutter-limited detection	223
Discussion	225
Performance Summary (V)3	231
Performance Summary (V)5	233
Comparison of APS 504 (V)3 vs APS 504 (V)5	235

Conclusions	237
Recommendations	239
Appendices for (V)3	
Appendix I-A Description of (V)3 model	I-1
Appendix I-B Clutter cross-sections transferred to tape	I-22
Appendix I-C Partial specifications	I-25
Appendix I-D Sea state and iceberg classification	I-26
Appendices for (V)5	
Appendix II-A Iceberg population documented in the flying program	II-1
Appendix II-B Radar calibration curves	II-10
Appendix II-C Telex comment on (V)5 by manufacturer ...	II-13

Glossary of Radar Terminology

References

LIST OF TABLES

TABLE	Page
0. Specifications of the APS 504 (V)5 and comparison with the APS 504 (V)3	18
1. Summary of environmental conditions	32
2. Specifications of APS 504 (V)3 and comparison with standard marine radar	34
3. Radar calibration in tabular form	37
4. Measured and estimated radar parameters	39
5. Summary of target radar cross-section statistics	46
6. Summary of sea clutter data	54
7. Comparison of normalized cross-section of sea clutter with Nathanson (1969)	58
8. Apparent signal-to-noise ratio as a function of threshold	69
9. Relationship of target cross-sections and observed blip-to-scan ratios	72
10. Cross-sections modelled for calibrated buoys	74
11. Cross-sections modelled for particular targets of interest ...	75
12. Calculated free space cross-section of small dome iceberg	77
13. Cross-sections modelled for targets on flights 2, 3, 5, 10 and 12	86
14. Cross-sections modelled for targets on flights 13, 15, and 17	87
15. Cross-sections modelled for targets on flight 19	88
16. Cross-sections modelled for targets on flights 7, 11, and 20	89
17. Cross-sections of iceberg targets by size class	92
18. Predicted performance for class 1, 2, and 3 conditions	117
19. Wind and wave heights for flights 3 and 8	121
20. Summary of hindcast environmental conditions	142

21.	Summary of radar signal data on targets, APS 504(V)5	146
22.	Summary of sea clutter data, APS 504(V)5	147
23.	Observed radar performance for a small iceberg target, 9 June 1987	163
24.	Observed radar performance for a small iceberg target, 17 June 1987	166
25.	Observed radar performance for a small iceberg target, 21 May 1987	168
26.	Observed radar performance for a bergy bit target, 21 May 1987	169
27.	Summary of flights with similar hindcasts	170
28.	Tabulated maximum range of detection (June 6, June 9, June 17)	171
29.	Tabulated maximum range of detection (May 5, May 21, June 19)	179
30.	Tabulated maximum range of detection (May 14, May 15, June 22)	190
31.	Range of detection comparison	197
32.	Radar parameters used for analysis	200
33.	Summary of iceberg radar cross-section statistics	206
34.	Ocean normalized radar cross-section statistics for sea state 5	213
35.	Comparison of performance of (V)3 and (V)5	235

LIST OF FIGURES

FIGURE	Page
1. Radar recording system interfaced with the APS 504 (V)3	36
2. Radar calibration - injected power versus recorded digital voltage	38
3. Calculated radar cross-section as a function of range for the 10-m ² reflector - unaveraged data	42
4. Calculated radar cross-section as a function of range for the 10-m ² reflector - moving average of five data points (scans) .	42
5. Cumulative radar cross-section probability distribution for the 10-m ² reflector and comparison with a negative exponential distribution	44
6. Calculated radar cross-section as a function of range for a growler - moving average of two data points (scans)	49
7. Cumulative radar cross-section probability distribution for a growler and comparison with a negative exponential distribution	49
8. Calculated radar cross-section as a function of range for a bergy bit - moving average of seven data points (scans)	50
9. Cumulative radar cross-section probability distribution for a bergy bit and comparison with a negative exponential distribution	50
10. Calculated radar cross-section as a function of range for a small iceberg - moving average of eight data points (scans) ..	51
11. Cumulative radar cross-section probability distribution for a small iceberg and comparison with a negative exponential distribution	51
12. Cumulative normalized radar cross-section probability distribution for sea clutter at a 3° grazing angle; upwind ...	55
13. Cumulative normalized radar cross-section probability distribution for sea clutter at a 3° grazing angle; downwind .	55
14. Cumulative normalized radar cross-section probability distribution for sea clutter at a 3° grazing angle; 360°	56
15. Cumulative normalized radar cross-section probability distribution for sea clutter at a 1° grazing angle; downwind .	56

16.	Cumulative normalized radar cross-section probability distribution for sea clutter at a 1° grazing angle; upwind ...	57
17.	Model flow chart	60
18.	Apparent detection signal-to-noise ratio as a function of threshold	68
19.	Modelled free-space cross-section required for flight 9	80
20.	Modelled free-space cross-section required for flight 8	81
21.	Modelled free-space cross-section required for flight 14	83
22.	Distribution of free-space cross-sections: bergy bits, small and medium icebergs	93
23.	Distribution of free-space cross-sections: medium icebergs ...	94
24.	Distribution of free-space cross-sections: small icebergs	95
25.	Distribution of free-space cross-sections: bergy bits	97
26.	Modelled free-space cross-section required for flight 17	100
27.	Modelled free-space cross-section required for flight 7	101
28.	Modelled free-space cross-section required for flight 11	102
29.	Modelled free-space cross-section required for flight 16	103
30.	Modelled free-space cross-section required for flight 14	104
31.	Modelled free-space cross-section required for flight 18	105
32.	Modelled free-space cross-section required for flight 3	106
33.	Modelled free-space cross-section required for flight 9	111
34.	Generalized prediction for class 1 conditions	114
35.	Generalized prediction for class 2 conditions	115
36.	Generalized prediction for class 3 conditions	116
37.	Sea clutter unit cross-section versus grazing angle for flight 3	122
38.	Sea clutter unit cross-section versus grazing angle for flight 8	123
39.	Sea clutter unit cross-section versus grazing angle and azimuth for flight 3	125

40.	Sea clutter unit cross-section versus grazing angle and azimuth for flight 8	126
41.	Data acquisition system	133
42.	Flight lines flown on 9 June 1987	143
43.	Flight lines flown on 9 June 1987	144
44.	Hand tracing from radar display, 23 April 1987	151
45.	Hand tracing from radar display, 23 April 1987	157
46.	Example of display grid used for visual aid	160
47.	Observed radar performance for iceberg detection using pulse width A at 500 ft June 6, 9, 17	173
48.	Observed radar performance for iceberg detection using pulse width B at 500 ft June 6, 9, 17	175
49.	Observed radar performance for iceberg detection using pulse width A at 1500 ft June 6, 9, 17	176
50.	Observed radar performance for iceberg detection using pulse width B at 1500 ft June 6, 9, 17	177
51.	Observed radar performance for iceberg detection using pulse width A at 500 ft May 5, May 21, June 19	182
52.	Observed radar performance for iceberg detection using pulse width B at 500 ft May 5, May 21, June 19	183
53.	Observed radar performance for iceberg detection using pulse width A at 1500 ft May 5, May 21, June 19	185
54.	Observed radar performance for iceberg detection using pulse width B at 1500 ft May 5, May 21, June 19	186
55.	Best observed radar performance for iceberg detection using pulse width A above 500 ft May 5, May 21, June 19	187
56.	Best observed radar performance for iceberg detection using pulse width B above 500 ft May 5, May 21, June 19	188
57.	Observed radar performance for iceberg detection using pulse width A at 500 ft May 14, May 15, June 22	193
58.	Observed radar performance for iceberg detection using pulse width B at 500 ft May 14, May 15, June 22	194
59.	Best observed radar performance for iceberg detection using pulse width A above 500 ft May 14, May 15, June 22	195

60.	Best observed radar performance for iceberg detection using pulse width B above 500 ft May 14, May 15, June 22	196
61.	Receiver calibration curve for the 30- μ s compressed pulse	201
62.	Sensitivity time control curve for an intermediate setting ...	201
63.	Cumulative radar cross-section probability distribution for a reference target using the 0.2- μ s pulse and fixed frequency operation	203
64.	Cumulative radar cross-section probability distribution for a reference target using the 10.0- μ s pulse and fixed frequency operation	203
65.	Cumulative radar cross-section probability distribution for a reference target using the 30.0- μ s pulse and fixed frequency operation	204
66.	Cumulative radar cross-section probability distribution for a bergy bit using the 10.0- μ s pulse and fixed frequency operation at an altitude of 500 ft	208
67.	Cumulative radar cross-section probability distribution for a bergy bit using the 30.0- μ s pulse and fixed frequency operation at an altitude of 500 ft	208
68.	Cumulative radar cross-section probability distribution for a bergy bit using the 30.0 μ s pulse and frequency agility at an altitude of 500 ft	210
69.	Cumulative normalized radar cross-section probability distribution of sea clutter for sea state 5, upwind at a 2.0° grazing angle, using the 0.2- μ s pulse and fixed frequency operation	215
70.	Cumulative normalized radar cross-section probability distribution of sea clutter for sea state 5, upwind at a 2.0° grazing angle, using the 30.0- μ s pulse and fixed frequency operation	215
71.	Cumulative normalized radar cross-section probability distribution of sea clutter for sea state 5, upwind at a 2.0° grazing angle, using the 10.0- μ s pulse and fixed frequency operation	216
72.	Cumulative normalized radar cross-section probability distribution of sea clutter for sea state 5, upwind at a 1.0° grazing angle, using the 10.0- μ s pulse and fixed frequency operation	216

73.	Cumulative normalized radar cross-section probability distribution of sea clutter for sea state 5, upwind at a 0.3° grazing angle, using the 10.0- μ s pulse and fixed frequency operation	217
74.	Measured mean and median signal-to-noise ratio as a function of range for a bergy bit using a 30.0- μ s pulse and fixed frequency operation	219
75.	Measured mean and median signal-to-noise ratio as a function of range for a bergy bit using a 30.0- μ s pulse and frequency agile operation	219

EXECUTIVE SUMMARY

The desire to improve the current airborne iceberg surveillance capability for ice management in support of offshore oil exploration has raised interest in alternative radar systems. Prior to 1986 the only operational airborne radar experience had been with imaging radars. These radars utilize a single high resolution look to image targets as they pass broadside to the aircraft. They are operated at altitudes that may preclude visibility for confirming target identity. Iceberg and ship targets are often indistinguishable on the basis of the radar imagery alone.

This experiment evaluated two generations of search radar, a different airborne system originally designed for military purposes. There were two primary reasons why search radar was potentially suited for operational iceberg surveillance. Search radar was designed to operate at low altitudes (below 1000 feet). This offered the use of a flight altitude with a greater chance of visibility. In addition search radar is a moderate resolution multi-look system using a rotating antenna similar to marine radar. The ability of the system to repetitively scan the region of a target, in the radar field of view, was expected to improve the probability of detecting the target.

The rotating antenna allows targets to be detected ahead of the aircraft allowing the aircraft time to divert from its normal course to view and confirm the identify of the target. This capability has appeal for offshore search and rescue operations because of its search potential.

Because of availability and the level of sophistication, it was decided to evaluate two generations of search radar, one already in use worldwide, the other a new state-of-the-art system. Both systems are manufactured by Litton Systems Canada Limited. The APS 504(V)5 model is the new system. The APS 504(V)3 model has already been in use for other surveillance activities for a number of years.

Husky/Bow Valley and Petro-Canada Inc. were preparing to use the (V)3 for operational ice surveillance in 1986 and subsequently replace it with the (V)5 to support their oil exploration activities off the east coast of Canada. The evaluation program was designed to take advantage of this operational program and add the experimental data collection required for evaluation onto the upcoming operational flights. The availability of operational support flights throughout the iceberg season would permit the program duration to extend over many months allowing personnel to gain experience with these new radars and lessening the impact of any initial equipment failures or data collection problems, and would permit the radar's capability to be observed over a broad range of conditions. Information on ice and environmental conditions would be provided from the exploration drilling platform and the other ice detection and data management system components in place to support operations.

The experimental program was divided into three subprograms. The first objective was to observe and document the radar's surveillance capability to detect icebergs under different conditions as opportunities presented themselves during normal surveillance operations. The second objective was to develop a model specific to each radar system, which extrapolated overall performance from the individual cases actually observed. The third objective was to collect signal data from both radars to investigate the radar properties of icebergs and the ocean. This data would also support the modelling effort.

The (V)3 program consisted of 20 data-collection flights starting in the spring of 1986, while the (V)5 program consisted of 14 flights beginning in the spring of 1987. The exceptionally light iceberg population in 1986 resulted in the (V)3 being assessed using data collected from 33 icebergs.

The (V)5 was assessed from data collected on 113 icebergs in 1987, a more plentiful iceberg year. Both programs documented the radars surveillance capability, and collected radar signal data. Emphasis was placed on detection of

the lesser iceberg size classes, particularly bergy bits and growlers.

Unforeseen events limited modelling to the (V)3 only and resulted in the use of dedicated flights for the (V)5 program. Both programs collected a substantial amount of data quantifying individual iceberg detectability, physical iceberg dimensions, applicable environmental conditions and the flight and radar parameters used. In addition a data base of radar signals was collected which has been only partially analyzed to date because of the large volume of data collected.

During the program it became evident that surveillance performance was a trade-off between achieving an acceptable iceberg detection probability, versus achieving an acceptable area of coverage per flight. Probability of detection was optimum for both radars at a flying height of 500 feet, the lowest practical flying altitude. Higher altitudes resulted in poorer detection capability as the radar signals reflected from the ocean (sea clutter) became larger, thereby masking signals from the iceberg targets. The percentage of icebergs detected in a given size class did increase to some maximum limit as the distance of the target to the flight track was reduced to some minimum value, but no improvement in percentage detection was observed inside this optimum distance. In other words, there was a limit to the highest percentage of bergy bits, (for example), that could be detected, and in order to achieve this percentage the aircraft had to pass within a fixed maximum range of each bergy bit. The maximum achievable percentage of detection, and the corresponding range at which it occurred, varied with the iceberg size class and the environmental conditions. This places limits on how far apart parallel flight lines can be for surveillance to maintain a high percentage of detection, which limits area of coverage. The fuel economy of the aircraft which is somewhat reduced at low altitude, can also limit coverage albeit to a lesser extent.

It was found that the overall iceberg surveillance capability of the APS504(V)5 exceeded that of the APS504(V)3. (A comparison is given in Table 35). Only the capabilities of the (V)5 will therefore be elaborated on. Large and medium icebergs were not observed to present a detection problem to the (V)5. At the other extreme, growlers were detected so poorly (25% or less) that routine growler surveillance during all operational flights with the (V)5 seems impractical.

Over the environmental conditions encountered, the (V)5 demonstrated a reasonably high percentage detection of small icebergs (80 to 90%) and a moderate capability to detect bergy bits (50 to 70%).

The (V)5 achieved its best combined detection of small icebergs and bergy bits for all observed conditions at an altitude of 500 feet using its shorter pulse width. The required flight line spacing ranged from 18 miles under calm sea conditions (90% detection for small icebergs, 70% for bergy bits) to 10 miles under the more extreme conditions observed (80% detection for small icebergs, 50-56% for bergy bits).

Since airborne iceberg surveillance for support of exploration drilling has a large area of coverage, there may be a distance beyond which bergy bits are no longer a concern because they will deteriorate before reaching the drilling area. Under calm sea conditions, a change of altitude to 1500 feet, and a change to the longer radar pulse width, will permit line spacing to increase to 38 nautical miles while retaining a high detection of small icebergs near 100%, (at the expense of bergy bit detection). Under the more extreme conditions observed, the same pulse width, and an altitude of 500 feet will allow a line spacing of 25 nautical miles while maintaining about 85% detection of small icebergs. Again, this assumes bergy bit detection is not required.

After the two-year evaluation program, the oil company operations personnel clearly preferred the use of search radar for iceberg (point target) surveillance

over Side-looking Airborne Radar (SLAR), which had been used during the two preceding years, because of its much superior "ground-truthing" and target confirmation capability. Because of the low flying altitudes used during search radar operations, this system is much more conducive to visual operations. Also the data processing and presentation time for search radar flight data was very substantially reduced from that of the SLAR system, an important consideration in operational decision making during iceberg/drilling unit encounters.

Further improvements in iceberg surveillance using airborne radar will probably be more readily achieved by concentrating on the statistical nature of the radar properties of icebergs and the ocean (sea clutter). Average values of these quantities alone are insufficient to describe the detection process, and do not fully indicate what changes to make to a radar system to improve detection and extend area of coverage.

It is felt that more can be gained by concentrating on the signal processing algorithms used to optimize detection, as opposed to trying to improve hardware capabilities. Competition in the radar industry tends to maintain available hardware at a state-of-the-art level. Signal processing techniques in use, have been optimized for the detection of ships, aircraft, etc. which is not necessarily synonymous with iceberg detection.

It is likely that the oil industry will have to approach the radar industry to get a custom radar system optimized specifically for iceberg detection. The radar industry will require the signal processing algorithms desired for iceberg detection. The choice of algorithms will depend on a thorough knowledge of the statistics involved, hence the emphasis on obtaining those statistics from existing data. These same statistics will also determine the choice of hardware.

RÉSUMÉ POUR LA DIRECTION

Le désir d'améliorer la capacité actuelle de surveillance aérienne des icebergs dans le cadre de la gestion des glaces à l'appui de l'exploration pétrolière en mer a suscité un intérêt pour les nouveaux systèmes radar. Avant 1986, seuls les radars imageurs avaient été utilisés en vol à cette fins. Ces derniers permettent une visée unique à haute résolution enregistrée perpendiculairement à la ligne de vol. Ils sont utilisés à des altitudes qui peuvent empêcher d'identifier la cible de visu. Il est souvent impossible de distinguer les icebergs des navires d'après l'image radar seulement.

L'expérience consistait à évaluer deux générations d'un radar de recherche, ce dernier étant un système aéroporté différent conçu à l'origine pour des fins militaires. Le radar de recherche semblait applicable à la surveillance des icebergs pour deux grandes raisons. Premièrement, il a été conçu pour être utilisé à faible altitude (en deçà de 1 000 pieds), ce qui accroît les chances de bonne visibilité. Deuxièmement, le radar de recherche est un système à visées multiples à moyenne résolution qui comprend une antenne rotative semblable au radar marin. Nous prévoyions que le balayage répétitif de la superficie d'une cible dans le champ de vision du radar améliorerait la probabilité de détecter la cible.

L'antenne rotative permet de détecter les cibles qui se trouvent à l'avant de l'aéronef, ce qui donne au pilote le temps de changer sa direction pour examiner la cible et confirmer l'identification. Cette caractéristique présente des avantages évidentes pour les opérations de recherche et de sauvetage en mer.

Étant donné la disponibilité et le degré de perfectionnement du radar de recherche, nous avons décidé d'en évaluer deux générations, l'une déjà utilisée partout dans le monde, l'autre un nouveau système de pointe. Les deux systèmes sont manufacturés par Litton Systems Canada Limited. Le modèle APS 504(V)3 est déjà utilisé pour d'autres activités de surveillance depuis un certain nombre d'années.

En 1986, Husky/Bow Valley et Petro-Canada Inc. se préparaient à utiliser le (V)3 dans le cadre d'opérations de surveillance des glaces et à le remplacer ultérieurement par le (V)5 pour appuyer leurs activités d'exploration pétrolière au large de la côte est du Canada. Les concepteurs du programme d'évaluation en ont profité pour demander que des données expérimentales nécessaires à l'évaluation soient recueillies au cours des vols opérationnels prévus. L'exécution de ces vols pendant toute la saison des icebergs permettrait d'étendre la durée du programme sur de nombreux mois, ce qui aiderait le personnel à bien connaître les nouveaux radars, à remédier aux défauts initiaux de l'équipement et à résoudre les problèmes de collecte de données. Cela permettrait en outre d'observer la capacité du radar dans une large gamme de conditions. La plate-forme de forage d'exploration ainsi que d'autres éléments des systèmes de repérage des glaces et de gestion des données déjà en place fourniraient de l'information sur l'état des glaces et de l'environnement.

Le programme expérimental a été divisé en trois volets. Le

but du premier volet consistait à observer la capacité du radar de détecter les icebers dans les différentes conditions qui se présenteraient au cours des opérations normales de surveillance, et à accumuler des données à ce sujet. Le but du deuxième volet était de mettre au point, pour chacun des systèmes radar, un modèle qui en extrapolerait le rendement général à partir de cas particuliers vraiment observés. Le but du dernier volet était de recueillir des données sur les signaux des deux radars, afin d'étudier leurs particularités dans le cas des icebergs et de l'océan. Ces données appuieraient également l'élaboration du modèle.

Le programme d'étude du (V)3 a comporté 20 vols de collecte de données débutant au printemps 1986, et celui du (V)5, 14 vols débutant au printemps 1987. En raison du nombre exceptionnellement faible d'icebergs en 1986, le (V)3 a été évalué d'après les données recueillies pour 33 icebergs

En 1987, le (V)5 a été évalué à partir de données recueillies pour 113 icebergs, nombre beaucoup plus imposant. Dans le cadre de ces deux programmes, nous avons étudié la capacité de surveillance des radars et recueilli des données sur leurs signaux. Nous avons mis l'accent sur la détection des icebergs de petite taille, en particulier les bergybits et les bourguignons. En raison d'événements imprévus, seule la modélisation du (V)3 a pu être réalisée à l'aide des vols prévus et le programme d'évaluation du (V)5 a nécessité des vols spéciaux. Dans le cadre des deux programmes, nous avons recueilli un nombre substantiel de données en vue de quantifier la possibilité de détecter des icebergs particuliers, les dimensions physiques des icebergs, les conditions environnementales applicables et les paramètres utilisés pour les vols

et le radar. En outre, nous avons constitué une base de données sur les signaux radar, laquelle n'a fait l'objet que d'une analyse partielle jusqu'à présent en raison du grand nombre de données recueillies.

Au cours du programme, nous nous sommes aperçus que l'efficacité de la surveillance était une question d'équilibre entre l'obtention d'une probabilité acceptable de détection des icebergs et une superficie acceptable couverte par chaque vol. Pour les deux radars, la probabilité de détection était optimale à la plus faible altitude de vol pratique, soit 500 pieds. Nous avons obtenu une capacité de détection moindre aux altitudes plus élevées, car les signaux radar réfléchis par l'océan (écho de vague) devenaient plus forts et masquaient les signaux provenant des icebergs cibles. Le pourcentage d'icebergs décelé dans une classe de taille donnée a augmenté jusqu'à une valeur limite à mesure que la distance entre la cible et la ligne de vol diminuait jusqu'à une valeur minimale, mais nous n'avons observé aucune augmentation du pourcentage de détection à l'intérieur de la distance optimale. Autrement dit, il y avait une limite dans le pourcentage de bergybits (par exemple) détectables et, afin d'atteindre ce pourcentage, l'aéronef devait passer à l'intérieur d'une distance maximale définie pour chaque bergybit. Le pourcentage de détection maximum que nous avons pu obtenir, et la distance correspondante ont varié selon la classe des icebergs et les conditions environnementales. Il faut donc limiter la distance entre les lignes parallèles de vol pour maintenir un haut pourcentage de détection, ce qui limite par le fait même la superficie couverte. La consommation de carburant, qui est quelque peu supérieure à faible altitude, peut également limiter la superficie couverte, mais dans une moindre mesure.

Nous avons observé que la capacité globale de détection des

icebergs du APS504(V)3 était supérieure à celle du APS504(V)3. (Le tableau 35 montre une comparaison.) Nous ne traiterons donc plus en détail que des capacités du (V)5. Le (V)5 n'avait pas de difficulté à détecter les icebergs de grande et de moyenne tailles. Par contre, nous avons observé que les bourguignons étaient détectés dans un pourcentage si faible (25% ou moins) que leur surveillance régulière dans le cadre de tout vol opérationnel semble impossible.

Dans toutes les conditions environnementales qui se sont présentées, le (V)5 a pu détecter un pourcentage assez élevé de petits icebergs (80 à 90 %) et un pourcentage moyen de bergybits (50 à 70 %).

Pour toutes les conditions observées, le meilleur pourcentage de détection combinée des petits icebergs et des bergybits obtenu par le (V)5 a été enregistré à une hauteur de 500 pieds et en utilisant la plus courte durée d'impulsion. L'espacement requis entre les lignes de vol a varié de 18 milles dans des conditions de mer calme (détection de 90 % des petits icebergs et de 70 % des bergybits) à 10 milles dans les conditions les plus extrêmes observées (détection de 80 % des petits icebergs et de 50 à 56 % des bergybits).

Puisqu'on utilise de grandes superficies de couverture pour la surveillance aérienne des icebergs effectuée à l'appui du forage d'exploration, il est possible qu'il existe une distance au-delà de laquelle les bergybits ne posent plus de problème parce qu'ils succomberont à l'érosion avant d'atteindre la zone de forage. Dans des conditions de mer calme, lorsque l'altitude de vol est 1 500 pieds et qu'on utilise la plus longue durée d'impulsion radar, on peut augmenter l'espacement des lignes de vol à 38 milles nautiques tout en conservant un fort pourcentage de détection des bergybits). Dans les conditions les plus extrêmes observées,

la même durée d'impulsion et une altitude de vol de 500 pieds permettront un espacement des lignes de 25 milles nautiques et la détection d'environ 85 % des petits icebergs. Encore là, il est supposé que la détection des bergybits n'est pas nécessaire.

Une fois le programme d'évaluation de deux ans terminé, le personnel des opérations de la société pétrolière a nettement préféré l'utilisation du radar de recherche pour la surveillance des icebergs (objectif ponctuel à l'utilisation du radar aéroporté à antenne latérale (RAAL), qui avait été utilisé auparavant, pendant deux ans; il l'estime très supérieur aux chapitres de la détection des réalités du terrain et de la confirmation de l'objectif. En raison des faibles altitudes de vol utilisées au cours des opérations avec le radar de recherche, ce dernier est beaucoup plus propice aux observations visuelles. De plus, les temps de traitement et de présentation des données obtenues à l'aide du radar de recherche étaient substantiellement réduits par rapport au système RAAL, facteur qui a de l'importance lorsqu'un iceberg dérive vers une plate-forme de forage.

Il sera probablement plus facile d'améliorer la capacité de détection des icebergs à l'aide des radars aéroportés en se concentrant sur l'étude statistique des caractéristiques des signaux radar obtenus pour les icebergs et l'océan (écho de vague). Les valeurs moyennes de ces seules quantités sont insuffisantes pour décrire le processus de détection et n'indiquent pas entièrement quels sont les changements à apporter à un système radar pour améliorer la détection et accroître la superficie couverte.

Nous pensons qu'il serait plus profitable de se pencher sur les algorithmes de traitement de signal utilisés pour optimiser la détection que d'essayer d'améliorer les capacités du matériel. La concurrence tend

à forcer l'industrie des radars à offrir du matériel d'avant-garde. Les techniques de traitement de signal utilisées ont été optimisées pour la détection des bateaux, des avions, etc., ce qui n'est pas nécessairement semblable à la détection des icebergs.

Il est probable que l'industrie pétrolière devra demander à l'industrie des radars de concevoir un système optimisé spécialement pour la détection des icebergs. Pour ce faire, l'industrie des radars devra disposer d'algorithmes de traitement de signal applicables à la détection des icebergs, et pour choisir ces algorithmes, il faudra bien connaître les statistiques applicables, de là l'accent mis sur l'obtention de ces statistiques à partir de données existantes. Les mêmes statistiques détermineront également le choix du matériel.

INTRODUCTION

Efficient resource exploration off Canada's east coast is hampered by the seasonal appearance of icebergs. An iceberg which manages to reach the area of an exploration platform can disrupt operations due to the potential for impact with the structure. Ice management procedures are in place to either divert icebergs before they become an unmanageable problem, or move the platform. These procedures rely on iceberg surveillance to provide iceberg positional information.

Because of the area of coverage required for efficient ice management, two aerial surveillance techniques have been used to provide long- and medium-range coverage of the Grand Banks for strategic planning of offshore operations. Airborne visual surveillance has been limited mainly by the availability of visibility at the lowest practical flying altitude.

Airborne microwave radar has provided an iceberg surveillance capability independent of visibility, however, its performance is limited by the fact that the smaller icebergs make poor radar targets.

To date experience has mainly been with SLAR (Side Looking Airborne Radar) and to a lesser extent with SAR (Synthetic Aperture Radar). These imaging radars operate in very different manners, however they have two things in common. They tend to fly at relatively high altitudes compared to visual surveillance and they basically have one high resolution look at a target as they fly by it. Side-looking airborne radar (SLAR) has been used for sea ice and iceberg surveillance, by offshore operators and government, and has provided satisfactory service for sea ice but less optimum service for icebergs. SLAR has found its major application in

radar imaging. Its use for point target detection is questionable because it only has one look at a target per pass. If there is any question as to the presence of a target a return pass may be required. Target identification is often a problem as SLAR operations take place at higher altitudes (for reasons of geometrical coverage) which may have less visibility than lower altitudes.

A recent study evaluating both SAR and SLAR iceberg surveillance capability (Rossiter et al, 1985), suggests SAR could be an improvement over SLAR, but also noted target identification from the imagery was not practical. It also noted that bergy bits and growlers could be momentarily obscured by waves which would have some impact on a single look system.

The alternative to a high resolution single look radar system is the coarser resolution multi-look search radar. Airborne search radar offers a multiple-look capability because of its 360° scanning antenna. This multi-look feature combined with increased visibility afforded by the typical lower flying altitudes make search radar a suitable candidate for iceberg surveillance. Prior to this study, there was very little experience with using a search radar to detect icebergs. One short term qualitative study had been done (Currie and Haykin, 1985) with an Eaton APS-128 search radar, in two basic configurations with and without pulse compression. It concluded that search radar would be a useful addition to an ice management system. Interest in determining the capabilities of search radar for iceberg surveillance provided the motivation to seek funding from the Environmental Studies Research Funds (ESRF) to evaluate two search radars.

ICEBERG DETECTION

The detection of icebergs with microwave radar depends on the ability of the radar to detect small target signals in a background of noise or ocean clutter. Apart from propagation considerations, the radar signal received from an iceberg is a complex function of the iceberg's size, shape, and surface characteristics, which determine its radar cross-section. Competing signals of system noise and ocean clutter limit detection when the received signal power is less than the noise power level (noise-limited) or clutter power level (clutter-limited). The system noise level is often expressed in terms of the receiver's minimum detectable signal (MDS) and is proportional to the receiver bandwidth. In general, the wide bandwidth requirements of short-pulse, high-resolution radars limit the MDS of the radar. The area of the ocean illuminated by the radar at an instant in time, referred to as the radar resolution cell, directly controls power received from ocean clutter. The radar resolution cell is defined by the radar's horizontal beamwidth and the radar pulse length. In general, the smaller the radar resolution cell the better the radar will perform when detection is clutter-limited.

Detection depends on many factors. Wind velocity and wave height determine the presence and extent of sea clutter. Altitude and range determine grazing angle (the angle between the ocean surface and the incident radar transmission) which affects the magnitude of sea clutter present. Iceberg radar cross-sections (their apparent quality as a reflector) are highly variable. These are just a few of the variables at work. Three separate areas must be investigated to anticipate the iceberg surveillance capability of a particular microwave radar. It is the radar cross-sections of icebergs, the radar cross-sections of sea clutter, and

the actual radar system in use which collectively determine the capability that can be achieved.

SYSTEM DESCRIPTION

The (V)3 and the (V)5 both use digital signal processing techniques and a 16-intensity level monitor to present the radar information to the operator. The onus is on the radar operator to recognize detection of a target from repetitive blips (localized signals that appear brighter than the display background).

The operators have various processing options at their disposal to compensate for conditions that affect all X-band radars to some extent. The signal from a target competes with the natural noise in the radar system and the backscattered signal from the ocean's surface (sea clutter). Detection requires that the target's signal exceeds both noise and sea clutter. A threshold control is available on both radars to place a lower limit on the signals displayed, and can be used to reduce or eliminate noise or sea clutter from the display. As sea state increases, sea clutter increases, stronger at closer ranges. An adaptive video technique called constant false alarm rate (CFAR) is available to remove the average sea clutter signal, leaving only the fluctuations. This counteracts the effect of stronger sea clutter signals at close range, and tends to flatten out the sea clutter background on the display.

The operator can choose the range scale on the display, and position identified targets with a digital cursor. Unlike SLAR which receives the target in its side-looking beam pattern for only a very short time, search radar has a rotating antenna (similar to marine radar) which allows the target to be scanned repetitively (swept by the antenna beam) about a

hundred times, or more, depending on aircraft speed and the range scale used.

The (V)5 being more recent in design than the (V)3 offers additional features. The (V)5 incorporates pulse-to-pulse frequency agility and pulse compression. Frequency agility is intended to improve target detection in sea clutter by decorrelating the sea clutter returns from pulse to pulse. Pulse compression provides increased system performance by transmitting higher average power and providing higher range resolution. Other important features provided by the (V)5 include scan-to-scan integration. Scan-to-scan integration is used to take advantage of the fact that sea clutter tends to decorrelate from scan-to-scan while targets stay correlated. When this is the case, scan-to-scan integration may be used to smooth the clutter background on the display, making targets more detectable.

The APS-504 (V)5 radar has two main modes of operation, anti-submarine watch (ASW) and maritime patrol application (MPA). The ASW mode was designed to detect small targets (submarine periscopes) in a sea clutter environment and should provide the best performance for small ice masses. Table 0 provides a summary of the APS-504 (V)5 specifications and a comparison with those of the APS-504 (V)3. As a general guide to performance the range at which the received signal from a target having a 10 m^2 radar cross-section is 10 dB above the system noise level is provided.

TABLE 0

Specifications of the APS-504 (V)5 and
comparison with the APS-504 (V)3

	APS 504(V)3		APS 504(V)5 ^d	
Transmitter peak power (kW)	100		8	
Transmitter average power (W) ^a	80	2.6	128.0	384.0
Antenna gain (dB)	32		32	
Pulse length (μ sec)				
- uncompressed	0.500	0.200	10.000	30.000
- compressed	-	-	0.030	0.200
Resolution cell size at 10 naut mi (m^2) ^b	55784	22316	3347	22316
Range for a 10 dB signal- to-noise ratio on a 10 m^2 radar cross-section (naut mi) ^c	22	10	28	35

^a Assume a pulse repetition frequency of 1600 Hz.

^b Based on 2.3° beamwidth.

^c Free space propagation.

Actual detection ranges for this target will be greater because of radar signal processing and propagation effects. These ranges demonstrate the relative performance differences between the (V)5 modes and the (V)3.

^d The columns under (V)5 are for three different operational modes. The (V)5 may be used to transmit a 0.200 μ sec pulse of fixed frequency without subsequent pulse compression. Transmission of a frequency coded 10.000 μ sec pulse results in an effective pulse width of 0.030 μ sec. Transmission of a frequency coded 30.000 μ sec pulse results in an effective pulse width of 0.200 μ sec.

STUDY OBJECTIVE

The objective of the study was to evaluate the iceberg detection capability of two search radars; an APS-504 (V)3 and an APS-504 (V)5. The program was designed to evaluate the radars during their operational use offshore, to document their performance over the iceberg season, and to collect scientific data necessary for a better description of the radar characteristics of icebergs, the ocean (sea clutter) and the processes affecting iceberg detection.

STUDY PROGRAM

Operational ice surveillance flights supporting ongoing exploration were scheduled for the winter of 1986 using the APS 504(V)3. The (V)3 was subsequently to be replaced with the APS 504(V)5. The proposed study program was designed to take advantage of the availability of ice surveillance flights to build up a large data base of iceberg targets in a wide range of environmental conditions. This program time frame was very attractive from the point of view of providing sufficient time for equipment mobilization, system debugging, and operator training before the actual evaluation began. The lack of this feature is often a problem for programs of short duration. The program was to take place over a nine month period with flying hours allotted to the evaluation of the two radars.

The evaluation would consist of two components. The first component would document observed detection performance capability during the program. The output of this component would, therefore, provide results for only those targets and situations encountered. Reference radar reflectors (fixed radar cross-section in horizontal plane) were to be

deployed offshore for performance evaluation against known targets. The second component included characterizing the radar system, recording received radar signals from sea clutter and selected icebergs, and modelling the operation of the radar. The recorded radar signals would provide a reference sample of iceberg radar cross-sections and a data base of sea clutter. The model was to provide the capability to extrapolate from the isolated cases of observed detection to the overall surveillance capability. In a two step process, the model would first use the sea clutter data and observed detection of each iceberg from each flight to calculate that iceberg's radar cross-section.

This would eventually provide the statistical distribution of iceberg radar cross-sections in each size class. The model would then be used (with the same sea clutter data) to calculate the percentage of icebergs detectable in each class for clutter distributions corresponding to different environmental conditions. Data collected on the radar reflectors would provide independent calibration points within the data set. Validation of the method would be provided by comparison of the results obtained from the analysis of recorded signals from selected test cases with the results obtained using the model.

An on-board digitizing capability was to be installed to record the radar signal before any digital processing occurred. This data would be used to look at target cross-section fluctuations from scan to scan as well as define sea clutter distributions during different wind and wave conditions.

This fundamental information was relevant not just to these radars, but also to SLAR and marine radar operating in the same frequency range.

In the spring and summer of 1986 the evaluation of the APS-504(V)3 was carried out using this methodology. It happened that 1986 was a light ice year and a significant portion of the iceberg data had to be collected by flying further north with dedicated flights. Sea clutter data were collected on both the operational flights over the Grand Banks and dedicated flights.

The assessment program used to evaluate the (V)3 concentrated on the smaller size classes of icebergs for which marine radar is known to have detection problems. Data collection was piggy-backed with existing surveillance operations, to collect documented cases of detection and non-detection over an extended period of time. The data was collected during twenty flights from May to July, 1986. The digital information was collected during 13 of 20 flights to build a data base of target and clutter statistics.

STUDY MODIFICATIONS

The original schedule called for the APS-504 (V)5 to be installed in July 1986, however, technical problems at the manufacturer's plant delayed delivery until late 1986. The second phase of the evaluation was rescheduled to take place in the spring of 1987.

During the (V)3 evaluation program it was discovered that the reference radar targets exhibited a significant amount of motion even in moderate seas and that care was required when using these targets for detection performance evaluation. Early in the (V)5 program it was decided to use these targets only for calibration purposes and only under calm sea conditions. An effort was made to find an alternative to these targets for reference in all sea conditions and at one point a Wave-rider

buoy was considered. It was found, however, that this target could not be detected reliably by the radar. Other alternatives of fabricating large omni-directional targets were investigated and were found not to be feasible. A major change in the methodology away from the (V)3 program was required when detailed data on the (V)5 radar system was not available from the manufacturer. The modelling component of the study was based on emulating the signal processing steps used in the actual radar. This involved knowing fairly precisely how signals were handled internally. The (V)5 was substantially different in design compared to the (V)3 particularly in its signal processing steps. Although the possibility of using calibration equipment to measure the radar's overall signal processing transfer function was considered, there was no assurance the method would be successful. It was concluded that without a technical description like that supplied for the (V)3 it was no longer possible to take the same approach for the (V)5. The radar modelling component of the study was eliminated and the emphasis was placed on documenting the observed performance and scientific data collection.

In late April, just after flying for the study had commenced, a fire on the drilling unit Bow Drill 3 halted operational flights until mid-June and brought the drilling unit in for repairs. The effects on the program were the loss of available operational flights, and accurate environmental data in the vicinity of sea clutter data collection. This limited the amount of sea clutter data that could be collected. A Wave-rider buoy was installed about 10 naut mi off the Newfoundland coast and sea clutter data was collected in that area. Environmental conditions were obtained from hindcast data.

As with the (V)3 the (V)5 assessment program concentrated on the

smaller iceberg size classes. A total of 14 flights occurred between April and July, 1987. Radar signal data was collected on 11 of these flights.

REPORT FORMAT

Because of the change in methodology between the (V)3 and (V)5 assessment programs, the reporting emphasis differs between Part I and Part II. This is mainly because of the emphasis placed on modelling the overall (V)3 surveillance capability versus summarizing the observed (V)5 capability.

The non-technical reader will find both radars' performance capability summarized in Discussion along with other pertinent comments, and is also directed to Comparison of APS 504 (V)3 vs APS 504 (V)5.

Appendix I-D contains summary tables, relating sea state to significant wave height and wind speed, and iceberg size classification to above water dimensions.

PART I: APS 504 (V)3

METHODOLOGY

As described in the study program there were a number of elements in the (V)3 program. One objective was to mathematically define the radar system being assessed. A second objective was to document the capability of the radar system for events of opportunity as they occurred. A third objective was to develop a model to extrapolate from the isolated cases observed to the overall detection capability of the radar. The fourth objective was to collect fundamental information pertaining to the process of iceberg detection with X-band radar.

Two calibrations were performed during the program to measure some of the radar system parameters and confirm manufacturer specifications.

Throughout the flight program the performance of the radar was documented with the radar's video tape system providing in-flight recording of the radar display. These video tapes were subsequently reviewed on the ground. The resulting information provided the observed detection performance of the radar. Observed performance was complimented with environmental information in the area of interest, and aerial photography of icebergs, to form an overall database of observed (V)3 performance.

One of the key elements in the program was a digital recording system installed onboard the aircraft which sampled the radar signals after reception by the radar but before any signal processing occurred. The system was used to record the radar signals from both selected icebergs and sea clutter, providing some of the basic information used to describe iceberg detection with X-band radar.

An important feature was that the radar signals from sea clutter were sequentially stored in a format that was basically a duplicate of the radar signals received in actual operation. This data was also used as the first step in simulating real time operation of the (V)3 for the purposes of performance prediction and extrapolation.

A computer model of the (V)3 radar signal processing was developed based on a detailed technical description supplied by the manufacturer. The model emulated the radar from the point at which radar signals were recorded by the digital system. By starting the model with the recorded radar signals from sea clutter the real time operation of the radar system was emulated. This avoided the problem of having to model sea clutter. The model was used to calculate how much signal was required from an iceberg to be detected in sea clutter (or system noise) for different environmental conditions, and particular altitudes and radar modes.

The radar cross-sections of documented icebergs were calculated by modeling actual detection cases and calculating the radar cross-sections required to match the observed detection.

Calibrated radar reflectors were deployed offshore and their radar signals recorded in flight. These targets were used to measure some of the radar system parameters during typical operation as well as compare their measured radar cross-sections with those calculated by the model.

Similar comparisons were also made with the radar cross-section calculated from the recorded radar signals from icebergs and the model's predicted radar cross-sections.

At the conclusion of data collection the resulting statistical distributions of iceberg radar cross-sections, the data sets of collected sea clutter, and the model were used to calculate general detection

performance.

DOCUMENTATION AND DATA BASE

Iceberg dimensions were calculated mainly from photographs taken in-flight with a hand-held, 35-mm camera equipped with a zoom lens. The radar range was recorded during the photo session to provide a scaling factor.

The radar display was recorded on a high-resolution tape deck (part of the (V)3 system matched to display resolution) and was analysed on the ground. This analysis provided the record of detection actually observed during radar operation for documented targets.

Environmental conditions, usually measured at the drilling unit Bow Drill 3, were catalogued with the above data. This resulted in a volume of video-tapes from the radar display and a data base of original weather observations, iceberg photographs, flight paths, original observations on target detection, and so on. Analysis produced 20 rather lengthy flight documentation files. The files contained target dimensions, class and location, condensed environmental conditions, analysis of target ranges, bearings, blip-to-scan ratios, flight parameters, radar parameters, and comments.

Received power representing sea clutter was converted to unit radar cross-section and was stored on multiple 2,400 ft magnetic tapes, as well as being plotted on graphs.

This data base is currently (December 87) stored at Centre for Cold Ocean Resources Engineering (C-CORE) and because of the length and number of flight documentation files and quantity of sea clutter graphs, most of these items are not included in this report.

THE RADAR SYSTEM

A description of the radar was obtained in three areas.

- a) Litton Systems Canada Limited provided a working description of most of the signal processing methods used in the (V)3 and the characteristics of the (V)3 receiver amplifier and antenna pattern.
- b) The radar receiver amplifier voltage output was measured independently as a function of injected power.
- c) Receiver output was recorded with an on board digital system as the aircraft flew by the radar reflectors on operational flights.

The receiver calibration indicated the level of noise in the radar system and related received power to output radar signal. The received power from the calibrated buoys calculated from their radar signals recorded in flight was used to check system performance under operating conditions, provide data for comparison with modeled results, and calculate signal to noise ratios required for detection.

RADAR SIGNAL RECORDING

The onboard digital system was also used to record the radar signals from selected icebergs and sea clutter. These recorded signals were then converted to received power using the calibration data.

Analysis of received power provided

- time series of radar cross-sections of targets as a function of range (Item 1);
- fluctuation statistics of radar cross-sections for each target in item 1 (Item 2); and
- sea clutter cross-sections as a function of range and azimuth (Item 3).

Item 1 was used to assess the effect of multipath propagation (see Blake 1980) for point targets (i.e., the calibrated radar buoys), to assess the multipath effect for spatially distributed targets (i.e., icebergs), and to provide average cross-section values for targets. Item 2 was used to check the statistical probability distributions of radar cross-sections of both point targets and spatially distributed targets. Item 3 provided a record of the sea clutter distribution in range and azimuth.

MODELLING AND PERFORMANCE PREDICTION

The technical description of the signal processing methods used in the (V)3 allowed an emulation model to be developed. The radar was simulated from the point where the digital system recorded the radar signals in flight.

The model calculated the average free-space radar cross-section of an iceberg from its record of detection as observed on the radar display and the received signals recorded from sea clutter on the day detection was observed.

Essentially the model solved for the radar cross-section that would produce the same record of detection.

The record of detection was the blip-to-scan ratio over a well defined range segment of the radar screen. (The blip-to-scan ratio is the number of detections divided by the number of times the target was scanned by the antenna beam). This resulted in statistical distributions of radar cross-section for iceberg classes that were detectable.

The model was also used to calculate the required target

cross-sections for reliable detection from the sea clutter data collected under different environmental conditions.

The accuracy of the model was assessed by comparing its calculated cross-sections with the measured cross-sections of isolated cases.

The model operates in free space, where received power varies with inverse fourth power of range. Therefore, the scattering effect of the ocean surface on the radar signal received from the target is ignored. This approach was adopted because an iceberg's radar cross-section is distributed from the sea surface to its maximum height, and the apparent maximum height of the lesser size classes was expected to vary considerably with swell. This was expected to smear multipath effects (associated with point targets), so that received power on average would vary as the inverse fourth power of range (see Blake 1980). Targets were assumed to follow Swerling statistics (Case 1) (see Skolnik 1980) because of their complex geometry and random aspect. Case one statistics assumes the target's radar cross-section is constant from pulse to pulse during one scan, but uncorrelated from scan to scan. One basic feature is that the probability density of obtaining a particular radar cross-section decreases exponentially with increasing radar cross-section. This statistical distribution requires the average radar cross-section of the target to be specified.

A summary of the model is given in "Model Used for APS 504 (V)3", and a more technical description can be found in Appendix I-A.

ENVIRONMENTAL CONDITIONS FOR EACH FLIGHT

Environmental characteristics such as wind speed and significant wave height, were documented for each flight, and describe the conditions during which radar signal data were collected to characterize sea clutter.

Operational flights recorded radar signal data on the inbound approach to the drilling unit Bow Drill 3. For these flights, environmental data were extracted from measurements made at the drilling unit Bow Drill 3. Dedicated flights collected radar signal data in an area adjacent to the first documented target, often far removed from drilling operations. Environmental data for these flights came from coastal stations in the vicinity such as lighthouses, (combination of measurement and visual observation), and hindcasts both from government and from private agencies for that area.

Table 1 provides a basic assessment of sea state for each flight. Wind speed and significant wave height (SWH or $H_{1/3}$) have been used to identify the approximate Douglas sea state number associated with each flight.

Studies involving radar usually try to relate radar backscatter from the ocean to Douglas sea state number, as opposed to the Beaufort scale (of wind force). Appendix I-D summarizes the wind speed and significant wave height corresponding to each Douglas sea state number. The Beaufort scale is not used in this report.

TABLE 1

Summary of environmental conditions

Flight no.	Wind (knots)	$H_{1/3}^a$ (m)	H_w^b (m)	H_{w1}^c (m)	H_{w2}^d (m)	Douglas sea state
1	13	2.1	1.2	1.2	1.2	3 to 4
2	30	4.3	4.3	0	0	6
3	29	4.9	2.4	4.3	0	6
4	5	3.0	0	3.0	0	1?
5	21	1.7	1.2	1.2	0	4
6	18	1.9	0.6	2.0	0	4
7	8	2.0	0	2.0	0	2
8	30	2.7	2.4	1.2	0	5 to 6
9	28	3.9	2.4	3.0	0	6
10	25-30	2.0	1.0	2.0	0	4 to 5
11	15	1.2	0	1.2	0	3
12	~18	1.3	~1.0	~1.0	0	3 to 4
13	~10	1.3	~1.0	~1.0	0	2 to 3
14	20	4.0	0	4.0	0	5
15	20	2-3		(2-3 total)		4
16	19	2.4	0	2.4	0	4 to 5
17	<10	0	0	0	0	1
18	21	2.7	1.2	2.4	0	5
19	5-10	~1.0		(~1 total)		1 to 2
20	7	2.0	0	2.0	0	1 to 2

^a significant wave height (SWH)

^b wind driven wave (SWH)

^c primary swell wave (SWH)

^d secondary swell wave (SWH)

CALIBRATION AND DIGITAL ANALYSIS

The performance evaluation of the APS-504 (V)3 radar required an accurate calibration of the transfer characteristics of the radar and recording system. Otherwise quantitative estimates of iceberg and sea clutter radar cross-sections from radar signals recorded in flight would not have been possible.

The following sections describe system calibration results, selected results from the radar target analysis, and a presentation of representative sea clutter data. Only selected data products produced for the calibration and digital analysis are presented here, with all other data being stored with Sigma Engineering Limited.

SYSTEM DESCRIPTION

The APS-504 (V)3 airborne radar system is a non-coherent pulsed radar similar in many respects to standard marine radar. Table 2 provides a comparison of the specifications of the (V)3 with a marine radar.

Table 2

Specifications of APS-504(V)3 and comparison with a standard marine radar

Feature	APS-504(V)3	Marine radar (Racal-Decca RM1629)
Transmitter power (kW)	100	25
Antenna gain (dB)	32	33
Minimum detectable signal (dBm)	-105 ^a	-102 ^a
Resolution cell size at 10 nautical miles (m ²)	55784 ^b	38806 ^b
Maximum range of detection for a 10-m ² radar cross-section (naut. mi.)	22 ^c	14 ^c
Processing: Automatic CFAR	Yes	No (manual) ^d
STC	Yes	Yes

^a. Assume a 5 dB noise figure for both radars and a 2 MHz receiver bandwidth for the (V)3 and a 4 MHz bandwidth for the RM1629.

^b. Based on 2.3° beamwidth and 0.5 μ s pulse length for the (V)3 and 0.8° beamwidth and 1.0 μ sec pulse for RM1629.

^c. Assume 10 dB signal-to-noise ratio and free space propagation.

^d. CFAR is implemented using a logarithmic amplifier followed by a high pass filter having a fast time constant (FTC).

A digital recording system was interfaced to this radar to permit the recording of raw, unprocessed radar signals. The recording system was set up to sample the 0.5- μ s radar pulse data at a 5-MHz rate with 8-bit amplitude resolution.

Figure 1 provides a block diagram of the recording system as it was interfaced to the radar. The system was configured to operate in two modes:

- a) Window mode provided a movable window 22.5° in azimuth and 4 naut mi in range that was placed over the target of interest during data collection. The window position was updated using navigation data from the HP 310 computer on board the aircraft so that data could be collected for a target as the aircraft flew by it. These data have been used for target cross-section measurements.
- b) Full scan mode provided for the collection of 360° of radar data in four range rings. These data were used for radar modelling and sea clutter analysis.

SYSTEM CALIBRATION

The system calibration established the relationship between the digital value recorded by the recording system and the radio frequency (RF) power received at the antenna. This calibration took place in three steps:

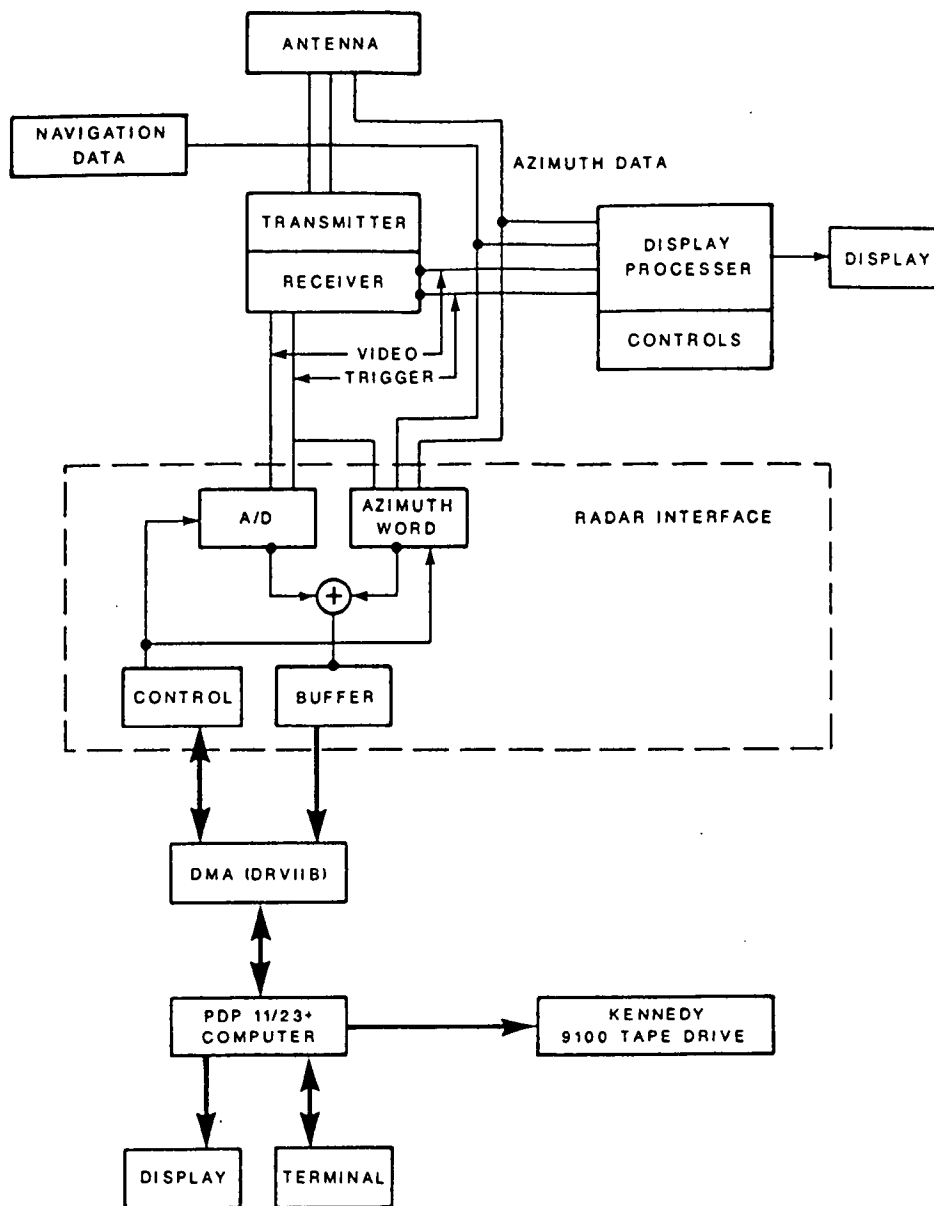


Figure 1. Radar recording system interfaced with the APS-504(V)3.

a) Establish the receiver and recording system transfer characteristics directly by using injected signals from a signal generator (HP 8684B) and by digitizing and recording the resultant output on tape. The voltage output of the receiver was also measured so that the transfer characteristics of either the receiver or recording system could be plotted separately. Figure 2 presents the plot of injected power versus recorded digital level. This calibration was carried out twice for the experiment, once at the beginning and once at the end, with no measurable change in characteristic. Table 3 presents the calibration data in tabular form.

TABLE 3

Radar calibration in tabular form

Power (dBm)	Digital voltage
-110	5
-105	8
-100	18
-95	37
-90	58
-85	82
-80	101
-75	119
-70	140
-65	161
-60	181
-55	197
-50	218
-45	233
-40	245

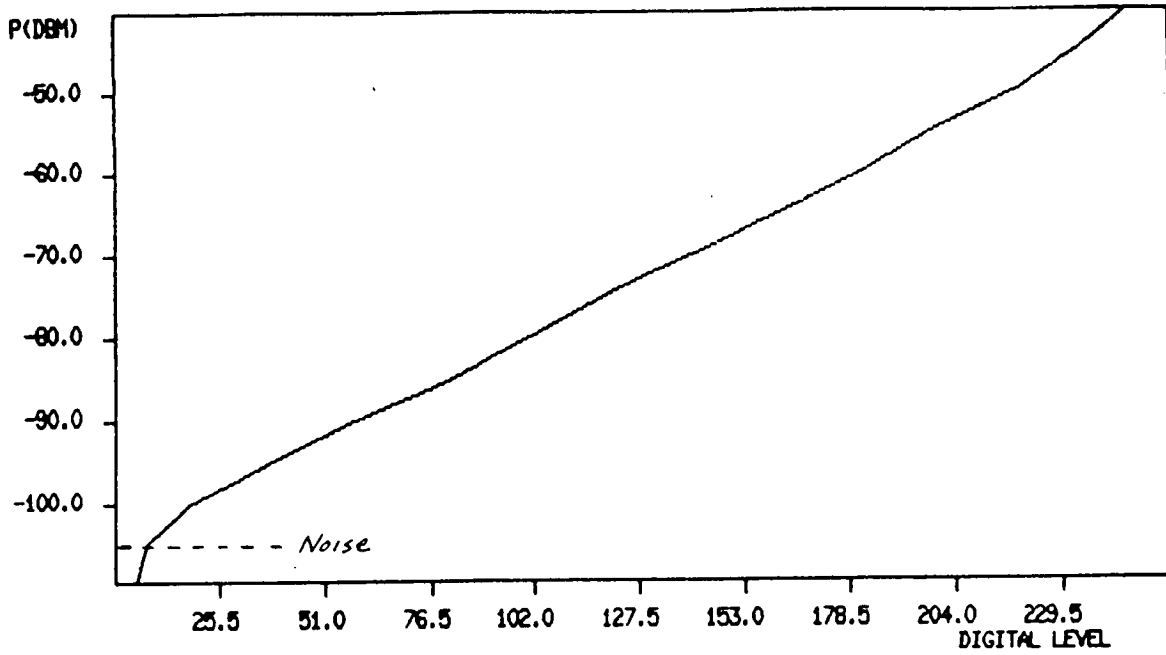


Figure 2. Radar calibration - injected power versus recorded digital voltage.

b) Establish the radar system parameters required for use in the radar equation. Several times throughout the experiment the radar transmitter power and receiver sensitivity were measured using a HP8900D peak power meter and HP8684B signal generator. These measurements met Litton's specifications. Litton provided estimates of other system losses and antenna gain pattern. A summary of the resultant radar parameters and their comparison with measured values is provided in Table 4.

TABLE 4
Measured and estimated radar parameters

Feature	Specification	Measured value	Date (1986)	Estimated value	Source
Transmitter power (kW)	100	95	Apr. 03	-	-
		98	Apr. 20		
		115	Apr. 26		
Minimum detectable signal (dBm)	-	-104	Apr. 03	-105	Sigma Eng.
		-105	Apr. 20		
		-106	Apr. 26		
Antenna gain (dB)	32	-	-	-	-
System two-way losses (dB)	-	-	-	1.6	Litton

- c) Close the calibration by using the results of a) and b) with the radar equation and recorded signals from reference targets of known radar cross-section.

During the experiment 2- and 10-m² Luneburg lens omni-azimuth reflectors were deployed offshore and used as reference targets for the performance evaluation. Data collected on 14 July 1986 on the 10-m² reflector were used to close the system calibration.

As the closure of the calibration was being attempted over the ocean it was necessary to establish multipath effects on the cross-section measurements. Multipath propagation is caused by the presence of a reflecting surface, the ocean, between the radar and the target giving the radar signal two paths to the target, one direct and one via reflection from the ocean surface. When the geometry of range, antenna height and target height is such that there is 180° phase shift between the direct and reflected signals, they cancel causing a multipath null. Alternatively, when the phase difference is 360° the signals add causing a multipath lobe.

In order to consider the effect of multipath on radar cross-section the radar equation may be written as,

$$\sigma F^4 = \frac{P_r (4\pi)^3 LR^4}{P_t G^2 \lambda^2} \quad (1)$$

where P_r = received power, watts
 L = system 2-way losses
 R = range to target, m
 P_t = transmitter power, watts

G = antenna gain
 λ = radar wavelength, m
 F^4 = multipath propagation factor
 σ = radar cross-section, m²

For free space propagation the multipath propagation factor F^4 , is unity and the equation may be used to calculate radar cross-section from the received power and range when the other parameters are known. F^4 may be calculated using the spherical earth formulation provided by Blake (1980) for a given antenna and target height. Data were collected at ranges from 4.3 km (2.3 naut mi) to 30.2 km (16.3 naut mi) and the free space radar cross-section ($F^4 = 1$) calculated. These cross-sections are plotted in Figure 3 with the quantity σF^4 for a 10-m² radar cross-section, antenna height of 152 m, and target height of 2.5 m. From this figure it is seen that there are substantial swings in the measured cross-section and nowhere are multipath nulls observed in the data. These effects are not surprising as both aircraft height and target height (1.5-m ocean swell) are continuously varying over the data collection path thereby making the multipath plot of Figure 3 only valid in some average sense. Figure 4 plots the same data as Figure 3 except a moving average of five points (or scans corresponding to 10 s elapsed time) has been taken. The trends illustrated here clearly show some correspondence with the multipath plot with cross-section maximums and minimums being located close to multipath maximums and minimums.

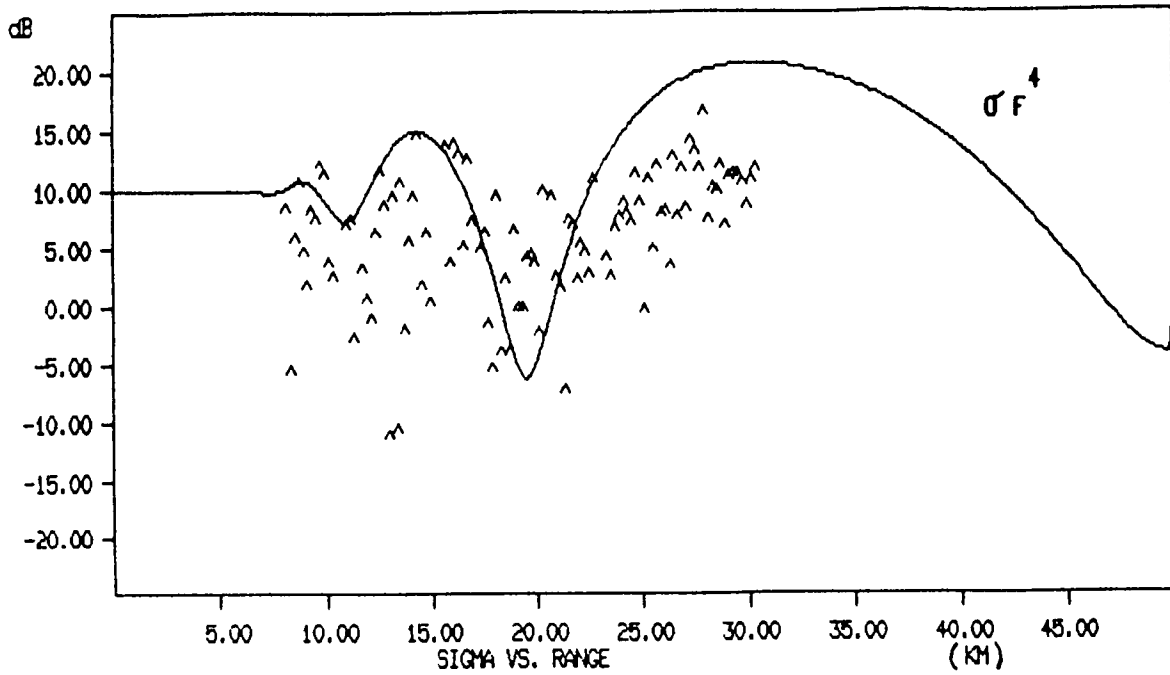


Figure 3. Calculated radar cross-section as a function of range for the 10-m² reflector - unaveraged data.

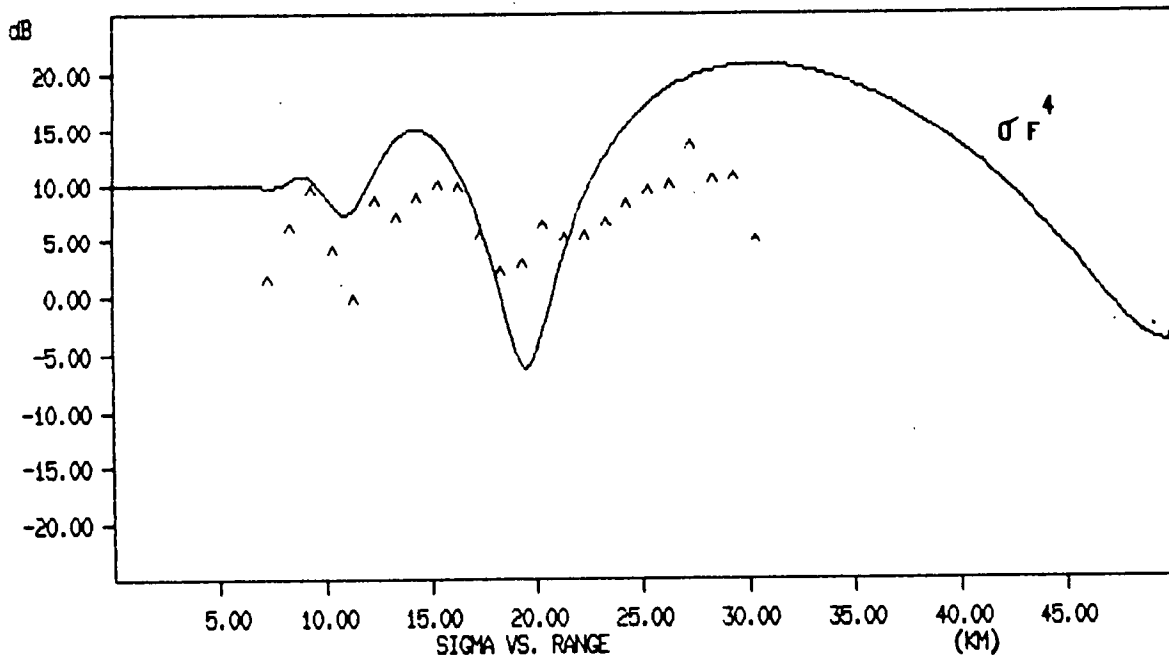


Figure 4. Calculated radar cross-section as a function of range for the 10 m² reflector - moving average of five data points (scans).

Figure 5 presents the amplitude distribution of the data in Figure 3 plotted as a cumulative radar cross-section (RCS) probability distribution. Also, plotted in the same figure is the negative exponential distribution typical of Swerling Case 1 target fluctuation for which the average cross-section is taken as the average calculated from the data points. (For further discussion on Swerling Case 1 statistics see Appendix I-A). The average cross-section for these data points is 8.9 m^2 and the median is 6 m^2 . Another similar pass by this target gave an average cross-section of 16.9 m^2 and a median of 13 m^2 . As a Swerling Case 1 target fluctuation model was initially selected for use in the blip-to-scan analysis, it was important to compare the actual data to this model. Figure 5 shows excellent agreement between the data and this model, however, as Figure 4 illustrates, there could be a possible contamination of the statistics by multipath. Further investigation revealed that the data in Figure 3 follow a negative exponential distribution out to about 12.4 naut mi, (23 km) and then starts to look more normally distributed. This investigation was carried out by segmenting the data in range and generating new cumulative RCS probability density plots. The average cross-section for these segments varied from about 5 m^2 to 16 m^2 with the average of 5 m^2 coming from the region of (17 to 23 km). Therefore, estimates of the reflector cross-sections using the blip-to-scan method (which relies on a Swerling Case 1 model) should be best out to a range of 12.4 naut mi, (23 km) after which the change in amplitude distribution will cause the blip-to-scan method to estimate higher than actual cross-sections. This effect was confirmed by examination of the results of the blip-to-scan analysis for the reflector on this day.

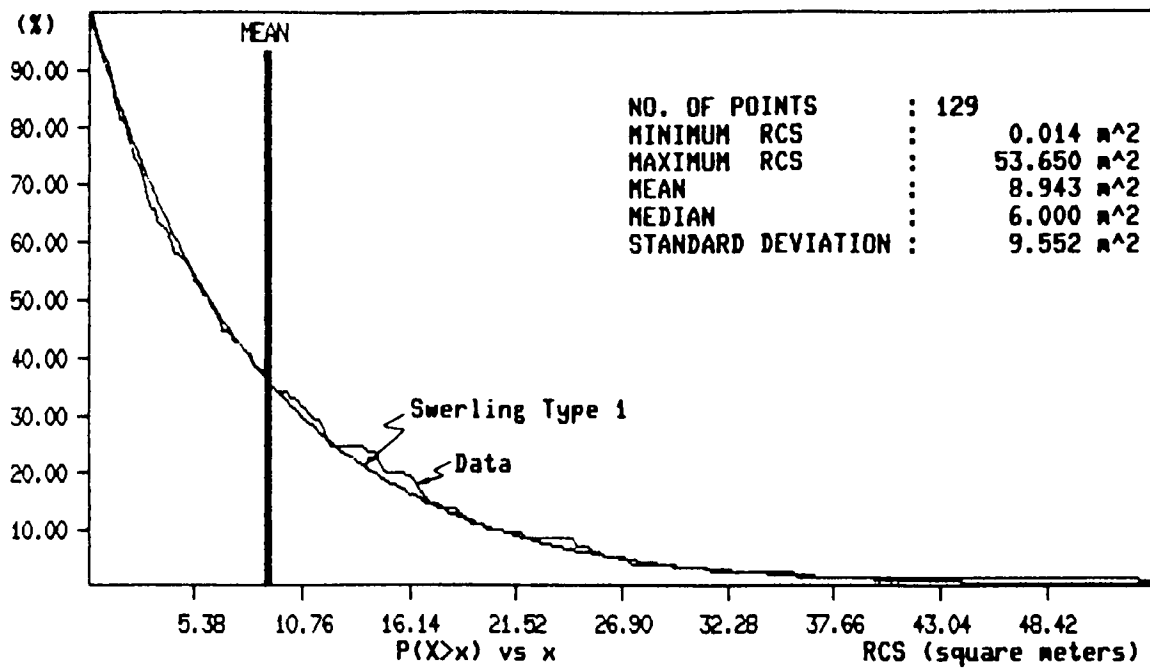


Figure 5. Cumulative radar cross-section probability distribution for the 10-m² reflector and comparison with a negative exponential distribution.

In conclusion, two passes by the 10-m^2 reflector have been used to close the radar system calibration. After segmenting data of Figure 3 into three ranges, a spread of average cross-section was observed to be from 5 to 16 m^2 and the average over the full pass was 8.9 m^2 . The agreement in all cases is better than 3 dB.

In addition, the choice of negative exponential distribution or Swerling Case 1 fluctuation model for the 10-m^2 target appears to work out to a range of about 12.4 naut mi, (23 km) after which the distribution starts to look more normal. If this result is also true for icebergs the best cross-section estimates using the blip-to-scan method will be obtained at closer ranges.

TARGET ANALYSIS

The analysis was conducted on digital data for seven icebergs and the 10-m^2 radar reflector. The digital data resulted from sampling unprocessed radar video data for the $0.5\text{-}\mu\text{s}$ radar pulse at a rate of 5 MHz with an 8-bit amplitude resolution.

A number of radar scans were collected on each target as the aircraft flew by. The position of the target within data collection window varied from scan to scan so that it was necessary to analyse the data on an individual scan basis. For each radar scan, the peak signal return for a particular target was extracted from the data. Free-space cross-sections were then calculated for each data point using the radar equation and radar calibration and compiled as target cross-section statistics (Table 5). Note that these statistics represent all the data points collected on a particular target as the aircraft flew by it. Graphical presentation of the data on the 10-m^2 target has been presented in the

TABLE 5

Summary of target radar cross-section statistics
APS-504(V)3

Target No.	Iceberg class	Min. (m ²)	Max. (m ²)	Mean (m ²)	50% (m ²)	S.D. ^a (m ²)
1	medium	26.480	16712.4	1625.94	935.0	2254.2
2	bergy bit/ small	0.014	28.9	1.86	0.6	3.9
3	growler	0.003	0.6	0.06	0.04	0.1
7	bergy bit	0.076	35.0	4.64	2.5	6.2
12	small	0.024	227.3	41.28	22.5	47.0
13	small	0.309	77.0	17.10	12.5	16.3
14	growler	0.019	8.4	0.81	0.3	1.4
<hr/>						
10-m ²	reflector					
	run 1	0.014	53.7	8.94	6.0	9.6
	run 2	0.138	136.7	16.91	12.9	19.8

^a S.D. is standard deviation

proceeding section.

Table 5 illustrates the wide range of cross-sections obtained from the different iceberg classes and the large fluctuation that can occur for any particular piece of ice. Most of the icebergs seemed to follow a negative exponential distribution corresponding to Swerling Case 1 fluctuation. However, there were exceptions in the medium size icebergs encountered. The closest agreement appears to occur in the small iceberg class.

The following figures present graphical data on three of the icebergs in Table 5. Figures 6, 8, and 10 present radar cross-sections as a function of range for a growler, bergy bit, and a small iceberg respectively. Figures 7, 9, and 11 provide corresponding plots of the cumulative radar cross section (RCS) probability distribution for each of these pieces of ice.

It has been suggested that the effect of multipath on an iceberg face may be to enhance its RCS above its free space value, (Dawe 1985; Ryan 1985). Therefore, also plotted on Figures 6, 8 and 10 is the quantity $\sigma_{MP} F^4$ where F^4 was defined in equation 1 and here is averaged over the iceberg's height.

An estimate of the overall average multipath enhancement was obtained using the free space cross sections calculated from the data. The average radar cross section in the presence of multipath, σ_{MP} , was calculated using,

$$\sigma_{MP} = \frac{\sigma_{FS}}{\frac{1}{n} \sum_{i=1}^n F_i^4(R)}$$

Where $F_i^4(R)$ = calculated propagation factor at range R averaged over the target height,

σ_{FS} = calculated average free space radar cross section.

n = number of data points

For $F_i^4 = 1$ $\sigma_{MP} = \sigma_{FS}$

The multipath calculations were made using a radar propagation model based on spherical earth geometry. This model has been used in previous studies (Harvey and Ryan 1986; Ryan 1985) and, more recently, to predict maximum detection ranges successfully for the APS-504 (V)5.

In Figure 6 for the growler there is no difference between the average free-space RCS, σ_{FS} , and the average multipath RCS, σ_{MP} . However, for the bergy bit and small iceberg of Figures 8 and 10 the multipath RCS is 3 and 4 dB lower than the free-space value indicating a possible enhancement of 3 and 4 dB respectively.

Although this enhancement may indeed be real, it cannot be proven unless the same exact iceberg were to be observed under different environmental conditions. Even then the variability of a particular iceberg could cause more than a 3- to 4-dB change in its average value.

The multipath plots do indicate that the observed cross-section from enhancement should increase slightly with range, but this increase is only observed in the data in Figure 8 for the bergy bit.

The effect is the opposite in Figure 6 with the cross-section of the growler decreasing with increasing range. Data for this growler were taken with a background of 1-m height combined sea, comprised mainly of swell. This effect was noticed on other small targets and has been attributed to a combination of the change in grazing angle and shadowing of portions of the iceberg by the ocean swell.

In conclusion, all but the larger icebergs seem to follow Swerling Case 1 target fluctuation. It is possible that some enhancement of radar cross-section is occurring in the bergy bit and small iceberg sizes. This enhancement cannot be proven conclusively from the data on hand. The decrease in radar cross-section with increasing range for the growlers and small bergy bits appears to provide evidence of either a shadowing or a grazing angle effect on apparent radar cross-section.

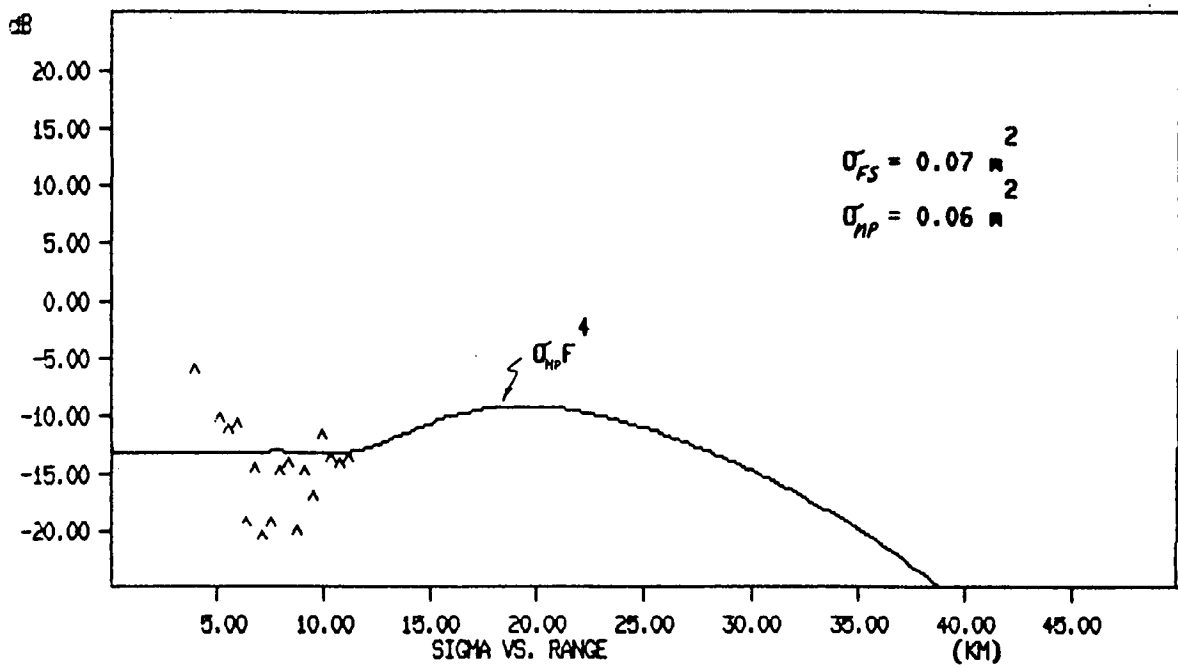


Figure 6. Calculated radar cross-section as a function of range for a growler - moving average of two data points.

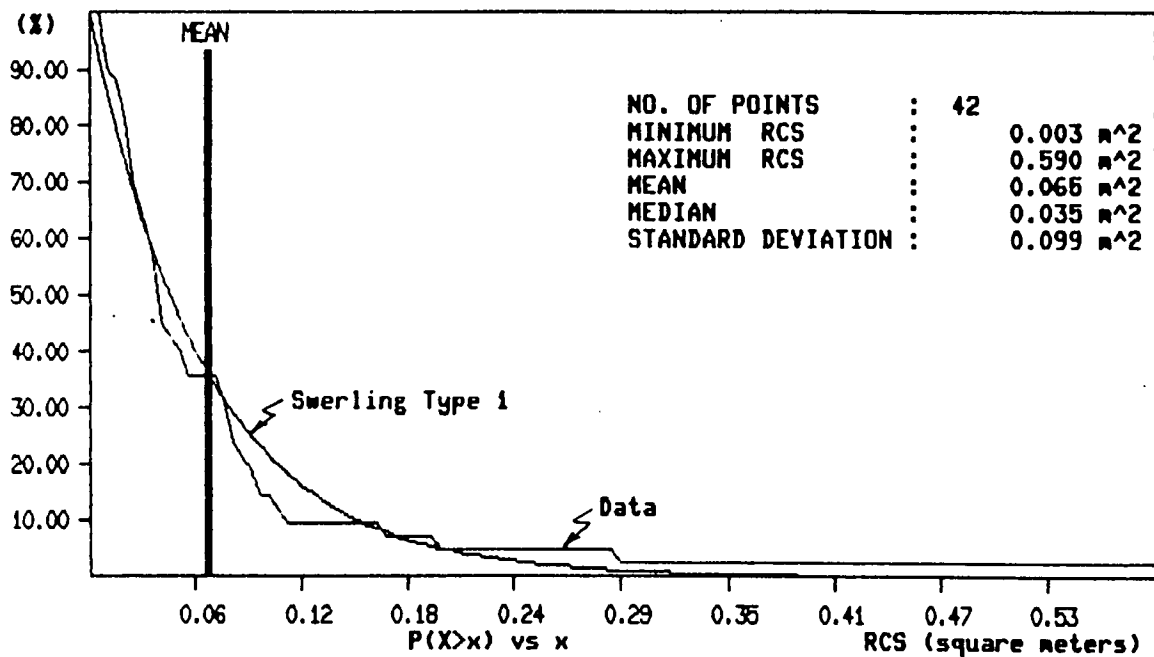


Figure 7. Cumulative radar cross-section probability distribution for a growler and comparison with a negative exponential distribution.

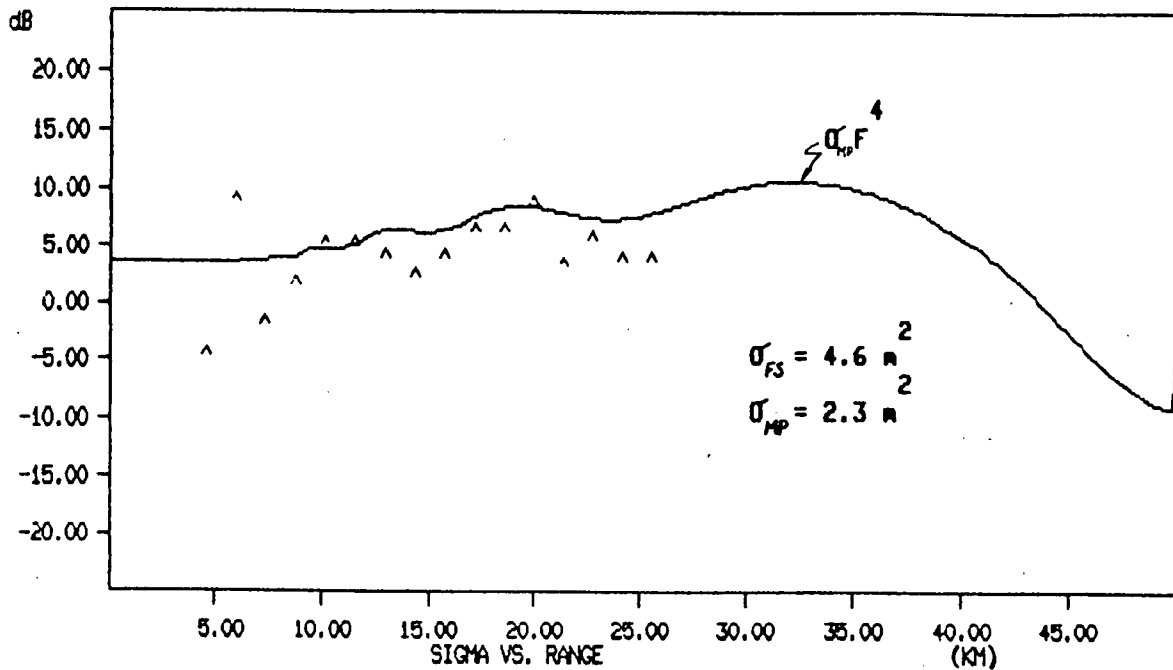


Figure 8. Calculated radar cross-section as a function of range for a bergy bit - moving average of seven data points (scans).

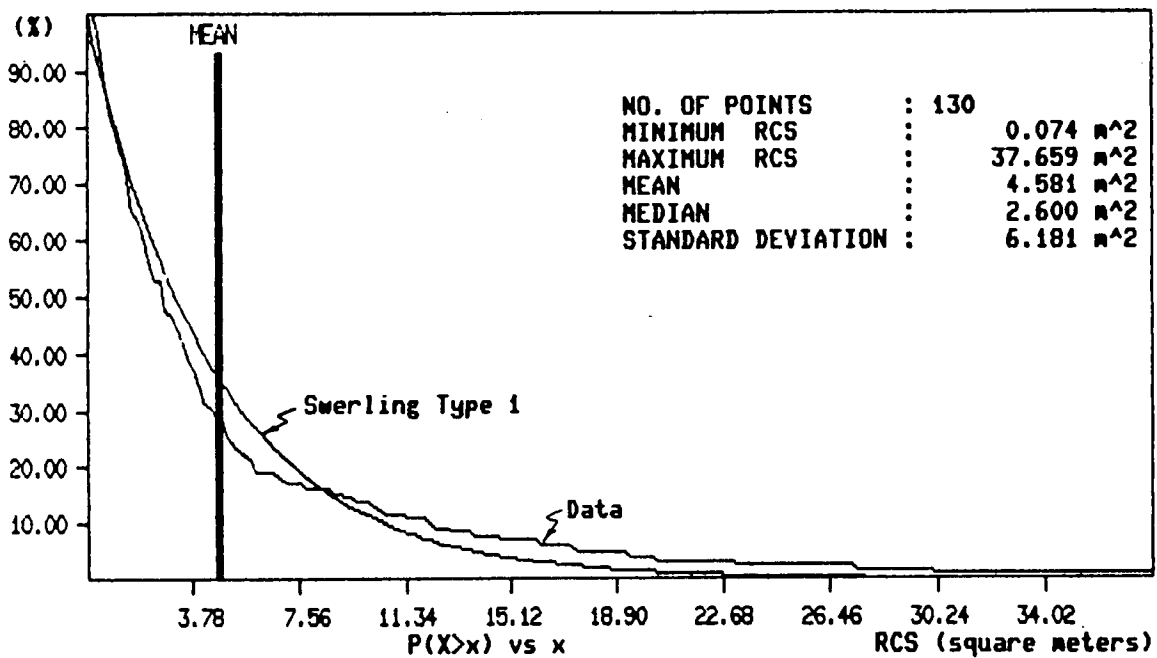


Figure 9. Cumulative radar cross-section probability distribution for a bergy bit and comparison with a negative exponential distribution.

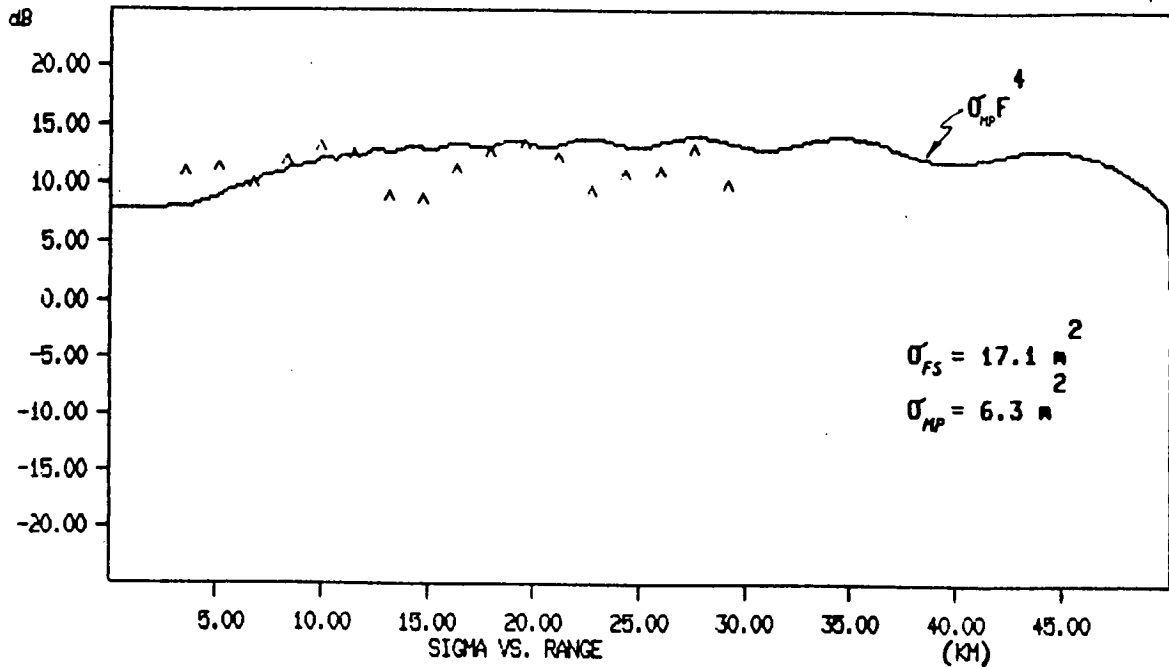


Figure 10. Calculated radar cross-section as a function of range for a small iceberg - moving average of eight data points (scans).

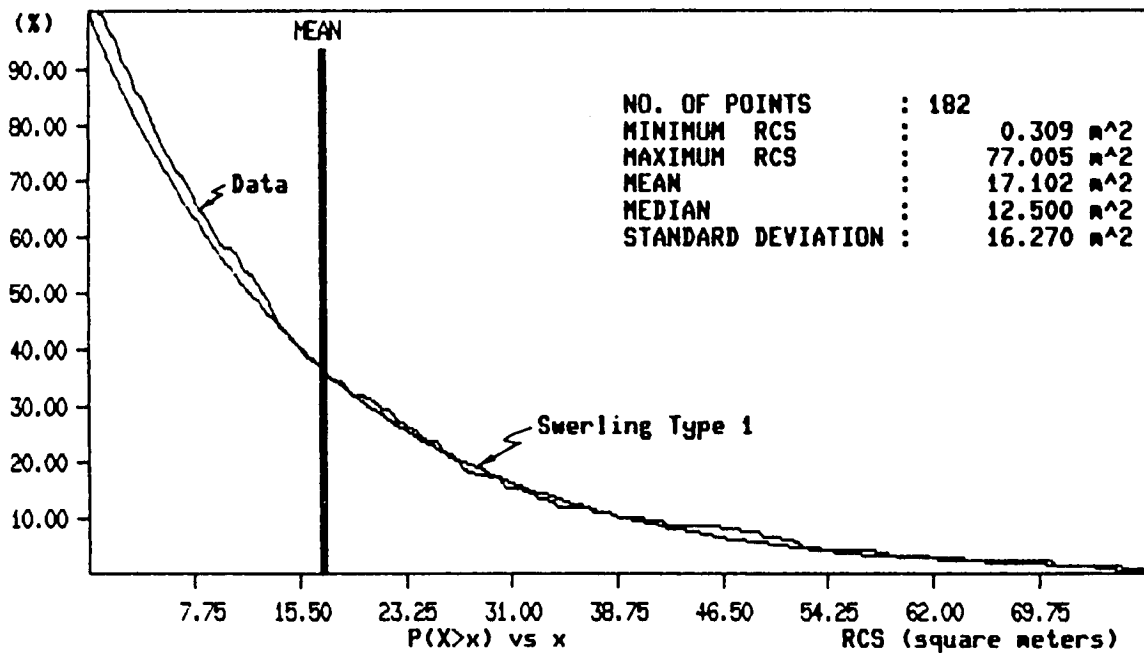


Figure 11. Cumulative radar cross-section probability distribution for a small iceberg and comparison with a negative exponential distribution.

SEA CLUTTER STATISTICS

During the APS-504 (V)3 evaluation, digital data were collected on 11 different days covering a range of sea states from 1 to 6. Table 6 provides a summary of the data collected and the wind and significant wave height (SWH) that were present at the time.

The sea clutter data have been used with the (V)3 model to extract iceberg radar cross-sections using the blip-to-scan method and to provide contour plots of the normalized radar cross-section, σ° , of the ocean. The data may also be used to investigate sea clutter amplitude distributions. The following section presents amplitude distributions for σ° for a sea state 5 to 6 situation that occurred on 31 May 1986. The upwind and downwind distributions were constructed using uncorrelated samples of clutter in 11.25° of azimuth and 1 naut mi in range.

Figures 12 and 13 provide upwind and downwind, cumulative normalized radar cross-section (NRCS) distributions for a 3° grazing angle. Figure 14 presents the distribution for 360° of azimuth for the 3° grazing angle. Figures 15 and 16 provide downwind and upwind distributions for a 1° grazing angle. Cross-wind distributions were also plotted but are not presented here. Table 7 presents a summary of mean NRCS values observed 31 May 1986 compared with Nathanson (1969). All the values calculated from the data are lower than those of Nathanson. This trend has also been noted using data collected on other days.

In conclusion, digital data for 11 different sea conditions were collected. These data have been used to model (V)3 performance and to calculate the NRCS of the ocean. Comparison of these values from one

particular day with published data reveals the present data to be 6 to 13 dB lower than the published data.

TABLE 6

Summary of sea clutter data

Tape	Date (1986)	Alt. ^b (ft)	Ant. Tilt ^c (deg.)	Wind spd/dir (kt) (°T)	SWH ^a (m)	Swell dir. (°T)
6	May 08	4000	-8.0	20/320	5.0	50
		4000	-5.0			
		500	-3.5			
7	May 26	4000	-8.0	8-10/50	1.5	340
		4000	-5.0			
		500	-3.5			
8	May 31	4000	-8.0	30/200	2.7	210
		4000	-5.0			
		500	-3.5			
9	Jun 04	4000	-8.0	26/250	4.5	180
		4000	-5.0			
		500	-3.5			
11		500	0.0	25/220	3.0	
12	Jun 08	4000	-8.0	16/230	1.0	220
		4000	-5.0			
		500	-3.5			
13	Jun 13	500	-0.5	0-10/260	1.5	
		330	-0.5			
14		4000	-8.0	15/260	3.0	40
		4000	-5.0			
		500	-3.0			
		330	-3.0			
15	Jun 19	4000	-8.0	18/170	2.0	190
		4000	-5.0			
		500	-3.0			
		330	-3.0			
17	Jun 27	500	-0.5		< 0.3	
		330	-0.5			
20		500	-1.0		< 0.3	
		330	-1.0			
21	Jul 03	4000	-8.0	32/210	3.0	240
		4000	-5.0			
		500	-3.0			
		330	-3.0			
24	Jul 04	500	-1.0	8/110	0.5	30
		330	-1.0			
25	Jul 14	4000	-8.0	7/290	1.5	260
		4000	-5.0			
		500	-3.0			
		330	-3.0			

a. Significant wave height.

b. Altitude.

c. Antenna tilt.

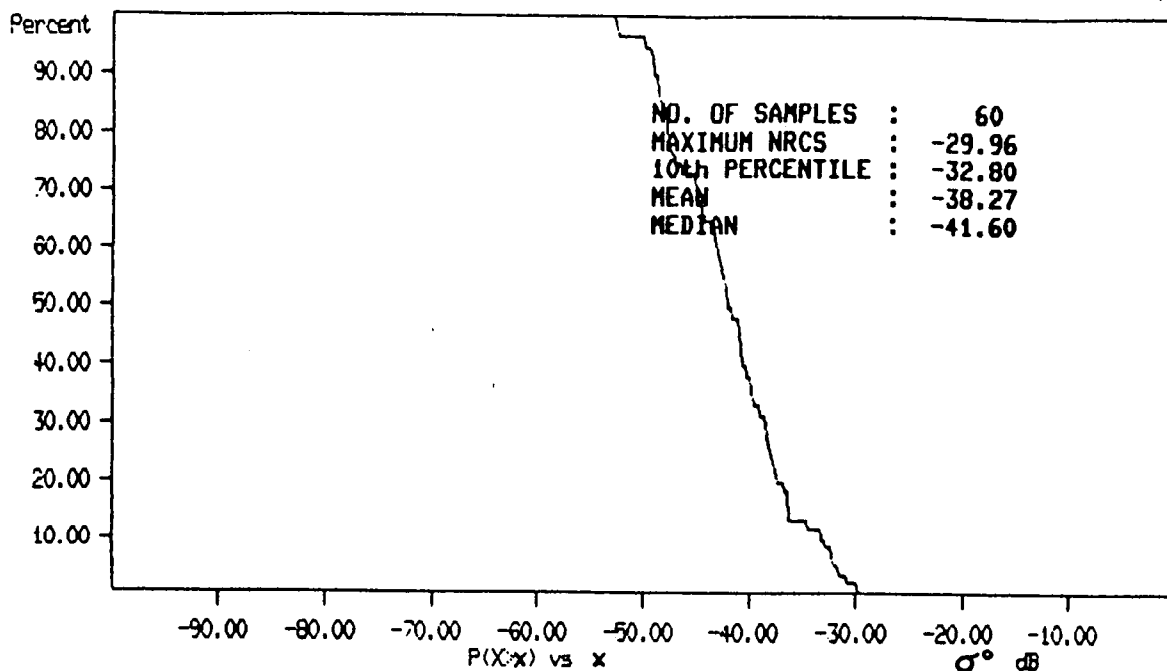


Figure 12. Cumulative normalized radar cross-section probability distribution for sea clutter at a 3° grazing angle (upwind, wind = 30 kt, SWH = 3 m).

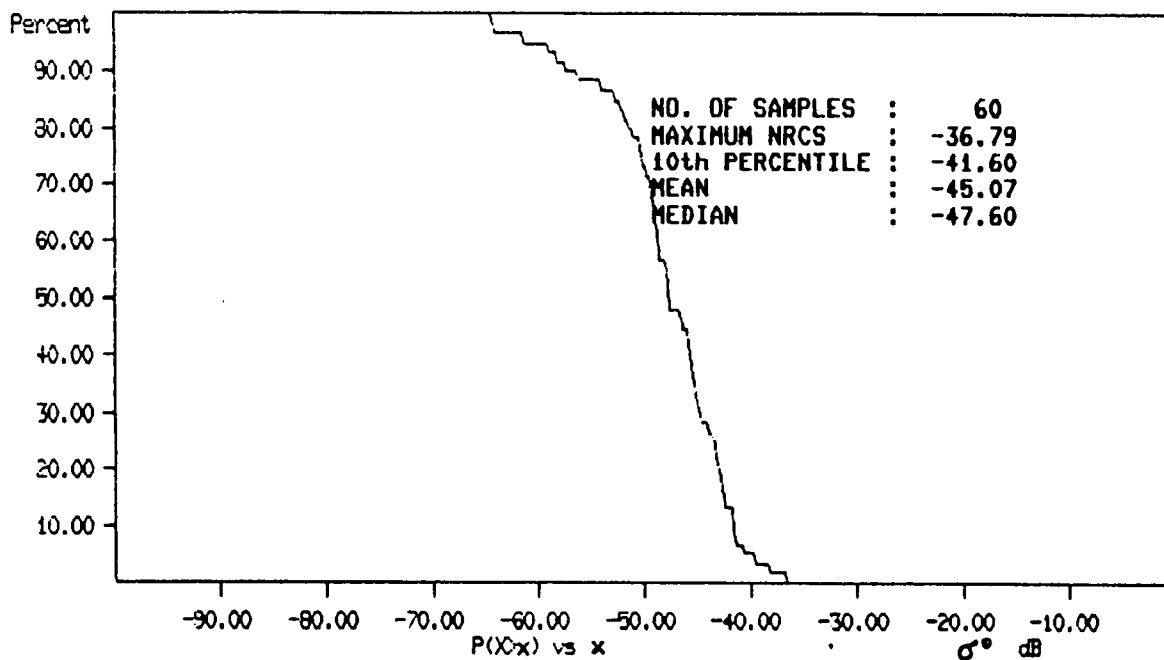


Figure 13. Cumulative normalized radar cross-section probability distribution for sea clutter at a 3° grazing angle (downwind, wind = 30 kt, SWH = 3 m).

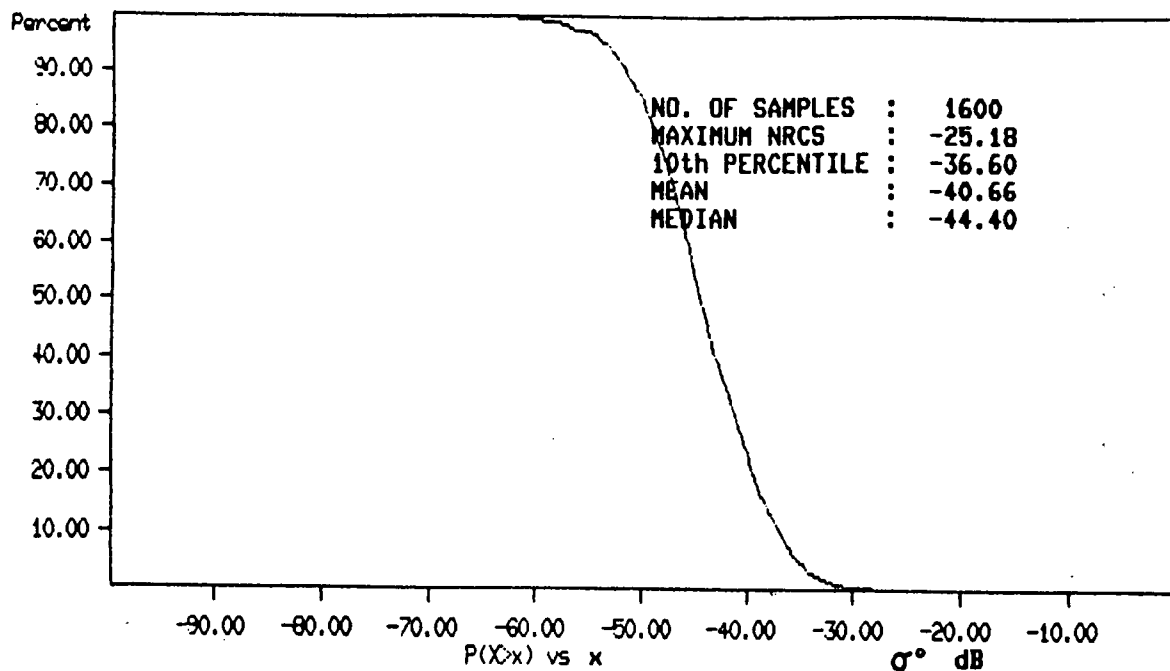


Figure 14. Cumulative normalized radar cross-section probability distribution for sea clutter at a 3° grazing angle (360°, wind = 30 kt, SWH = 3 m).

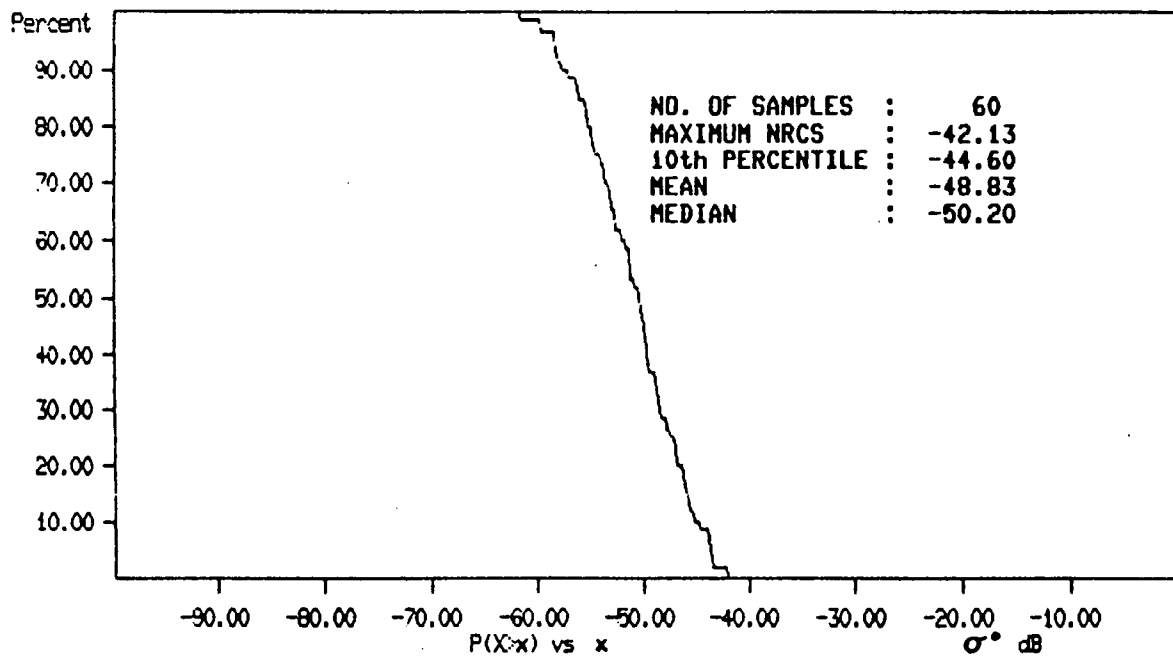


Figure 15. Cumulative normalized radar cross-section probability distribution for sea clutter at a 1° grazing angle (downwind, wind = 30 kt, SWH = 3 m).

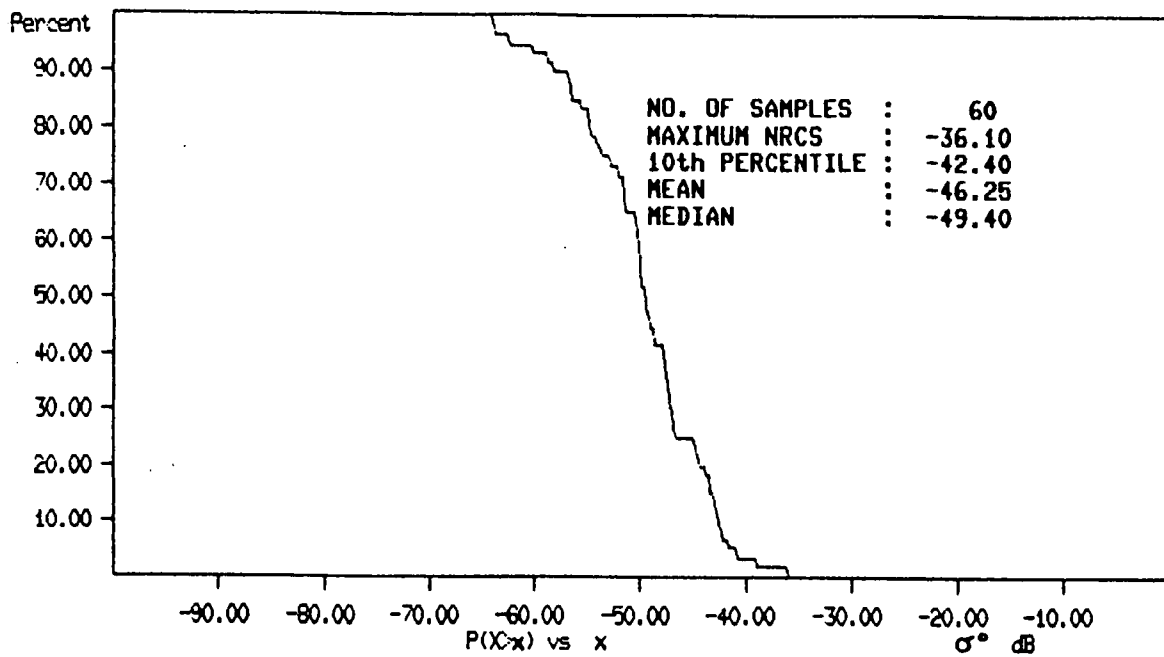


Figure 16. Cumulative normalized radar cross-section probability distribution for sea clutter at a 1° grazing angle (upwind, wind = 30 kt, SWH = 3 m).

TABLE 7

Comparison of normalized radar cross-section
of sea clutter with Nathanson (1969).

Grazing angle (deg.)	Backscatter coefficient (dB below $1\text{m}^2/\text{m}^2$)				Nathanson ^a (SS5)
	Orientation with respect to wind direction				
	Up ^b	Down ^c	Cross ^d	360	
0.6	49	-	-	-	36
1.0	46	49	48	47	33
3.0	38	45	41	41	32

^a. The data from Nathanson is for sea state 5 and has been interpolated at 0.6°

^b. Looking upwind.

^c. Looking downwind.

^d. Looking crosswind.

MODEL USED FOR APS 504 (V)3

GENERAL DESCRIPTION

The model of the APS 504 (V)3 was developed at C-CORE to emulate the signal-processing functions occurring in the (V)3, in order to calculate both required target cross-sections for detection as well as probability of detection for a specific target radar cross-section. (A full technical description is provided in Appendix I-A.)

Following each transmission by the radar, the power received at the antenna is converted into voltage as a function of time. The voltages then undergo a variety of signal processing operations by the radar culminating in a presentation of the processed signals on a screen display. The radar uses digital techniques for all of its processing.

During flights over open ocean, this same signal voltage arising from power received at the radar antenna was sampled and recorded by Viatic Resource Systems Inc. These data are a record of power received as a function of time and are taken to be representative of typical ocean backscatter (power reflected back to the radar from the ocean for a particular environmental condition). The samples of signal voltage are the input to the model, and represent the signals from multiple scans (360° sweeps) of the radar antenna over the ocean.

The model takes this record of signal voltage, converts it to received power (Figure 17) and applies the same signal processing operations, in the same order, taking into account the finite accuracy of digital processing. Incorporated into the model are the calibration results (discussed earlier) of the logarithmic amplifier, and the stated antenna beam pattern.

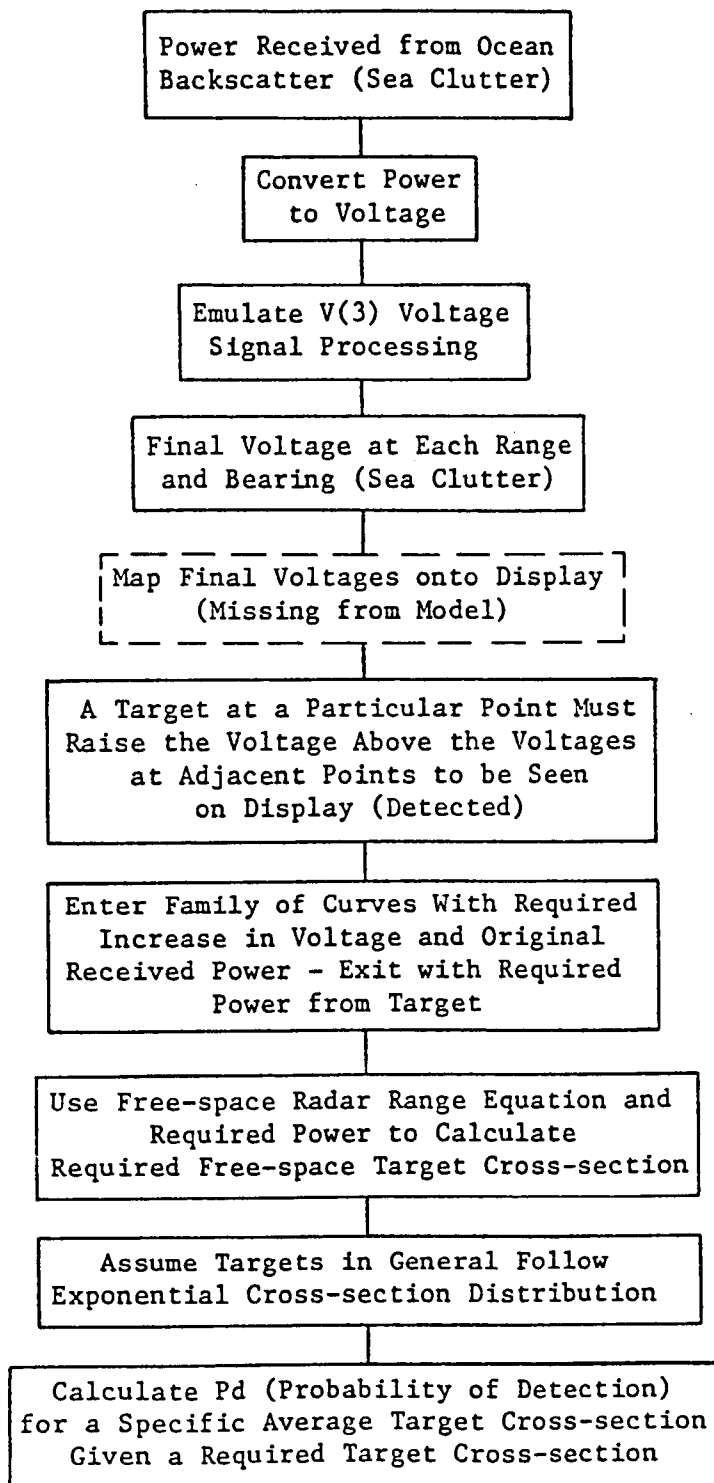


Figure 17. Model flow chart.

The emulation of the radar is taken as far as the final voltage just before transformation to the radar display. The (V)3 uses an internal look-up table which maps the final processed output voltage onto one of 16 display intensity levels. The look-up table description is unavailable and therefore is not incorporated into the emulation of the (V)3.

The emulation of (V)3, starting with received power, produces calculated final voltages representing multiple scans of the radar antenna over open ocean. Each voltage corresponds to a particular range and bearing, and represents the radar's response to sea clutter (ocean backscatter). Up to this point in the calculations, only the background of the radar display has been calculated (i.e. the signals resulting from sea clutter and system noise). A potential target has to compete with this background to be detected. The next step is to calculate at each point of interest the necessary signal a target must have to stand out from the background.

Each point in range and bearing, which has a particular voltage associated with it, is competing with adjacent points with different voltages. Detection of a target in sea clutter was modelled as the requirement that the power from the target further raise the voltage to equal the maximum of the adjacent points. Therefore, if a target were at the point of interest, the target power must be sufficient to raise the signal voltage to compete with its strongest neighbour. A separate formulation calculated the signal voltage increase above background as the radar antenna sweeps through a region containing a target. The voltage increase changes if the received power from either sea clutter or the target changes. This related the desired signal voltage increase required for detection to target radar cross-section.

A family of curves was calculated that relate the required increase in signal voltage (for the point of interest to be a local maximum compared to its neighbours), to the required power from the target.

The model enters this family of curves with the necessary voltage increase required, and the original power received at the point of interest and exits with a number indicating the power required from the target.

The basic radar range equation (free space) is then used to calculate the required target cross-section for detection at the point of interest, from the power required and the radar range.

The model assumes that targets in general have an exponential probability distribution of cross-section (Swerling Case 1). At the point of interest a particular cross-section is required for detection. The probability of detection for a target with a fluctuating cross-section is then calculated from this distribution (see Appendix I-A).

Once the distribution of required cross-sections across the radar screen have been calculated and a probability distribution of radar cross-section assumed for targets, two data products are possible.

The model was used to calculate average target cross-sections from their observed blip-to-scan ratio. The requirement for this calculation was that the sum of the calculated probabilities along the modelled target track across the radar screen, normalizing to the number of target scans, equal the observed blip-to-scan ratio.

Similarly the calculated cross-sections for detection as a function of range and azimuth were used to produce contour plots of required cross-section for detection at $P_d = 0.5$, for different environmental

conditions.

LIMITATIONS OF THE MODEL

The samples of radar-received power, described in the previous section, form the input to the model. These samples are taken to be representative of typical ocean backscatter (sea clutter) for the observed environmental conditions.

The system that collects these samples collects only one radial in six. Although the model takes this reduction in data into account, it forces certain calculations to be done with averaged values as opposed to unaveraged individual data points. For instance, the area of a target would be swept by about 21 radials (i.e., 21 radar transmissions) per radar sweep, on 25 naut mi range scale. As the data available are reduced by a factor of 6, only three radials of received power are available per scan to emulate radar signal processing. Inherent in using a reduced number of radials for modelling is the tacit assumption that sea clutter is well correlated from radial to radial. (i.e. that the clutter signal changes slowly from pulse to pulse at a given range).

The available description of the (V)3 does not include the range of signal voltage corresponding to each screen intensity. There are only 16 intensity levels on the radar display. The range of information compressed into one intensity level would be expected to introduce some loss in the detection process. The model works only up to the final voltage, and any loss associated with this data compression has been omitted out of necessity. This omission is expected not only generally to bias calculated target cross-sections below their true value, but also to lower predicted required cross-sections for detection by a similar

amount.

Although a maximum of 12 radar scans of received power is available for input to the model, calculated target cross-sections based on 12, 6, 3, or 1 scan generally show little variation in the result. The number of radar scans of received power used for modelling does not appear to be a limiting factor. To be safe, however, a minimum of three scans were used to calculate target cross-sections, and to predict required cross-sections for probability of detection (Pd) of 0.5.

The power received from sea clutter is related to its radar cross-section per m^2 which is a function of grazing angle. Altitude and radar slant range determine grazing angle. The model takes the altitude and slant range used to record received power, and calculates both the sea clutter radar cross-section per m^2 and the corresponding grazing angle. Power received from sea clutter for a different altitude is calculated using the sea clutter cross-section for the appropriate grazing angle of interest.

Collection of received power was limited to a radar slant range of about 16.6 naut mi. This range corresponds to a grazing angle of 0.284° for an altitude of 500 ft. When the model emulates the (V)3 for the same altitude at which the received power was collected, its range of prediction is limited to 16.6 naut mi. If the altitude used for prediction is greater than the altitude at which received power was collected, then the range of prediction increases. When the model emulates detection at 1,500 ft altitude with received power collected at 500 ft, matching grazing angles results in extending the range of prediction out to 24.6 naut mi.

Care was taken when predicting detection at a higher altitude to avoid converting radar system noise into apparent sea clutter. If the received power represented a noise-limited case below grazing angles of some value, then predictions at higher altitudes would only be valid out to the same grazing angle region. When the prediction altitude was below received-power altitude, the calculated received-power was not allowed to fall below the true noise level of the radar.

As the model assumes free-space propagation, any multipath effects will be absorbed in the calculated cross-sections of targets. This effect may appear as a target, the average cross-section of which, exhibits fluctuations when calculated over different range intervals, assuming that all other conditions such as aspect, remain constant.

Lastly, the model is based on the technical description available to C-CORE. Errors or omissions in the technical description of the (V)3 would introduce errors into the model and its calculations.

APPARENT REQUIRED SIGNAL-TO-NOISE RATIO AS A FUNCTION OF THRESHOLD

This section uses observed maximum range of detection of targets with known cross-sections under noise-limited conditions to draw conclusions about the apparent required signal-to-noise ratio (S/N) for detection, as a function of the threshold control setting on the (V)3. Apparent S/N is used as a convenient means of calculating the required increase in signal strength for detection as the threshold of detection is raised.

The threshold control knob was replaced prior to the start of data collection with a 10-turn potentiometer dial. Threshold could be set in a region from 0.55 to 1.47. The threshold control determines what voltage,

if any, is subtracted out of radar video signal and apparently also determines the shape and extent of the display look-up table described earlier.

Measurements of power required just to exceed the threshold were made during calibration and are described fully in Appendix I-A.

Basically, above a setting of about 0.96, noise is no longer visible on the radar display. As the threshold increases above 0.96, so does the received power required for detection. In the region from about 0.8 to 0.96 noise is visible on the radar display but does not appear to occupy too many of the 16 intensity levels available. Well below 0.8 the noise region seems to be fairly brightly displayed.

Thirteen data points were found during analysis to have the following conditions;

- a) Maximum range of detection took place outside the clutter zone of the radar, where detection was noise limited.
- b) The average radar cross-section of the target was known.
- c) The threshold setting was documented.

The apparent S/N required for detection was then calculated (based on an average noise value of -135 dB) from the free space radar range equation,

$$P_r = \frac{P_t G^2 \lambda^2 L\sigma}{(4\pi)^3 R^4}$$

where; P_r = power received

$$P_t = 10^5 \text{ W}$$

$$G = G_0 (1 - 134.16 \sin^2 \alpha)$$

$$G_0 = 1584.9 \text{ (antenna gain at } \alpha = 0^\circ)$$

$$\alpha = \text{vertical deviation from beam center}$$

$$\lambda = 0.032 \text{ m}$$

$$L = 0.6918 \text{ (two way loss)}$$

$$\sigma = \text{average target cross-section (m}^2\text{)}$$

$$R = \text{radar slant range (m)}$$

$$10 \text{ Log S/N} = 10 \text{ Log Pr} + 135 \text{ dB.}$$

The thirteen data points are plotted as a function of threshold in Figure 18. The flight number, aircraft altitude, and maximum range of detection are included in brackets beside each point. Between 0.73 and 0.93, a S/N of 4.6 to 10.0 dB is required for detection. (This agrees in general with the family of curves used by the model, described briefly earlier and more fully described in Appendix I-A, Figure I-A4, which predict a minimum S/N for detection of 6 to 8 dB). As one would expect the apparent S/N rises as the threshold is increased above 0.96.

The region below 0.73 is an apparent anomaly. The apparent S/N required for detection would not normally be expected to exceed S/Ns required at higher threshold settings.

Table 8 summarizes the results of Figure 18. The data indicates an additional loss of about 7.5 dB between the region at which noise is allowed to fully enter the display look up table (0.55 to 0.65) and at which the threshold is set at about the level of the noise (0.73 to 0.93).

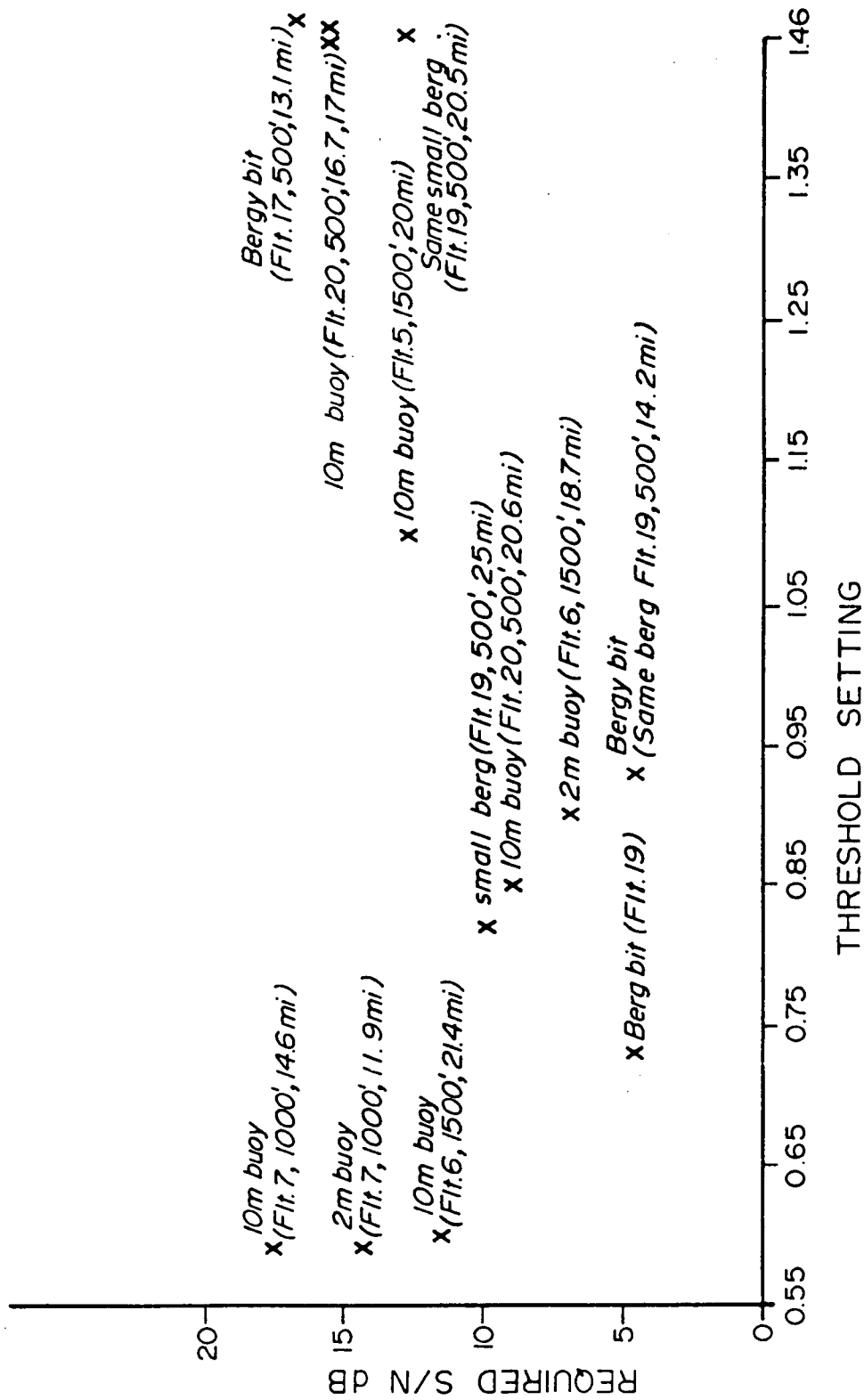


Figure 18. Apparent detection signal-to-noise ratio as a function of threshold.

TABLE 8

Apparent signal-to-noise ratio as a function of threshold

Threshold setting	Apparent average S/N observed (dB)
0.55 to 0.65	14.6 \pm 3.0
0.73 to 0.93	7.3 \pm 2.7
1.10	-12.8
1.46 to 1.47	14.8 \pm 2.0

This loss is not taken into account in model calculations, but the target cross-sections calculated from blip-to-scan ratios observed with thresholds below 0.73 have been increased by 7.5 dB to adjust for this apparent loss.

The source of this loss is not clear. A comment consistently recorded during blip-to-scan analysis of the radar display for threshold settings below 0.73 is, "display background is too bright, and makes target blips difficult to see".

On flight 11, the calibrated buoys were detected inside the clutter zone, but then the threshold was reduced, clutter appeared to saturate the display, and the buoys were lost.

The conclusion reached is that either the look-up table is being partially saturated when the threshold is set too far below local signal levels or the background is too bright for weak blips to contrast well. In either case, a potentially detectable target may not be readily visible to the operator.

When the source of the local background is noise, a threshold above 0.73 would be expected to be sufficient. When the local background rises because of sea clutter, however, the threshold may have to be raised to limit the range of video signals entering the look-up table.

CALIBRATED RADAR BUOYS

The calibrated radar reflectors mounted on buoys were intended to provide basic reference targets with known radar cross-sections. Both reflectors have a beam pattern in their vertical plane of about $\pm 18^\circ$ (at $\pm 18^\circ$ their reflectivity would be down by 50%) and are omnidirectional in their horizontal plane.

A videotape of the buoys in a sea state with no apparent wind and 1- to 2-m swells (relatively low sea state) indicates that the buoys tilt back and forth through the vertical with deviations of up to 10° . It is possible that in heavier sea states, under the influence of wind, the buoys may not only exhibit deviations from vertical that exceed their beam patterns, but also may list down wind.

This movement presents a problem to the data analysis that cannot be accounted for in the model, because the apparent cross-section of the buoys could be a function of wind direction and sea state, presumably dropping their values at certain radar-to-wind look angles.

RELATIONSHIP BETWEEN BLIP-TO-SCAN RATIOS AND CROSS-SECTIONS

The ratio of free-space cross-sections of two targets that follow the same path across the radar screen at slightly different times can be approximately related to their respective blip-to-scan ratios, under the following conditions:

- a) Both target tracks on the radar display extend well inside their respective absolute maximum range of detection.
- b) Neither target has 100% detection in the range interval of interest.
- c) Both targets exhibit Swerling Case 1 statistics.

Operational flights by the calibrated buoys resulted in one buoy following the other across the radar screen, separated by about 1 naut mi. Their observed blip-to-scan ratios from flights 5, 6, 7, and 11, and their range intervals are presented in Table 9.

The model calculates (see Appendix I-A, equation 9) probability of detection based on,

$$Pd = e^{-\sigma_{req'd} / \sigma_{av}} \quad (2)$$

where Pd = probability of detection

$\sigma_{req'd}$ = required free-space cross-section at some point in range

σ_{av} = average free-space cross-section of the target in question.

Although $\sigma_{req'd}$ changes from point to point, it seems reasonable that a particular segment of a target track have an average $\sigma_{req'd}$ associated with it. If two targets cross the same path then both will be required to compete with this average value for detection.

Applying this equation for two targets as described and re-arranging,

$$\sigma_{av1} \ln Pd_1 = -\sigma_{req'd} = \sigma_{av2} \ln Pd_2 \quad (3)$$

where the subscripts indicate targets 1 and 2 respectively. Similarly, the blip-to-scan ratios for each target reflect the average values of their Pd. Substituting,

$$\sigma_{av1} \ln (B/S_1) = \sigma_{av2} \ln (B/S_2) \quad (4)$$

and re-arranging,

$$\frac{\sigma_{av1}}{\sigma_{av2}} = \frac{\ln (B/S_2)}{\ln (B/S_1)} \quad (5)$$

This method has been applied in Table 9 in the last column, estimating the ratio of the 2-m² buoy's cross-section to that of the 10-m² buoy. Ideally the ratio should be 0.2. From the results this method appears to be accurate to within 3.5 dB.

TABLE 9
Relationship of target cross-sections and observed
blip-to-scan ratios

Flight	Target	Range interval	Blip-to-scan ratio	$\frac{\text{Ln} (B/S_{10m^2})^a}{\text{Ln} (B/S_{2m^2})}$
5	10-m ²	12.5-20.6	48/126	0.35
5	2-m ²	15.3-21.6	8/126	
6	10-m ²	9.8-5.5	51/61	0.25
6	2-m ²	8.5-5.2	25/51	
7	10-m ²	6.2-10.6	171/174	0.15
7	2-m ²	6.4-9.2	156/175	
11	10-m ²	19.8-12.6	69/86	0.33
11	2-m ²	19.7-11.8	49/96	
11 ^b	10-m ²	16.7-12.6	40/45	0.45
11 ^b	2-m ²	16.7-11.8	43/56	

^a Ratio of natural logarithms of observed blip-to-scan ratios, of 10-m² buoy to 2-m² buoy.

^b These are segments of the longer range intervals of flight 11.

COMPARISON OF MODELLED RESULTS AND SURFACE DATA

Comparison can be made in two main areas between modelled results and ground verification data.

Cross-sections calculated by the model are compared with measured or known cross-sections. Cases of non-detection of the calibrated buoys are compared with the model's prediction of required cross-section, within the uncertainty of the apparent cross-sections of the calibrated buoys in strong sea states (discussed earlier).

Radar cross-sections calculated by the model:

Tables 10 and 11 list the results for all targets that were verified on the ground. All cases were observed with the radar in log mode with constant false alarm rate (CFAR) on. As an example, on flight 17, run number 2, the radar was set on 12/1g/cf, 12 naut mi range scale, log mode, CFAR on. Altitude was 500 ft, with the antenna dipped down 0.5°. The target was a bergy bit. The aircraft heading was 358° relative to magnetic north. The bergy bit was observed on the radar display at ranges from 6.0 to 11.5 naut mi. The target offset, or distance between the flight line of the aircraft and the bergy bit was 0.0 naut mi. Thus, the aircraft was flying directly away from the bergy bit. The threshold was set at 1.47 (the maximum). This high setting was often used for strong radar targets to increase the required cross-section for detection and reduce the blip-to-scan ratio below 100%. Cross-section calculations require ratios less than 100%. The threshold setting is taken into account by the model. The blip-to-scan ratio was 56/73, i.e., the target was detected 56 times during 73 scans. The model calculated a cross-section of 5.3 m².

TABLE 10

Cross-sections modelled for calibrated buoys

Run no.	Radar mode	Alt. (ft)	Antenna dip (deg.)	Thresh- old	Target type	A/C ^a HDG (deg.)	Target range (naut mi)	Final	Target offset (naut mi)	Blip-to-Scan ratio	Model σ AV	Viatec σ AV
<u>Flight 7</u>												
1	25/1g/cf	1000	-2.0	0.59	2-m ² buoy	113	5.6	10.0	4.3	156/175	1.1±0.1	-
2	25/1g/cf	1000	-2.0	0.59	10-m ² buoy	112	6.0	9.2	4.3	171/174	9.0±0.1	-
<u>Flight 11</u>												
1	25/1g/cf	500	-1.0 ^a	0.96 ^b	10-m ² buoy		19.8	12.6	3.5	69/86	-	-
2	25/1g/cf	500	-1.0	0.96	2-m ² buoy		19.7	11.8	4.1	49/96	-	-
3 ^c	25/1g/cf	500	-1.0	0.96	10-m ² buoy	126	16.7	12.6	3.5	40/45	10.9±1.3	-
4 ^c	25/1g/cf	500	-1.0	0.96	2-m ² buoy	124	16.7	11.8	4.1	43/56	4.1±0.3	-

^a Estimated only.

^b Estimated only.

^c Runs 3 and 4 are segments of runs 1 and 2 of flight 11, limited to 16.7 miles, to allow calculation of σ .

^d Aircraft heading.

Note: See text for definitions and units of measure.

TABLE 11

Cross-sections modelled for particular targets of interest

Run no.	Radar mode	Alt. (ft)	Antenna dip (deg.)	Thresh-old	Target type	A/C HDG (deg.)	Target range (naut mi)	Final	Target offset (naut mi)	Blip-to-Scan ratio	Model σ AV	Viatec σ AV
<u>Flight 17</u>												
1	6/lg/cf	500	-0.5	1.47	bergy bit	358	1.6	6.0	0.0	64/65	8.5 \pm 4.0	-
2	12/lg/cf	"	"	"	"	358	6.0	11.5	0.0	56/73	5.3 \pm 1.8	4.9 \pm 5.0
4	25/lg/cf	"	"	"	"	358	13.2	4.7	0.0	71/95	5.9 \pm 1.6	-
5	6/lg/cf	"	"	"	"	358	3.6	5.7	3.5	26/42	0.6 \pm 0.12	-
<u>Flight 19</u>												
11	6/lg/cf	500	-1.0	1.46	small dome	77	3.2	5.6	0.0	27/28	2.5 \pm 1.5	-
12	12/lg/cf	"	"	1.46	"	76	6.5	11.2	0.0	35/58	2.8 \pm 0.7	-
14	25/lg/cf	"	"	0.92	"	254	15.9	9.8	0.0	43/72	1.0 \pm 0.1	-
15	12/lg/cf	"	"	0.92	"	256	8.9	4.9	0.0	40/43	0.9 \pm 0.1	-
16	6/lg/cf	"	"	0.92	"	253	4.3	1.5	0.0	31/32	0.4 \pm ?	-
17	6/lg/cf	"	"	0.92	"	256	2.2	6.0	0.0	34/42	<0.2	-
18	12/lg/cf	"	"	0.92	"	256	6.2	12.0	0.0	64/66	3.4 \pm 1.4	-
19	25/lg/cf	"	"	0.92	"	256	12.9	18.8	0.0	51/69	2.5 \pm 0.3	-
21	12/lg/cf	"	"	1.46	small iceberg	125	6.0	12.0	0.0	74/84	13.0 \pm 3.5	15.1 \pm 16.7
22	25/lg/cf	"	"	1.46	"	126	12.6	20.5	0.0	62/108	17.8 \pm 4.2	-
24	25/lg/cf	"	"	1.46	"	296	19.7	9.5	2.4	110/126	46. \pm 12.5	-
25	25/lg/cf	"	"	1.46	"	273	5.9	15.5	5.3	88/140	2.75 \pm 0.75	-
<u>Flight 20</u>												
2	25/lg/cf	500	-0.5	1.46	10-m ² buoy	109	13.7	6.1	0.0	66/83	9.25 \pm 2.75	-
3	25/lg/cf	"	"	1.46	"	118	11.8	17.0	0.0	42/56	23.75 \pm 7.0	10.4 \pm 8.2
4	25/lg/cf	"	"	1.46	"	298	15.1	11.7	6.4	35/40	36.0 \pm 13.0	26.0 \pm 21.4
5	12/lg/cf	"	"	1.46	"	293	10.6	11.2	5.3	209/239	6.0 \pm 1.4	8.4 \pm 9.8
6	25/lg/cf	"	"	1.46	"	294	12.0	16.7	4.8	53/65	32.5 \pm 11.0	-

Note: See text for definitions and units of measure.

The corresponding time history of power received for that range interval produced by Viatec calculates to an average free-space cross-section of 4.9 m^2 . The value of ± 5.0 is the standard deviation of an exponential distribution and, therefore, not indicative of the accuracy of measurement.

The results from flights 7 and 11 indicate that the model is calculating reasonable values within 3 dB for the calibrated buoys with theoretical cross-sections of 2- and 10-m^2 . Similarly, the measured values of the buoys on flight 20 support the values obtained on flights 7 and 11 and also agree with the modelled values for that flight within 3.6 dB (worst case). The modelled cross-sections for the bergy bit on flight 17 and for the small iceberg on flight 19 are in somewhat closer agreement with their measured values.

The small dome iceberg on flight 19 was initially the source of some confusion. This flight overflew an area with a wide variety of targets ranging from growlers to medium icebergs. Received power was collected accidentally from a group of three targets 2.5 naut mi south and slightly west of the small dome. Blip-to-scan analysis was done only for the small dome, while ignoring the three targets nearby because their identity was not known.

The modelled cross-sections calculated from the blip-to-scan ratios in the 6.0- to 18.8- naut mi regions range from 1.0 to 3.4 m^2 , with an average value of $2.425 \pm 1.021 \text{ m}^2$, and, of course, did not agree with analysis of received power from totally different targets.

This problem warranted some calculations of cross-section based on maximum range of detection. Ocean conditions that day were quite calm (sea state of 1 to 2) resulting in a small clutter zone and, therefore,

detection would be mostly noise-limited for targets with cross-sections in the order of square metres. The small dome iceberg was observed on the display at maximum ranges of detection of 18.0 and 18.8 naut mi with thresholds between 0.78 and 0.92 on two separate passes but was observed at a detection range of only 11.2 naut mi with a threshold of 1.46.

The average free-space cross-sections were calculated for these three maximum ranges, assuming a noise-limited situation, in the same manner as described earlier. The results are given in Table 12, and are within 3 dB of the average of the modelled cross-sections. They also suggest that the average radar cross-section does not appear to vary substantially with range in this particular case.

TABLE 12

Calculated free space cross-section of small dome iceberg

Maximum range (naut mi)	Threshold setting	Apparent S/N required (dB)	Calculated cross-section required (m ²)
18.0 miles	0.78	7.5 dB	2.57
18.8	0.92	7.5	3.06
11.2	1.46	15.0	2.12

On flight 2, the supply vessel MV Placentia Bay was observed to have an approximate blip-to-scan ratio of 50% at 12 naut mi, upwind, in Douglas sea state of about 6. The threshold setting was very low, at about 0.65, which introduced an additional loss of 7.5 dB. The flight altitude was 800 ft. Although no digital power was collected on that flight, flights 3 and 9 also occurred during sea state 6 conditions and model predictions are available for an altitude of 500 ft.

The predictions were aligned according to wind direction and the

required free-space cross-sections ($P_d = 0.5$) predicted from those flights at the 12 naut mi location of the MV Placentia Bay average $15 \pm 3 \text{ m}^2$ for thresholds well above 0.65.

The altitude of 800 ft on flight 2 raises the average clutter cross-section at 12 naut mi by about 3 dB over that observed at 500 ft. Assuming the same average signal-to-clutter ratio (S/C) is required for detection at 12 naut mi at both altitudes, then the radar cross-section of the MV Placentia Bay was estimated in dB as,

$$10 \text{ Log } 15 + 7.5 \text{ dB} + 3 \text{ dB} = 22.26 \text{ dB}$$

or about 168 m^2 .

Radar cross-sections for Husky/Bow Valley supply vessels measured with X-band marine radar were obtained from the drilling unit Sedco 706 in 1984 (Ryan et al. 1985), and averaged between 146 and 192 m^2 , at a range of 8 to 10 naut mi. These values agree with the model's prediction within 3 dB.

It appears that cross-sections calculated by the model have a typical accuracy of ± 3 dB based on the surface measurement data available.

Predictive accuracy of model:

The three flights to be discussed occurred in sea states of 4 and greater, and represent cases for the model to predict regions of both detection and non-detection for the calibrated buoys. It is not clear whether the calibrated buoys, because of their directional pattern, retain their cross-sections observed at low sea states in moderate and stronger sea states.

All that can be assessed is the possible error on the part of the model assuming that the buoys do retain their cross-sections in strong sea

states.

On flight 9, the aircraft flew by the calibrated buoys in sea state of 6, at an altitude of 500 ft. The radar was set on 25-naut mi range scale, log mode, with CFAR on. Unfortunately the threshold was set at 0.75, much too low for the conditions encountered, and would have incurred an additional loss of 7.5 dB. Neither buoy was detected.

The model's prediction for that day at the same altitude is given in Figure 19. The values on the contours are the required free-space cross-section required in square metres for $P_d = 0.5$ when a substantially higher threshold is used. All values must be multiplied by 5.6 to account for the additional loss in using a threshold of 0.75. The approximate path of the buoys has been drawn in. The best region for detection is the area where the 5- and 6- m^2 contours are crossed, but, with the additional loss, even these contours represent a minimum of 28 to 33.6 m^2 and, therefore, non-detection is predicted for both the 2- and 10- m^2 buoys.

On flight 8, conditions were similar. The aircraft flew by the buoys along the same route in a sea state of 5 to 6, in the same radar mode as flight 9 with an altitude of 500 ft, without detecting either buoy. The model's prediction for 500 ft and the path of the buoys is illustrated in Figure 20. Unfortunately, threshold settings were not documented. Again for the first half of the buoy's path across the radar screen, the clutter zone appeared too bright, indicating the threshold was too low which introduced excessive loss. The contours in this region indicate a minimum cross-section required of about 6 m^2 at a relatively high threshold. Therefore, given the low threshold setting, non-detection is predicted.

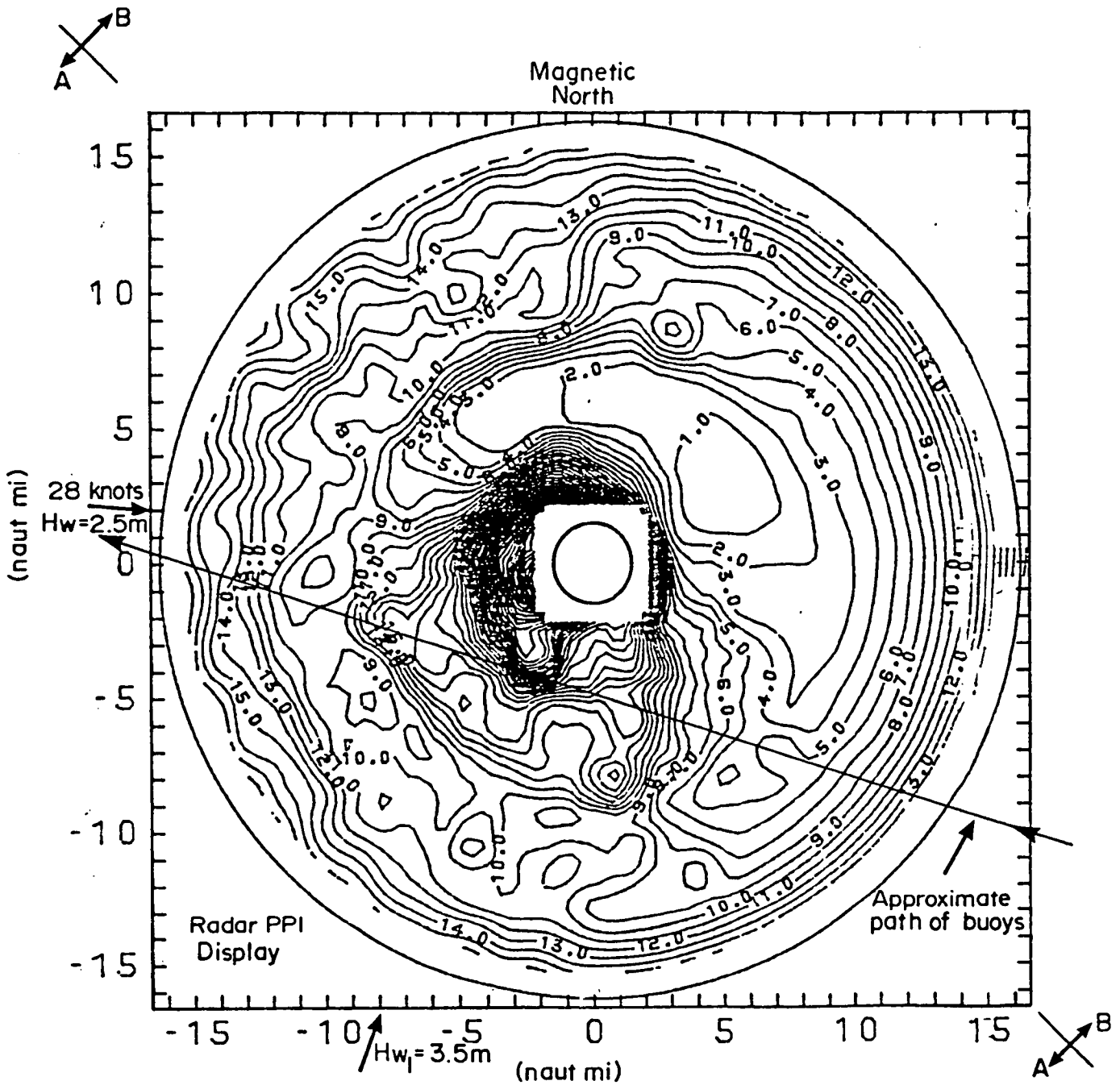


Figure 19. Modelled free-space cross-section (m^2) required for $P_d=0.5$ for flight 9: altitude 500 ft, CFAR'on', sea state 6.

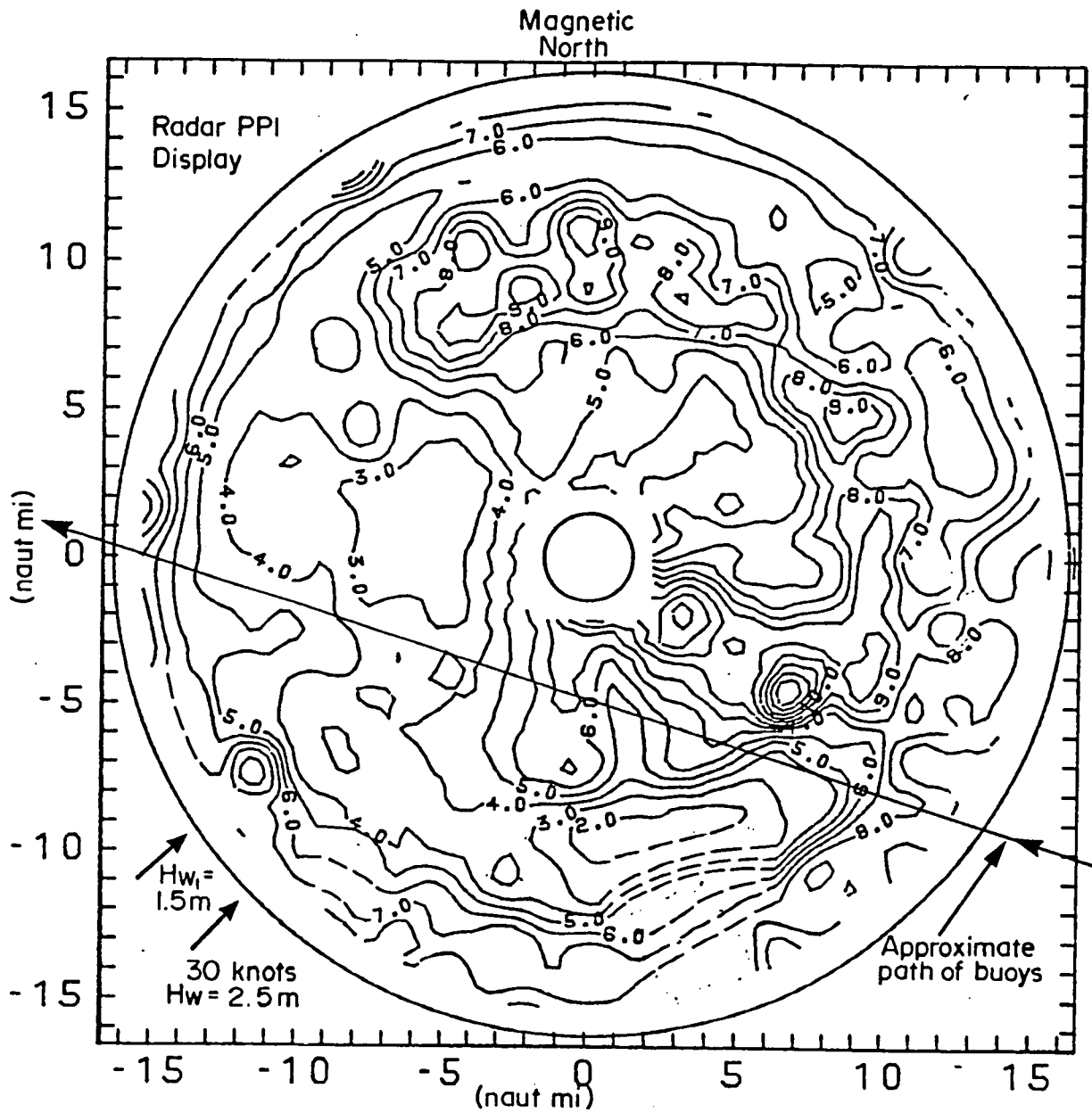


Figure 20. Modelled free-space cross-section (m^2) required for $P_d=0.5$ for flight 8: altitude 500 ft, CFAR'on', sea state 5-6.

During the second half of the buoy's path, however, the threshold was raised sufficiently to remove the background clutter beyond 18 naut mi, (i.e., the very edge of the clutter zone). Whether this setting was sufficient to eliminate excessive loss is unknown. Assuming that it was, the lowest contour region crossed was 4 m^2 . Therefore, the model predicts that the 2-m^2 buoy will not be detected, but that the 10-m^2 buoy should be detected. As the 10-m^2 buoy was not detected, the possible error is that the model underestimated the minimum required cross-section by 4 dB.

On flight 5, the aircraft flew by the buoys with a sea state 4 background at an altitude of 1,500 ft, in the same radar mode as flights 8 and 9, but using a more appropriate threshold of 1.1 to 1.2. As no received power was recorded that day, a prediction was made using received power from flight 14, and the prediction was aligned for the differing wind direction. Flight 14 had the same wind speed as flight 5, but more SWH and is represented as a sea state 5. The prediction is for a 1,500 ft altitude, and is illustrated in Figure 21. The different path of the buoys, compared to previous figures, is a result of alignment to wind direction.

On flight 5 the 2-m^2 buoy was almost undetectable along the entire path with a blip-to-scan ratio of 8/126, and was observed only because its location was already known. The 10-m^2 buoy was not detected until the aircraft was 12.5 naut mi past it and had a marginal blip-to-scan ratio of 48/126, with its last discernible blip at 20.6 naut mi. The model predicts the 10-m^2 buoy should not be detected until it is within 7 naut mi ahead of the aircraft and then should remain easily detectable until it is 17.5 naut mi past the aircraft. The lowest contour in this

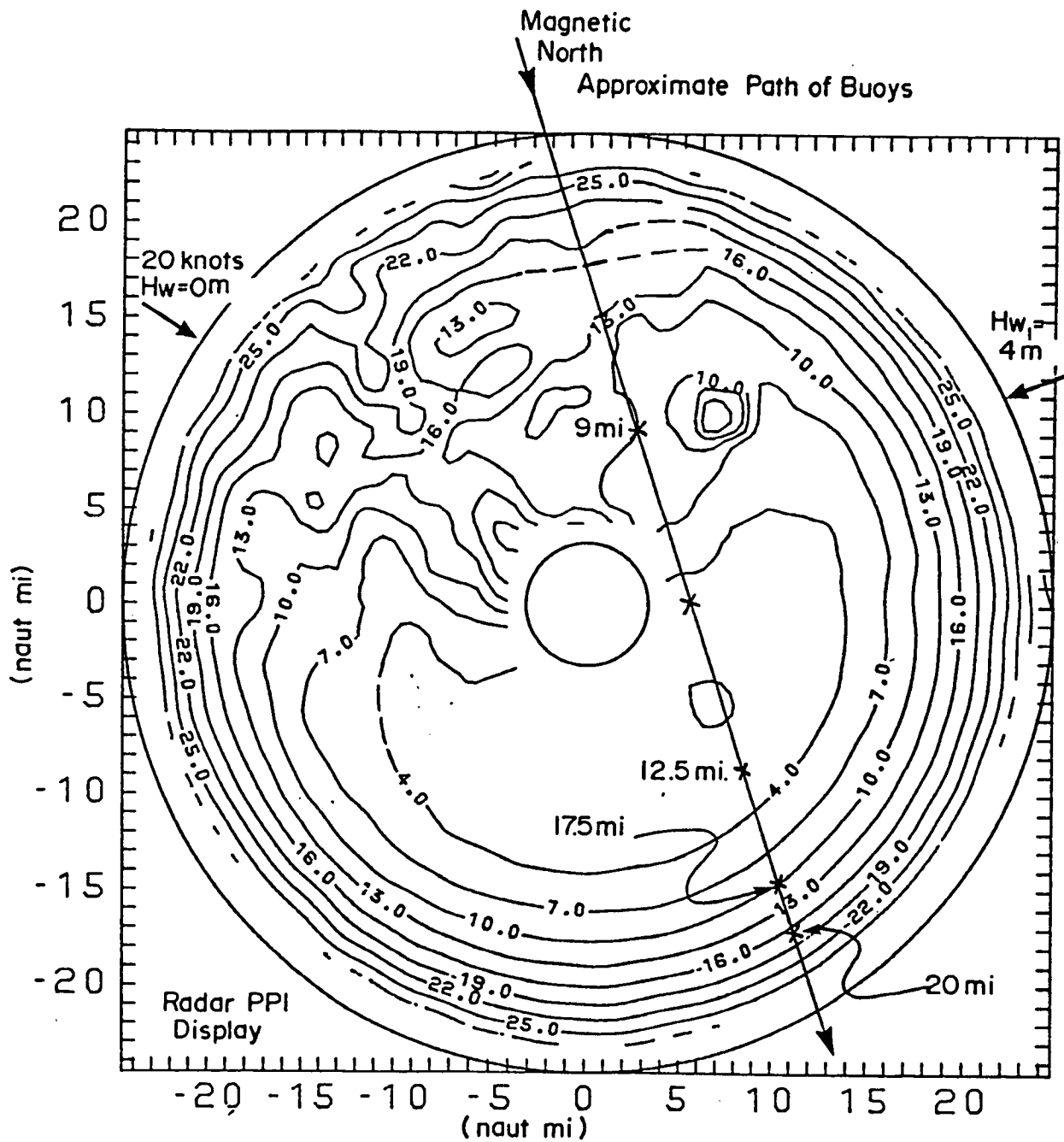


Figure 21. Modelled free-space cross-section (m^2) required for $P_d=0.5$ for flight 14: altitude 1,500 ft, CFAR'on', sea state 5.

region is 4 m^2 but because of the region it encompasses, probably 3 m^2 would be more appropriate as a minimum value. As the buoy remained undetected until it was 12.5 naut mi past the aircraft, the worst possible error is that the model underestimated the minimum cross-section required by 5 dB.

The clutter cross-sections calculated for flight 14 allow an estimate of the average S/C to be made for the 10-m^2 buoy. Assuming the buoy retained its free-space average cross-section of 10 m^2 , then at 5 naut mi its average S/C would have been +19.5 dB, while remaining undetected at this range. Normally this S/C would be expected to be sufficient for detection.

However, no measurements of received power exist to indicate what the apparent cross-sections of the buoys are in medium-to-strong sea states. To be conservative, it was assumed that the model can underestimate required cross-sections for $P_d=0.5$ by 4 to 5 dB.

DISTRIBUTION OF MODELLED RADAR FREE-SPACE CROSS-SECTIONS

Cross-sections for all the modelled icebergs are listed in this section, with the flight and radar parameters applicable.

Subsequently, cross-sections are grouped together to examine the statistical spread observed. The cross-sections are then broken down statistically according to iceberg size classifications, in preparation for predicting overall performance.

CALCULATED CROSS-SECTIONS

Tables 13 to 16 list all the calculated cross-sections broken down by flight number under the following headings from left to right:

Run number:	cross reference to flight documentation files which use same number to identify flight path range segment.
Radar mode:	radar range/mode/options radar range scale in naut mi mode: always lg (log) options used: cf (CFAR) gs (ground stabilized display)
Altitude:	aircraft altitude in feet
Antenna dip:	antenna dip in degrees. -1° means the antenna vertical beam center was pointed 1° down from the horizontal
Thresh:	threshold setting on the radar ~ approximate > greater than value stated < less than value stated
Target type:	as stated. Collapsed: multiple targets were painted as one blip because of radar resolution. DDK: drydock iceberg Pin: pinnaclcd iceberg

TABLE 13

Cross-sections modelled for targets on flights 2, 3, 5, 10, and 12

Flt/run radar mode	Alt (ft)	Dip (°)	Thresh	Target type	A/C HDS	Target Range Initial Final	Target offset	B/S	Model σ AV	σ Maximum range from S/N	Predicted σ AV from similar conditions	Comments
<u>Flight 2</u>												
2	25/1g/cfcs	800	0.65	Med. DDK ^a	287	-	14.2	-	-	-	151.5	Predicted σ _{AV} calculated from predictions @ 500' from flights 3 and 9. Adjusted for increased altitude.
3	6/1g/cf	800	~0.65	"	334	3.0	5.3	24/31	-	-	182.8	
	25/1g/cf	"	"	Med. pin ^b	280		12	~50%	-	-	168.7	
	25/1g/cf	"	"	Placentia Bay	280		12	~50%	-	-	168.7	
<u>Flight 3</u>												
4	25/1g/cf	1000	>0.96	Small DDK	305	-	>16	0.0	-	-	>39.	
<u>Flight 5</u>												
6	6/1g/cf	1000	1.0	Bergy bit	339	3.6	1.7	1.0	11/24	-	1.9	Predicted σ _{AV} calculated from predictions @ 500' and 1500' from flight 14.
<u>Flight 10</u>												
2	25/1g/cf	500	~0.6	Med pin	282	7.7	12.6	~7.	76/90	-	211.	Predicted σ _{AV} calculated from predictions for this flight (Pd = 0.5) and adjusts for B/S observed.
<u>Flight 12</u>												
3	6/1g/cf	500	<1.08	Bergy bit	333	1.0	5.3	0.0	32/62	-	~0.1	Predicted σ _{AV} calculated from predictions from flights 11 and 16.
3	"	"	"	"	"	-	6.0	"	-	-	-	

^a Dry dock.^b Pinnacle.

Note: See text for definitions and units of measure.

TABLE 14

Cross-sections modelled for targets on flights 13, 15, and 17

Flt/run radar mode	Alt (ft)	Dip (°)	Thresh	Target type	A/C HDG	Target Initial	Target Range Initial Final	Target offset	B/S	Model σ AV	σ Maximum range from S/N	Predicted σ AV from similar conditions	Comments	
Flight 13														
1	6/lg/cf	500	1.22	Small berg	164	1.35	3.1	1.0	14/28	0.12+0.02	-	-	For small berg plus 4 bergy bits: Target size classes from 34mm photo where images small. Sizes may be overestimated by one size class. Targets in very close proximity to each other. It is possible that targets have been interchanged unknowingly. Runs 6, 7, 8, and 9 targets collapsed into same range cell; cross-sections calculated are for targets together.	
2	6/lg/cf	"	"	Bergy bit ₍₁₎	"	1.0	2.7	0.9	23/28	0.61+0.15	-	-		
3	6/lg/cf	"	"	Bergy bit ₍₂₎	"	1.35	2.9	1.2	20/28	0.32+0.06	-	-		
4	6/lg/cf	"	"	Bergy bit ₍₃₎	"	1.5	3.1	1.3	4/28	0.02+0.01	-	-		
5	6/lg/cf	"	"	Bergy bit ₍₄₎	"	1.65	3.3	1.6	15/28	0.11+0.03	-	-		
6	25/lg/cf	"	0.86	Collapsed	345	-	12.0	0.0	-	-	0.49	-		
7	25/lg/cf	"	0.75	"	326	9.1	15.3	0.0	39/86	~4.4	1.29	-		
8	25/lg	"	0.83	"	121	9.0	7.5	6.0	79/113	~1.9	-	-		
9	25/lg	"	0.83	"	120	-	14.0	6.0	-	-	0.90	-		
Flight 15														
3	12/lg/cf	500	1.23	Med. DK	131	7.8	10.8	-8.	80/84	-	-	113.7	Predicted σ _{AV} calculated from prediction @ 500' from flight 18. Calculation for Med. wedge adjusted for increased altitude. Maximum range of 10 miles observed for small berg.	
7	12/lg/cf	500	0.85	"	233	4.1	6.3	0.0	27/40	-	-	18.5		
2	12/lg/cf	500	1.23	Small DK	131	6.9	12.0	-6.5	54/84	-	-	15.7		
5	25/lg/cf	500	1.23	"	129	12.0	18.5	-6.	38/66	-	10.9	-		
9	6/lg/cf	1800	1.08	Med. wedge	053	2.7	6.0	0.0	16/33	-	49.	-		
11	6/lg/cf	500	0.90	Small berg	251	1.3	6.0	0.0	50/73	-	-	7.3		
11	12/lg/cf	500	0.90	"	251	-	10.0	0.0	-	-	-	5.0		
Flight 17														
1	6/lg/cf	500	1.47	Bergy bit ₍₁₎	358	1.6	6.0	0.0	64/65	8.5+4.0	-	-		Maximum range observed just after aircraft turning, bergy bit (2).
2	12/lg/cf	"	"	"	358	6.0	11.5	0.0	56/73	5.3+1.8	-	-		
4	25/lg/cf	"	"	"	358	13.2	4.7	0.0	71/95	5.9+1.6	-	-		
5	6/lg/cf	"	"	"	358	3.6	5.7	3.5	26/42	0.6+0.12	-	-		
25/lg/cf	500	-1.0	<0.96	Bergy bit ₍₂₎	-	-	16.5	-	-	-	1.8	-		
19	12/lg/cf	"	>0.96	Bergy bit ₍₃₎	027	-	10.9	0.0	-	-	>0.34	-		
20	12/lg/cf	500	>0.96	Bergy bit ₍₃₎	209	-	10.5	0.0	-	-	>0.29	-		
24	25/lg/cf	"	"	"	210	-	>18	0.0	-	-	>2.57	-		
29	12/lg/cf	"	"	Bergy bit ₍₄₎	328	-	10.7	0.0	-	-	>0.32	-		
8	25/lg/cf	"	>0.96	Small DK	151	-	>18	2.0	-	-	>>2.57	-		

Note: See text for definitions and units of measure.

TABLE 15

Cross-sections modelled for targets on flight 19

Flt/run radar mode	Alt (ft)	Dip (°)	Thresh	Target type	A/C HDG	Target Range Initial Final	Target offset	B/S	Model σ AV	σ Maximum range from S/N	Predicted σ AV from similar conditions	Comments
Flight 19												
1	6/1g/cf	500	0.93	Berry bit	063	2.4	5.5	0.0	36/39	0.16±0.04		
2	12/1g/cf	"	0.93	"	062	5.9	10.9	0.0	43/64	0.25±0.05		
3	25/1g/cf	"	0.93	"	062	11.9	14.2	0.0	18/30	1.19±0.15		
4	25/1g/cf	"	0.73	"	259	14.3	11.5	5.5	27/38	1.06±0.06		
5	12/1g/cf	"	0.73	"	260	10.3	5.4	4.5	70/73	1.06±0.16		
6	12/1g/cf	"	0.73	"	267	5.1	7.3	4.5	69/90	0.50±0.03		
7	6/1g/cf	"	1.05	"	129	3.9	1.3	0.4	24/33	0.33±0.04		
8	6/1g/cf	"	1.05	"	129	0.9	5.3	0.4	44/55	0.07±0.05		
9	12/1g/cf	"	1.05	"	129	5.7	11.0	0.0	40/60	0.29±0.04		
11	6/1g/cf	"	1.46	Small dome	77	3.2	5.6	0.0	27/28	2.5±1.5	2.12	
12	12/1g/cf	"	1.46	"	76	6.5	11.2	0.0	35/58	2.8±0.7	2.57	
13	25/1g/cf	"	0.78	"	252	-	18.0	0.0	-	-	-	
14	25/1g/cf	"	0.92	"	254	15.9	9.8	0.0	43/72	1.0±0.1		
15	12/1g/cf	"	0.92	"	256	8.9	4.9	0.0	40/43	0.94±0.1		
16	6/1g/cf	"	0.92	"	253	4.3	1.5	0.0	31/32	0.4±?		
17	6/1g/cf	"	0.92	"	256	2.2	6.0	0.0	34/42	<0.2±		
18	12/1g/cf	"	0.92	"	256	6.2	12.0	0.0	64/66	3.4±1.4		
19	25/1g/cf	"	0.92	"	256	12.9	19.8	0.0	51/69	2.5±0.3		
21	12/1g/cf	"	1.46	Small bergs	125	6.0	12.0	0.0	74/84	13.0±3.5		
22	25/1g/cf	"	1.46	"	126	12.6	20.5	0.0	62/108	17.8±4.2		
24	25/1g/cf	"	1.46	"	296	19.7	9.5	2.4	110/126	46. ±12.5		
25	25/1g/cf	"	1.46	"	273	5.9	15.5	5.3	88/140	2.75±0.75		
26	25/1g/cf	"	1.46	Small DDK	267	5.9	18.3	5.3	169/174	73.0±22.0	>43	Predicted σ_{max} calculated by ratio method compared to small berg. (see p.70).

Note: See text for definitions and units of measure.

TABLE 16

Cross-sections modelled for targets on flights 7, 11, and 20

Flt/run radar mode	Alt (ft)	Dip (°)	Thresh	Target type	A/C HDG	Target Range		Target offset	B/S	Model σ AV	
						Initial	Final				
<u>Flight 7</u>											
1	25/1g/cf	1000	-2.0	0.59	2-m ² buoy	113	5.6	10.0	4.3	156/175	1.1±0.1
3	25/1g/cf	"	"	0.59	10-m ² buoy	112	6.0	9.2	4.3	171/174	9.0±0.1
<u>Flight 11</u>											
1 ^a	25/1g/cf	500		0.96	10-m ² buoy		19.8	12.6	3.5	69/86	-
2 ^a	25/1g/cf	"		0.96	2-m ² buoy		19.7	11.8	4.1	49/96	-
3 ^b	25/1g/cf	500	-1.0	0.96	10-m ² buoy	126	16.7	12.6	3.5	40/56	10.9±1.3
4 ^b	25/1g/cf	"	"	0.96	2-m ² buoy	124	16.7	11.8	4.1	43/56	4.1±0.3
<u>Flight 20</u>											
2	25/1g/cf	500	-0.5	1.46	10-m ² buoy	109	13.7	6.1	0.0	66/83	9.25±2.75
3	25/1g/cf	"	"	1.46	"	118	11.8	17.0	0.0	42/56	23.75±7.0
4	25/1g/cf	"	"	1.46	"	298	15.1	11.7	6.4	35/40	36.0±13.0
5	12/1g/cf	"	"	1.46	"	293	10.6	11.2	5.3	209/239	6.0±1.4
6	25/1g/cf	"	"	1.46	"	294	12.0	16.7	4.8	53/65	32.5±11.0

Note: See text for definitions and units of measure.

^a Antenna tilt and threshold estimated.

^b These are segments of runs 1 and 2, limited to 16.7 miles, to allow calculation of σ_{av}.

A/C Hdg: aircraft heading in degrees relative to Magnetic North.

Target Range Initial: slant range in naut mi from aircraft to target at beginning of target track analyzed.

Target Range Final: slant range in naut mi at end of target track analyzed

Target Offset: perpendicular distance in naut mi between target track across screen and parallel flight path

B/S: number of detections/number of scans on target (blip-to-scan ratio)

Model σ_{av} : average free-space cross-section of target calculated by the model in m^2 error based on the B/S being ± 1 count off in detection on one additional scan

Maximum range from S/N: average free-space cross-section calculated from maximum range of detection observed and apparent S/N required for detection. (determined by threshold setting).

Predicted σ_{av} from similar conditions: for targets which were documented on a flight which did not collect received power, σ_{av} was estimated using the model's prediction ($P_d = 0.5$) from another flight with similar environmental conditions. Corrections were made to allow for differing wind directions, altitudes, and blip to scan ratios other than 0.5 (see P.70).

In some cases the cross-sections calculated have a > (greater than) or < (less than) qualification. Usually this designation means that the target was never detected and, therefore, only a minimum value can be calculated below which its cross-section must lie. Alternatively, the target had perfect detection out to some maximum range at which point the range scale was decreased to look at some other target, in which case only a lower limit is established on the cross-section.

STATISTICAL DISTRIBUTION OF MODELLED ICEBERG FREE-SPACE CROSS-SECTIONS

A total of 33 icebergs, from growler to medium iceberg in size, were sufficiently well documented to have a cross-section calculated in some form. Some of the targets were observed from multiple aspects and exhibited substantial changes in cross-section, whereas the radar and flight parameters (except for aircraft heading) remained essentially constant.

Table 17 lists the targets, subdivided by size class and in chronological order by flight. Cross-sections listed are the average value when more than one value was available, with the number of points averaged indicated.

Figure 22 illustrates the spread in all cross-sections using cumulative percentage. The cross-sections were ranked in decreasing size. The percentage of targets with cross-section greater than or equal to that of the n th rank is $n \times 100/m$, (m = total population size).

For instance, using Figure 22, of 27 icebergs, 26% had cross-sections greater than about 40 m^2 , and 40% had cross-sections greater than about 6 m^2 .

The large spread in values prevents the tail of the distribution from being graphed accurately.

Figure 23 illustrates medium icebergs only. The population is small but it appears that medium icebergs can be expected to exhibit cross-sections in the order of tens of square meters and up.

Figure 24 illustrates small icebergs only. Note the change of scale

TABLE 17

Cross-sections of iceberg targets by size class

Flight no.	Mean cross-section (m ²)	No. of points averaged	Detection
<u>Growlers</u>			
5			no
5			no
12			no
12			no
15			no
15			no
<u>Bergy bits</u>			
5	<1.9	1	no
5	1.9	1	
12	0.32	2	
12	<0.1	1	no
13	0.61	1	
13	0.32	1	
13	0.02	1	
13	0.11	1	
17	5.08	4	
17	1.8	1	
17	>1.1	3	
17	>0.32	1	
19	0.55	9	
19	<0.1	1	no
<u>Small icebergs</u>			
3	>39	1	
13	0.12	1	
15	13.3	2	
15	6.15	2	
17	>2.57	1	
19	19.88	4	
19	73.0	1	
19	1.84	10	
<u>Medium icebergs</u>			
2	167.15	2	
2	168.7	1	
10	211.0	1	
15	66.1	2	
15	49.0	1	

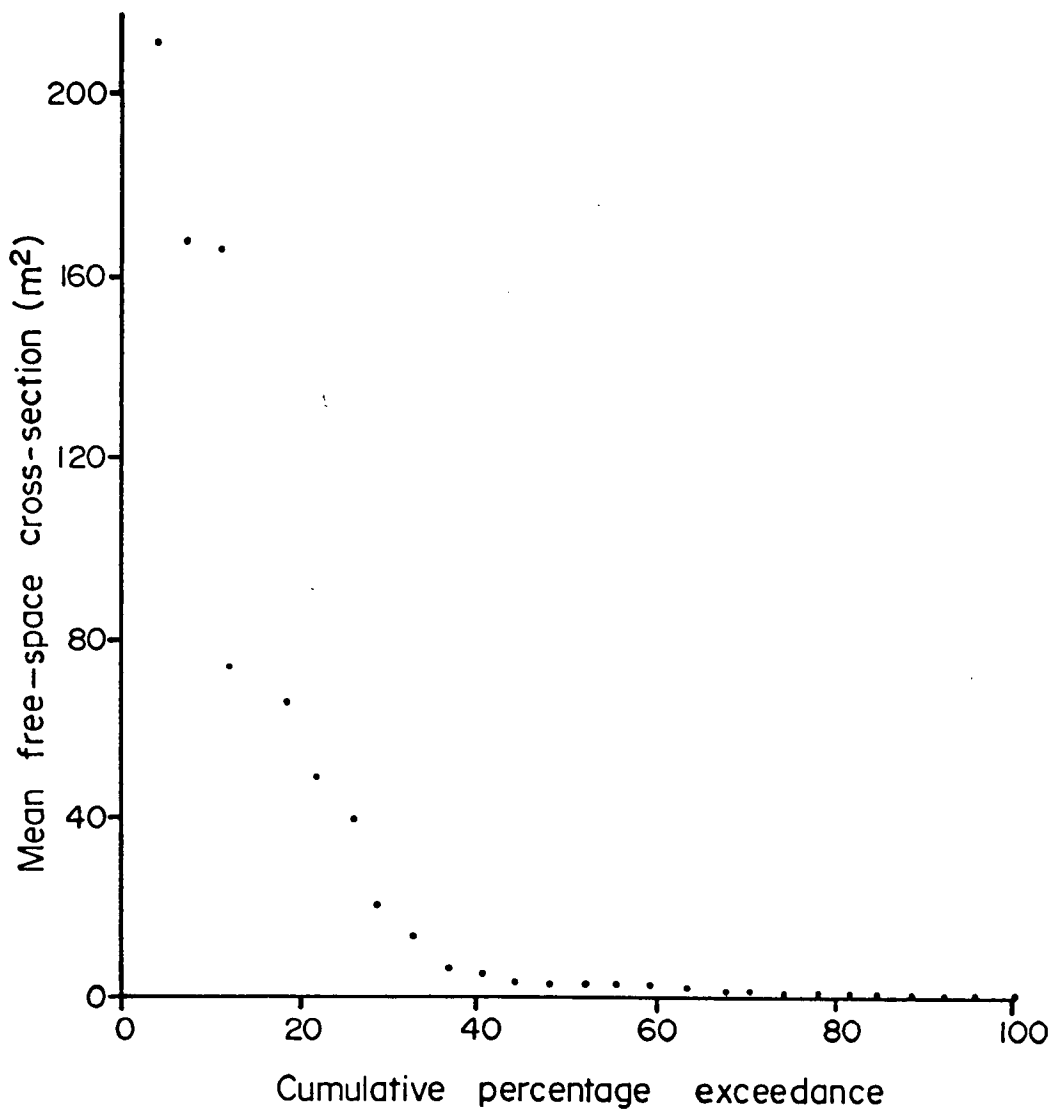


Figure 22. Distribution of free-space cross-sections:
 bergy bits, small and medium icebergs (population 27).

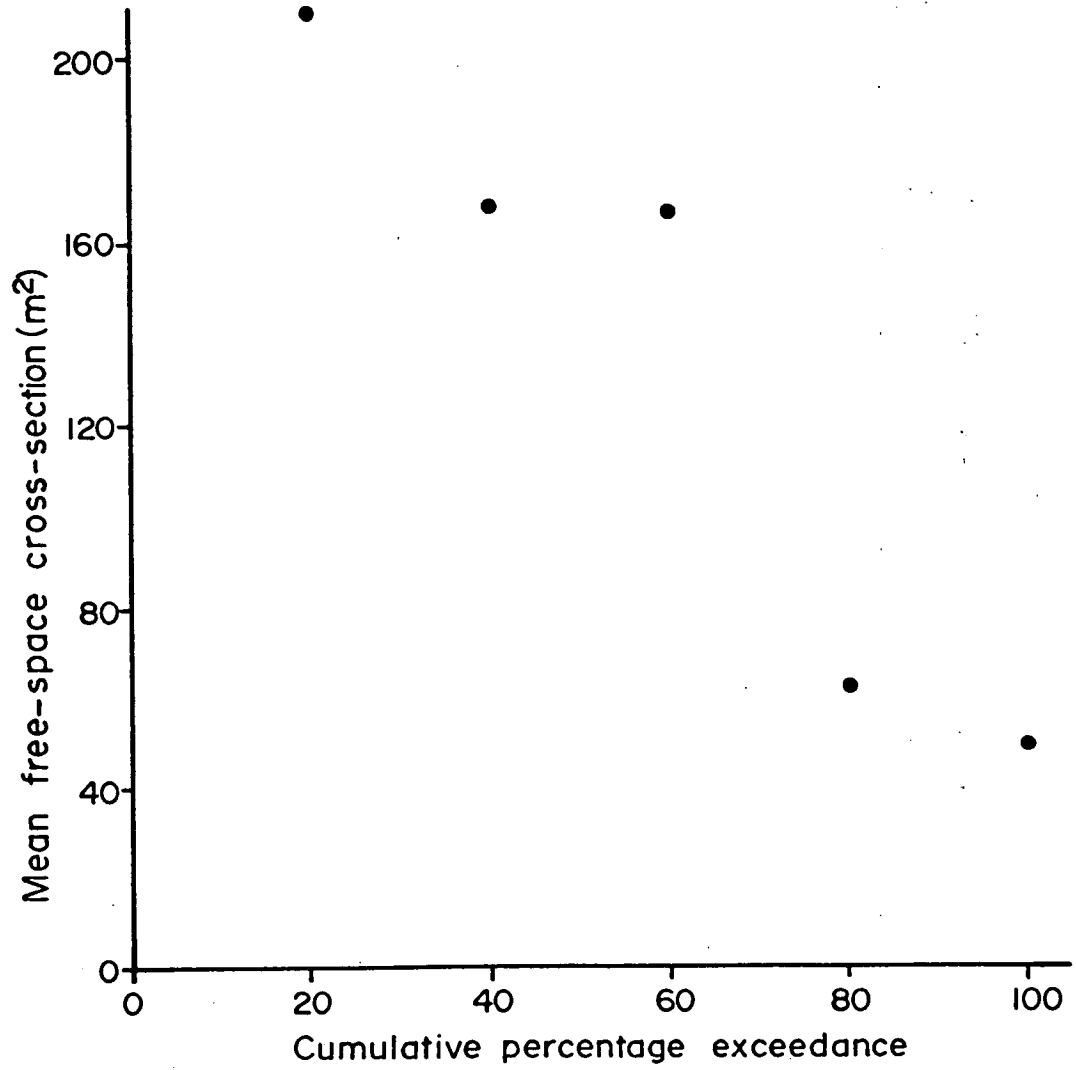


Figure 23. Distribution of free-space cross-sections: medium icebergs (population 5).

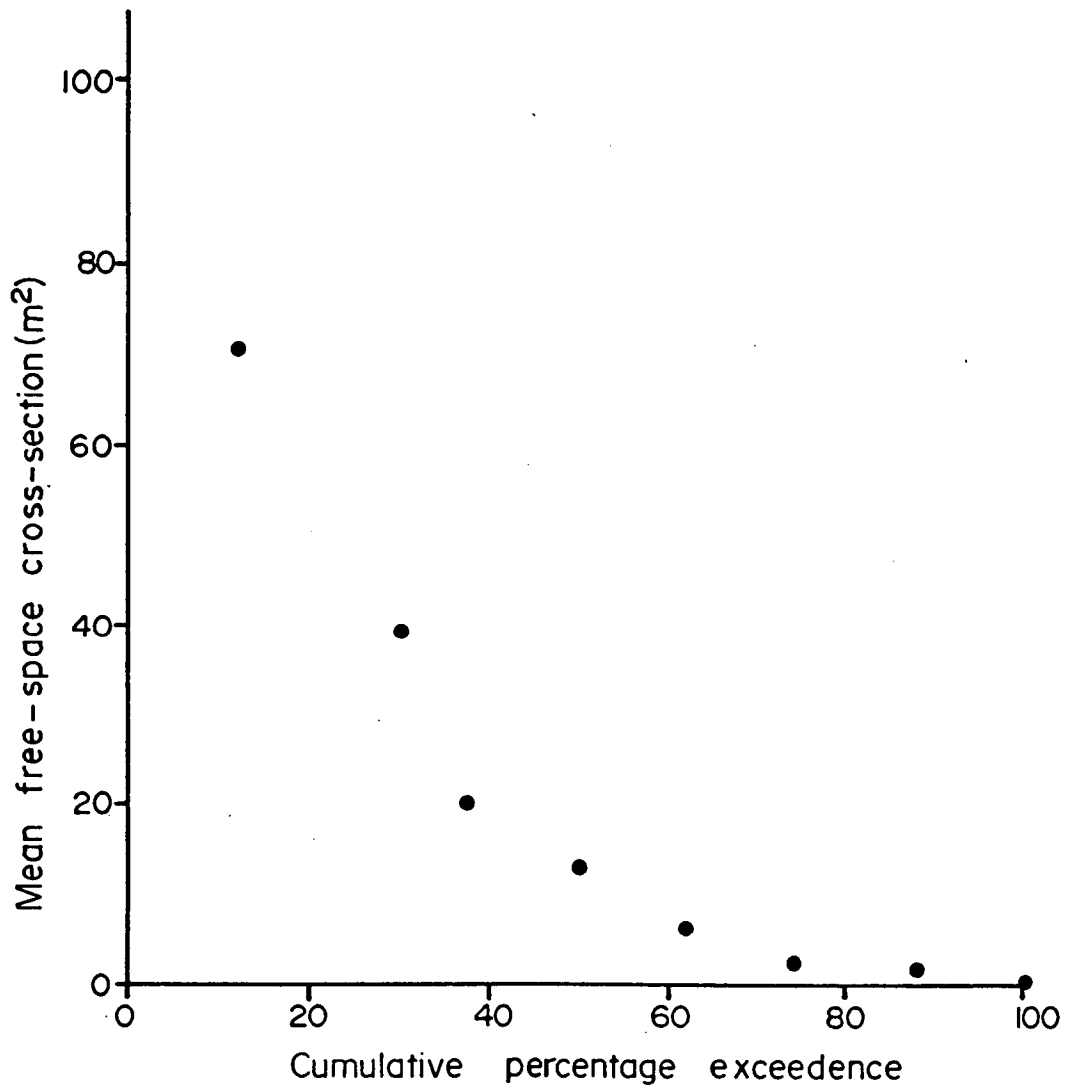


Figure 24. Distribution of free-space cross-sections: small icebergs (population 8).

on the vertical axis. The population is slightly larger, and it appears at least 50% can be expected to exhibit cross-sections above 10 m^2 , and 75% are in the order of 2 to 3 m^2 or greater.

Figure 25 illustrates bergy bits only. Again, note the change of scale on the vertical axis. The population is substantially increased over previous classes. It appears that 40% of bergy bits can be expected to exceed 0.6 m^2 , and 70% exceed 0.3 m^2 .

All the individual size class distributions seem to exhibit similar shapes but on different scales. It is always possible that the peak or tail of each distribution may contain a point from the adjacent size class, as some of the targets were border cases between two size classes. Thus large bergy bits could be called very small 'small' bergs, and so on.

Finally, the individual classes are related to the calibrated buoys. All five medium icebergs look like multiple 10-m^2 buoys. Of eight small icebergs, four look like 10-m^2 buoys or larger, whereas the other four look like something in between the 10-m^2 buoy and the 2-m^2 buoy. Of 14 bergy bits, only four have the capability to look like the 2-m^2 buoy.

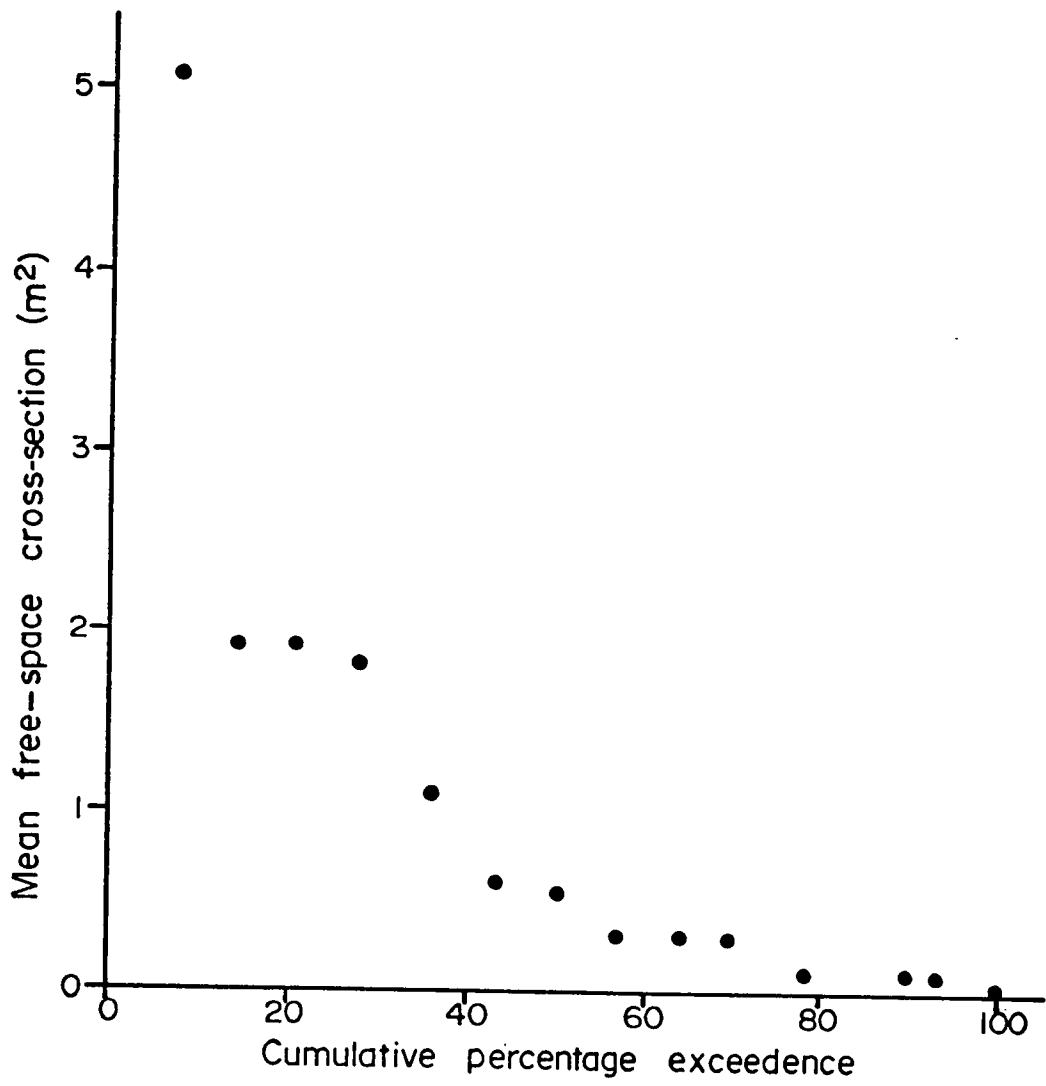
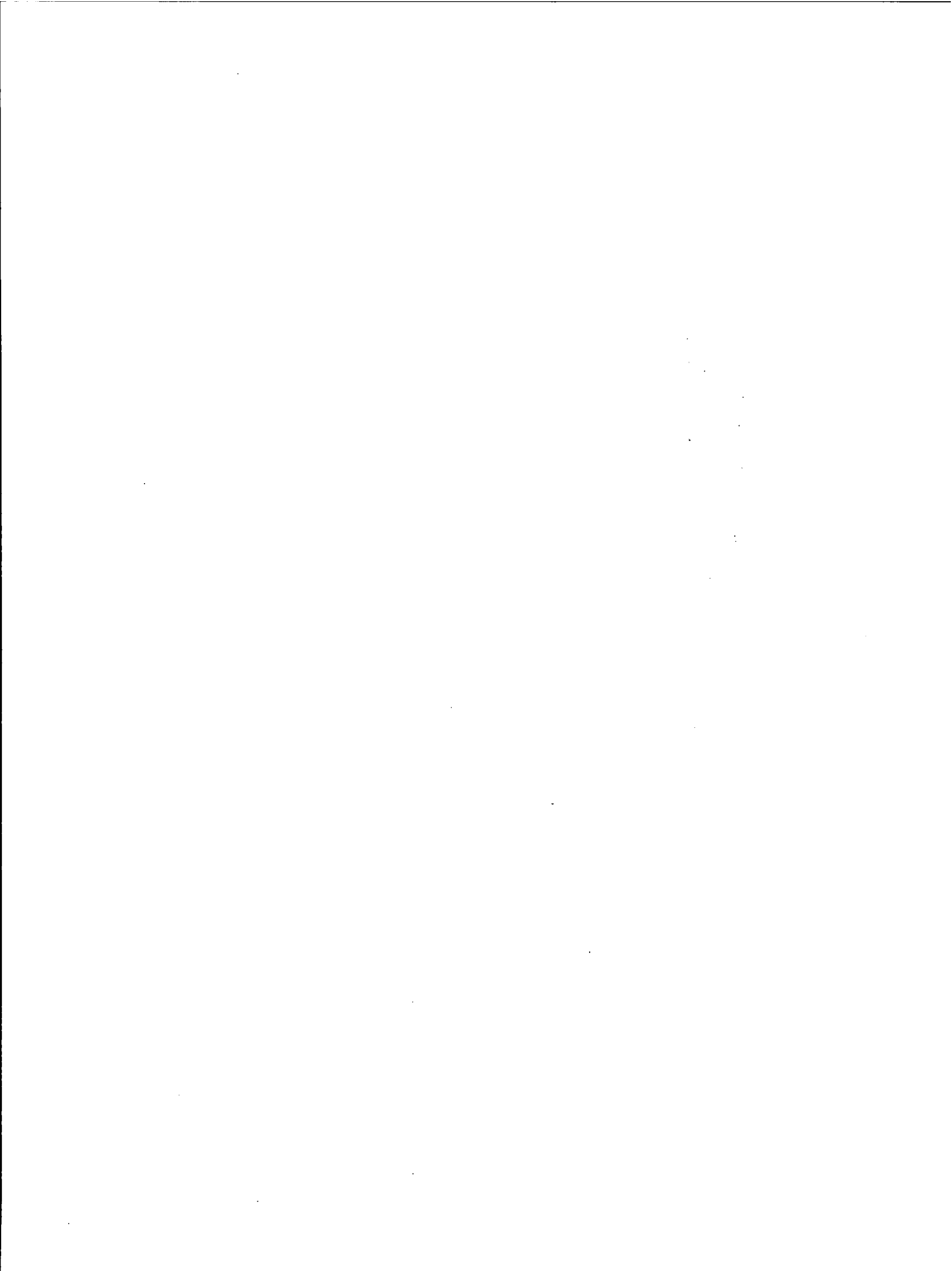


Figure 25. Distribution of free-space cross-sections: bergy bits (population 14).



MODELLED PERFORMANCE PREDICTIONS

The model's predictions are examined for six different sea states, at a flight altitude of 500 ft. It is shown that large fluctuations in required cross-section can occur for apparently similar conditions and that the shape of constant cross-section contours can vary widely. The effects of increasing altitude above 500 ft are illustrated. Predictions for apparently similar sea states which occurred on different days are compared. It is necessary to group similar detection requirements and to classify the range of environmental conditions for which they were observed to occur. The results of the previous section are then introduced to illustrate some general predictions. Lastly, the effect of these results on operational flying is discussed.

PERFORMANCE PREDICTIONS FOR SIX SEA STATES

Figures 26 to 32 illustrate the model's prediction of free-space cross-section in square metres required for detection, in order of increasing sea state. The aircraft is assumed to be flying at an altitude of 500 ft with the radar set on 25-naut mi range scale. CFAR is turned on and the threshold is set to limit the noise and clutter signals to the lower levels of the look-up table at 16.6 naut mi, the maximum range of prediction limited by the available range of received power collected. Each prediction was generated from a separate data set collected on a different flight. The scale is illustrated in nautical miles on two axes. Arrows illustrate the direction of the wind and wind driven waves (H_w), and primary swell (H_{w1}). Wind speed is given in knots, and significant wave height in metres. Each prediction is specific to the

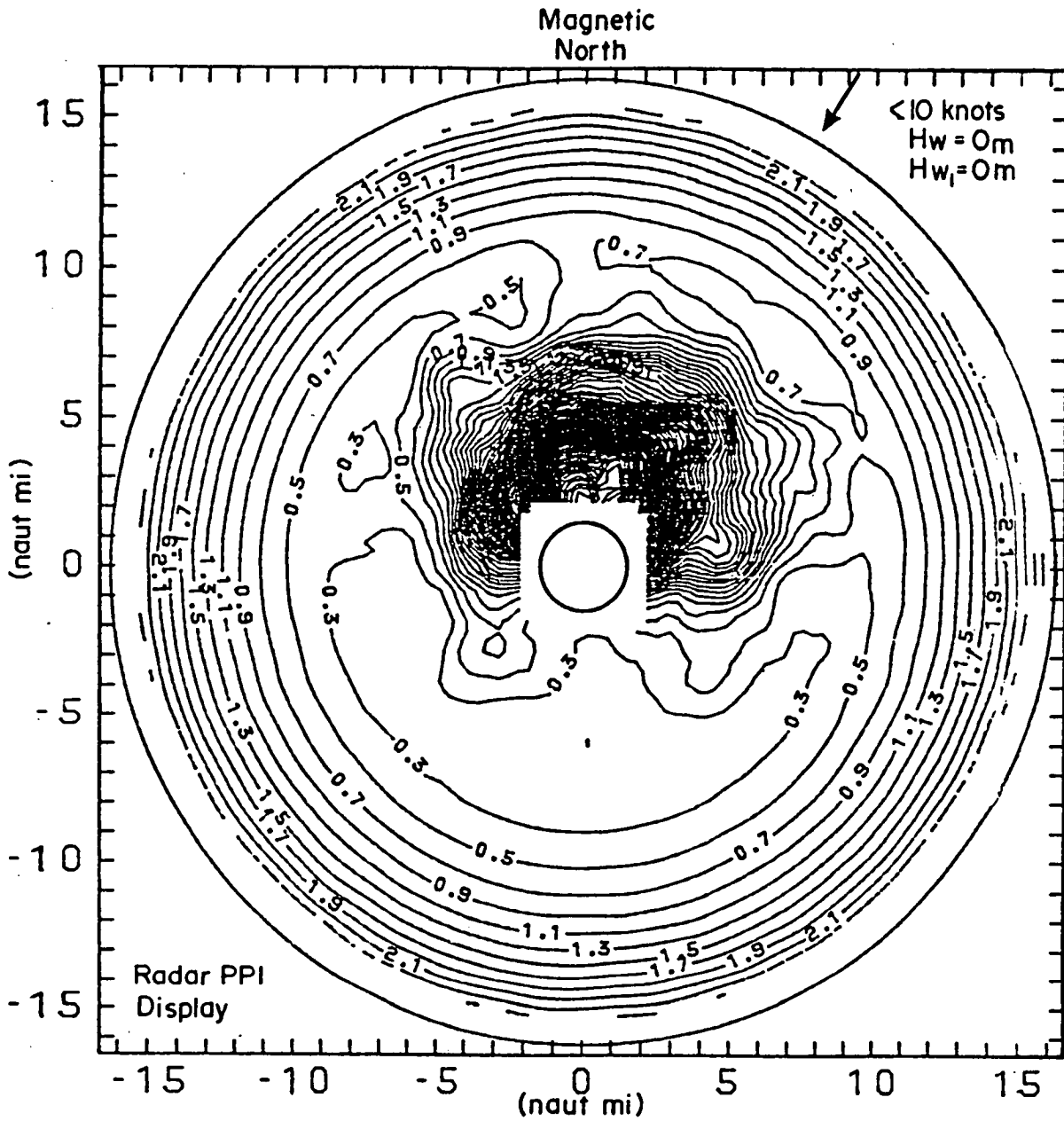


Figure 26. Modelled free-space cross-section (m^2) required for $P_d=0.5$, flight 17; altitude 500 ft, CFAR'on', sea state 1.

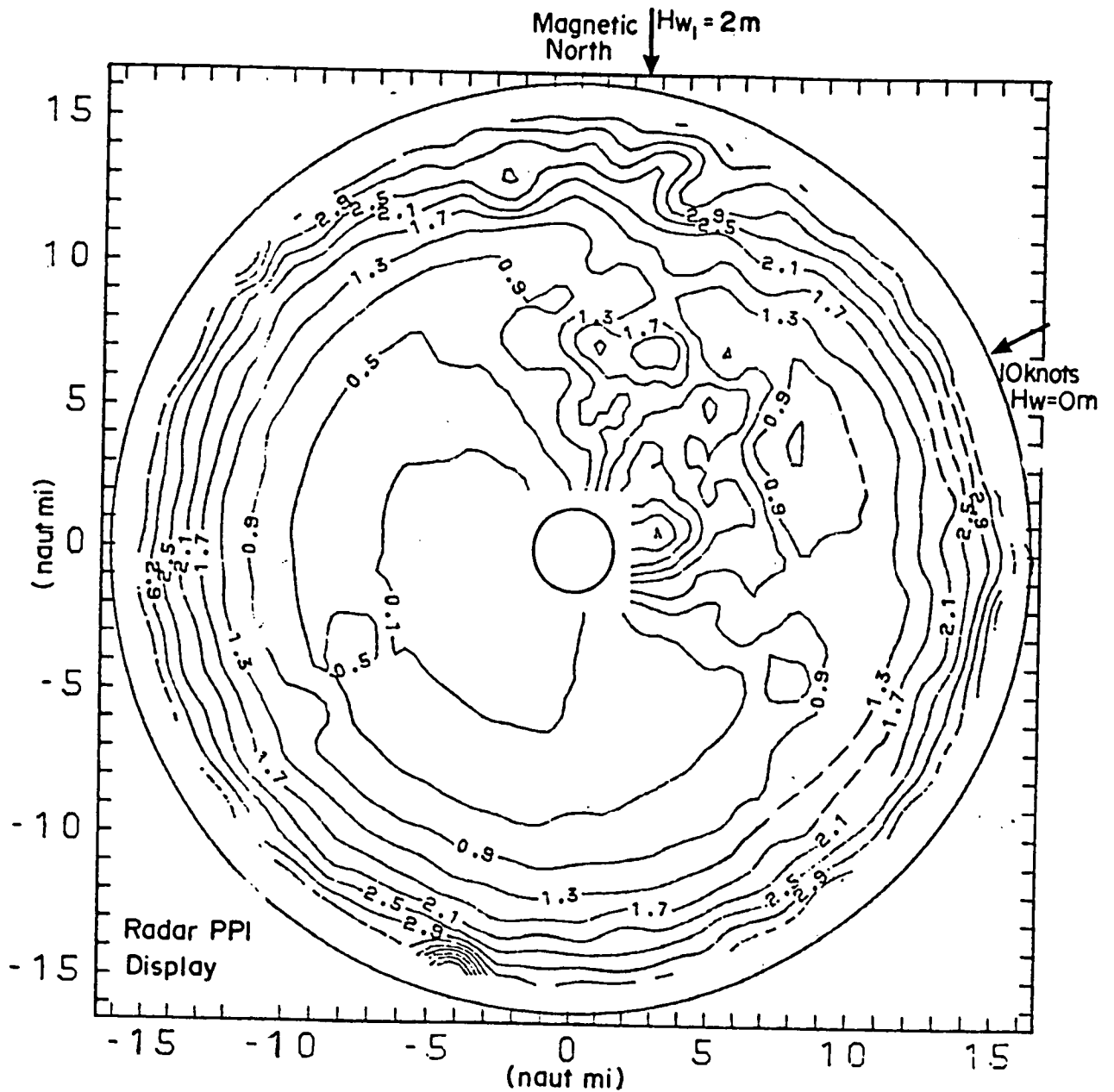


Figure 27. Modelled free-space cross-section (m^2) required for $P_d=0.5$, flight 7; altitude 500 ft, CFAR 'on', sea state 2.

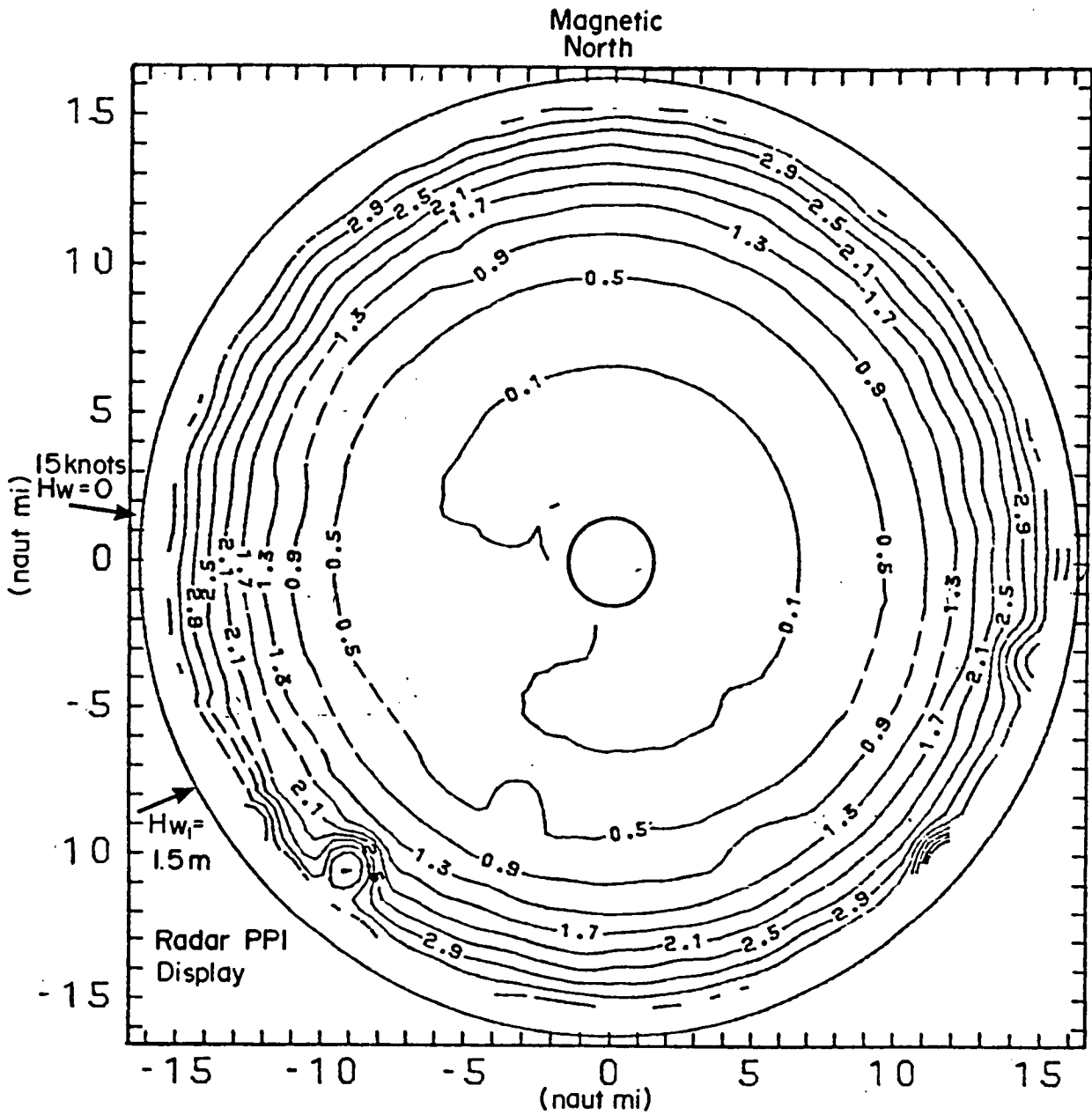


Figure 28. Modelled free-space cross-section (m^2) required for $P_d=0.5$, flight 11; altitude 500 ft, CFAR 'on', sea state 3.

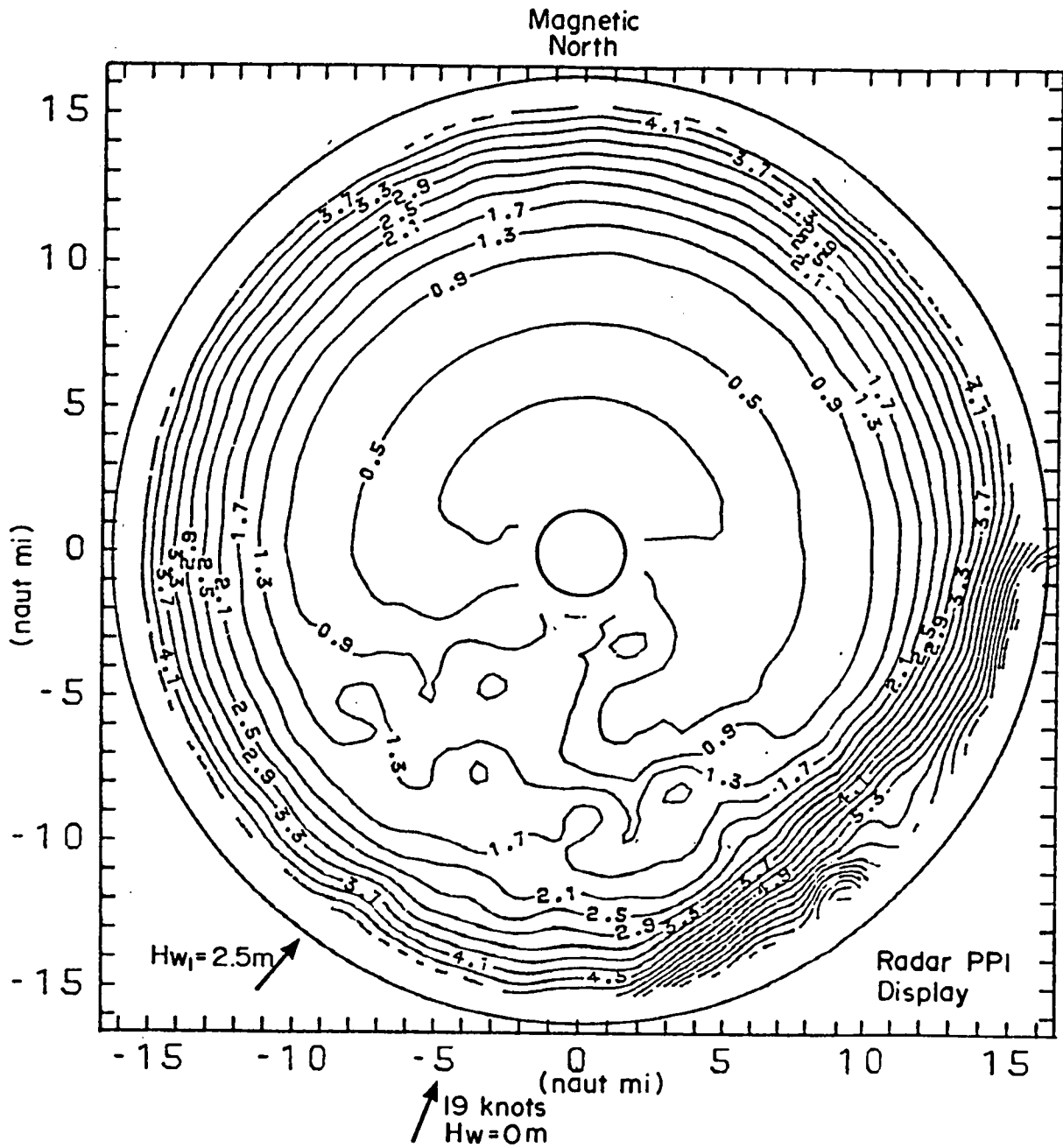


Figure 29. Modelled free-space cross-section (m^2) required for $P_d=0.5$, flight 16; altitude 500 ft, CFAR'on', sea state 4-5.

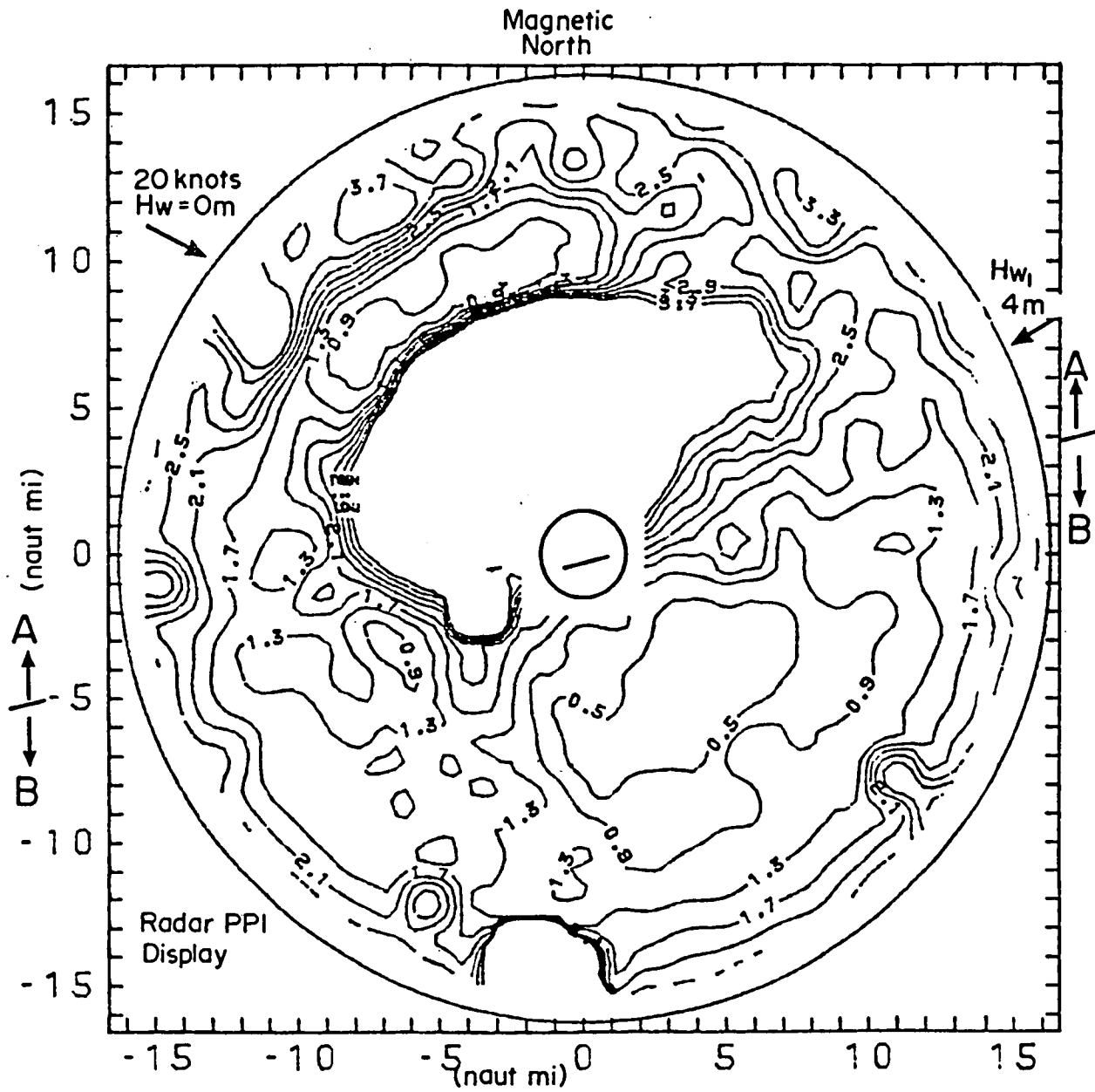


Figure 30. Modelled free-space cross-section (m^2) required for $P_d=0.5$, flight 14; altitude 500 ft, CFAR'on', sea state 5.

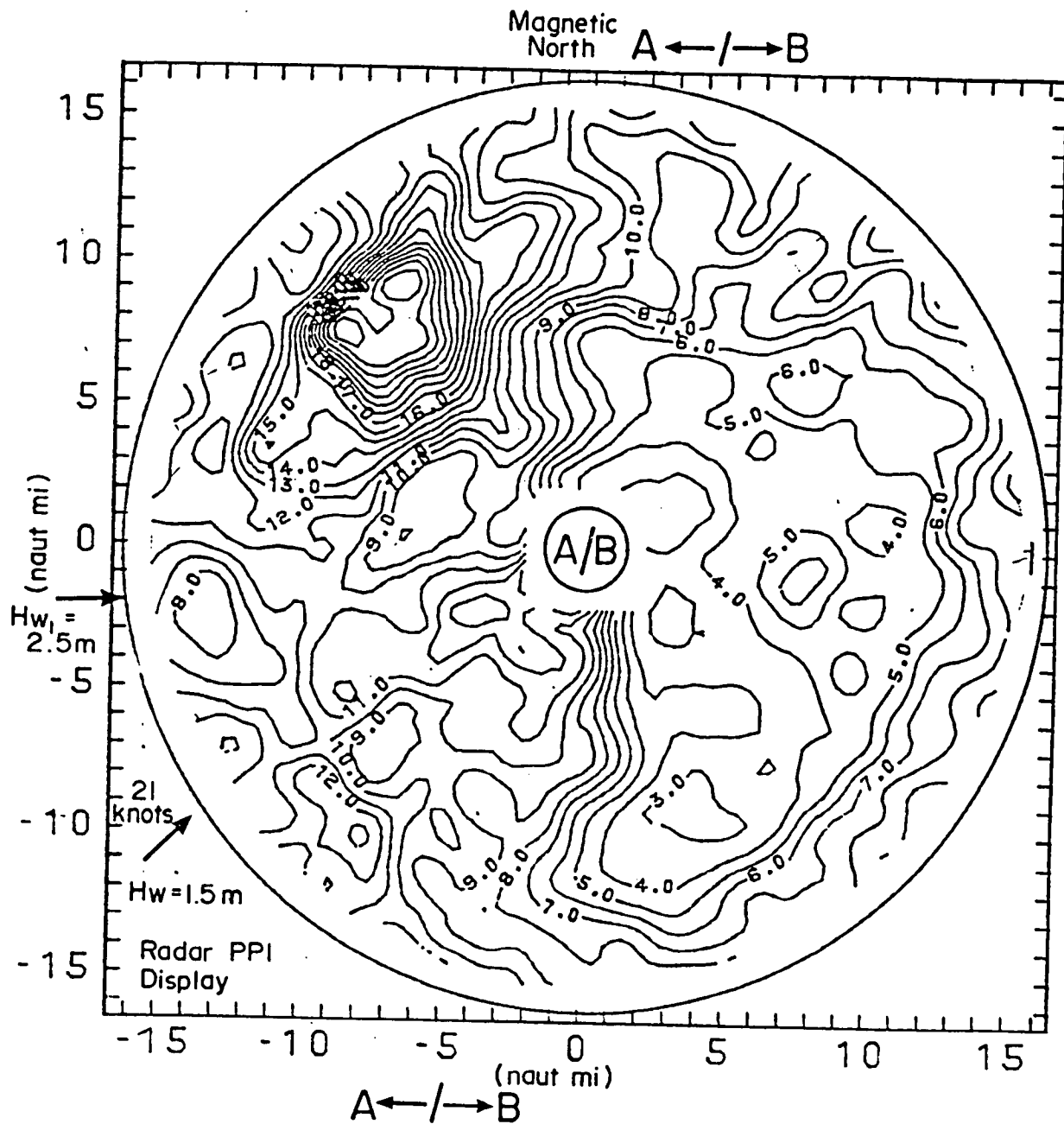


Figure 31. Modelled free-space cross-section (m^2) required for $P_d=0.5$, flight 18; altitude 500 ft, CFAR 'on', sea state 5.

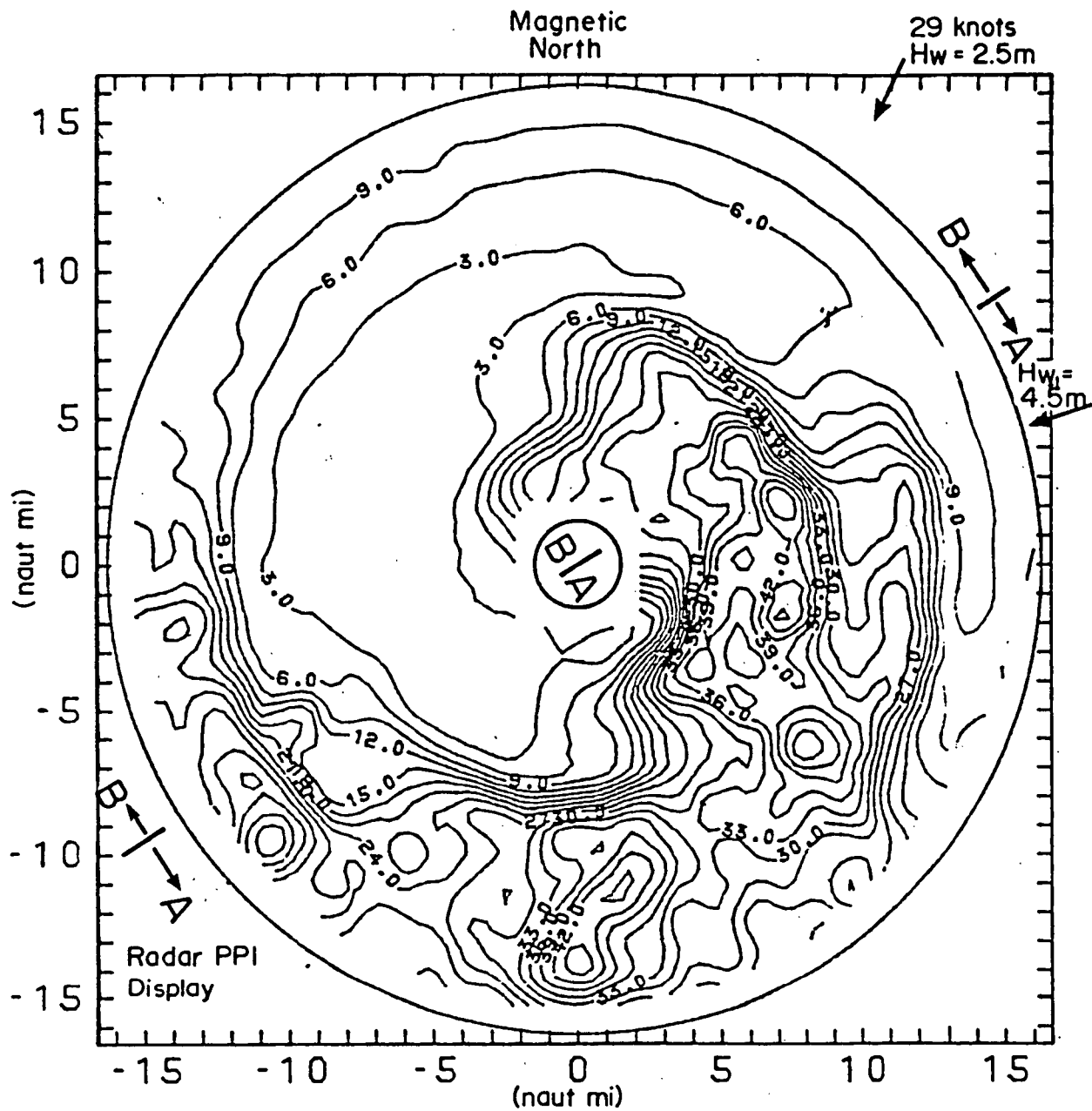


Figure 32. Modelled free-space cross-section (m^2) required for $P_d=0.5$, flight 3; altitude 500 ft, CFAR'on', sea state 6.

wind and wave conditions as shown.

Sea states 1, 2, and 3 are considered first. Beyond 10 naut mi the required cross-sections were similar for all three sea states, generally increasing with range independent of wind or wave direction (indicating that detection was noise-limited, not clutter-limited). Within 10 naut mi there was a clutter zone roughly upwind which required larger cross-sections for detection than downwind. In Figure 26 the clutter zone is the region of dense contours close to the radar display origin facing magnetic north. In Figure 27 the clutter zone faces NE from the radar display origin extending out to the 1.3 m^2 contour. In Figure 28 a weak clutter zone appears to face W-SW, where the 0.1 m^2 contour is pushed in towards the display origin. From the predictions, increasing sea state number does not necessarily promise larger required cross-sections in the clutter zone. Although sea state 3 has more wind it did not generate the clutter cross-sections required to increase required target cross-sections. Possibly the seas were under developed during collection of received power for this flight. In other words the wind may not have been blowing sufficiently long enough for the waves to fully develop, lessening the amount of sea clutter. By comparison, sea states 1 and 2, although lower in wind speed, required 10 to 20 times more cross-section in the clutter zone than in the corresponding downwind region. For these three cases, if a 2-m^2 target was within 13 naut mi of the flight track it would cross contours below 2 m^2 in most cases and detection is predicted.

There is no prediction available for a sea state 4 condition, but Figure 29 illustrates a sea state 4 to 5 condition. More cross-section was required for detection than in the previous examples. Again, the

clutter zone appeared upwind facing south and required more cross-section for a target to be detectable than the corresponding region downwind. The contours beyond 10 naut mi are basically circular, except for one non-circular region from 11 naut mi outwards facing SE. Possibly this distortion was the effect of some ocean structure like a shear zone but this is only speculation. Detection is predicted for a 2-m^2 target within 11 naut mi of the flight track since it would cross contours below 2-m^2 .

Figures 30 and 31 illustrate two predictions for sea state 5 from different flights. The clutter zone in Figure 30 faces N-NW extending out to about 10 miles. In Figure 31 the clutter zone appears to take up a full semi-circle facing West. Both have a clutter zone more or less on the upwind side that requires more cross-section for detection of targets than the corresponding region on the opposite side. The main difference between the two is the typical cross-section required. In Figure 31 the cross-sections required are five to 10 times greater than in Figure 30. Again, it may be that during flight 14 (Figure 30) the seas are under developed, since the wind driven component of the waves (H_w) was not observed to be present, while 1.5m (H_w) was present for flight 18 (Figure 31). It is also worth noting that unlike the previous examples, the radar screen can now be broken into two halves, with region A requiring substantially more cross-section than region B. Somewhere beyond 16.6 naut mi the radar would become noise-limited and circular contours would re-appear, although their values could be quite high. Lastly, a 2-m^2 target is only predicted for detection in region B, Figure 30 and not at all in Figure 31.

Figure 32 is one prediction for sea state 6 which can be compared with Figure 19 which is for a sea state 6 observed on a different day. In Figure 32 there is a substantial difference between the region B where required cross-sections range from 3 to 9 m² and region A where 40 m² will be required. The separation into two halves is only for comparison, being somewhat inappropriate because of the spiral geometry. By comparison, Figure 19 could be divided by a line running from the upper left-hand corner to the lower right hand corner of the box. Within 12 naut mi the area facing SW contains the clutter zone where 10 m² to 15 m² was required whereas the corresponding area in the upper region required only 2 m² to 8 m² of cross-section.

It appears that cross-sectional requirements are not well related to sea state numbers within 16.6 naut mi. The shape and value of the contours defining detection appear to exhibit large variations for apparently similar sea states. One partial cause of this discrepancy may be under developed seas. Wind and significant wave height alone may be an insufficient description of sea state for the purpose of evaluating radar detection. Another factor would be distributions of sea clutter with different spatial geometry.

DETRIMENTAL EFFECT OF INCREASING ALTITUDE

Two examples will illustrate that, as a general rule, increasing altitude lowers detection capabilities substantially. Figure 21 illustrates the required free-space cross-sections of targets at an altitude of 1,500 ft and should be compared with the prediction for 500 ft altitude in Figure 30. Both figures are from the same flight. Note

the different scale of 24.6 naut mi for Figure 21. Whereas target cross-sections of 0.5 m^2 to 3.7 m^2 were required at 500 ft, 4 m^2 to 13 m^2 cross-sections are now required at 1,500 ft for the same 0 to 16.6 naut mi range. This is a consequence of increasing grazing angles by increasing altitude, therefore increasing clutter cross-sections, and as result, required cross-sections for detection.

Secondly, a more extreme case is illustrated in Figure 33 with a prediction for 4,000 ft and should be compared with the prediction for 500 ft in Figure 19. Again, both figures are from the same flight. Whereas cross-sections of 1 m^2 to 16 m^2 were required at 500 ft, 20 m^2 to 68 m^2 were required at 4,000 ft.

The conclusion is that 500 ft is an optimum altitude. Even for days when the radar is apparently noise limited at 10 to 16 naut mi, raising the altitude could change a noise-limited situation into a clutter-limited situation and, therefore, could lower the detection capabilities of the radar.

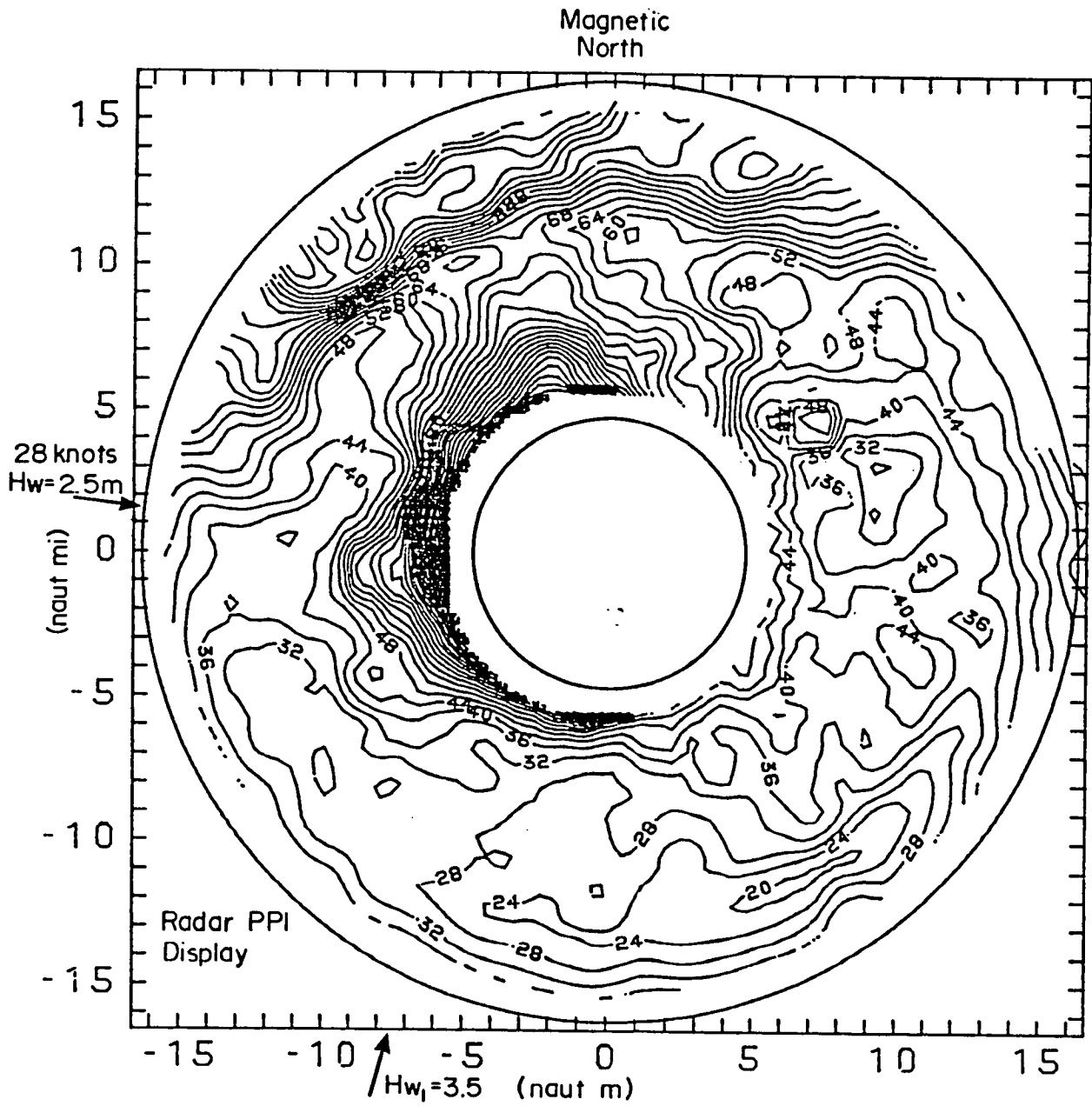


Figure 33. Modelled free-space cross-section (m^2) required for $P_d=0.5$ for flight 9; altitude 4,000 ft CFAR'on', sea state 6.

MODELLED ICEBERG DETECTION

The statistical distributions of iceberg radar cross-sections were related to the performance predictions to obtain the percentage of targets detectable in each class. Since required radar cross-sections were not found to be well related to seastate numbers, it was judged preferable to break the detection contour plots into groups having similar requirements, generalize those requirements at the expense of some detail, and then characterize the range of environmental conditions responsible for these predictions.

Environmental conditions were broken down into three classes, each containing similar detection characteristics but possibly spanning a range of sea state numbers:

Class 1:	Wind	\leq	20 knots
	Hw	=	0 m
	Hw ₁	=	0 to 4 m
Class 2:	Wind	\sim	10 to 30 knots
	Hw	\sim	1 to 2.5 m
	Hw ₁	\sim	1 to 2.5 m
	(Hw + Hw ₁)	\sim	2 to 4 m
Class 3:	Wind	\sim	20 to 30 knots
	Hw	\sim	2.5 m
	Hw ₁	\sim	3 to 4.5 m
	(Hw + Hw ₁)	\sim	6 to 7 m

The best detection performance can be expected during class 1 conditions. The environmental parameters represent calm conditions or under developed seas before a wind wave component develops. The undefined region of Hw \sim 0.5m stems from a lack of data, and probably corresponds to the transition between class 1 and 2 conditions. Class 2 and 3 conditions represent increasing amounts of sea clutter respectively. In all cases an

altitude of 500 ft was assumed, with CFAR on.

Figures 34, 35, and 36 illustrate the results of generalizing the predictions for classes 1, 2, and 3, respectively.

For class 1 conditions, the 15 naut mi contour requires 2.3 m^2 to 4.1 m^2 for detection, the 13 naut mi contour requires 1.2 m^2 to 2.5 m^2 , and the 10 naut mi contour requires 0.5 m^2 to 0.9 m^2 . If a clutter zone is present, that region will limit detection to about targets of 1.7 m^2 cross-section, otherwise the figure quoted for the 10 naut mi contour applies. Detection requirements for classes 2 and 3 are illustrated in similar fashion.

The distributions of cross-sections for each iceberg class were used to determine the approximate percentage detectable as a function of range.

Table 18 summarizes the results of combining the observed population statistics for each iceberg class and the generalized predictions for the three classes of conditions.

A range of percentage is indicated with the lesser of the two figures calculated, assuming the model underestimates required cross-section by 4 dB (approximate factor of 2.5). The form of the calculations is illustrated for class 1 conditions and small icebergs at 13 naut mi.

At 13 naut mi 1.5 m^2 to 2.5 m^2 is predicted to be required with an average of 2.0 m^2 . Using Figure 24, 84% of the population has a cross-section greater than 2 m^2 . If the model is underestimating by 4 dB, then 5 m^2 is required (factor of 2.5) and 66% of the population exceeds this value. Thus 66 to 84% are indicated as detectable at 13 naut mi for class 1 conditions.

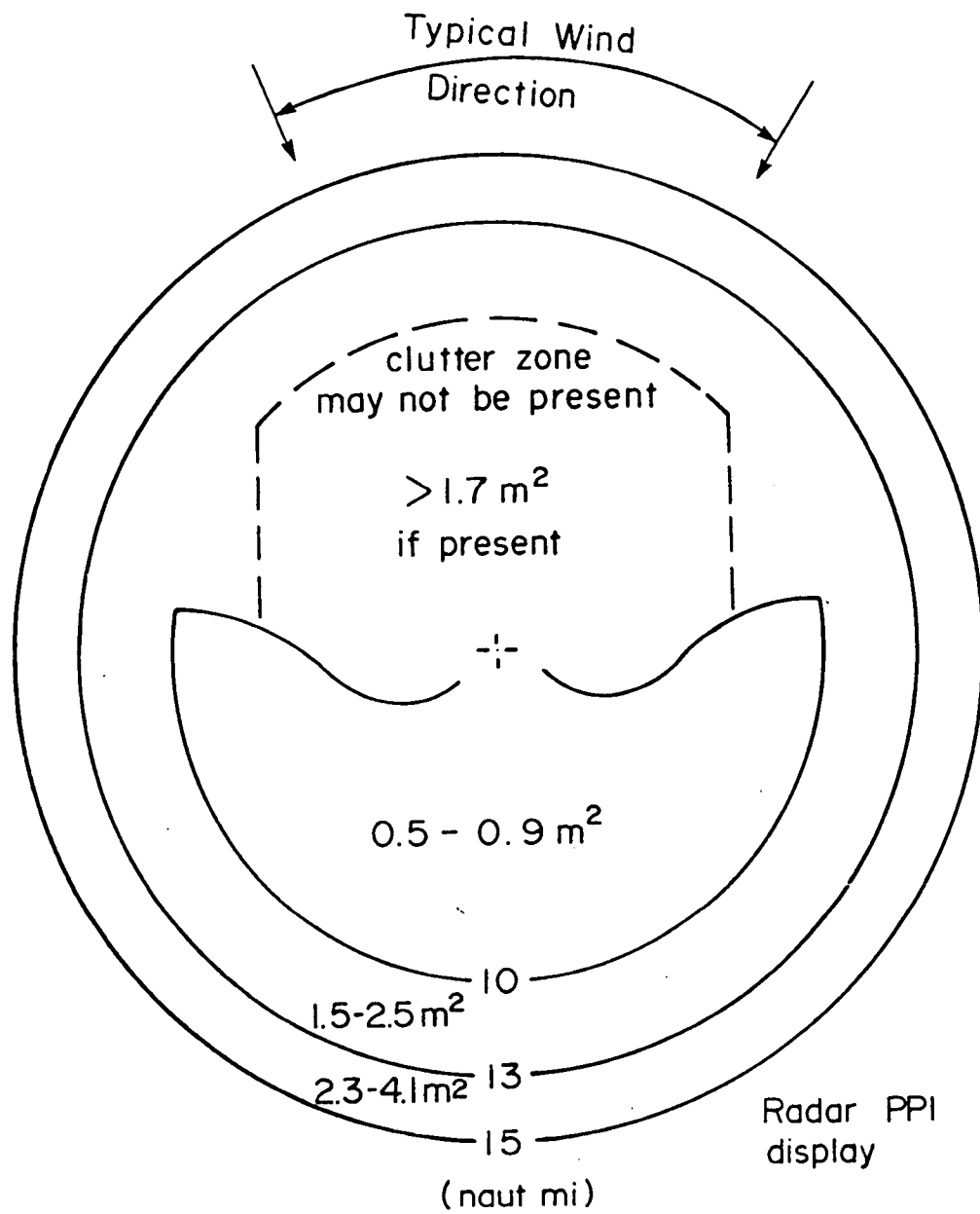


Figure 34. Generalized prediction for class 1 conditions, (V)3.

Required cross-sections for detection ($P_d=0.5$)
 Altitude: 500 ft.

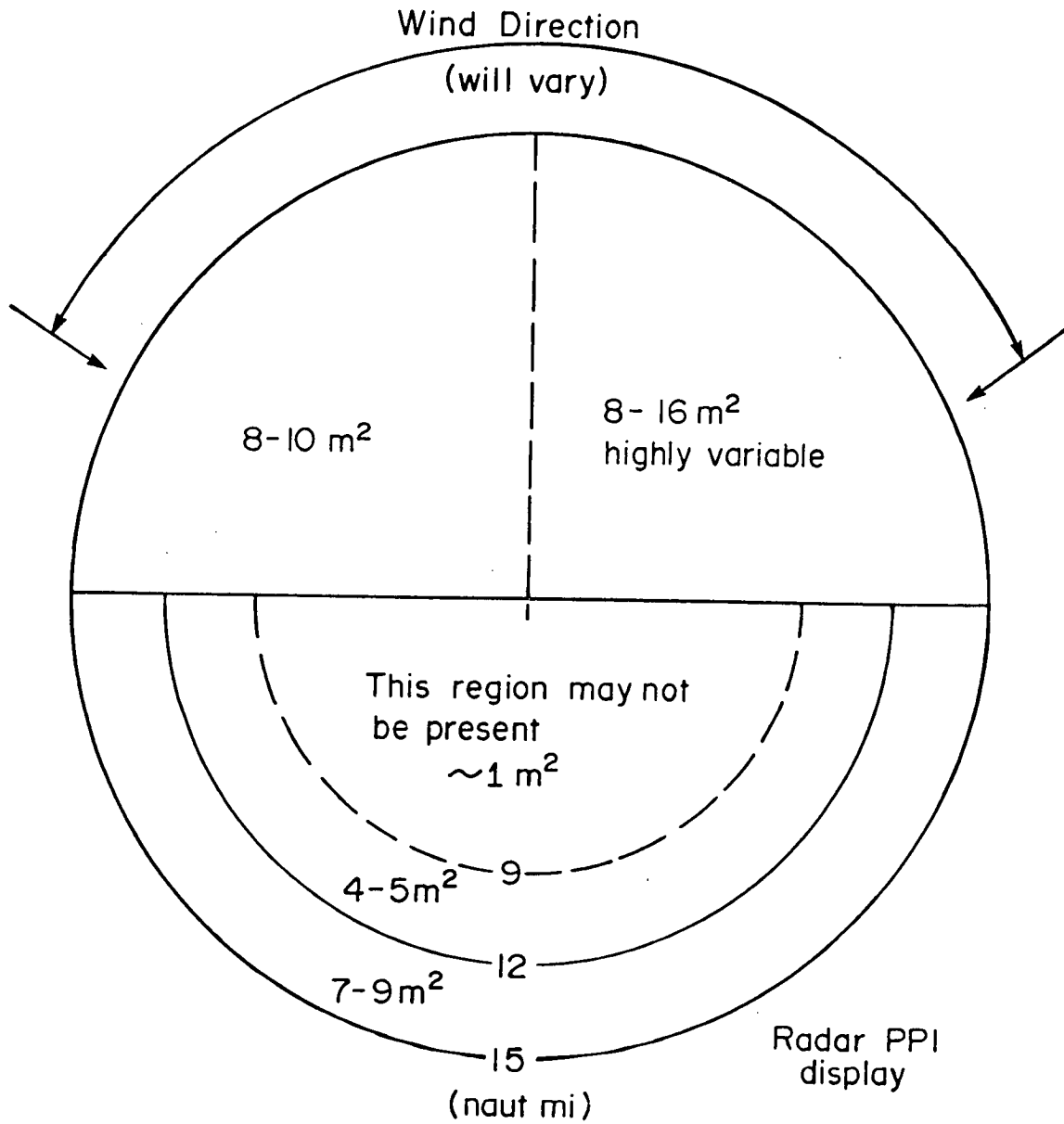


Figure 35. Generalized prediction for class 2 conditions, (V)3.

Required cross-sections for detection (Pd=0.5)
Altitude: 500 ft.

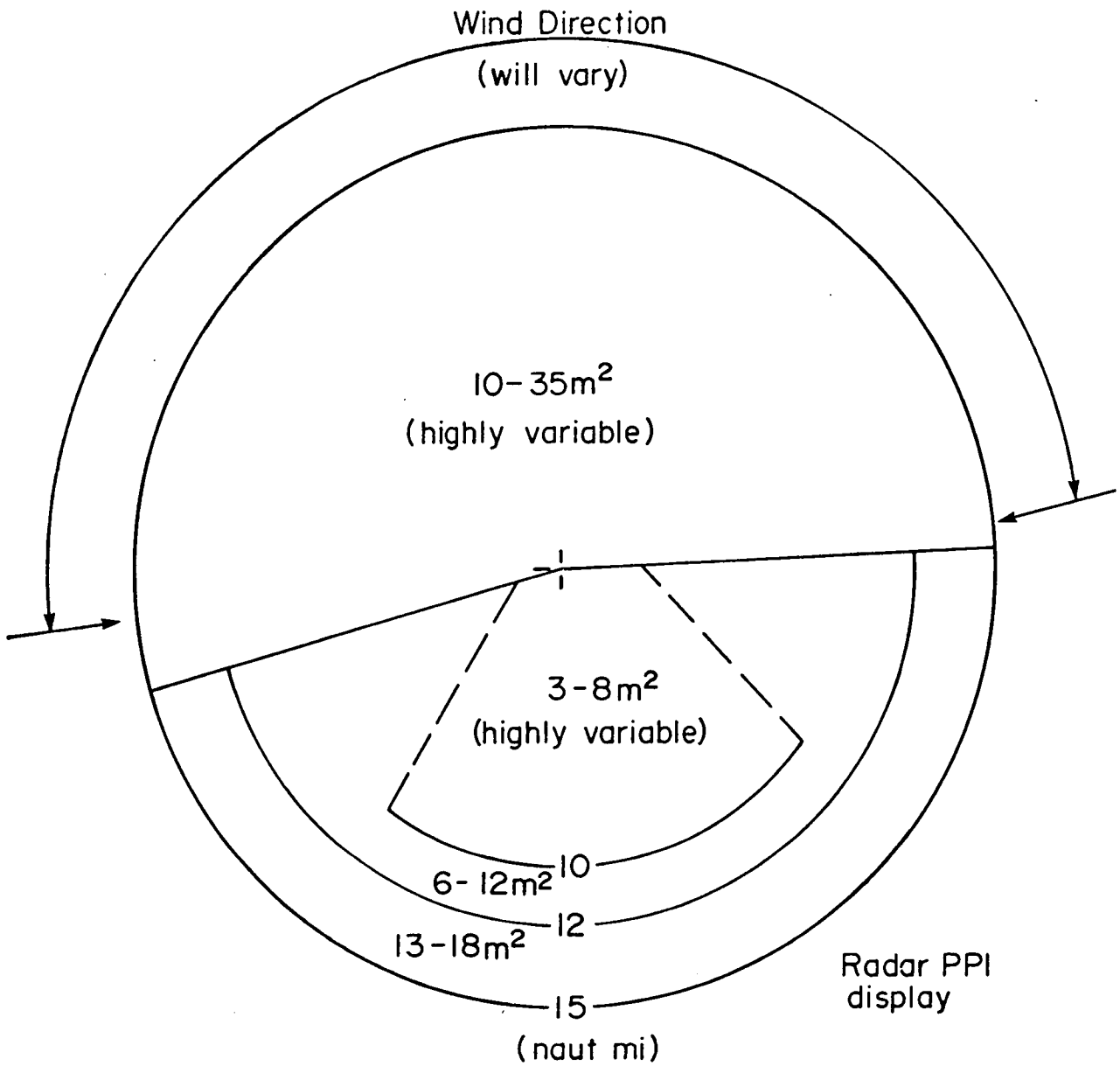


Figure 36. Generalized prediction for class 3 conditions, (V)3.

Required cross-sections for detection (Pd=0.5)
Altitude: 500 ft.

TABLE 18

Predicted (V)3 performance for class 1, 2 and 3 conditions

Range (naut mi)	Comment	Expected percentage of detectable icebergs by size class for each indicated region of the radar screen ^d		
		Bergy bit	Small iceberg	Medium iceberg
Class 1 Conditions ^a				
10	contour opposite clutter zone	28-41	87-95	100
0-10	clutter zone	8-28	69-87	100
13	contour	<8-12	66-84	100
15	contour	~0-10	59-72	100
Class 2 Conditions ^b				
9	contour of lower region if present	12-37	74-93	100
12	contour of lower region	0-8	53-68	100
15 miles	contour of lower region	0	37-59	100
0-15 miles	Upper left region	0	36-57	100
0-15 miles	Upper right region	0	34-52	100
Class 3 Conditions ^c				
0-10	Lower region	0	49-64	100
12	contour of lower region	0	36-57	100
15	contour of lower region	0	30-45	100
0-15	Upper region	0	20-36	88-100

^a Refer to figure 34^b Refer to figure 35^c Refer to figure 36^d The orientation of the clutter zone with respect to the flight direction, and the distance between the flight path and target, will determine the regions the target will intersect and therefore the expected percentage of detection.

It should be noted that for class 1 conditions, the operator can visually determine from the display where the regions indicated in Figure 34 are probably located.

For class 2 conditions, it is possible that the operator can still locate which half of the screen is the better half.

However, it is doubtful that under class 3 conditions that the regions are discernible visually.

EFFECT ON OPERATIONAL SURVEILLANCE

The detection capability of the (V)3, which is poor at best for bergy bits, is non-existent for growlers.

If it is necessary to search for bergy bits, which is only possible during class 1 conditions, then parallel flight lines would appear to be limited to about 10-naut mi spacing.

For small icebergs, a 26-naut mi spacing seems appropriate for class 1 conditions, 12-naut mi for class 2 conditions, and 10-naut mi spacing for class 3 conditions.

For medium icebergs, 26-naut mi spacing is expected to provide reasonable detection capabilities for all three classes of conditions.

The flight line spacing has been calculated assuming that the radar operator can identify only the best region for detection under class 1 conditions.

Under classes 2 and 3 the line spacing was chosen so that during two parallel lines in opposite directions the space between the lines would be swept at least once by the best region for detection. The choice of flight line spacing, therefore, depends on the detection required for the

lowest size class.

It is assumed that the aircraft is confined to 500-ft altitude and that a threshold setting can be found to limit background display intensity without removing regions of the display entirely. If the altitude has to be increased it will be at the expense of detection, possibly not too severely for class 1 conditions, but it would appear to impose a serious detection loss for class 2 and 3 conditions.

SEA CLUTTER ANALYSIS

Examples of the calculated cross-section of sea clutter are given for two somewhat similar sea states.

The two examples were produced from received power collected on flights 3 and 8, both flown at an altitude of 500 ft, both with the same antenna dip, using 0.5 μ s pulse width.

Wind and wave height were recorded as indicated in Table 19.

Table 19

Wind and wave heights for flights 3 and 8

Flight No.	Wind (m)	Hw (m)	Hw ₁ (m)
3	29	2.5	4.5
8	30	2.5	1.5

Figures 37 and 38 illustrate the maximum value observed (curve 4), the minimum value observed (curve 3), the mean value (curve 1), and standard deviation (curve 2), of the calculated unit cross-section of sea clutter as a function of grazing angle, for flights 3 and 8, respectively. These quantities were calculated from multiple scans, over 360° of azimuth. The minimum observed value follows a smooth curve in the area where received power is noise-limited.

From 7.2 to 1.6° grazing angle, the mean value curves from both flights appear somewhat linear in shape, although their slopes are quite different.

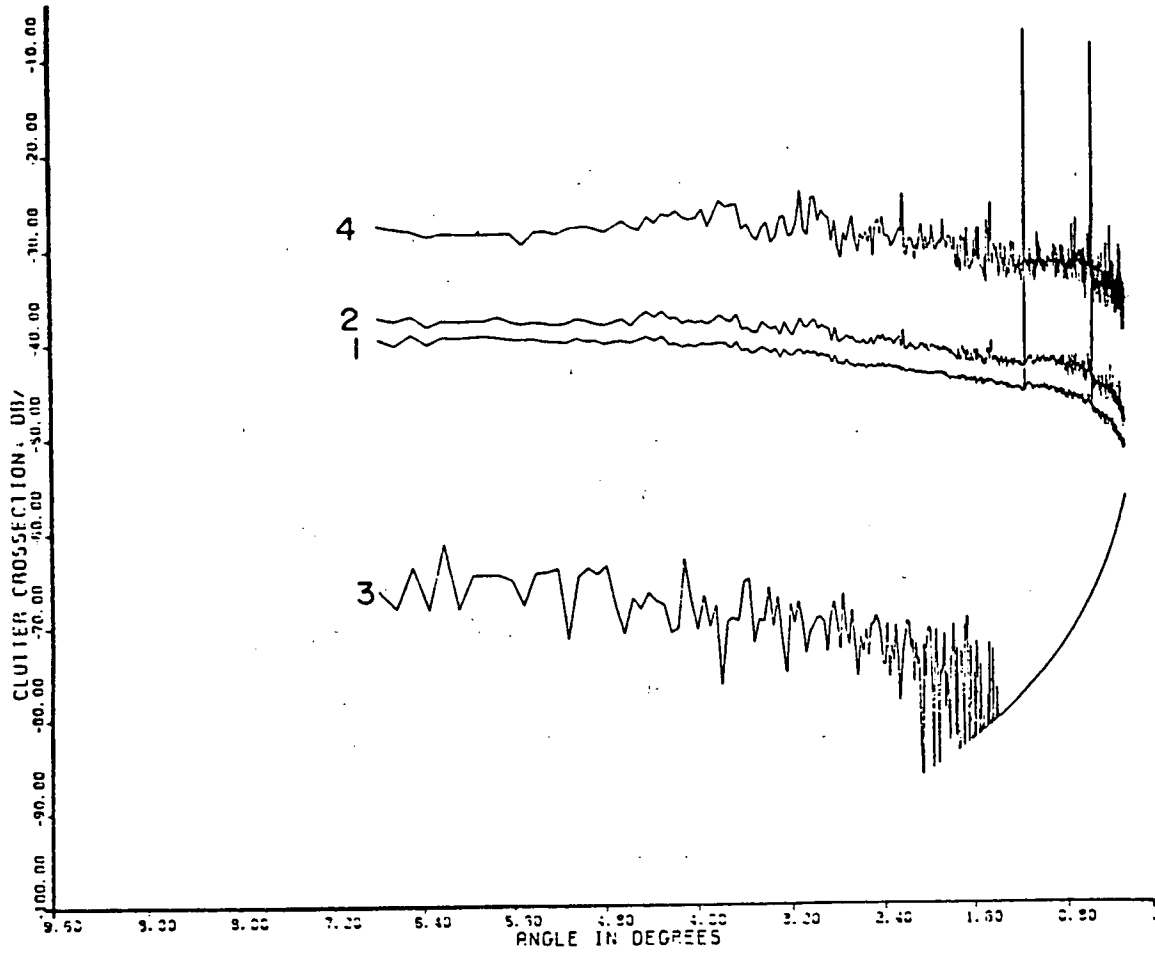


Figure 37. Sea clutter unit cross-section versus grazing angle for flight 3.

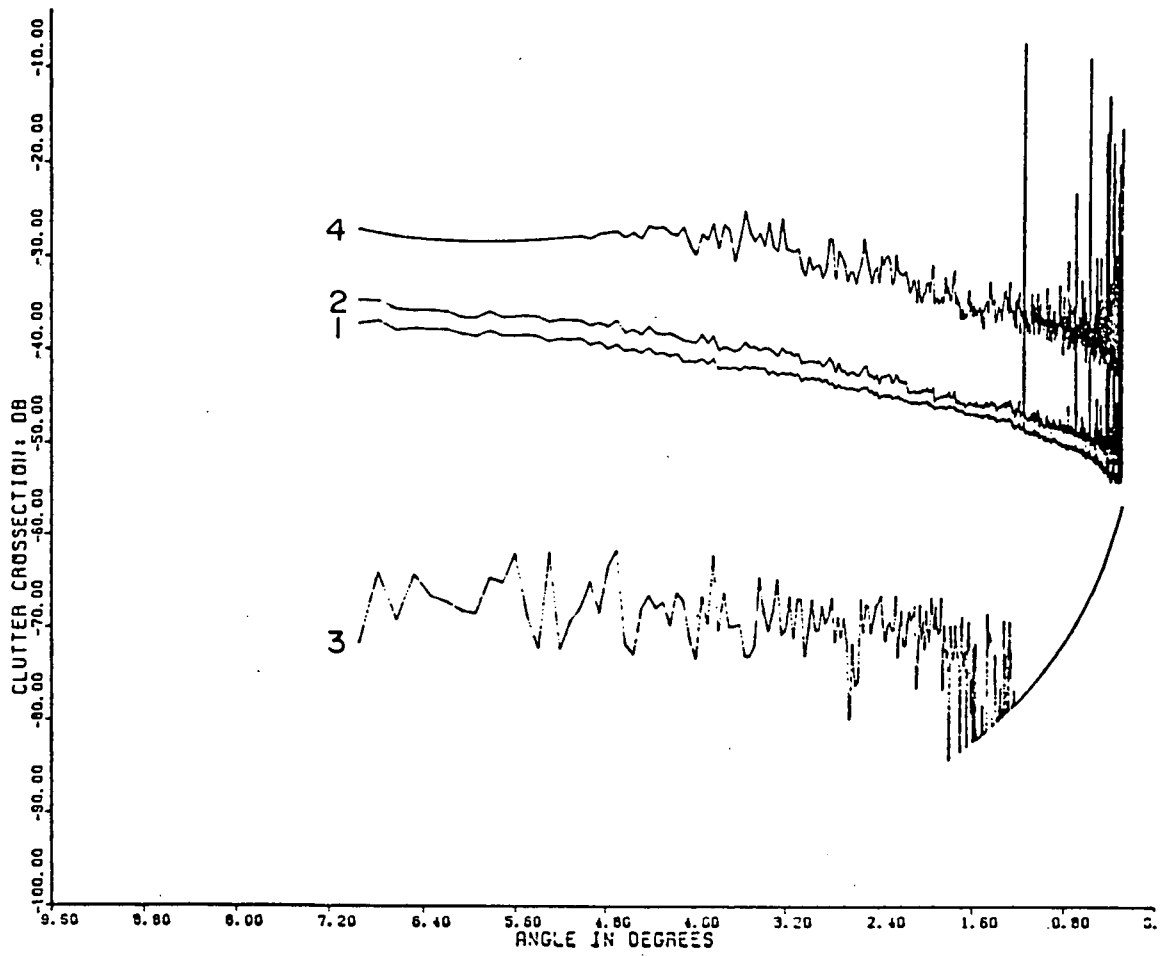


Figure 38. Sea clutter unit cross-section versus grazing angle for flight 8.

Figures 39 and 40 illustrate the azimuthal distribution of the same two data sets in the form of contour plots for flights 3 and 8, respectively. The inner circle locates a grazing angle of 6.78° and the outer circle locates a grazing angle of 0.28° . Between the circles, grazing angle decreases linearly from inner to outer ring. The contour values are in dB. An interesting feature is the off-centre -39 dB contour enclosed by the -42 dB contour in Figure 39, and the lack of cardioid shape in the contours. The contours in Figure 40 are more cardioid in appearance by comparison. In both cases, there is a substantial drop in values from the upwind region to the downwind region.

Detection is sometimes predicted using published values of average sea clutter radar cross-section. Nathanson's (1969) tabulated average value for sea clutter cross-section at X-band frequency in sea state 5, at grazing angles of 3° and 1° respectively is, -32 dB and -33 dB, dropping to -39 dB and -40 dB for sea state 3 at the same respective angles. Figures 37 and 38 indicate much lower values for sea state 5 to 6 between -41 and -49 dB, in the same grazing angle region. It may be that the discrepancy stems from trying to predict sea clutter based on sea state number.

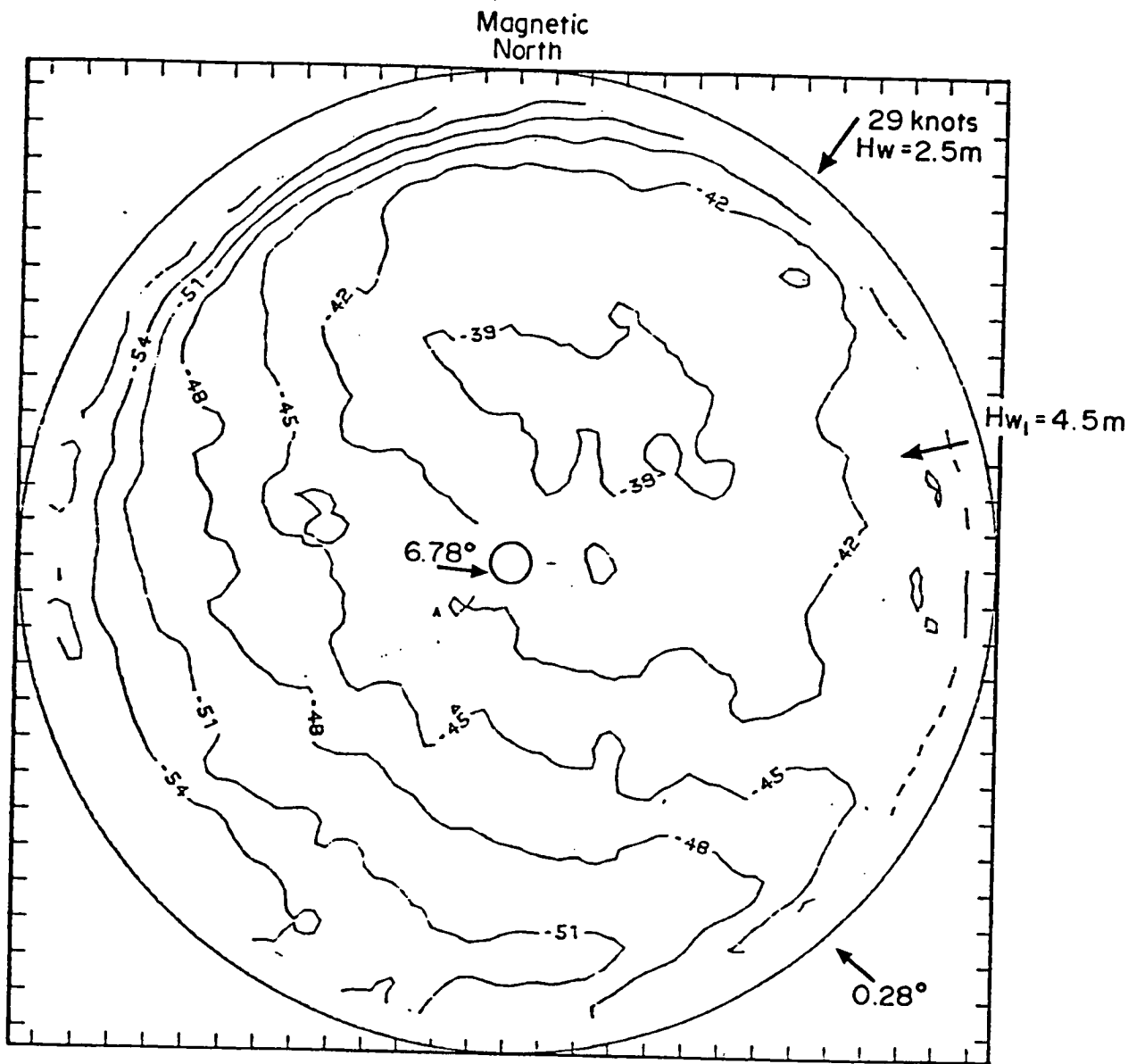


Figure 39. Sea clutter unit cross-section (dB) versus grazing angle and azimuth for flight 3.

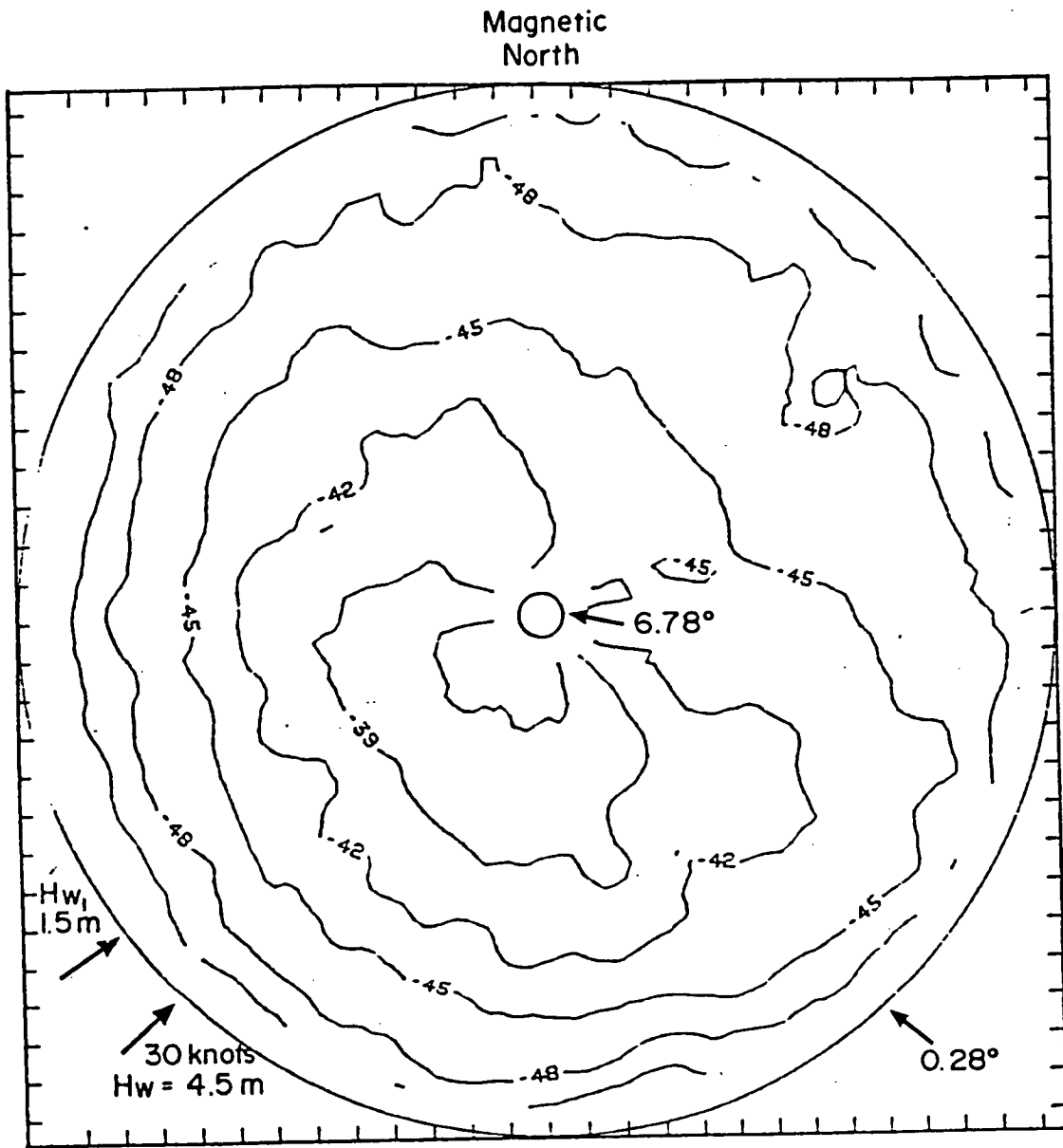


Figure 40. Sea clutter unit cross-section versus grazing angle and azimuth for flight 8.

PART II: APS 504 (V)5

METHODOLOGY

In many respects the (V)5 program was very similar to that of the (V)3. Calibrations were performed to measure some of the radar system parameters and confirm manufacturer specifications. During the flight program the performance of the radar was documented with the radar's video tape system in flight recording of the radar display. These video tapes were subsequently reviewed on the ground and provided the observed detection performance of the radar. Observed performance was complimented with environmental information in the area of interest, and aerial photography of icebergs, to form an overall database of observed performance.

Because of the increased iceberg densities during the (V)5 program the data base of observed performance contains about three times as many targets compared to the (V)3 database. As in the (V)3 program, radar signals were recorded in flight from icebergs and sea clutter with the same digital system.

The main difference between the two programs was the lack of a technical description sufficient to model the signal processing of the (V)5. The impact of this was twofold. The influence on detection of flight and radar parameters could only be assessed by trying different combinations and noting the change in detection, which consumes more flight time per target, and requires operations in the air to be extremely efficient. Increased iceberg densities over the previous year and increased experience in data collection mitigated this factor somewhat,

but not entirely.

Secondly, it was no longer possible to extrapolate detection of an iceberg size class from one set of environmental conditions to another. Therefore, the detection capability of the radar could only be established for those combinations of iceberg size class and environmental conditions where sufficient numbers of the size class were observed.

The introduction of the (V)5 substantially increased the number of signal processing options available, compared to the (V)3. It was not practical to collect data for every processing combination on each piece of ice. As the primary output of the study would be documented performance, it was desired to build a data base that was large enough to have statistical significance with the emphasis on the modes that make use of all of the features of the (V)5. Most of the data were collected between the altitudes of 500 ft and 1,500 ft with some test cases flown at higher altitudes. Typically each target was overflown twice, changing either pulse length or altitude, with radar-processing options selected as deemed necessary. When radar signal recording was carried out STC was normally disabled, which had some consequence on the display set up. Tests cases were flown to evaluate the effect of frequency agility, pulse length, and altitude on radar cross-section of the icebergs.

SYSTEM PARAMETERS

The large number of operational and radar features available required the selection of specific data collection modes such that the important questions regarding the performance of the (V)5 could be answered with the data collected. The features available for

consideration are provided below with a description of their expected effect on performance.

Altitude: Aircraft altitude changes the grazing angles on both targets and ocean for a given range. In general, the higher the grazing angle the more sea clutter the radar will image. However, the radar cross-section of an iceberg will also be incidence-angle dependent. The (V)5 may be operated over the altitude range of 100 ft to 20,000 ft.

Pulse length: Radar pulse length directly alters the radar resolution cell size. As the radar resolution cell decreases so does the average clutter level competing with a target's signal. Because of a different minimum detectable signal (MDS) on each of the compressed pulses of the (V)5, pulse length will also affect detection when there is no clutter present.
Modes: 10.00 μ s compressed to 0.03 μ s (pulse A) and 30.00 μ s compressed to 0.20 μ s (pulse B).

Frequency agility: Pulse-to-pulse decorrelation of sea clutter returns with frequency agility will result in an increase in detection capability in rougher sea states.
Modes: OFF,AG1,AG2

CFAR: Removal of mean sea clutter background.
Modes: ON/OFF

STC: Removes range dependence of clutter and prevents receiver saturation.
Modes: Range and Depth

Scan-to-scan integration: Smooths out signals that are not correlated from scan-to-scan improving target detection in sea clutter.
Modes: FF,FS,SF,SS; where the first letter refers to the rise time constant and the second refers to the decay time constant; F(fast); S(slow).

SURFACE VERIFICATION

Verification of iceberg characteristics consisted primarily of Hasselblad vertical photography and also hand-held 35-mm camera side-

looking photography. Lenses of focal length from 70 mm to 140 mm were used on the Hasselblad which provided a plan view of iceberg dimensions. Hasselblad photos were located with a latitude and longitude from the aircraft navigation system as the iceberg was photographed, together with the altitude and aircraft heading. In addition to the observer's estimate of iceberg size class and type, the iceberg's horizontal dimensions and orientation with respect to magnetic north were known or could be calculated. Telephoto lenses with a focal length of 200 mm to 350 mm were used on the hand-held, 35-mm camera for perspective views. Using aircraft heading, the iceberg face could be related to the plan view. When both types of photos were taken, iceberg height was calculated from the ratio of apparent height to width on the 35-mm photograph, times the length at the given aspect on the Hasselblad photograph. Usually bergy bits and growlers were photographed by both cameras. Hasselblad photos were taken of small icebergs and often 35-mm photographs as well. Medium and large icebergs were documented with a 35-mm photograph when convenient.

The drilling unit Bowdrill 3 provided environmental data for the single operational flight just before the drilling unit was pulled off location. All environmental data for subsequent flights were obtained from the following sources. Wind records were obtained from government weather stations at St. John's, Bonavista, and Gander. Observed pressure charts were obtained from the Atmospheric Environment Service (AES) weather office in Gander and were used to generate a wind hindcast for the area of interest at the time of data collection.

Sea state information came from a Waverider buoy located 15 naut mi east of Torbay upper air station (AES), from estimates of sea state and swell direction made by the observer on board the aircraft, and Meteorological and Oceanographic Centre (METOC) wave charts for the region of interest at the time of coverage. The wind hindcast and the sea state information were used to generate a swell and wind-wave hindcast.

RADAR SIGNAL DATA ACQUISITION

To characterize the detection process of icebergs in a rough sea environment it is necessary to develop an understanding of the radar characteristics of icebergs and ocean. The radar signal data acquisition program was directed towards this objective. The primary requirement was to collect data representative of the capabilities of the (V)5. Selected data was analysed to provide reference points within the data base that would assist the observed performance analysis. This section describes the data collection program including the data acquisition equipment, system calibration, and data collection modes.

Data Acquisition System

A digital data acquisition system was used to record the radar video voltage at the output of the logarithmic amplifier just before the radar's signal processing unit. The system was configured to sample the radar video at 10 MHz with 8-bit amplitude resolution. The sample rate was adequate for the 200 ns uncompressed pulse as well as for the 30 μ s compressed pulse. To sample the wide bandwidth video on the 10 μ s compressed pulse a compromise was made by using interleaved sampling.

Four consecutive sample sweeps were interleaved by 0-, 25-, 50- and 75 ns to achieve an effective sampling rate of 40 MHz. This sampling would take advantage of the pulse-to-pulse correlation of the radar signal on targets and would permit the extraction of radar cross-sections from the data by providing one received power measurement per target per scan. Figure 41 shows the general arrangement of data acquisition equipment and how it was interfaced to the radar. As the radar video was collected, antenna position was converted to digital form and placed in a data header word with range and video data before it was stored on magnetic tape. The data acquisition was carried out under computer control using a PDP 11/23+ computer.

System Calibration

Radar system calibration was required such that the receiver output video voltage could be related to power received at the radar antenna. The calibration took place in three steps:

a) The first included the use of a fixed frequency microwave signal generator to inject known signals into a directional coupler installed in the waveguide between the transmitter/receiver unit and the antenna, while recording the radar video in a digital form on magnetic tape. Injected pulse lengths were chosen to maximize the output radar video voltage for a particular radar compressed pulse. A $0.20 \mu\text{s}$ injected pulse length was used for the $0.20 \mu\text{s}$ uncompressed radar pulse. The injected power levels were varied over the radar's dynamic range so that a calibration curve of

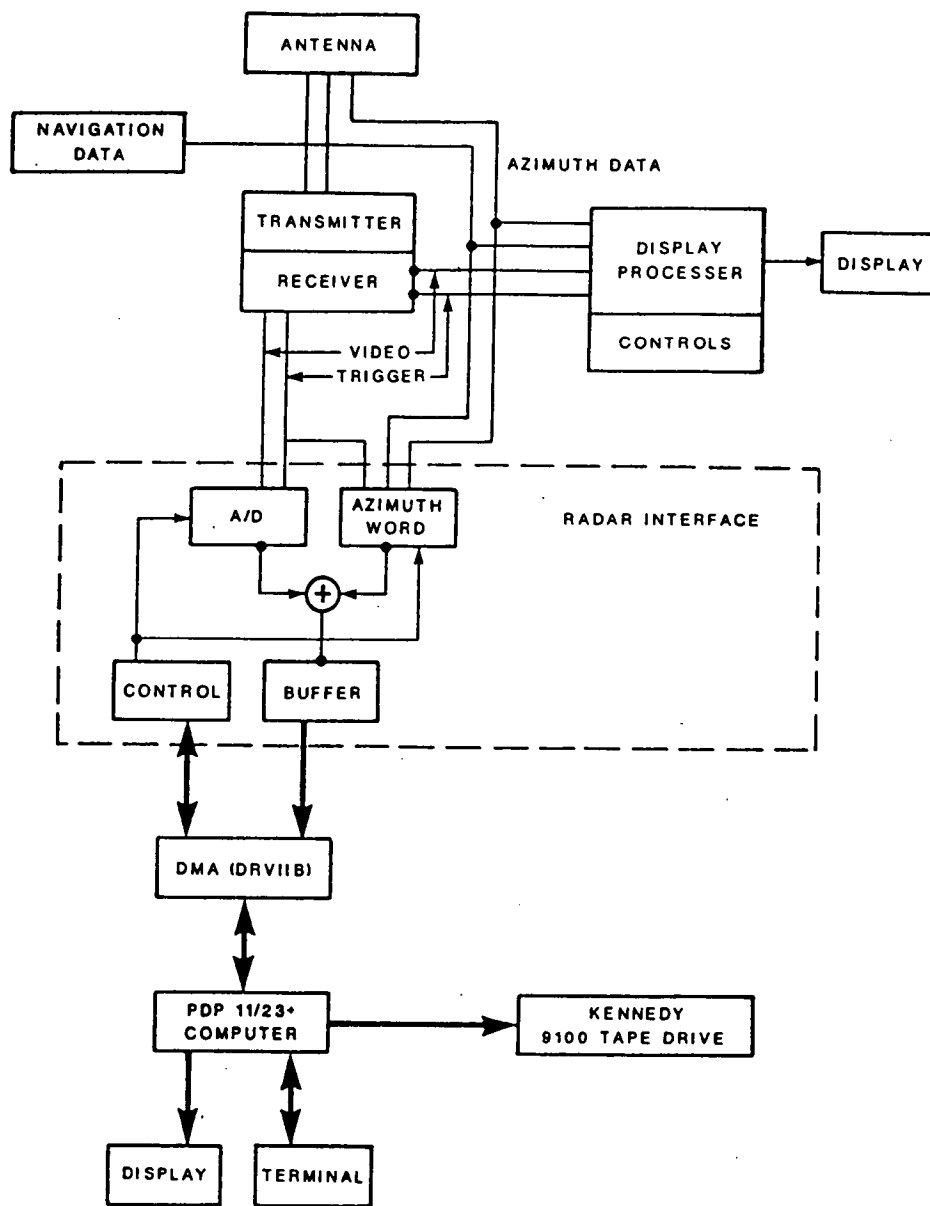


Figure 41. Data acquisition system interfaced to the APS-504 (V)5.

injected power versus recorded digital voltage could be generated. This procedure ensured the complete system including the recording system would be calibrated. The process was carried out for the three available pulse lengths (0.2-, 10.0-, and 30.0- μ s). The radar uses a non-linear frequency modulation technique to generate a pulse compression waveform on the 10.0- and 30.0- μ s pulses. A pulse compression gain is achieved when the received signal is compressed in a surface acoustic wave (SAW) device from 10.0 μ s and 30.0 μ s to 30 ns and 200 ns, respectively. Using a fixed frequency signal generator for calibration results in the generation of a curve of relative power versus receiver output voltage. This relative calibration is made absolute in the third step of the calibration. The sensitivity time control (STC) was calibrated by injecting a constant power level and varying the STC over its available range.

b) The second step of the calibration consisted of the estimation of the radar parameters required in the radar range equation. Transmitter peak power was measured several times throughout the data collection program and estimates of system losses were provided by the manufacturer.

c) The final step was the closing of the calibration by collecting data on a reference target having a known radar cross-section. The target chosen was an omni-azimuth Luneburg lens with a specified radar cross-section of 10 m². The lens target was mounted at a height of 2.5 m on a fiberglass buoy. The 0.20- μ s uncompressed pulse data were used with the results of calibration steps a) and b) and the free-space radar range equation ($1/R^4$) to close the calibration loop, ensuring that all system

parameters had been properly accounted for. Once closure on this pulse was achieved, data on the target using the compressed pulses were analysed using the relative calibration of step a) and the system parameters and radar cross-section data from the 0.20- μ s pulse data, and, from, this an effective processing gain was calculated. The processing gain may then be used with the relative calibration of step a) to find the absolute received power for use in the free-space radar equation.

Data Collection Modes

Different data collection modes were used depending on the type of data being collected. Three different modes available and their application are described.

Tracking-Window Mode. The data on the reference targets and icebergs were collected using a tracking-window mode. A 10 MHz sampling rate was used with a 10 bit azimuth resolution (1024 sweeps per scan). A window 2 naut mi in range and 22.5° in azimuth (256 samples in range and 64 sweeps in azimuth) was positioned over a target of interest using range and bearing data obtained from the active cursor on the radar operator's console. Radar data were collected for every radar scan once initiated and displayed in real-time on a colour monitor in either a plan-position-indicator (PPI) format or B-scan format. Aircraft position data, available over an RS232 communications line, were used to update the window position as the aircraft flew by the target. Data acquisition hardware limited the maximum data collection range to about 22 naut mi. This mode is economical in terms of data storage requirements and provides convenient format for data analysis.

Full-Scan Mode. The full-scan mode was used only to collect data for sea clutter analysis. Data were collected over 360° with a 9-bit azimuth resolution (512 sweeps per scan). Sampling rates of 10.0 MHz and 2.5 MHz were used sequentially to collect data on the 10.0-, 30.0-, and 0.2- μ s radar pulses. At a 2.5-MHz sampling, 18 scans of radar data were collected to a range of 31 naut mi for the 10.0- μ s pulse and to a range of 29.5 naut mi for the 30.0- μ s pulse. At a 10-MHz sampling rate six scans of data were collected over the range from 6.0 to 22.5 naut mi for the 10.0- μ s pulse and from 4.5 to 21 naut mi for the 30.0- μ s pulse. This data collection procedure provided statistically independent sea clutter returns for use in the generation of sea clutter probability distributions.

Stationary-Window Mode. This mode was used for sea clutter data collection. Data were collected with 10-bit azimuth resolution and a 10-MHz sampling rate. During data acquisition, windows of 22.5° in azimuth were positioned in each of the up-wind (direction of maximum clutter), cross-wind, and down-wind directions and data were collected in all three windows in every radar scan. The mode provided for the collection of sea clutter data for the 10.0-, 30.0-, and 0.2- μ s pulses with and without frequency agility. The data were collected to a range of 7.5 naut mi on the 0.2- μ s pulse, to 22.5 naut mi on the 10.0- μ s pulse and to 21 naut mi for the 30.0- μ s pulse.

Parameters of Interest

Radar signal data collection was carried out to investigate the effects of radar pulse length, aircraft altitude, and frequency agility on the radar cross-section of icebergs and ocean. To limit the number of combinations required a reference data collection mode was chosen and other parameters varied when particular comparisons were desired. Pulse length was chosen as the primary parameter for investigation and, as a result, most of the target and sea clutter data were collected on both the 10.0- and 30.0- μ s pulses using frequency agility at a primary altitude of 500 ft. Selected data were collected for different altitudes, mainly 1,500 ft. Other sequences included fixed frequency operation.

OBSERVED PERFORMANCE DATA COLLECTION

The objective of this aspect of the data collection was to obtain a data base of performance that could quantify detection as a function of iceberg class, flight parameters, radar mode, and environmental conditions. This would be used to identify the optimum mode for detection and the detection performance in an operational context. Documented detection describes the range interval over which the target was within radar range, and was either detected or not detected. It includes the radar mode, flight parameters in use, and the clutter region in which detection or non-detection occurred. Emphasis was placed on documenting the detection of small icebergs, bergy bits, and growlers, at the expense of the larger icebergs.

The (V)5 offered two substantially different pulse widths, scan integration with a choice of four time constants, STC, CFAR, frequency

agility, and a choice of range scales. Given that each iceberg class exhibits variability in detection, it was understood that multiple cases would be required to define performance for each class for a particular environmental condition and radar mode.

Basic configurations were chosen from the start of the experiment to give observed detection statistical meaning and to simplify data collection procedures.

From experience with the (V)3, the 25 naut. mi range was chosen as the prime scale at which to collect data, because it encompassed the anticipated region of detection, and because operationally a reasonable area of coverage is required. Both pulse widths needed to be examined. Pulse A, with an effective width of 30 ns (4.5-m resolution), was expected to reduce the effect of sea clutter substantially, and seemed suited to the dimensions of small targets like growlers. Pulse B, with an effective width of 200 ns (or 30-m resolution) although much longer than pulse A, was 2.5 times shorter than the shortest pulse width of the (V)3, also offered potential clutter reduction and was a reasonable match to bergy bit dimensions.

Altitude was considered to play a potentially large role. Although sea clutter would increase with increasing altitude, so would the grazing angle, presumably exposing more area of the smaller targets to the radar and reducing the shadowing effect of swell. Higher altitudes are attractive (operationally) because they reduce fuel consumption, thus extending the area of coverage.

Pulse width and altitude combinations were given preference in the data collection. As sea clutter was observed to decrease with decreasing

altitude on the (V)3, 500 ft was chosen as the reference altitude to which all other altitudes would be compared. Pulse A and B would both be used initially pending any obvious advantage to one over the other. The four basic data collection modes were;

- . 500 ft, pulse A (primary)
- . 500 ft pulse B (primary)
- . other altitude, pulse A
- . other altitude, pulse B.

Processing options such as STC, CFAR, frequency agility, and scan integration would be observed to see which combination worked best. Observed performance and radar signal data collection had to share some of the flights. Different radar modes were used for each type of data collection. During radar signal data acquisition STC was normally not used on either pulse. Pulse B was operated in rotary (ROT) mode where the display was not stabilized, and no scan integration was possible. To obtain sufficient cases of detection, the radar performance during this data collection was also used in the performance evaluation.

Flying time per flight was limited in duration to about 5.0 to 5.5 h. Within that time icebergs had to be located and photographed, sea clutter information had to be collected, and repeat passes had to be made on each iceberg of interest using different altitudes and pulse widths. Therefore, because the flight usually ended up farther north with time, as a rule of thumb, about 1 h from takeoff could be spent looking for bergy bits and growlers. After 1 h, whether they were present or not, data collection had to start on the smallest pieces of ice available.

Although the greatest effort was made to find ice in the smaller classes, there were always lots of medium (and some large) icebergs in the area, that required only their position to be noted and possibly a 35-mm photograph taken to document their presence in the radar field of view, without having to divert the aircraft. This ease of documentation is predominantly why they are in the data base.

Usually as time grew short, a series of about five icebergs would be located as the aircraft returned to St. John's to obtain five additional ranges of detection.

SUMMARY OF DATA COLLECTED

This section summarizes the iceberg population on which observed performance was based, and the environmental conditions for each flight. An example of lines flown during data collection is given. The collected radar signal data are summarized.

HINDCAST ENVIRONMENTAL CONDITIONS

The environmental conditions for each flight are given in Table 20 in terms of wind speed in knots, wind wave (Hw) in metres, and swell (Hw₁) in metres. Wind and swell directions, and the direction of maximum sea clutter observed on the radar display are also given in degrees (true north).

ICEBERG POPULATION

The icebergs upon which performance was observed are summarized by individual flight in Appendix II-A. The positions were measured using the aircraft navigation system. Dimensions were calculated from Hasselblad and 35-mm photographs.

EXAMPLE OF FLIGHT LINES

Figures 42 and 43 illustrate the flight lines flown on 9 June 1987. This flight collected data both for observed performance and for digital

TABLE 20

Summary of hindcast environmental conditions

Flight date	Wind speed (kt)	Hw (m)	Hw ₁ (m)	Wind Dir °TN	Swell Dir °TN	Radar Display Clutter Dir °TN
April 23	15-20	1.0	0.0	300 - 360	none	highly variable
May 5	10-20	<0.5	1.0	190 - 250	340	154 - 194
May 13	20-25	0.5	1.0-1.5	250 - 260	340	-
May 14	25-35	1.5-2.5	0.0	220 - 230	none	199 - 244
May 15	20-35	1.0-2.0	0.0	210 - 240	none	154 - 219
May 21	10-25	0.5-1.0	1.0-2.0	320 - 030	330-340	334
May 24	5-10	0.0	0.8	270	360	-
June 6	5-15	0.0	1.5	130 - 150	070	120 - 135
June 9	5-15	0.0-0.5	1.5	140	090	155 - 225
June 17	10-15	0.5	1.5	300	330	none
June 19	10-20	0.0-0.5	1.5	220 - 260	000-060	154 - 184
June 22	15-20	1.0	1.5-2.0	240 - 340	330	334
June 26	20-25	1.0	0.0	280 - 300	none	-

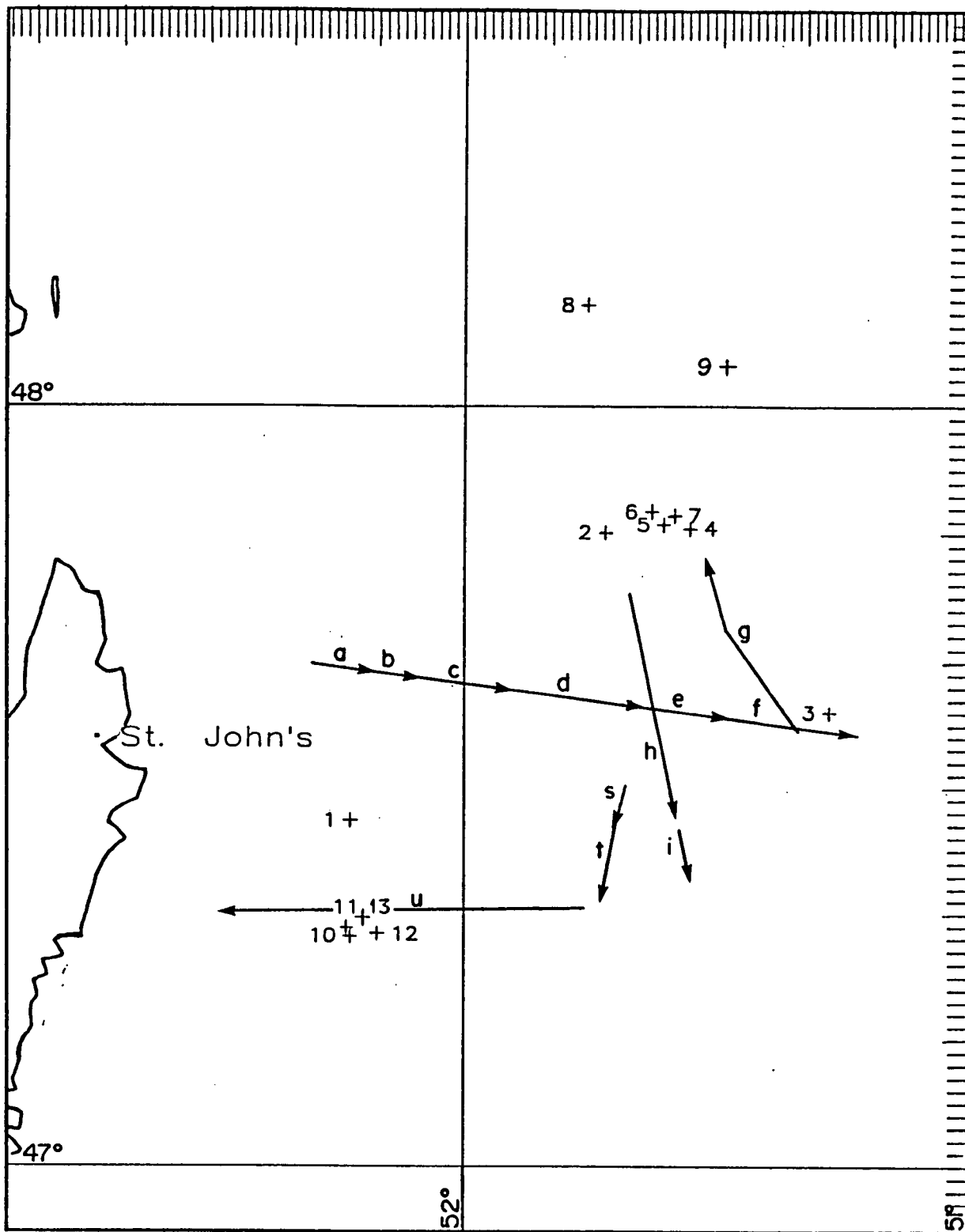
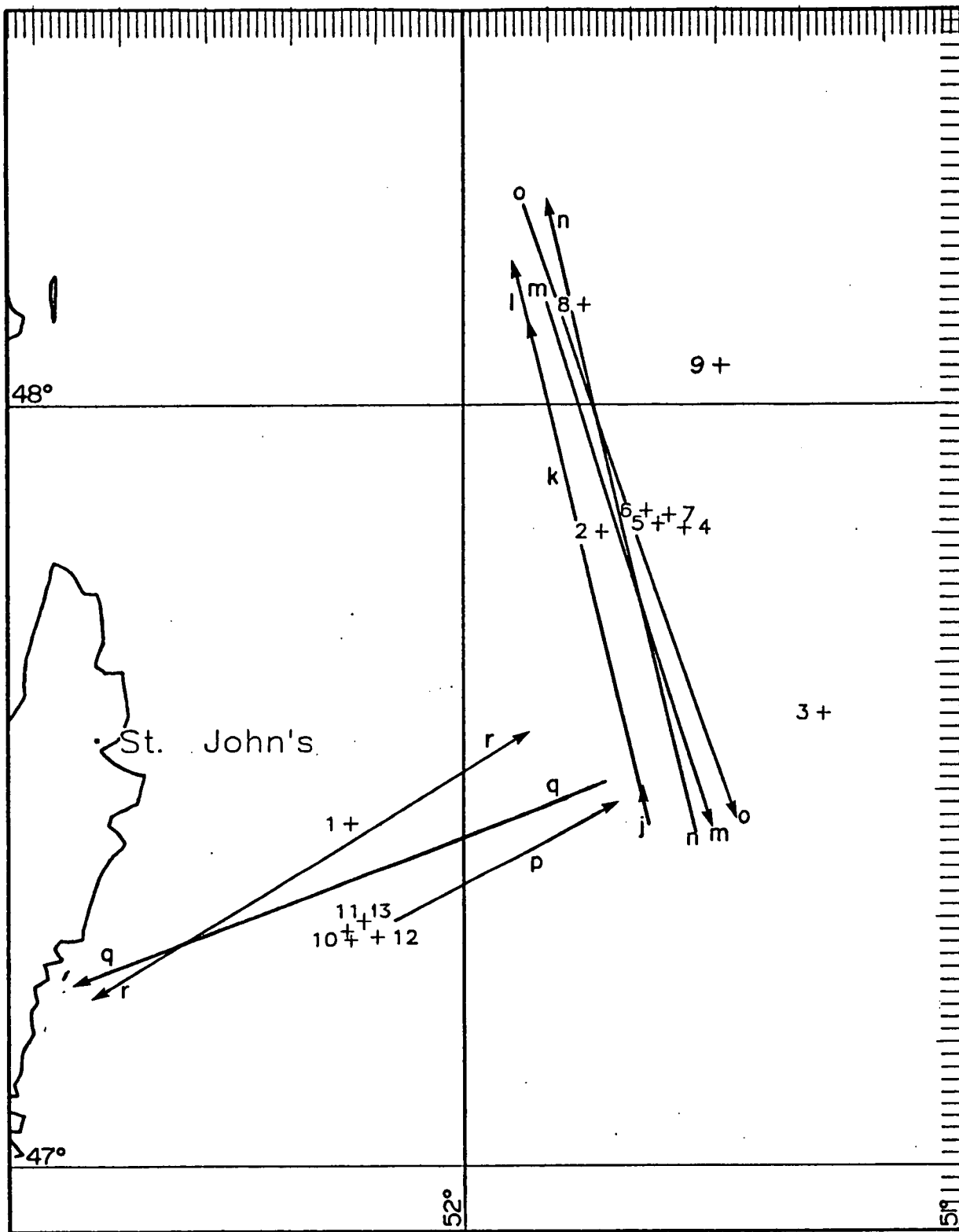


Figure 42. Flight lines flown on 9 June 1987.
 Numbers indicate the targets of interest (see appendix II-A).
 Flight lines a to u were flown in alphabetical order.



Flight 43. Flight lines flown on 9 June 1987.

data collection. Runs a to f were used for collecting sea clutter. The rest of the runs collected both observed performance and digital data.

RADAR SIGNAL DATA

All target and sea clutter data collected are summarized in Tables 21 and 22 respectively. Note that some of the sea state numbers provided in Tables 21 and 22 may differ from those in Table 20 and represent cases when estimates were made from the aircraft. These estimates are used in some cases, over the hindcast data of Table 20 as the local clutter situation was frequently observed to change during a data collection flight.

TABLE 21

Summary of radar signal data on targets, APS-504 (V)5

Target	Ref.	Tape/File	Date (1987)	Description	Position (deg:min)	Alt. (ft)	Pulse (μ sec)	Freq.	Sea state		Scans
									Swell Hght.(m)/Dir.($^{\circ}$ T)	Wind-wave	
1	7	7/(1-3)	May 15	Small	49:05.3 52:37.7	1000	10/30	AG1	3.0/225		90/250
2	5	7/(4-5)	May 15	Small	49:21.2 53:00.5	1000	30	AG1	1.0/225		248
3	16	7/6	May 15	Medium	49:28.7 53:25.4	1000	30	AG1	1.0/225		140
4	17	7/6	May 15	Small	49:07.2 53:17.6	1000	30	AG1	1.0/225		105
5	2	9/2	May 21	Small	48:42.8 52:13.6	500	30	F-8	3.5-4.0/355		90
6	3	9/2	May 21	Small	48:45.6 52:14.2	500	30	F-8	3.5-4.0/355		75
7	4	9/4	May 21	Large	49:13.8 52:21.3	1000	30	F-8	5.0/355		150
8		10/(1-2) 11/(1-5)	May 24	10-m ² buoy	47:40.1 52:24.2	500/1500	200/10/30	F-8	1.0/360	0.25/	150/50/140
9	2	17/(1-2)	Jun 06	Small	47:46.1 52:19.3	500	10/30	AG1	1.5/070		100/300
10	3	17/3 18/1	Jun 06	Small	47:46.6 52:16.8	500	10/30	AG1	1.5/070		200/300
11	3	17/3 18/1	Jun 06	Bergy Bit	47:46.6 52:16.8	500	10/30	AG1	1.5/070		50/100
12	9	18/(2-3)	Jun 06	Small	47:29.3 52:16.5	500	10/30	AG1	1.5/070		100/150
13		18/3	Jun 06	Growler	47:28.2 52:17.7	500	30	AG1	1.5/070		50
14		18/3	Jun 06	Growler	47:26.3 52:19.3	500	30	AG1	1.5/070		50
15	4	20/(1-5)	Jun 09	Small	47:50.5 51:33.6	500	10/30	AG1/F-8	2.0/090		200/200
16	4	20/(1-5)	Jun 09	Bergy Bit	47:50.5 51:33.6	500	10/30	AG1/F-8	2.0/090		200/200
17		20/(1-5)	Jun 09	Growlers(6)	47:49 51:34	500	10/30	AG1/F-8	2.0/090		75/75
18	10	21/(2-3)	Jun 09	Small	47:18.3 52:13.2	500/1500	30	AG1	2.5/090	0.25/140	100
19	11	21/(2-3)	Jun 09	Small	47:19.0 52:13.7	500/1500	30	AG1	2.5/090	0.25/140	75
20	5	22/(2-3)	Jun 17	Large	48:43.4 52:11.4	500/1000 1500	10/30	AG1	2.5-3.0/000		300/300
21	5	22/(2-3)	Jun 17	Bergy Bits(8)	48:43.4 52:11.4	500/1000 1500	10/30	AG1	2.5-3.0/000		250/250

TABLE 22

Summary of sea clutter data, APS-504 (V)5

Tape No.	Alt. (ft.)	Date (1987)	Start time (h:m:s)	Start position (lat.,lon.)	Finish time (h:m:s)	Finish position (lat.,lon.)	Pulse (μ s)	Sea state		Wind spd./dir. (kt./°T)	Freq.
								Swell H.(m)/Dir(°T)	Wind-Wave		
4	500	May 13	19:55:00	47:55.5 N 51:44.5 W	20:09:04		10/30		2.0	20-25/260	AG1
5	500	May 14	15:39:08	49:02.0 N 52:40.0 W	15:54:00	49:02.0 N 51:50.0 W	10/30		1.5-2.0	25-30/230	AG1
6	500	May 15	13:19:27	47:56.0 N 52:12.0 W	13:35:00	48:37.0 N 52:04.0 W	10/30		2.0	20-25/240	AG1
8	500	May 21	14:13:51	47:48.0 N 51:45.6 W	14:28:54	48:13.1 N 52:01.5 W	10/30		3.0	20/320	F-8
12	500	May 24	16:14:37	48:00.0 N 51:52.0 W	16:29:13		10/30	1.0/360	0.25	5/	F-8
13	500	May 24	16:33:25	47:49.0 N 51:10.0 W	16:47:28		30/200	1.0/360	0.25	5/	F-8
16	1500	Jun 06	13:08:49	47:39.2 N 52:14.9 W	13:25:00	47:36.5 N 51:39.0 W	10/30	1.5/070		5-10/150	F-8
19	1500	Jun 09	11:00:26	47:39.4 N 52:14.6 W	11:14:56	47:34.9 N 51:21.0 W	10/30	1.7/090		5-10/140	AG1
23	1000	Jun 19	16:39:40	49:32.8 N 52:45.0 W	16:56:17	49:18.2 N 52:47.5 W	10/30	2-2.5/060/300(2)		15-20/220	F-8
24	500	Jun 22	12:18:09	49:45.0 N 53:45.0 W	12:33:50	50:45.0 N 53:45.0 W	10/30	1.5-2.0/330	1.0	15-20/250	F-8
25	1500	Jun 26	14:02:38	47:43.8 N 52.40.3 W	14:19:44	48:04.1 N 50:45.4 W	10/30	1.5/000 200	1.5	20-25/280	F-8/AG1
	500	Jun 26	14:21:56	48:04.4 N 50:56.2 W	14:37:50	47:54.2 N 51:42.5 W	10/30	1.5/000 200	1.5	20-25/280	F-8/AG1
26	1500	Jul 02	16:41:20	46:30.0 N 49:51.2 W	17:02:32	46:30.4 N 48:23.0 W	10/30	1.0/250	2.5	20-25	AG1
27	1500	Jul 02	17:42:21	47:00.0 N 48:20.0 W	17:58:00	47:00.6 N 49:18.4 W	10/30	1.0/250 200	2.5	20-25	F-8/AG1
	500	Jul 02	17:59:10	47:00.6 N 49:18.4 W	18:14:14	47:00.3 N 50:11.3 W	10/30	1.0/250 200	2.5	20-25	F-8/AG1
28	1000	Jul 02	19:32:34	48:00.4 N 49:07.2 W	19:46:58	48:00.5 N 49:57.2 W	10,30	1.0/250	2.5	20-25	AG1

OBSERVATIONS AND PERFORMANCE

In this section, observations made early in the program are discussed. The (V)5 offered a number of operational modes, each with a set of signal processing options which could be combined, disabled or used individually. Observations early in the program identified which options had the most effect on detection for a given mode, and which modes of operation were not suitable for assessment.

The conclusions based on these observations reduced the number of modes to assess while indicating the hierarchy of signal processing options to use with each mode during data collection. They also identified a problem with an internal test signal in the radar. Some examples are described to illustrate how early conclusions were drawn. It is important to define "performance" and "detection", so that their context indicates the basis on which the (V)5 was assessed. These terms are explained in this section.

The area of radar coverage and the iceberg densities during data collection resulted in a large data base on radar performance. Formation of this data base is described. Since the data base required several passes to reduce the information into a usable form the reduction techniques are explained, in particular indicating the criteria applied to extract "reliable detection".

The last reduction step combined the results of many measurements into one number. Examples are given of this last step to give the reader a feel for the format and context associated with the result.

The remainder of this section presents the results of data reduction. The results are discussed, the optimum radar and flight parameters identified for different environmental conditions and conclusions drawn.

INITIAL OBSERVATIONS AND CONCLUSIONS

STC, CFAR, frequency agility

On 23 April, on pulse A with no CFAR or STC, the circular clutter zone displayed by the radar contained two regions, an interior region of display saturation with an outer annulus of moderate intensity, outside which only noise was present (Figure 44).

When CFAR was enabled, the saturation zone shrank from about 10 to about 7 naut. mi, with the transition zone expanding inwards, but not reducing its outer limit. The same basic effect was observed with AG1 (frequency agility) enabled and CFAR off. Raising the threshold was not effective because it eliminated the noise region entirely (no displayed intensity) before the saturation zone was affected. Scan integration and CFAR together could not eliminate the saturation region either. Also the overall clutter zone size did not appear to change. The blip contrast of the ships, in the transition region, improved substantially when CFAR was applied. With CFAR off, the ships at the transition zone edge could be missed. Another example occurred with an unknown target observed inside the saturation zone while scan integration was on and the STC was repeatedly being varied up (more attenuation) and down (less attenuation). As STC was turned down the target was lost as the zone saturated, while being exposed consistently as the STC was raised.

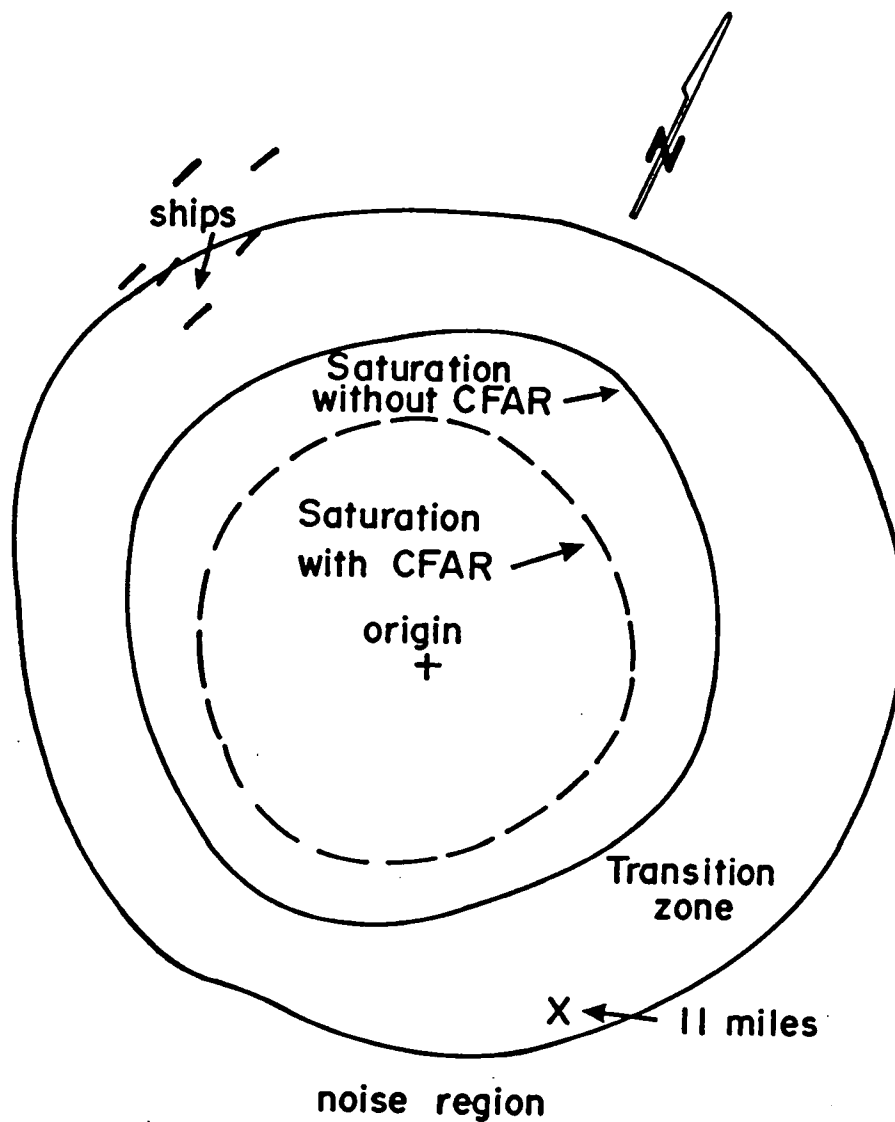


Figure 44. Hand tracing from radar display, 23 April 1987.
 Displayed clutter with CFAR on and off. Altitude 500 ft.

On 5 May 1987, at an altitude of 2,000 ft, on pulse A with STC on, AG1 reduced the displayed clutter zone from 21 to 17 naut. mi., and removing AG1 caused the clutter zone to bloom. With STC at maximum attenuation, AG1 enabled, but without CFAR, a small dome iceberg that was detected beyond 20 naut. mi. was lost in the clutter zone at 12 naut. mi., and was subsequently exposed with the addition of CFAR.

The conclusion (drawn from these examples and others) is that to eliminate the saturating effect of clutter during pulse A operation, STC was required first before CFAR and AG1 would be most effective. CFAR and AG1 both demonstrated similar reduction in clutter and CFAR also could improve target contrast.

From similar observations, pulse B could at times be operated with just CFAR or STC without incurring a zone of saturation on the display.

Frequency agility was again observed to reduce somewhat the extent of displayed clutter on pulse width B. In addition, in the region outside the major clutter zone, where clutter spikes appeared randomly, frequency agility appeared to suppress them substantially, lowering the background intensity and improving target contrast.

For more severe clutter, however, STC alone could not decrease the size of clutter zone saturation nearly as well as CFAR when operating on pulse B. The conclusion was reached that CFAR was very effective in reducing clutter zone saturation on pulse B, and more effective than STC, the addition of which could still be required.

Obtaining a stable display with a uniform background was not easy, and required a fair bit of adjustment by the operator.

Compared to the (V)3, the format of the (V)5 was considered by the operator not to be user friendly. It was difficult to keep the background visible, but not excessively bright. The threshold and STC settings used for pulse width A were not compatible with the threshold and STC settings for pulse width B making the transition from one to the other awkward.

Scan integration

With the appropriate mixture of STC, CFAR, and frequency agility, noise and clutter could be restrained in an average sense to what appeared to be the lower intensity levels of the display for both pulses. However, statistical fluctuations were still present in both regions and appeared as many isolated bright dots popping on and off at random (i.e., very spiky). This effect was noticeable on both pulses, and it should be emphasized that it was very pronounced on pulse A. By trying various combinations it was found that FF (fast rise, fast decay) was sufficient to remove the distraction presented by the spikes on pulse B. On pulse A, FF was insufficient and SS (slow rise, slow decay) was necessary. In general, FS (fast rise, slow decay) emphasized spikes by holding them too long. As a result, the operator would start chasing clutter spikes treating them as potential targets. SF (slow rise, fast decay) was looked at briefly, but appeared to lose information faster than it retained it.

Non-optimized modes

The radar antenna is usually stabilized (to compensate for sudden orientation changes of the aircraft) so that its plane of rotation remains

horizontal. In ASW mode, and when pulse A is used in MPA in ROT mode (PPI format) the antenna is not stabilized.

The two modes were looked at briefly. Both use the same pulse width but have faster antenna rotation rates than any other mode.

On 23 April 1987, it was found that while on pulse A, switching from MPA STB (stabilized antenna) to MPA ROT (unstabilized antenna) caused the display to change to a series of tiny segments looking like pie slices. Blips from ships that had been continuous in azimuthal extent became segmented and less visible. ASW mode presented a worse display. While working with a bergy bit and two growlers, on pulse B with STC, with at least six other larger pieces of ice detected on 5 May 1987, ASW was tried briefly with STC and scan integration. Almost all targets were lost. Neither mode was considered suitable for assessment.

Radar Display Test Pattern

The radar uses a 16-level look up table (16 intensities) to present the radar video. Ideally, the radar display should be matched so that all these levels are properly presented, and distinct.

A test pattern is available to set the radar display contrast and brightness. Sixteen vertical bars of increasing intensity are displayed, and the contrast and brightness then adjusted to make all 16 bars visible and distinct.

Post-flight observations from the operational flight on 23 April indicated that noise and clutter could easily enter the higher intensity levels saturating the display and washing out detectable targets. STC, CFAR, AGI, and scan integration were used as required on the next flight

to suppress this undesirable effect.

But post-flight playback of the radar videotapes revealed saturation was still a problem. Clutter and noise intensities that looked satisfactory in flight (i.e. not apparently reaching the higher display intensity levels), appeared to reach the higher intensity levels when reviewed on the playback system on the ground.

The solution was found by taking advantage of a new black and white display that had been installed at the observer's position since the completion of the V(3) program. This display doubled both as a Hasselblad viewfinder and as the observer's radar monitor. After the operator's display was adjusted to the test pattern, the two displays were compared.

The noise and clutter on the observer's display was judged excessively bright, and the radar settings were adjusted to reduce this background intensity on the observer's display. The intensity on the operator's display then had to be raised substantially to recover the background. The test pattern was then examined and found to be too bright with the higher intensities saturated together. Post-flight review now showed reasonable background display intensities, and targets did not seem to be washed out by the background.

Apparently, the test pattern is not matched to the radar video signal range. It seems to represent a stronger signal range than the radar video. Consequently, the brightness on the operator's display would be set too low, and the loss of apparent intensity would be compensated for by lowering either the STC or the threshold to raise the radar video, which brightens up the background, and presumably pushes the video higher into the display look-up table. In the air the display would appear

normal, but on the ground the background would appear too bright. All flights after 5 May 1987 used the observer's display as reference. The test pattern was considered unsuitable and was never used again.

Altitude

The extent of the displayed clutter zone was very sensitive to increasing altitude. The limits of the clutter zone were traced from the display (Figure 45). The radar was operating on pulse A, AGI enabled, STC on, with FS (fast rise, slow decay) scan integration. The settings were the same for both altitudes.

MEASURE OF PERFORMANCE

The performance of the V(5) was measured in terms of the maximum reliable range of detection observed for each target. Thus, the results would indicate how close the aircraft had to be to a given iceberg before detection could be expected.

The word "detection" needs definition. Detection means the target of interest is reasonably obvious on the radar display and would attract the attention of the operator. The presentation of noise and clutter on the radar display can determine if a target is obvious. As such, assessing whether a target is detected by reviewing videotape records of the radar display is a judgement call by the analyst.

When sea clutter was minimal on calm days detection would be observed and would usually continue as long as the iceberg's range was

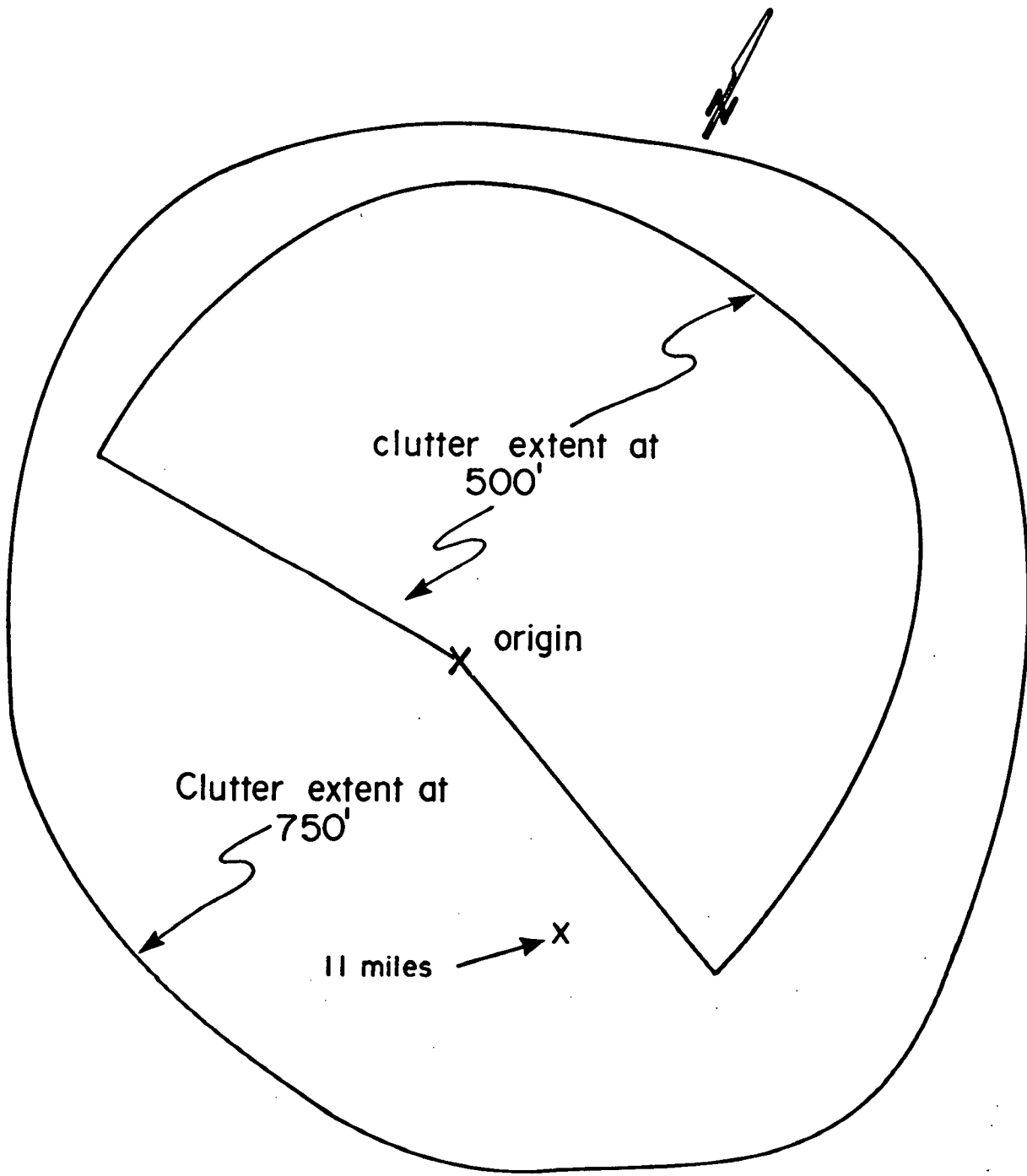


Figure 45. Hand tracing from radar display, 23 April 1987. Displayed clutter at 500 and 750 ft.

less than the maximum range. However a word of caution is in order. On range scales such as 25 naut mi, ranges below approximately 3 to 5 naut mi occupy a very small area at the center of the display. This central region is susceptible to congestion by sea clutter even on relatively calm days. It is not unusual to lose a well detected target as it enters this central region. However this is still predominantly noise-limited detection.

When sea clutter was significant, and often limited detection at much larger ranges, maximum range alone was insufficient to quantify detection for operational flying. As the target gets closer, it is competing with more sea clutter and detection can be lost. It was necessary to also look at the range interval inside maximum range where detection can be expected. As an example, an iceberg on a given day is first detected 18.5 naut. mi. away outside the clutter zone but gets lost at the edge of the clutter zone at 18 naut. mi. Only 0.5 naut. mi. interval is available for detection, which is insufficient.

Therefore, detection was quantified in terms of the maximum observed range and the interior interval of detection (e.g., detectable 18.5 naut. mi. to 18.0 naut. mi; undetectable 18.0 naut. mi. to 5.0 naut. mi.).

DATA REDUCTION

Several passes through the data set were required before the data were in a concise, usable form for assessing performance. Videotape is used by the radar to record the radar display in flight, and contains an audio track available only to the operator. These tape records were the main source of analysis for detection performance.

During the first pass by the aircraft, the altitude, positional coordinates, the radar mode and settings, the targets in the field of view, and their individual records of detection were documented.

The location of the up- and down-clutter regions were noted when visible. Typically, of ten to fifteen icebergs which had been photographed sequentially throughout a flight, six to ten were in the radar's field of view simultaneously on any given run. A transparent grid, with latitude, longitude, and the locations of the icebergs was made, which fit the display scale of the playback monitor. The grid (Figure 46) was used to determine when targets were in the radar field of view, and as an aid for separating them from other targets in the region that were not tested during the program. It was particularly useful in determining when a target was definitely in the radar field of view but undetected, and to locate targets that were to be tested later in the flight.

Data from the first pass were combined with any in-flight notes, the observer's log sheet of target positions and sea state observations, the iceberg photographs, and the calculated iceberg dimensions.

During the second pass, Mercator projection maps were used to plot the flight lines relative to the targets, and to locate the direction of maximum clutter. The records of detection for each run were then converted to range using the plotted flight paths, which also determined which clutter region each target was in at the time of detection or non-detection. The dimensions of the targets were checked, and the size were reclassified if necessary.

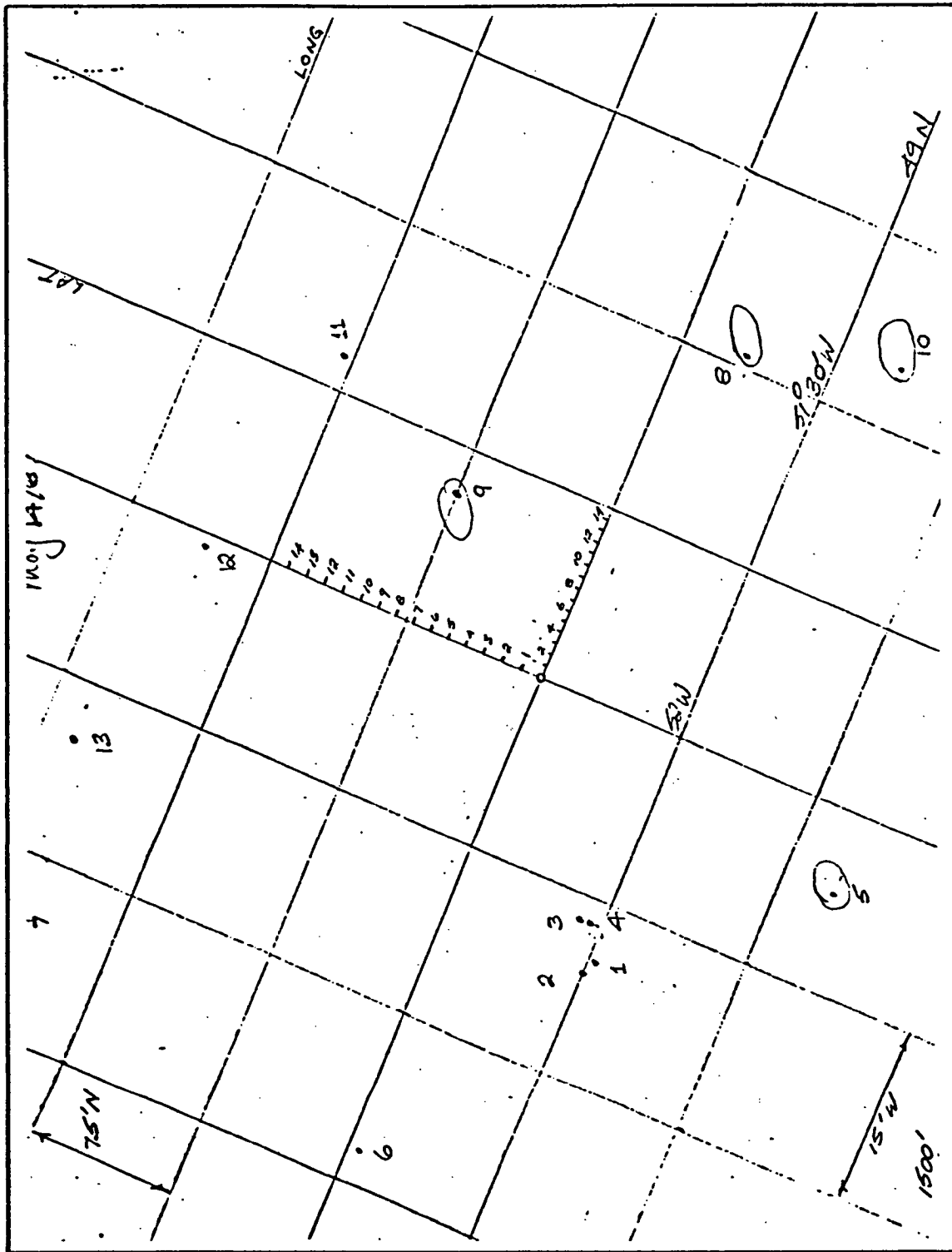


Figure 46. Example of display grid used for visual aid.

During the third pass, the records of detection applicable to each iceberg were summarized so that each iceberg was identified by a complete list of detection as a function of altitude, radar mode, range, and clutter region if applicable.

Estimating Reliable Range of Detection

A typical dedicated flight was used to locate and photograph a small number of targets in a region, to document their detection by the (V)5 radar during straight flight lines, and then to look for more targets. The length of each flight line was determined by the necessary distance to establish range of detection and subsequent non-detection for the target of interest. Other targets in the radar field of view were automatically recorded and most were later photographed as icebergs of interest.

As a result, targets of interest have multiple records of detection. Some of the records document the region of detection and subsequent non-detection. Other records may only document a range interval inside the region of detection or a range interval outside the range of detection.

The object is to summarize this type of data set into one number representing a reliable range within which detection can be expected and beyond which detection is not probable, for each iceberg.

Detected targets were sometimes observed to disappear from the display (non-detection) for short intervals on an otherwise continuous range interval of detection. These intervals were typically a couple of nautical miles. Targets that were basically undetectable over a long range interval sometimes were momentarily detected for a short interval. Again, the intervals were typically a couple of nautical miles.

It was decided that if an apparent maximum range of detection had been reached it should be followed by a sufficiently long interval of non-detection. Similarly, a region of detection had to be demonstrated by a sufficiently long interval.

The minimum interval chosen to apply to both cases was about 2.5 naut. mi. This value was chosen based on the typical fluctuations in detection previously mentioned, and because the radar operator needed time to observe a possible target and to judge whether detection had occurred. A range of 2.5 naut. mi. corresponds to 1.0 to 1.5 min. of flying time, depending on ground speed and closest point of approach.

Four examples illustrate how this criteria was applied, and what conclusions were drawn. The first two examples were taken from cases in which detection was basically noise-limited and clutter was almost nil.

The last two examples were taken from cases where sea clutter was significant.

Example 1 of data reduction. The results of observed performance for a small iceberg (reference #4, 9 June 1987) are given in Table 23. The flight lines are identified by letter (see Figures 42 and 43). In Table 23, the mode of the radar indicates the type of processing used. A stabilized display is indicated by STB, whereas ROT indicates rotary display. Frequency agility is indicated with AG1, whereas fixed frequency transmission is illustrated with F-8 (the centre of the radar frequency range). No additional processing is indicated by :--. CFAR is indicated by CF. Scan integration is identified with :FF (fast rise, fast decay) and :SS (slow rise, slow decay). The range intervals of detection and

TABLE 23

Observed radar performance for a small iceberg target (#4)
at two altitudes, 9 June 1987

Run	Pulse width	Mode	Range interval detected (naut mi)	Range interval not detected (naut mi)
<u>Altitude: 500 ft</u>				
(h)	A	STB AG1-:SS	7.0-22.2	22.2-23.0 ^a
(j)	A	STB AG1-:-	22.5-21.0 ^a	23.0-22.5 ^a
(k)	A	STB AG1-:-	21.0-8.0-20.0	-
(l)	A	STB AG1-:SS	20.0-22.7	22.7-25.0
(m)	A	STB F-8-:-	21.0-6.7 7.2-17.8	6.7-5.0-7.2 17.8-23.0
(i)	B	STB AG1-:-	-	24.0-27.5
(n)	B	ROT F-8-:-	24.0-5.0-23.0	-
(o)	B	ROT AG1-:-	23.2-5.5 4.3-21.7	5.5-4.0-4.3 21.7-23.0 ^a
(r)	B	STB AG1 CF:-	-	26.9-20.0
<u>Altitude: 1500 ft</u>				
(c)	A	STB AG1 CF:SS	25.0-19.0	-
(e)	A	STB AG1 CF:-	14.0-15.0 ^a	-
(f)	A	STB AG1 CF:SS	15.0-21.0	-
(g)	A	STB AG1 CF:-	18.5- 3.0	-
(t)	A	STB AG1 CF:SS	-	24.5-30.0
(u)	A	STB AG1 CF:SS	-	31.0-44.0
(b)	B	ROT AG1 CF:-	25.0 ^a	-
(d)	B	ROT AG1 CF:-	19.0-14.0	-
(s)	B	STB AG1 CF:FF	21.5-23.7 ^a	23.7-24.0 ^a

^a Inconclusive result based on a minimum 2.5 naut mi interval.

non-detection for each run are listed. For example, run (o) occurred at 500 ft altitude, on pulse B, with the display in rotary mode. Frequency agility was enabled, but neither CFAR or scan integration was used. The target was visible on the display at the start of this run at a range of 23.2 naut. mi. and was detected as the aircraft approached to within 5.5 naut. mi. The target was then lost. The target remained lost as the closest point of approach (CPA) occurred at 4.0 naut mi. Detection was recovered, as the target was receding from the aircraft, at 4.3 naut mi. Detection continued until 21.7 naut mi, when the target was lost and remained undetected to the end of the run at a final range of 23.0 naut mi

Performance at 500 ft on pulse width A will be considered first. Detection intervals shorter than the 2.5 naut mi previously described were discarded as inconclusive. The tabulated maximum range of detection of runs (h), (k), (l), and (m) lie between 17.8 and 22.7 naut mi, or 20.2 ± 2.4 naut mi.

For pulse B at the same altitude, runs (i), (n), and (o) place the maximum range interval between 21.7 and 24.0 naut mi. Run (r) indicates less than 20.0 naut mi. In cases like this, where detection has been reasonably demonstrated (beyond 20 naut mi) the maximum range interval is taken to be 20 to 24 naut mi or 22.0 ± 2.0 naut mi.

For pulse A at 1,500 ft, detection is demonstrated without contradiction to 21.0 naut mi by runs (f) and (g). Runs (c) and (t) fix the absolute maximum at 24.5 naut mi. The maximum range interval is then taken to be 21.0 to 24.5 naut mi or 22.7 ± 1.7 naut mi.

Lastly, for pulse B at 1,500 ft all that can be deduced is a maximum range of detection greater than 19.0 naut mi.

Example 2 of data reduction. The results of observed performance for a small iceberg (reference #1 17 June) are given in Table 24. At 500 ft, pulse A, the runs indicate a range of detection demonstrated out to 16.3 naut mi (run b) but limited to no more than 18.5 naut mi (run c). The maximum range of detection was taken to be 17.4 ± 1.1 naut mi. For pulse B at the same altitude, maximum range of detection was taken as >22.9 naut mi.

For 1,500 ft, pulse A, maximum range was set equal to 22.0 naut mi. The minimum range interval was relaxed slightly for pulse B at 1,500 ft. Run (g) demonstrates detection to at least 25 naut mi, whereas run (i) limits detection to 22.6 naut mi. Maximum range of detection was set at 23.8 ± 1.2 naut mi.

Table 24

Observed radar performance for a small iceberg target (#1)
at two altitudes, 17 June 1987

Run	Pulse width	Mode	Range interval detected (naut mi)	Range interval not detected (naut mi)
<u>Altitude: 500 ft</u>				
(b)	A	STB AG1 CF:SS	7.0-16.3	16.3-18.0 ^a
(c)	A	STB AG1 CF:SS	-	18.5-30.5
(d)	A	STB AG1 CF:SS	-	32.5-28.5
(e)	A	STB AG1 CF:SS	18.7-16.5 ^a	26.0-18.7
(h)	B	ROT AG1 -:-	11.5-22.9	22.9-25.0 ^a
<u>Altitude: 1500 ft</u>				
(f)	A	STB AG1 CF:SS	17.5-22.0	22.0-36.0
(g)	B	ROT AG1 CF:SS	25.0-11.0	-
(i)	B	ROT AG1 -:-	22.6-11.0	25.0-22.6

^a Inconclusive result based on a minimum 2.5 naut mi interval

Example 3 of data reduction. The data shown in Table 25 were collected on 21 May 1987 for a small iceberg. A clutter zone was present, the size and extent of which was dependent on pulse width and altitude. The quantities of interest are observed maximum range of detection, the interior interval of detection demonstrating detection into the clutter and the region of clutter over which this occurred. Clutter was divided into two regions. The stronger clutter region was denoted as up-clutter,

analogous to upwind. Down-clutter was the weaker clutter region. It should be noted that up-clutter and wind directions are not necessarily the same direction (see Table 20). Runs on which the target was in the transition area between up - and down-clutter (cross-clutter) were treated as up-clutter. STC and CFAR were used together, and are indicated with 'CS:'.

At 500 ft on pulse A the maximum range in the down-clutter region is indicated to be at least 26.5 naut mi or greater, with an interior range extending into 12.5 naut mi , which is summarized as ">26.5-12.5" (down-clutter). On pulse B at the same altitude, run (c) limits down-clutter detection to within 26.5 naut mi whereas runs (d₁), (d₂), and (i) indicate down-clutter detection from 0 to 27.7 naut mi. Therefore, down-clutter detection was taken to be "= 27.1 - 0 (\pm 0.6)" naut mi. Up-clutter detection is indicated by run (d₂) to be ">18.3-12.6" naut mi.

At 1,500 ft, on pulse A, run (f) indicates a down-clutter detection range "= 23.1-2.3." On pulse B at 1,500 ft, run (g) indicates a maximum down-clutter range of 26.0 naut mi extending into 4.0 naut mi whereas run (h) limits the interior range to 13.6 naut mi. Down-clutter detection was summarized as "= 26.0-13.6" naut mi.

TABLE 25

Observed radar performance for a small iceberg target (#2)
at two altitudes, 21 May 1987

Run	Pulse width	Mode	Range interval detected (naut mi)	Range interval not detected (naut mi)	Clutter region
<u>Altitude: 500 ft</u>					
(b)	A	STB AG1 CS:SS	12.5-26.5	@26.5 ^a	down-clutter
(c)	B	STB AG1 CS:FF	-	26.5-29.0	down-clutter
(d ₁)	B	STB AG1 CS:-	27.7-16.5	29.0-27.7 ^a	down-clutter
(d ₂)	B	ROT AG1 CS:-	16.5-0.0	0.0-12.6	down-clutter
			12.6-18.3	18.3-20.5 ^a	up-clutter
(i)	B	STB AG1 CS:FF	18.5-22.0	-	down-clutter
<u>Altitude: 1500 ft</u>					
(f)	A	STB AG1 CS:SS	2.3-23.1	23.1-32.0	down-clutter
(g)	B	STB AG1 CS:FF	26.0-4.0	30.0-26.0	down-clutter
(h)	B	STB AG1 CS:FF	13.6-15.5 ^a	8.0-13.6	down-clutter

a Inconclusive result based on a minimum 2.5 naut mi interval

Example 4 of data reduction. The data shown in Table 26 were also collected on 21 May 1987, for a bergy bit.

At 500 ft, pulse A, down-clutter detection was summarized as ">18.0-9.1" naut mi from runs (m) and (n), whereas up-clutter detection is indicated as "<3.0-13.0."

At 1,000 ft, pulse A, run (1) indicates down-clutter detection to be "<3.0-17.5" naut mi.

TABLE 26

Observed radar performance for a bergy bit target (#13)
at two altitudes, 21 May 1987

Run	Pulse width	Mode	Range interval detected (naut mi)	Range interval not detected (naut mi)	Clutter region
<u>Altitude: 500 ft</u>					
(m)	A	STB F-8 CF:SS	9.0-18.0	5.0- 9.0	down-clutter
(n)	A	STB F-8 CF:SS	17.5- 9.2	9.2- 3.0 3.0-13.0	down-clutter up-clutter
<u>Altitude: 1000 ft</u>					
(1)	A	STB F-8 CS:SS	-	17.5-3.0	down-clutter

MATRIX OF RESULTS AND ANALYSIS

Observed performance was based on data collected between 5 May 1987 and 22 June 1987. The results from flights with similar hindcast environmental conditions were combined as shown in Table 27. More weight was placed on windspeed, wind-wave height (Hw), and displayed clutter observations than swell (Hw₁).

TABLE 27

Summary of flights with similar hindcasts

Date (1987)	Hw (m)	Hw ₁ (m)	Wind (kt)
June 6, June 9, June 17	0 - 0.5	1.5	5 - 15 ^a
May 5, May 21, June 19	0.5 - 1.0	1.0 - 2.0	10 - 25 ^b
May 14, May 15, June 22	1.0 - 2.5	0.0 - 2.0	15 - 35 ^c

^a equivalent to class 1 conditions as described in Part I APS 504 (V)3

^b transition to class 2 conditions

^c equivalent to class 2 conditions as described in Part I APS 504 (V)3

The tabulated results from 6, 9, and 17 June are given in Table 28 as a function of pulse width and altitude. The radar display showed negligible sea clutter for these three flights, and, as such, they represent noise limited detection. The numbers in each horizontal line apply to the same iceberg, and gaps indicate a lack of data for a particular altitude and pulse width.

To illustrate the format, see the first iceberg in the small category. At 500 ft, pulse width A, its range of detection was equal to (=) 18.5 ± 2.3 naut mi. For pulse B at the same altitude, its range of detection was greater than (>) 22.0 ± 2.0 naut mi. At 1,500 ft, on pulse A, the range of detection was greater than (>) 19.0 ± 3.0 naut mi, and on pulse B it was equal to (=) 23.6 naut mi. The symbol '<' indicates the maximum range of detection must be less than the number indicated.

Although the matrix represents the reduction of data to the point where it can be worked with, its results are much better illustrated in a

TABLE 28

Tabulated maximum range of detection for 6, 9, and 17 June

Iceberg size class	Range of detection at 500 ft (naut mi)		Range of detection at 1,500 ft (naut mi)	
	PWA ^a	PWB ^b	PWA ^a	PWB ^b
Large	>34.0	>25.0	>27.2	>23.5
	>47.8	>28.0	>39.2	>25.0
	=35.1 ± 0.9	=38.0	>31.0	-
	-	>25.0	>23.0	>24.0
Medium	>34.0	>25.0	>27.2	>23.5
	=26.0 ± 2.8	>25.0	=31.6	>25.0
	=29.4	>25.0	>21.0	>22.5
	-	-	>16.0	>32.0
	=21.0	=22.6 ± 0.6	-	-
	>25.0	>24.0	>21.0	>25.0
	>28.5	>25.0	-	>25.0
	>33.8	>25.0	>32.0	-
	>28.5	>25.0	>34.5	>25.0
	=32.4 ± 2.4	-	-	-
	=32.5 ± 1.0	>25.0	>36.0	>25.0
	-	-	-	-
Small	=18.5 ± 2.3	>22.0 ± 2.0	>19.0 ± 3.0	=23.6
	=25.1 ± 3.6	=22.7 ± 2.3	-	>25.0
	=27.5 ± 1.0	>25.0	-	-
	=19.0 ± 1.3	=22.5 ± 2.4	>22.0	>21.5
	=20.0 ± 2.2	=22.0 ± 2.0	=22.7 ± 1.7	>19.0
	=27.8 ± 6.8	=23.8 ± 1.1	=20.6 ± 3.9	>25.0
	=19.5 ± 1.5	=20.9 ± 2.5	<16.7	>25.0
	=14.0 ± 3.0	=20.7 ± 2.3	<16.7	>25.0
	=17.5 ± 1.2	=22.9	=22.0	=23.8 ± 1.2
	< 4.0	<6.5	<2.8	-
	-	-	-	-
	-	-	-	-
Bergy Bit	=15.2 ± 5.7	=14.9 ± 4.2	-	-
	=13.0 ± 3.0	=14.3 ± 3.1	=14.0	<16.0
	=20.0 ± 2.7	=17.3 ± 1.0	=19.5	<20.0
	= 4.5 ± 4.5	<6.0	=19.0	<19.0
	< 4.5 ± 4.5	<2.0	<12.0	-
Growler	<3.0	=4.8 ± 4.8	-	-
	=4.5 ± 4.5	=5.3 ± 5.3	-	-
	=4.0 ± 4.0	<4.0	-	-
	<3.0	<3.0	<16.0	<13.0

a Pulse width A

b Pulse width B

graph of observed detection in an iceberg class versus range, for a particular altitude and pulse width.

Figure 47 illustrates observed detection at an altitude of 500 ft using pulse width A. From the matrix, maximum range of detection was observed for 10 small icebergs. By ranking them in order of decreasing range, the percentage detected as a function of maximum range can be calculated. The tenth point is <4.0 naut mi, and the ninth is $= 14.0 \pm 3.0$ naut mi. Nine of 10 icebergs, or 90%, had detection ranges greater than, or equal to, 14.0 naut mi, (see Figure 47). Similarly, the rest of the curve for small icebergs was developed.

Points that are encircled indicate that true observed detection should lie to the right of indicated point. All ten medium icebergs (100%) had a detection range greater than or equal to 21.0 naut mi. However, the next lowest value, >25.0 does not place an absolute limit on range of detection. Nine of 10 (90%) of medium icebergs had ranges of detection greater than 25.0 naut mi. The true range of detection curve for all ranges greater than, or equal to, 25.0 naut mi must, therefore, lie on the right-hand side of the curve as drawn. Special attention should be given to curves with points that are encircled.

In subsequent figures, usually only the 100% range of detection point has been plotted for the medium and large class of icebergs. These classes had such large ranges of detection that only a few cases of non-detection were actually observed with increasing range. An encircled point with an apparently low range value indicates that one medium or large iceberg was only observed at small range values and no data exist beyond that range.

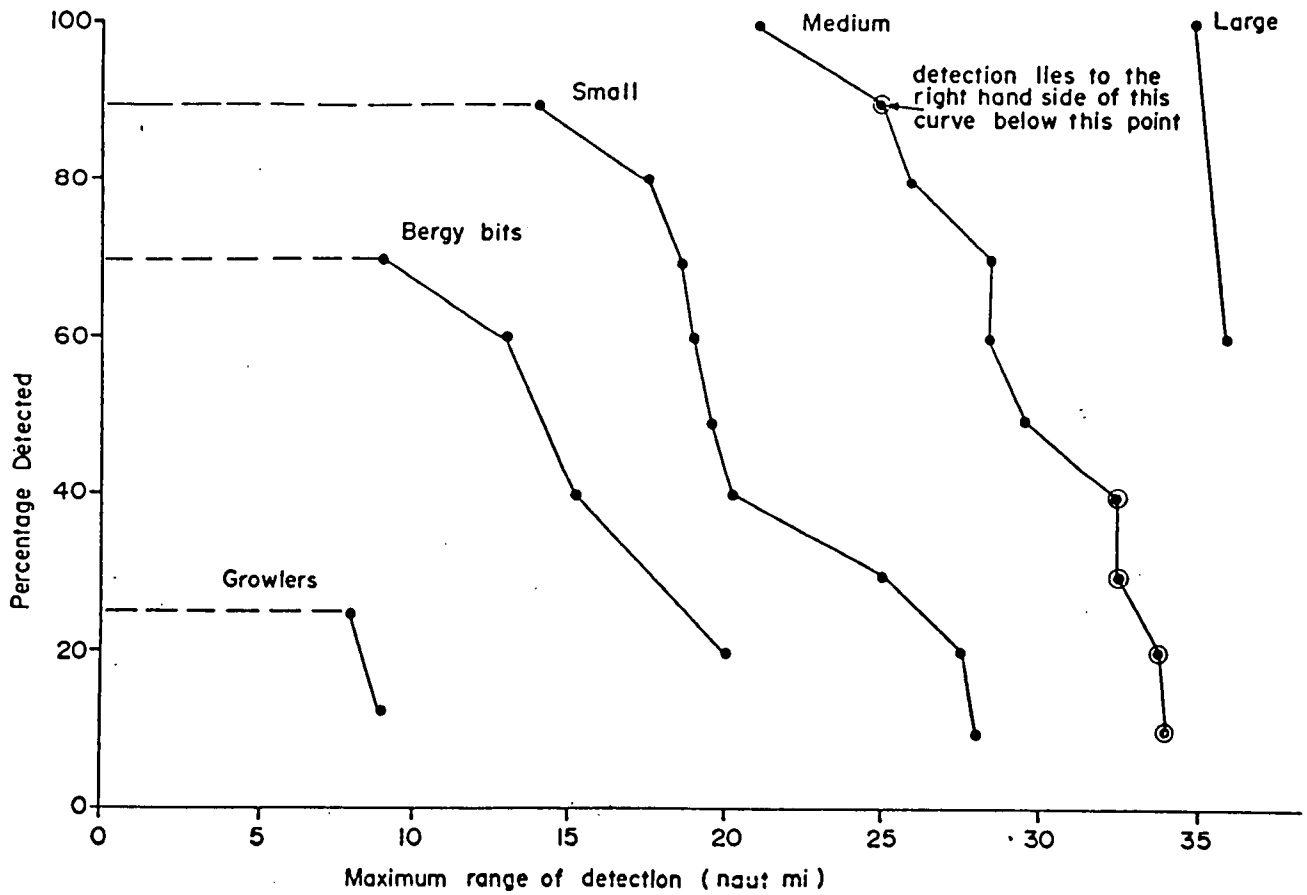


Figure 47. Observed radar performance for iceberg detection using pulse width A at 500 ft altitude (6, 9, and 17 June 1987). Populations = Large(3), Medium(10), Small(10), Bergy bits(5), Growlers(4).
Wind: 5-15kt Hw: 0-0.5m Hw₁: 1.5m

It should be noted that the curves are better defined as the population of cases increases in each class.

Since this graph format is used to illustrate detection performance, it is worth illustrating what can be inferred from Figure 47. For instance, small icebergs can be detected about 90% of the time if they are within about 14 miles radar range at the closest point of approach but one small iceberg in ten will not be detected regardless of range (i.e., the dashed line sets the maximum detection limit). A substantial drop in detection occurs as the closest point of approach moves out to 20 miles. Then, only 40% or four of ten small icebergs are likely to be detected.

For bergy bits, detection is limited to about 70% at about 9 miles closest point of approach, so about 3 of ten will be missed regardless of how close they are to the flight track. Although medium and large icebergs were not observed to pose a detection problem, even medium size icebergs do not have unlimited range of detection, and it was observed that one was only detected out to 21 naut mi.

The observed results for the other three combinations of pulse width and altitude are given in Figures 48, 49, and 50. The combination of altitude and pulse width observed to give the best performance for small icebergs is pulse B at 1,500 ft with 500 ft (same pulse width) a close second. Both combinations were observed to have a high percentage of detection at maximum ranges greater than 19 naut mi. Because of the finite number of cases it would be unwise to assume that pulse B at 1,500 ft truly has 100% detection capability. At 500 ft pulse A demonstrated shorter ranges of detection, although having a similar percentage detected. Pulse A at 1,500 ft had no detection capability for

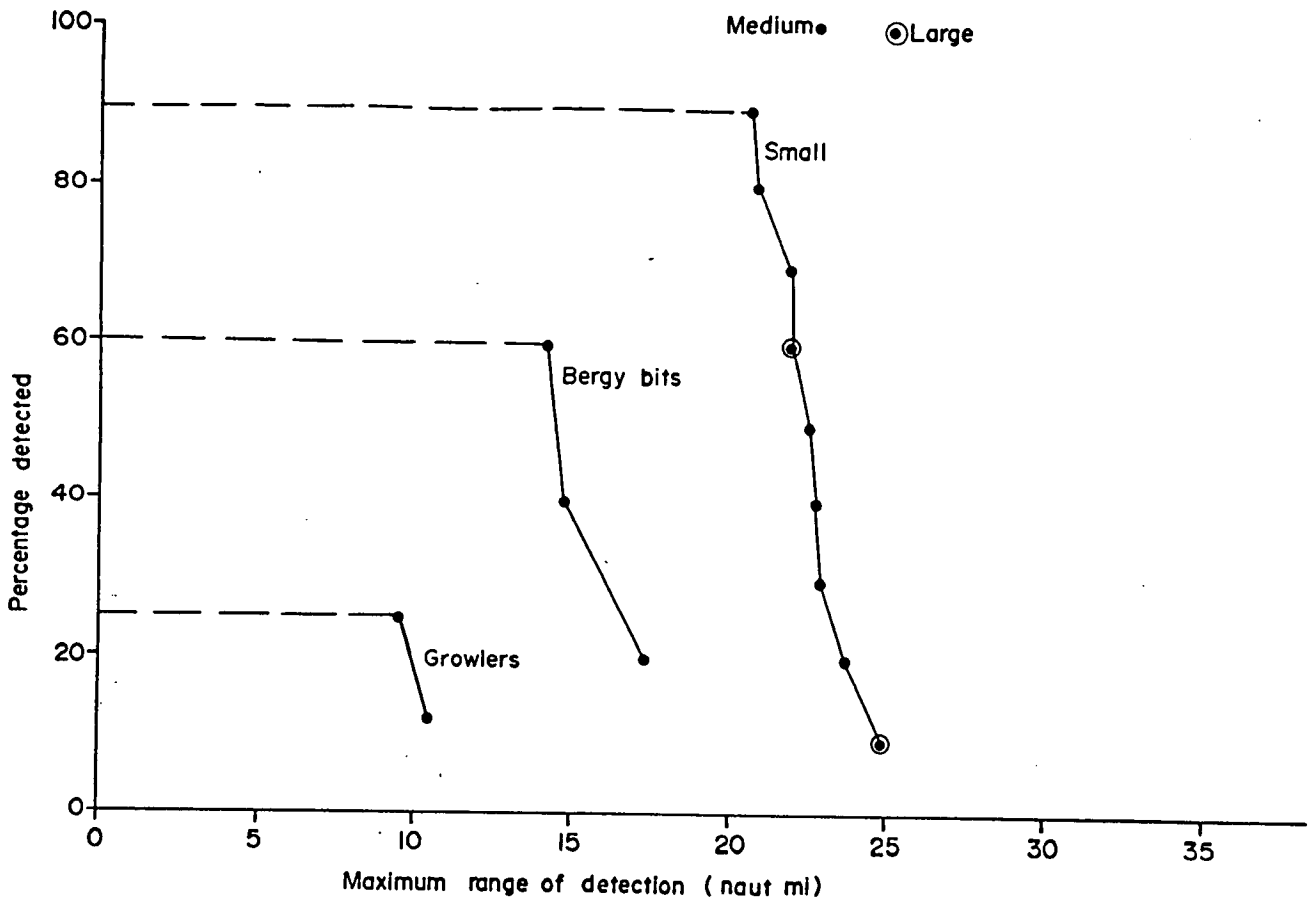


Figure 48. Observed radar performance for iceberg detection using pulse width B at 500 ft altitude (6, 9, and 17 June 1987). Populations = Large(4), Medium(9), Small(10), Bergy bits(5), Growlers(4)

Wind: 5-15kt Hw: 0-0.5m Hw₁: 1.5m

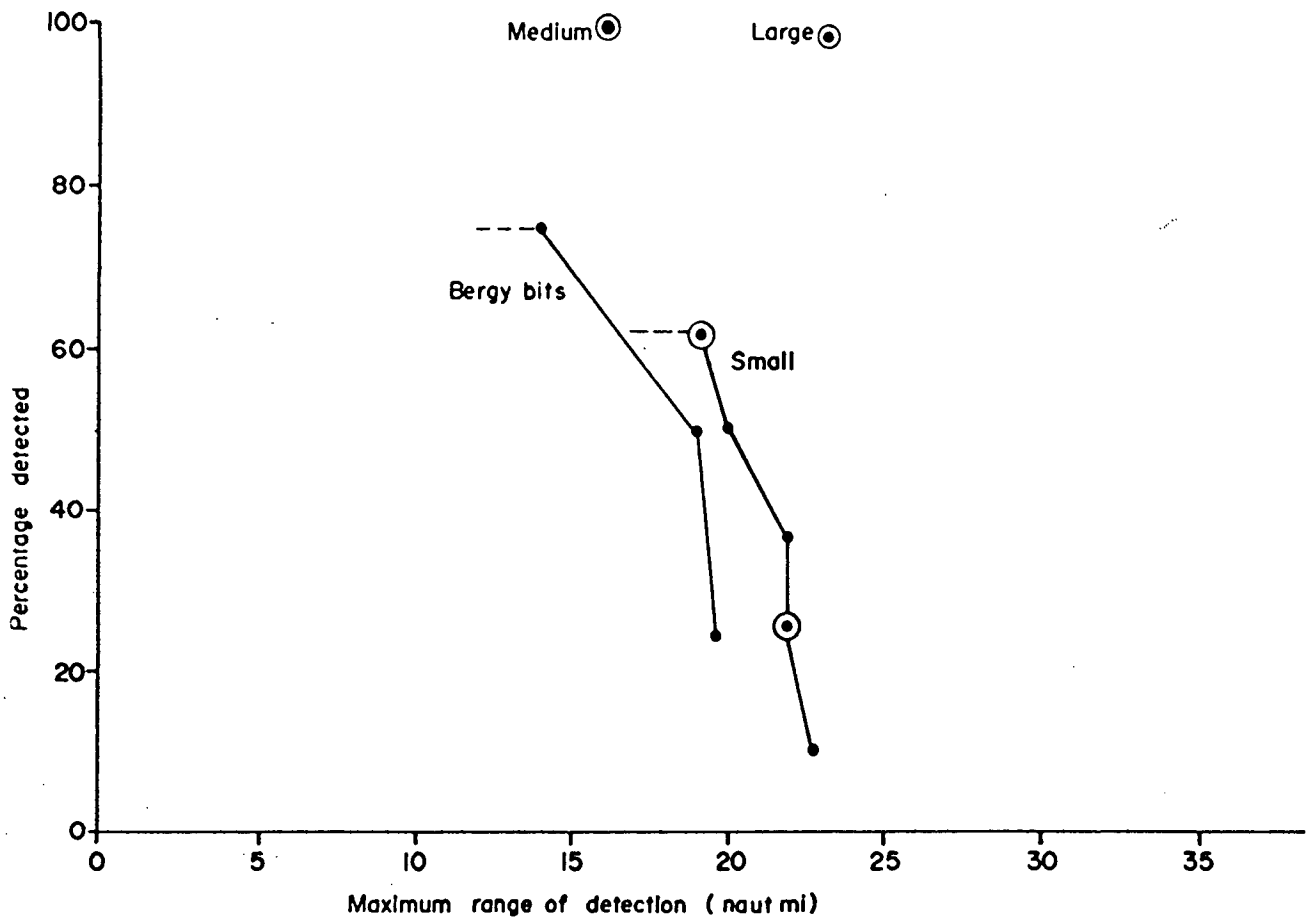


Figure 49. Observed radar performance for iceberg detection using pulse width A at 1500 ft altitude (6, 9, and 17 June 1987). Populations = Large(4), Medium(8), Small(8), Bergy bits(4), Growlers(0). Wind: 5-15kt Hw: 0-0.5m Hw₁: 1.5m

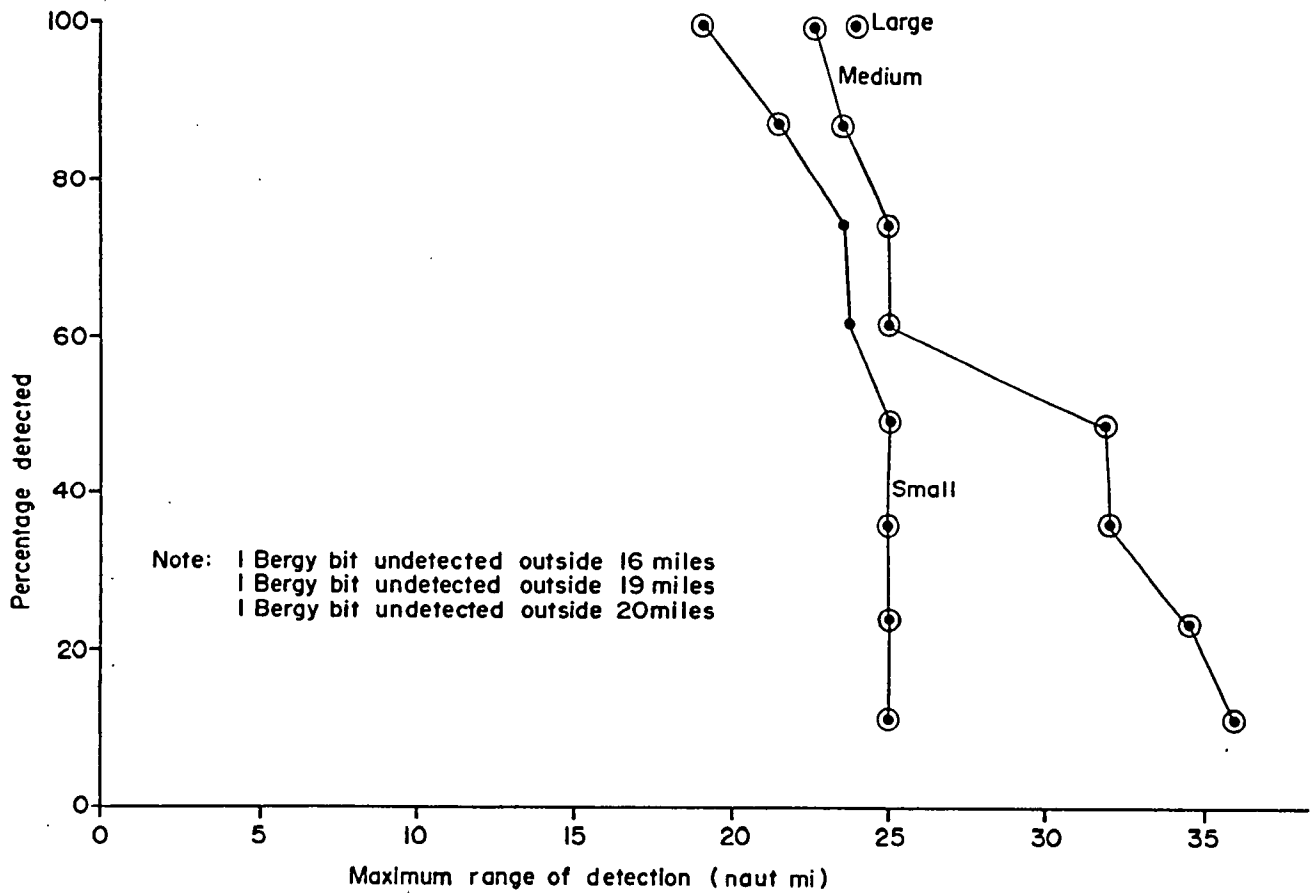


Figure 50. Observed radar performance for iceberg detection using pulse width B at 1500 ft altitude (6, 9, and 17 June 1987). Populations = Large(3), Medium(8), Small(8), Bergy bits(3), Growlers(0).

Wind: 5-15kt Hw: 0-0.5m Hw₁: 1.5m

38% (three of eight) outside 16.7 naut mi.

For bergy bits, on the other hand, pulse A was observed to have a slightly higher percentage of detection than pulse B that may not be statistically significant because of the differing population sizes. When range of detection is taken into account, however, pulse A at 1,500 ft was observed to have a definite edge.

Data on bergy bits for pulse B at 1,500 ft are limited; the regions of non-detection suggest its percentage detected could not be much better than pulse A at 1,500 ft.

Growlers were poorly detected at 500 ft on both pulse widths. There are insufficient data to form a conclusion for growler detection at 1,500 ft on either pulse width. The choice of best combination of pulse width and altitude depends on the application. When the region of coverage requires detection of bergy bits and small icebergs, the best combination appears to be pulse width A at an altitude of 500 ft, with pulse B at the same altitude a close second. Pulse B at 1,500 ft needs more investigation before an opinion can be formed.

When the region of coverage is sufficiently far removed from the platform to be protected, and only small icebergs and larger size classes are of interest then pulse B at 1,500 ft is the best combination. These conclusions are based on the observed performance of 6, 9, and 17 June when wind-wave (H_w) was 0 to 0.5 m, swell (H_{w1}) was about 1.5 m, and wind speed was 5 to 15 knots.

The tabulated results for 5, and 21 May, and 19 June are given in Table 29. The results have been subdivided to illustrate performance down-clutter (the weak half of the clutter zone direction) and up-clutter

TABLE 29

Tabulated maximum range of detection for data of 5 May, 21 May, and 19 June

Iceberg size class	Range of detection from 500 ft (naut. mi.)			Range of detection from 1,000 ft (naut. mi.)			Range of detection from 1,500 ft (naut. mi.)					
	FWA ^a		FAP ^b	FWA		FAP	FWA		FAP			
	Rdwn	Rup/cross ^d	Rdwn	Rup/cross	Rdwn	Rup/cross	Rdwn	Rup/cross	Rdwn	Rup/cross		
Large	—	>19.0-5.0	—	—	—	—	>20.5-3.0	—	—	—	>36.0-6.0	
	>30.0-25.0	>27.0-21.5	>33.0-17.0	—	—	—	>31.0-27.0	—	>31.5-23.5	—	>31.5-21.0	=16.2-13.5
	>19.0-5.0	—	>21.5-9.5	>25.0-4.0	—	—	—	—	>24.0-2.0	—	>22.0-0	>12.0-0
	=33.5-18.0	—	—	—	—	—	>32.0-13.5	—	—	—	—	—
Medium	>14.0-3.0	—	>29.1-17.6	—	—	—	>26.0-10.5	—	>25.5-6.5	—	—	—
	<6.5-8.0	<6.5-12.0	<7.5-10.0	>25.0-9.5	<30.0-34.2	—	=16.3-9.0	—	—	>22.0-4.0	—	=23.0-19.3
	—	—	—	—	—	—	>25.0-16.0	—	—	=26.7-19.0	—	<15.0-31.0
	—	—	—	—	>34.0-17.5	—	—	>23.5-11.0	—	—	—	—
Small	>28.0-4.0	—	—	—	>35.5-24.0	—	—	>23.5-17.5	—	—	—	—
	>17.6-10.9	—	>28.0-20.0	—	—	>26.5-11.0	—	—	—	—	—	—
	>19.0-5.0	—	>28.8-20.0	—	>13.5-4.5	—	>31.5-16.0	—	>31.0-5.5	—	—	—
	>19.5-5.0	—	>28.8-22.5	—	>14.0-6.5	—	=29.0-16.0	—	>31.0-8.0	—	—	—
Small	—	—	>31.5-4.5	—	—	—	—	—	—	—	—	—
	>24.0-1.0	>24.0-1.0	—	—	—	—	—	—	—	—	—	—
	=15.7-2.0	=15.5-8.7	—	—	=5.7-4.0	—	=22.3-16.0	—	—	—	—	—
	>26.5-12.5	—	=27.1-0	>18.3-12.6	—	—	=26.0-13.6	—	=23.1-2.3	—	=26.0-13.6	—
Small	=10.0-6.5	—	<2.0-26.5	<2.0-23.0	—	—	—	—	<3.0-29.0	—	<2.0-27.0	—
	>18.0-9.0	<13.5-21.0	>20.5-10.5	>25.0-9.0	—	—	<22.0-25.0	—	<7.0-21.0	<7.0-12.5	<5.5-20.0	<3.0-16.5
	—	>31.8-22.3	—	—	<13.0-28.5	—	—	<12.0-28.0	—	—	—	—

TABLE 29 (continued)

Iceberg size class	Range of detection from 500 ft (naut mi.)			Range of detection from 1,000 ft (naut mi.)			Range of detection from 1,500 ft (naut mi.)								
	FMB ^a		FMB ^b	FWA		FWB	FWA		FWB						
	Rdwn	Rup/cross ^d	Rdwn	Rup/cross	Rdwn	Rup/cross	Rdwn	Rup/cross	Rdwn	Rup/cross					
Bergy	<10.0-23.0	<4.0-15.0	<4.0-11.5	—	<10.0-28.0	<6.0-15.5	<0	-12.0	—	<1.0-15.5	<1.0-15.5	>27.8-9.1	—		
Init	=11.1-6.4	—	<20.5-28.0	—	<3.0-12.0	—	<15.0-30.5	—	—	=13.9-4.0	—	—	—		
	>20.0-6.0	—	>27.9-22.5	—	>12.9-6.0	—	=23.1-17.0	—	—	=24.0-7.0	—	—	—		
(33%)	=7.2-3.0	<1.0-14.0	—	—	—	<3.0-21.0	—	<3.0-22.0	—	—	—	—	—		
(66%)	<1.0-13.5	—	—	—	—	—	—	—	—	—	—	—	—		
	<1.5-18.0	<3.5-18.0	—	—	<3.5-18.0	—	<17.0-25.8	—	—	—	—	—	—		
	>18.0-9.0	<3.0-13.0	—	—	<3.0-17.5	—	—	—	—	—	—	—	—		
	=9.8-5.1	<1.0-12.0	—	—	>22.0-6.0	—	—	—	—	—	—	—	—		
	>18.0-5.9	—	—	—	—	—	—	—	—	—	—	—	—		
Growlers	<0	-31.0	—	—	<0	-11.5	<0	-17.0	<6.0-9.0	<11.5-21.0	—	<12.0-30.5	>10.0-4.7	<0	-12.0
	<0	-31.0	—	—	<0	-11.5	<0	-17.0	<6.0-9.0	<11.5-21.0	—	<12.0-30.5	>10.0-4.7	<0	-12.0
	<0	-31.0	—	—	<0	-11.5	<0	-17.0	<6.0-9.0	<11.5-21.0	—	<12.0-30.5	>10.0-4.7	<0	-12.0
	<0	-31.0	—	—	<0	-11.5	<0	-17.0	<6.0-9.0	<11.5-21.0	—	<12.0-30.5	>10.0-4.7	<0	-12.0
	<0	-13.0	<6.0-11.0	—	<0	-14.5	<20.5-28.5	<9.0-12.0	<9.0-12.0	<11.0-19.0	—	<11.5-28.0	<0	-12.0	<7.7-13.0
	<0	-13.0	<6.0-11.0	—	<0	-14.5	<20.5-28.5	<9.0-12.0	<9.0-12.0	<11.0-19.0	—	<11.5-28.0	<0	-12.0	<7.7-13.0
	<0	-13.0	<6.0-11.0	—	<0	-14.5	<20.5-28.5	<9.0-12.0	<9.0-12.0	<11.0-19.0	—	<11.5-28.0	<0	-12.0	<7.7-13.0
	<10.0-23.0	<5.0-16.0	<5.5-11.5	—	<10.5-27.0	<7.0-16.0	<0	-11.0	<0	-11.0	—	<1.0-10.5	<1.0-16.0	>27.1-9.1	—
	<10.0-23.0	<5.0-16.0	<5.5-11.5	—	<10.5-27.0	<7.0-16.0	<0	-11.0	<0	-11.0	—	<1.0-10.5	<1.0-16.0	>27.1-9.1	—
	<3.7-17.8	<4.0-17.0	<24.5-31.0	—	<6.0-11.0	<6.0-16.0	<17.0-25.3	—	—	—	—	—	—	—	—

^a Pulse width A
^b Pulse width B
^c Range interval in down-clutter region
^d Range interval in up- or cross-clutter region

(stronger half of the clutter zone). The results indicate that detection can be poorer up-clutter, for the icebergs of smaller size class, an expected result.

The results for both pulse widths at an altitude of 500 ft are illustrated in Figures 51 and 52, for observed detection in the down-clutter region. One assumption was made to increase the population size. It was assumed that an iceberg that was detected up-clutter would have the same detection range down-clutter.

At 500 ft, pulse A (see Figure 51) demonstrated 100% detection of small icebergs (nine of nine). For bergy bits, 62% were detected. It should be noted from the matrix, that some bergy bits exhibited variable detection from one run to the next. For example, the last bergy bit in the column was observed to be detected to 9.8 naut mi once and detected out to 18.0 naut mi the next time. Each run was given a 50% weighing before calculating percentage of detection versus range. Pulse width B, at 500 ft (see Figure 52), detected 86% (six of seven) small icebergs. Bergy bits are not illustrated because of the small population. As one bergy bit missed on pulse A was also missed on pulse B whereas another bergy bit was detected out to 20 naut mi or greater at both pulse widths, no conclusions have been reached for the performance of pulse B at 500 ft for bergy bits. Pulse width A did not detect any of 10 growlers. Pulse width B missed three growlers but only two were observed inside 10 naut mi. However, as both pulse widths were observed to have similar poor performance in the previous example for calmer conditions, it is doubtful that pulse B at 500 ft would outperform pulse A.

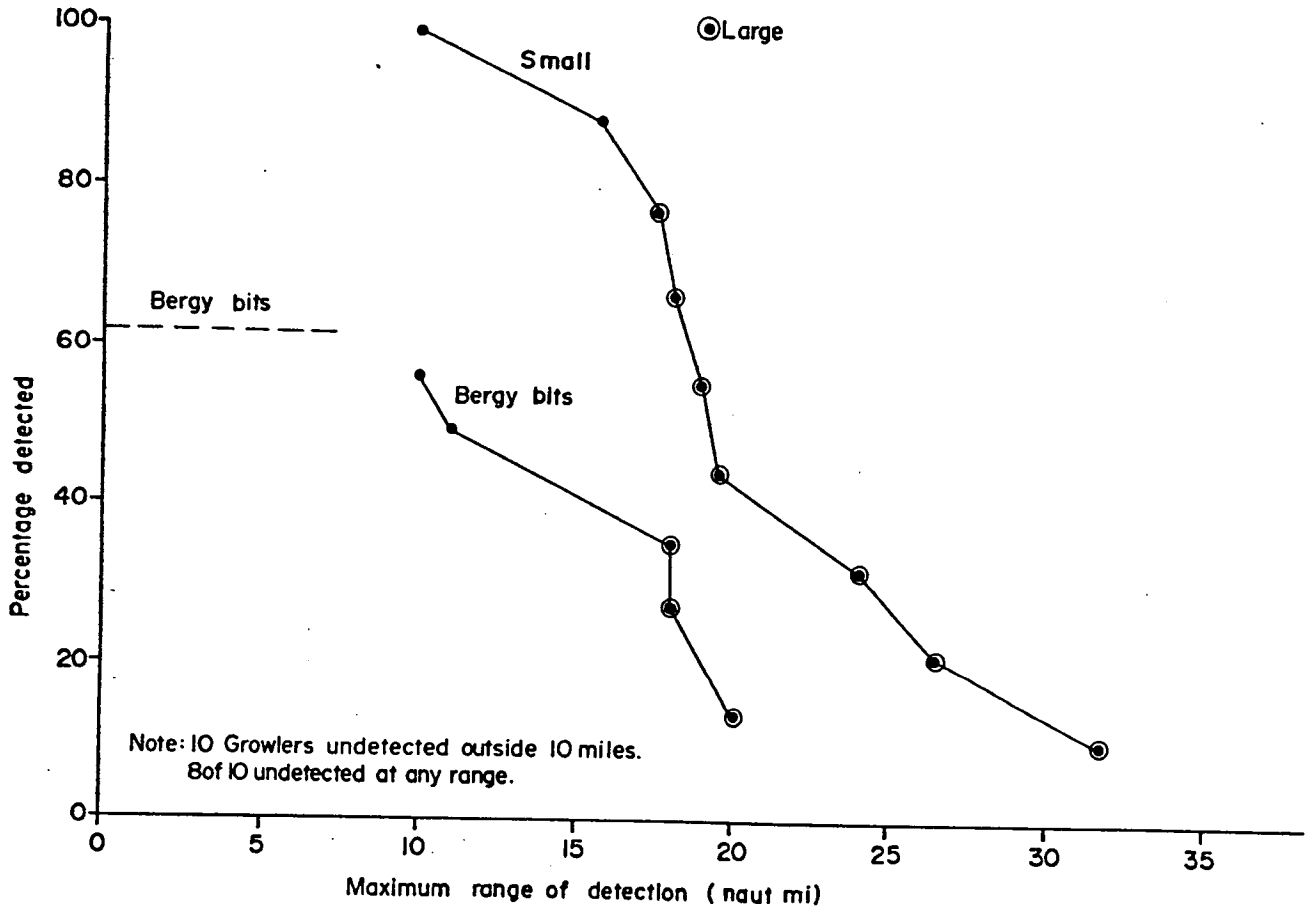


Figure 51. Observed radar performance for iceberg detection using pulse width A at 500 ft altitude (5 May, 21 May, and 19 June 1987). Down clutter region only. Populations = Large(4), Medium(0), Small(9), Bergy bits(7), Growlers(10).

Wind: 10-25kt Hw: 0.5-1.0m Hw₁: 1.0-2.0m

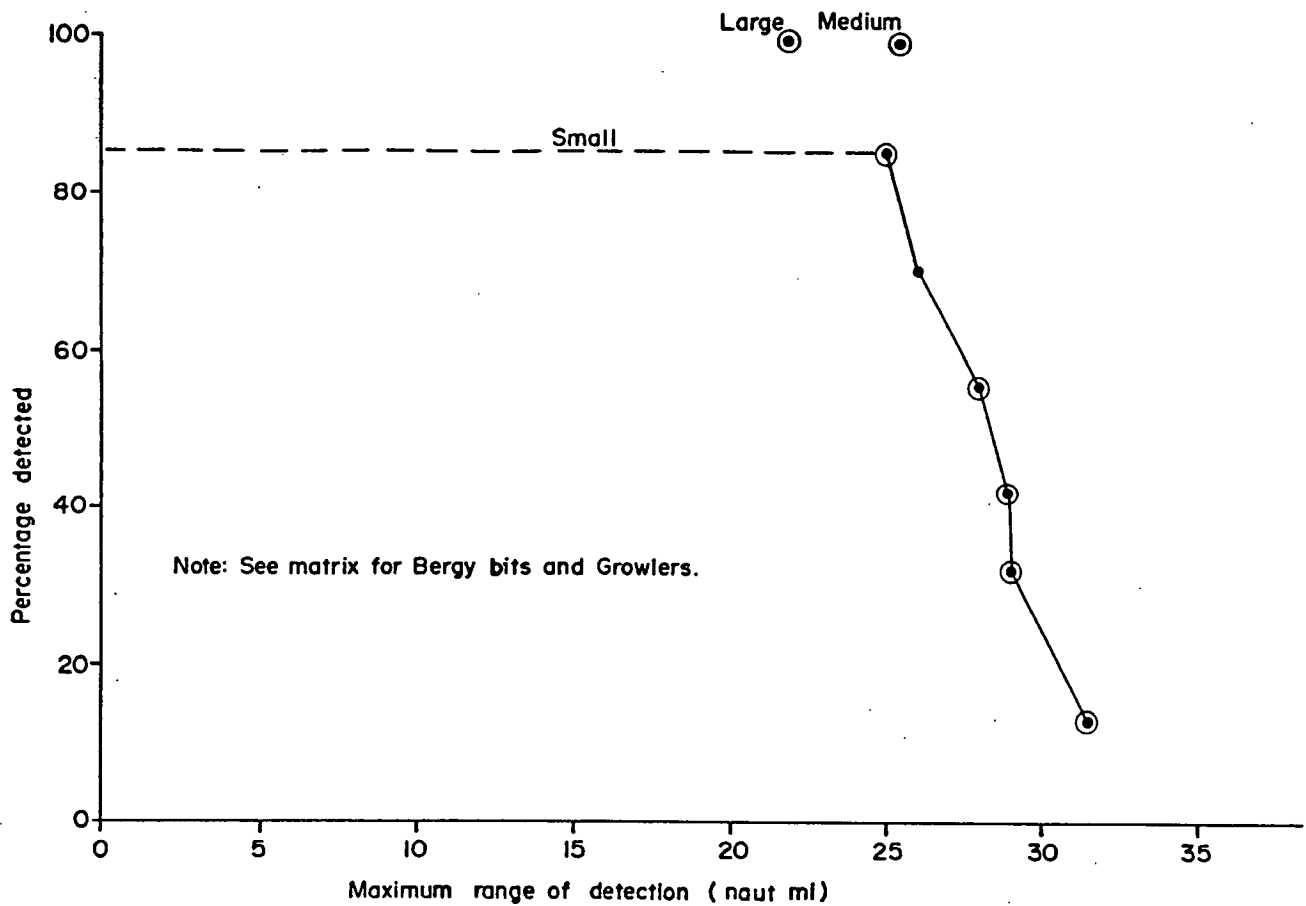


Figure 52. Observed radar performance for iceberg detection using pulse width B at 500 ft altitude (5 May, 21 May, and 19 June 1987). Down clutter region only. Populations = Large(3), Medium(2), Small(7), Bergy bits(3), Growlers(3). Wind: 10-25kt Hw: 0.5-1.0m Hw₁: 1.0-2.0m

Figure 53 illustrates the performance of pulse width A at 1,500 ft. The observed detection of small icebergs is poor (60%). From the matrix, it should be noted that two of the small icebergs detected at 500 ft were missed at 1,500 ft. The population of bergy bits is small and the same two bergy bits detected at 1,500 ft were detected to similar ranges at 500 ft. The small population is probably exaggerating performance at 1,500 ft. On pulse B at 1,500 ft, the same two small icebergs were missed, but growlers were surprisingly well detected, and may be an anomalous result (Figure 54). The five growlers were actually in two groups close together that were detected on one particular run on 5 May, as the aircraft approached them head on.

Figures 55 and 56 illustrate the trend in detection for all data observed above 500 ft, using the best observed performance on each iceberg (i.e. if an iceberg was undetected at 1,000 ft but was detected at 1,500 ft, the higher altitude result was used, and vice versa). These figures exaggerate true performance above 500 ft, and are only used to illustrate that increasing altitude will reduce detection.

For pulse widths A and B the detection of small icebergs is worse at 1,500 ft than on pulse A at 500 ft. From observed detection, 500 ft appears to be superior to higher altitudes. For small icebergs pulse A had better percentage detection but pulse B had longer range detection. The radar performance for bergy bit detection is well defined for pulse A, but insufficient information exists to quantify pulse B. Neither pulse width is expected to detect growlers at 500 ft. These conclusions are based on the observed performance of 5, and 21 May and 19 June when Hw (wind-wave) was 0.5 to 1.0 m, Hw₁ (swell) was 1.0 to 2.0 m and wind speed

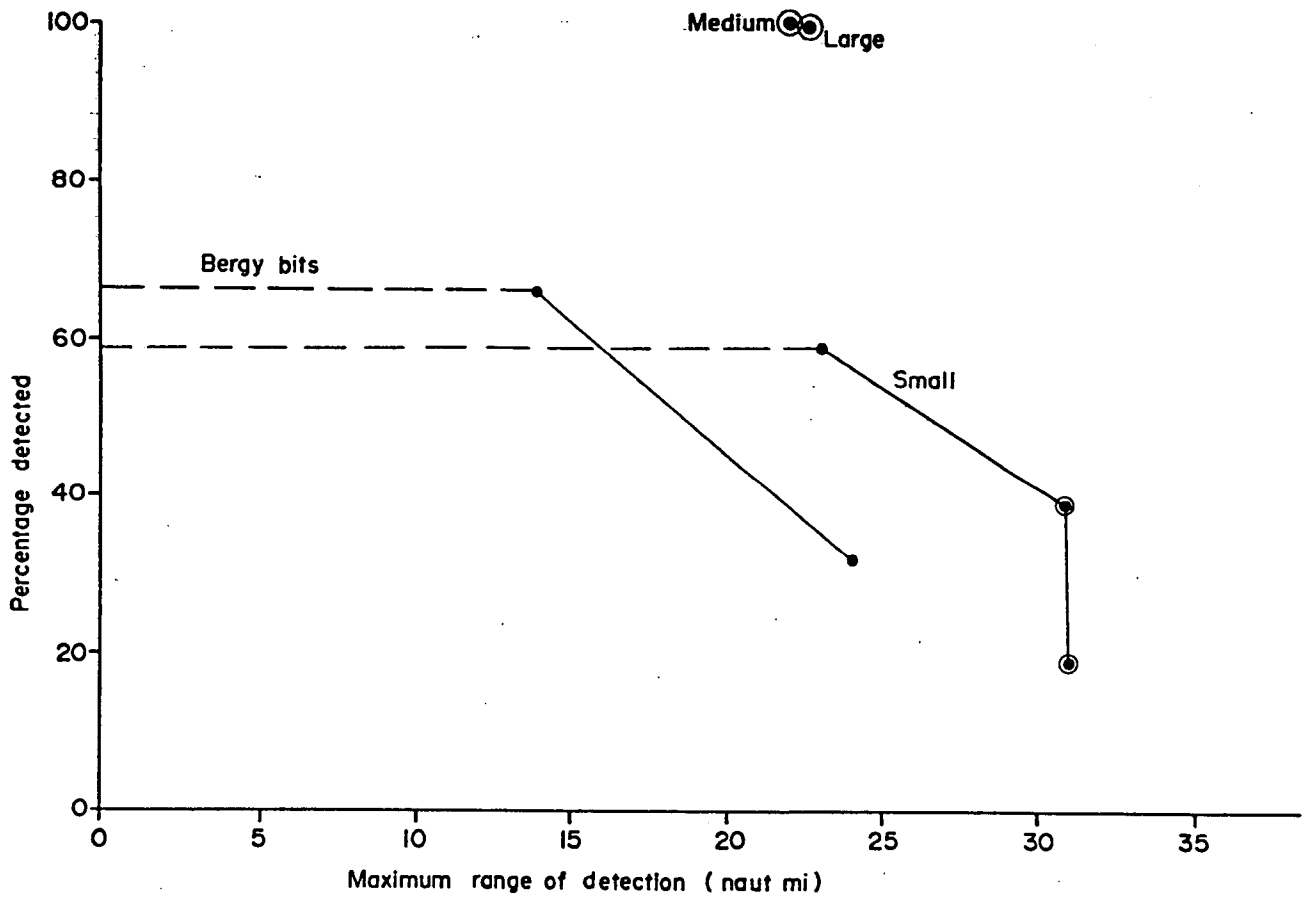


Figure 53. Observed radar performance for iceberg detection using pulse width A at 1500 ft altitude (5 May, 21 May, and 19 June 1987). Down clutter region only. Populations = Large(3), Medium(3), Small(5), Bergy bits(3), Growlers(0).

Wind: 10-25kt Hw: 0.5-1.0m Hw₁: 1.0-2.0m

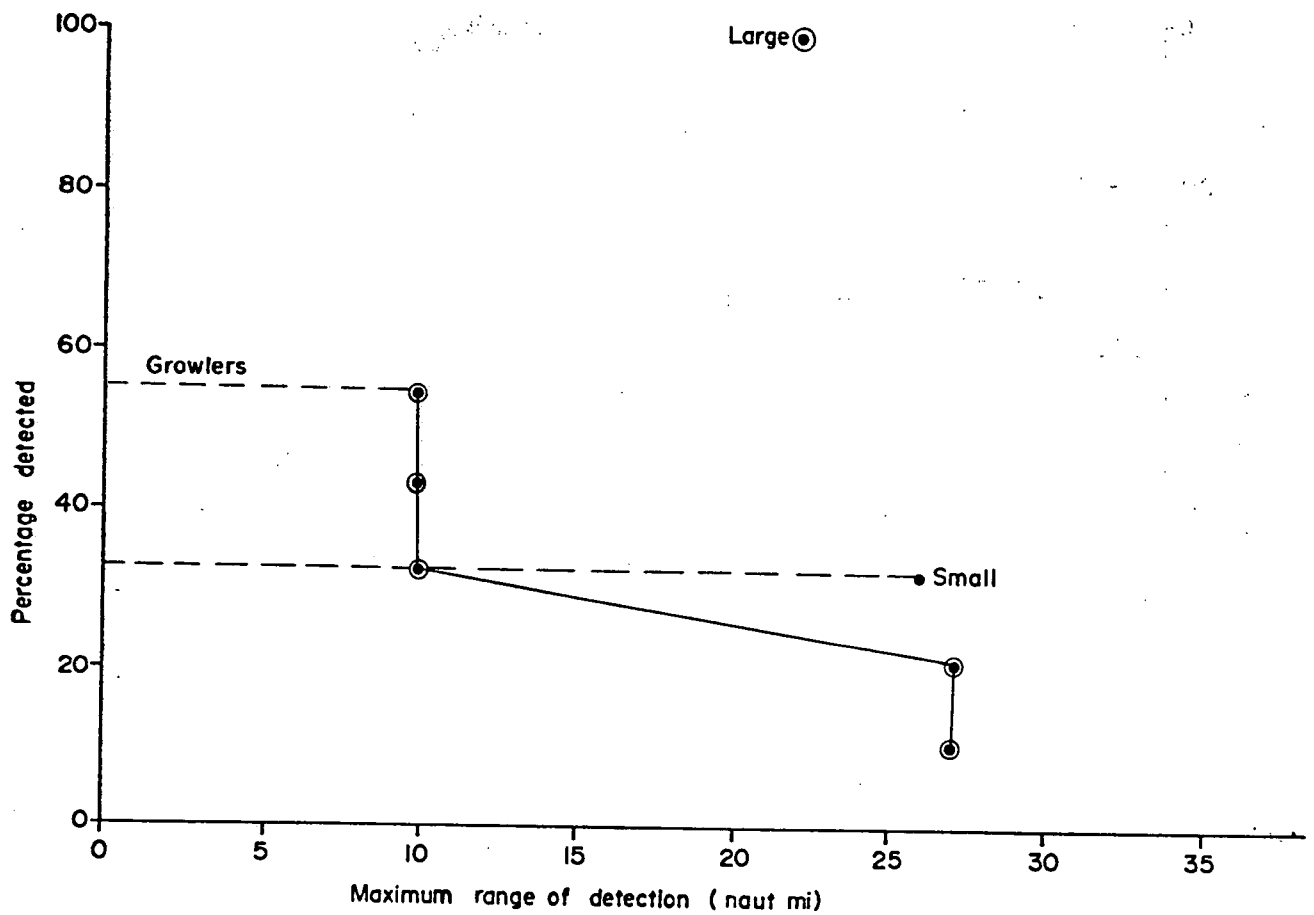


Figure 54. Observed radar performance for iceberg detection using pulse width B at 1500 ft altitude (5 May, 21 May, and 19 June 1987). Down clutter region only. Populations = Large(3), Medium(0), Small(3), Bergy bits(0), Growlers(9).
 Wind: 10-25kt Hw: 0.5-1.0m Hw₁: 1.0-2.0m

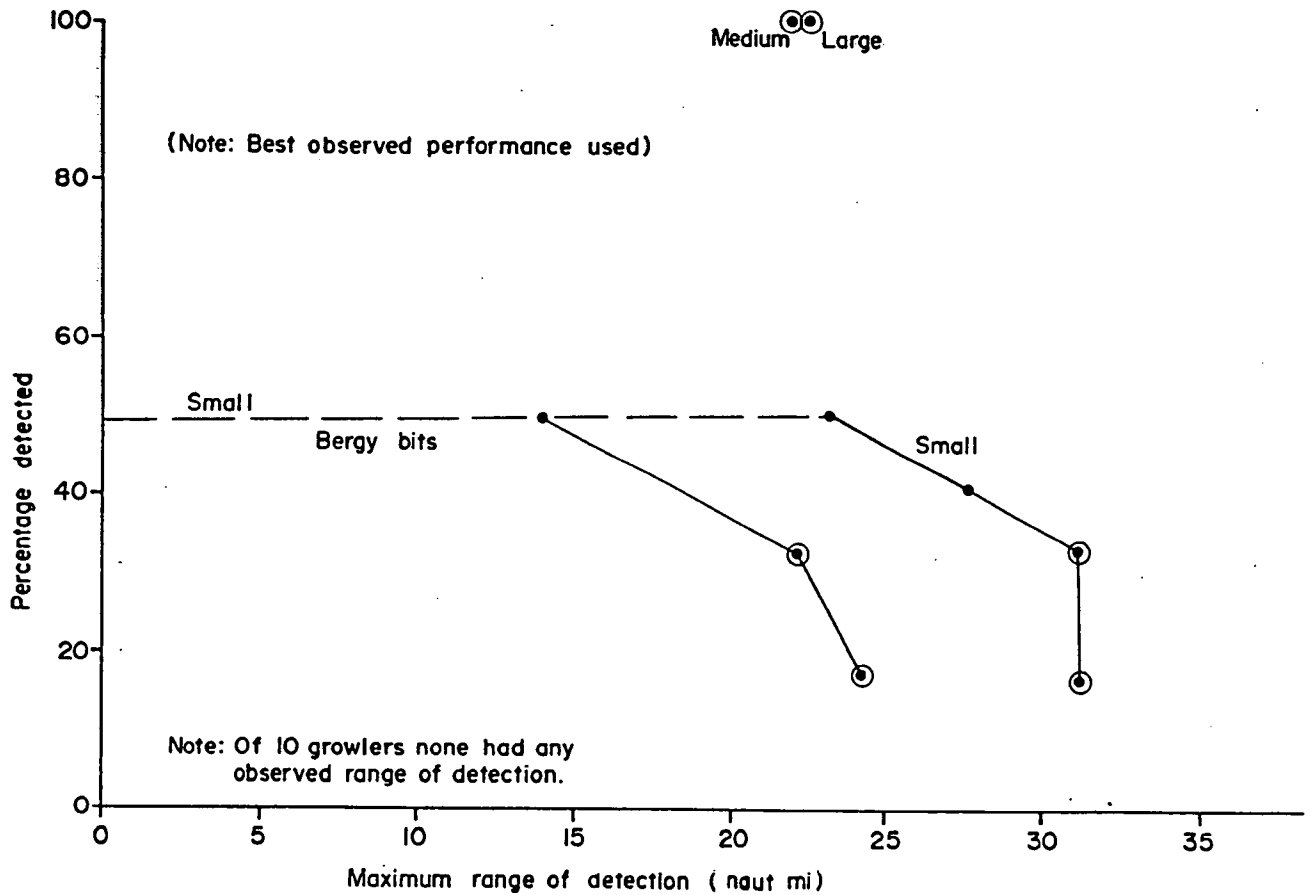


Figure 55. Best observed radar performance for iceberg detection using pulse width A at > 500 ft altitude (5 May, 21 May, and 19 June). Down clutter region only.

Populations = Large(3), Medium(6), Small(6), Bergy bits(6), Growlers(10).

Wind: 10-25kt Hw: 0.5-1.0m Hw₁: 1.0-2.0m

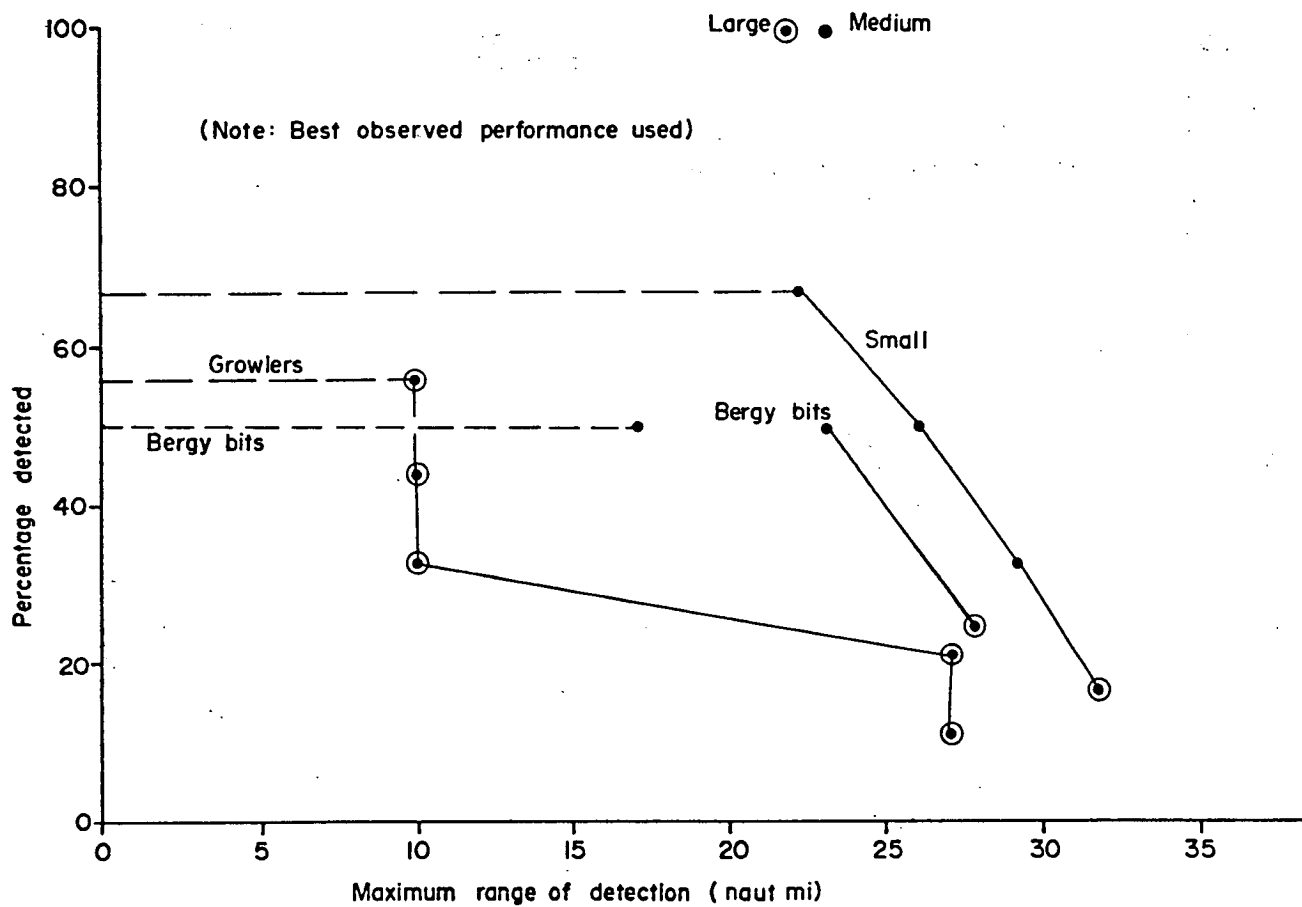


Figure 56. Best observed radar performance for iceberg detection using pulse width B at >500 ft altitude (5 May, 21 May, and 19 June). Down clutter region only. Populations = Large(4), Medium(5), Small(6), Bergy bits(4), Growlers(9).

Wind: 10-25kt Hw: 0.5-1.0m Hw₁: 1.0-2.0m

was 10 to 25 kt.

The tabulated results for 14, and 15 May and 22 June are given in Table 30. Again only the down-clutter region is being considered. For pulse A and 500-ft altitude (Figure 57), detection of small icebergs was 80% (four of five) and detection of bergy bits was 50% (two of four). For pulse B at the same altitude (Figure 58), 100% of four small icebergs were detected. Of four bergy bits, 75% were undetected outside 12.5 to 14.0 naut mi, indicating observed performance for bergy bits to be worse than for pulse width A. Of four growlers, two were observed down clutter to be undetected outside 8 naut mi.

Figures 59 and 60 illustrate the best observed radar performance for altitudes above 500 ft (derived in the same fashion as the previous case). Neither suggests any substantial improvement over the corresponding pulse width at 500 ft. From observed performance on 14, and 15 May, and 19 June, the best combination for bergy bit detection is pulse width A at 500 ft. For small icebergs, pulse width B at 500 ft provided better performance, although it was never used on the small iceberg missed with pulse A.

These flights occurred with Hw (wind-wave) between 1.0 and 2.5 m, Hw₁ (swell) between 0 and 2.0 m, with wind speeds between 15 to 35 kt.

Frequency agility and scan integration were earlier observed to suppress sea clutter on the radar display. How does this combination affect only the target? If there is an adverse trend it should be evident from cases of noise-limited detection when the target radar cross-section does not have to compete with sea clutter.

TABLE 30

Tabulated maximum range of detection, 14 May, 15 May, and 22 June

Iceberg size class	Range of detection from 500 ft (naut. mi.)				Range of detection from 1,000 ft (naut. mi.)				Range of detection from 1,500 ft (naut. mi.)			
	FWA ^a		FWB ^b		FWA		FWB		FWA		FWB	
	Rdn/F	Rup/cross ⁴	Rdn	Rup/cross	Rdn	Rup/cross	Rdn	Rup/cross	Rdn	Rup/cross	Rdn	Rup/cross
Large	>18.5-8.0	—	>32.0-10.0	—	—	—	>27.0-2.4	—	—	—	—	—
	>37.0-21.0	>31.0-10.5	>32.0-21.0	—	—	—	>36.0-30.5	—	—	—	—	—
	>16.0-4.0	—	—	—	—	>33.0-15.0	—	—	—	—	—	—
	>24.0-12.0	—	—	—	—	>11.0-7.5	—	>39.5-12.0	—	—	—	—
	—	—	—	—	>29.0-14.5	—	>37.0-7.5	—	—	—	—	—
	>12.5-4.0	—	>25.5-13.0	—	—	—	>34.0-22.5	—	—	—	—	—
	—	>24.0-15.0	>19.0-13.0	>16.5-12.0	—	—	>25.0-12.0	>25.0-21.5	—	—	—	—
	>25.0-2.0	>30.6-2.0	—	—	—	—	—	—	—	—	—	—
	—	>29.5-6.0	—	—	—	—	—	—	—	—	—	—
	—	—	—	—	—	—	—	—	—	—	—	—
Medium(a)	—	>27.0-10.0	—	>29.0-5.0	—	—	—	—	—	—	—	>30.0-8.0
	—	=37.0-12.0	—	>33.0-5.0	—	—	—	—	—	>23.5-10.0	—	>17.0-6.5
	(c)>30.0-24.0	—	>6.0-24.0	—	—	—	>36.0-22.4	—	>28.0-24.5	—	>44.0-28.5	—
	>20.0-16.5	—	>30. -16.5	—	—	—	>30.0-9.7	—	—	—	—	—
	>13.0-4.0	—	—	—	—	—	—	—	—	—	—	—
	—	—	—	—	>36.5-19.0	—	>41.5-10.0	—	—	—	—	—
	—	—	—	>22.0-3.0	—	—	>25.0-15.5	<2.0-20.5	—	—	—	—
	>9.5-6.0	>17.0-13.0	>20.0-5.5	—	—	—	>25.0-8.0	<17.0-20.0	—	—	—	—
	—	—	>25.5-9.5	—	—	—	—	—	—	—	—	—
	—	>28.5-20.0	>17.0-13.0	>20.0-16.0	—	>26.0-14.0	>25.0-7.5	>25.0-19.0	—	—	—	—
=27.6-13.0	=34.5-12.0	—	—	—	—	—	—	—	—	—	—	
—	=30.5-7.0	—	—	—	—	—	—	—	—	—	—	
>23.2-5.0	>19.5-8.0	>31.0-11.5	—	—	—	—	—	—	—	—	—	

(Same Icebergs at 3500 ft)

(a)
(b)
(c)

Table 30 (continued)

Iceberg size class	Range of detection from 500 ft (naut mi)			Range of detection from 1,000 ft (naut mi)			Range of detection from 1,500 ft (naut mi)				
	FWA ^a	FMB ^b	FMA	FWA	FMB	FMA	FWA	FMB	FMA		
	Rdwn	Rup/cross	Rdwn	Rup/cross	Rdwn	Rup/cross	Rdwn	Rup/cross	Rdwn	Rup/cross	
Small	< 6.0-28.0	—	—	< 4.0-32.5	—	< 2.0-16.0	—	—	—	—	
	—	—	>12.4- 7.8	>29.0-12.4	< 2.0-16.5	—	—	—	—	—	
	—	—	< 2.0-21.0	—	—	—	—	—	—	—	
(d)	>21.0- 8.5	>16.0- 8.5	>28.0-23.0	—	—	—	—	—	—	—	
(e)	—	—	>20.0- 8.0	>12.0- 3.0	>32.0-20.0	>21.0- 9.6	—	—	—	<22.5-44.5	
	—	—	—	—	>27.0- 3.0	—	—	—	—	—	
	>21.0-17.0	>29.0-17.0	>26.0-22.0	—	—	—	—	—	—	—	
	>25.0- 3.0	=30.0-20.5	—	—	—	—	—	—	—	—	
	(Same Icebergs at 3500 ft)										
				FWA			FMB				
				Rdwn	Rup/cross	Rdwn	Rup/cross	Rdwn	Rup/cross	Rdwn	Rup/cross
Bergy(f)	—	< 4.0-27.5	< 5.5-12.5	< 2.0-28.5	—	—	< 3.5-10.5	—	< 7.0-29.0	—	—
Bit (g)	>16.5- 5.9	>16.4-13.0	—	—	—	—	—	—	—	—	—
	< 0. -10.0	—	<10.0-21.0	—	—	—	—	—	—	—	—
	< 6.0-25.0	< 4.0-16.0	<14.0-33.0	—	< 2.0-13.5	<21.5-33.0	—	—	—	—	—
	—	=15.3† 1.0	< 1.0- 3.0	< 1.0-16.5	—	—	—	—	—	—	—
	—	< 3.0-31.4	—	<19.5-27.0	—	—	—	—	—	—	—
	—	< 4.5-16.5	—	—	—	—	—	—	—	—	—
	(Same Icebergs at 3500 ft)										
				FWA			FMB				
				Rdwn	Rup/cross	Rdwn	Rup/cross	Rdwn	Rup/cross	Rdwn	Rup/cross
(f)				—	< 6.0-34.0	—	—	—	<17.0-25.0	—	—
(g)				=13.6- 3.7	< 4.5-21.0	<10.0-18.0	—	—	—	—	—

Table 30 (continued)

Iceberg size class	Range of detection from 500 ft (naut mi)			Range of detection from 1,000 ft (naut mi)			Range of detection from 1,500 ft (naut mi)			
	FWA ^a		FMB ^b	FWA		FMB	FWA		FMB	
	Rblw ^c	Rup/cross ^d	Rblw	Rup/cross	Rblw	Rup/cross	Rblw	Rup/cross	Rblw	Rup/cross
Growlers	—	< 2.0-28.0	< 8.0-15.0	< 2. -27.0	—	< 0. -11.0	—	< 4. -31.5	—	<14. -22.0
	—	< 2.0-28.0	< 8.0-15.0	< 2. -27.0	—	< 0. -11.0	—	< 4. -31.5	—	<14. -22.0
	—	< 2.5-24.0	< 1.0- 3.0	< 1. -16.5	—	—	—	—	—	—
	—	< 2.5-24.0	< 1.0- 3.0	< 1. -16.5	—	—	—	—	—	—

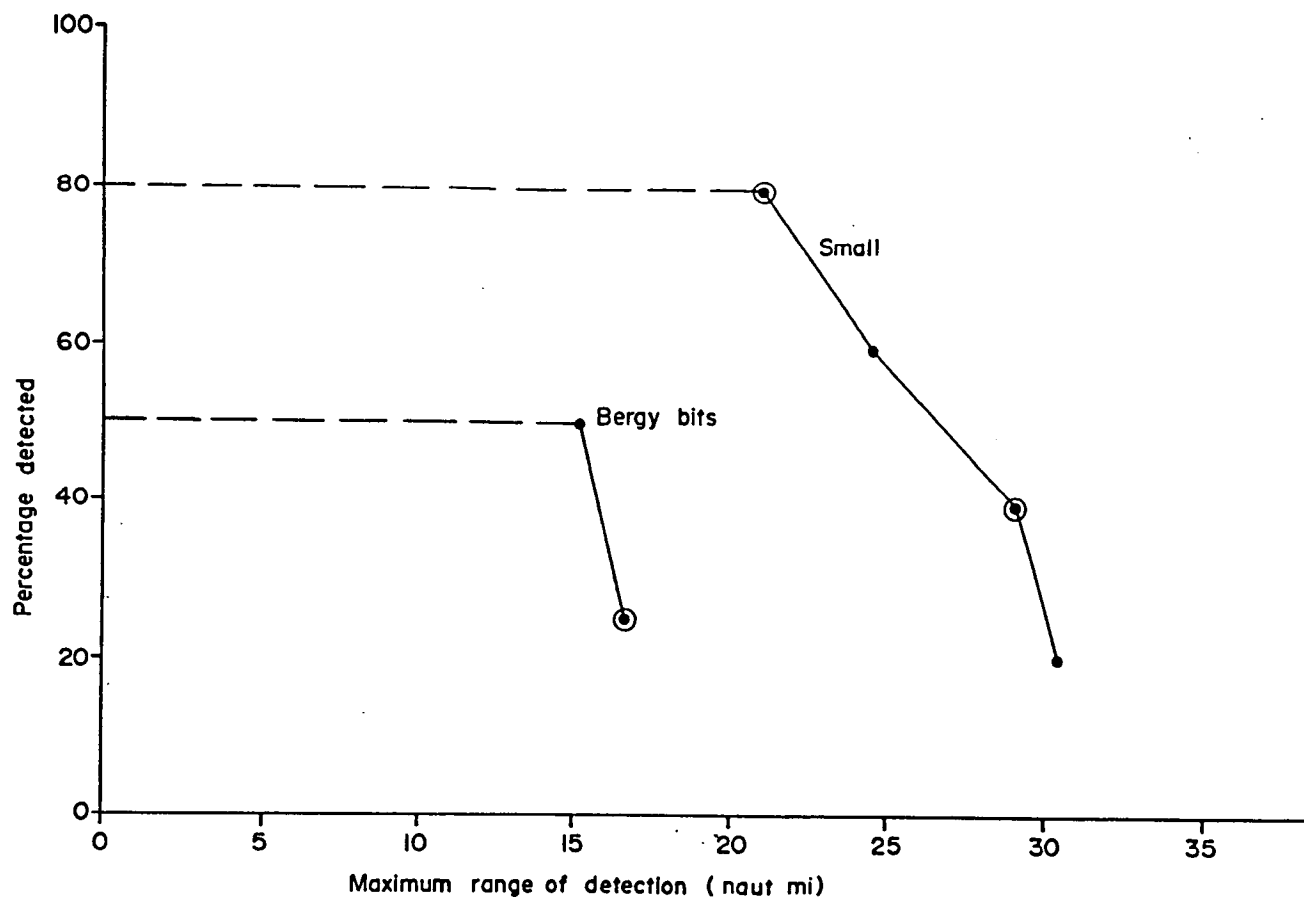


Figure 57. Observed radar performance for iceberg detection using pulse width A at 500 ft altitude (14 May, 15 May, and 22 June). Down clutter region only. Populations = Large(0), Medium(0), Small(5), Bergy bits(4), Growlers(0). Wind: 15-35kt Hw: 1.0-2.5m Hw₁: 0.0-2.0m

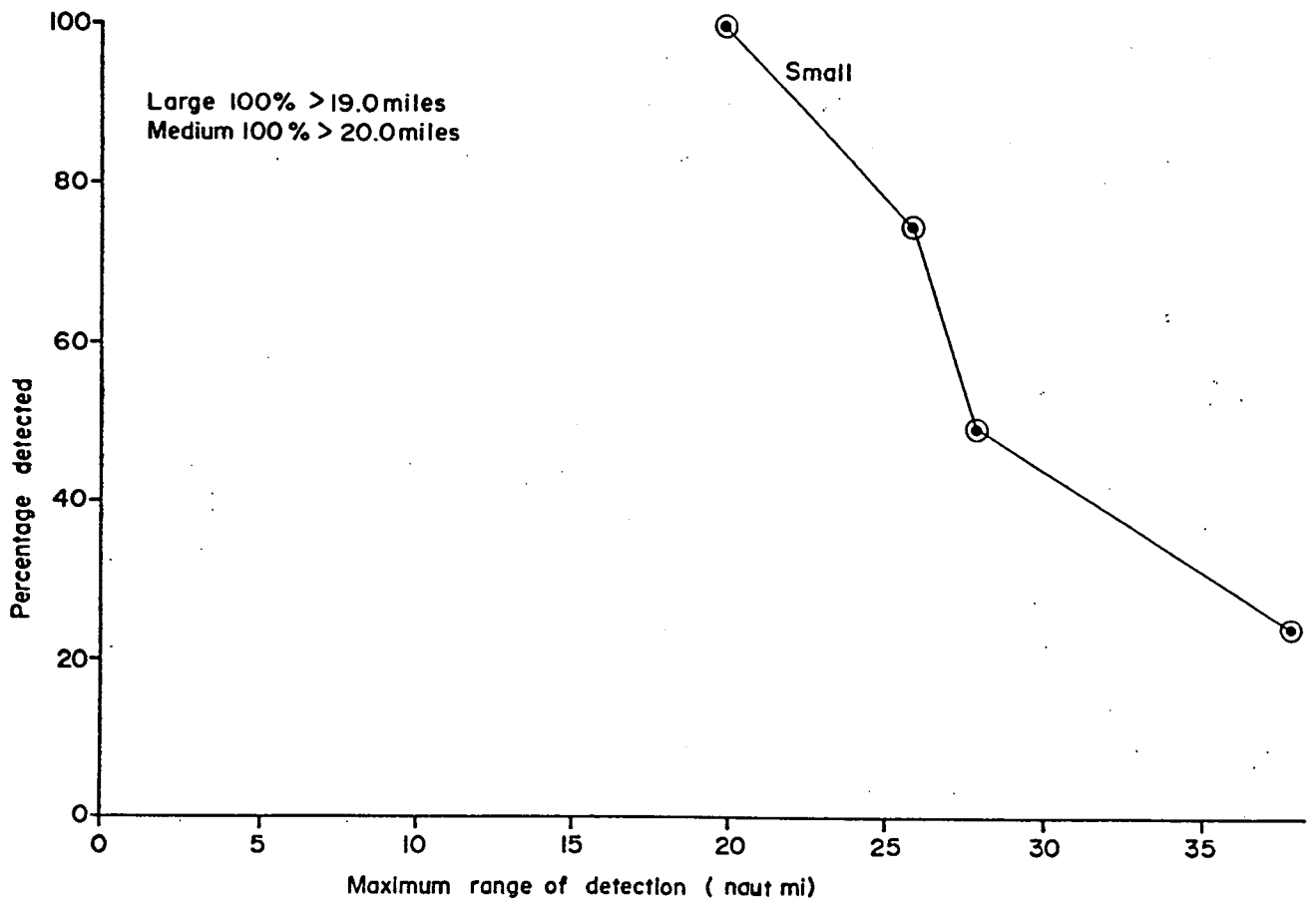


Figure 58. Observed radar performance for iceberg detection using pulse width B at 500 ft altitude (14 May, 15 May, and 22 June). Down clutter region only.
Populations = Large(4), Medium(9), Small(4), Bergy bits(4), Growlers(0).
Wind: 15-35kt Hw: 1.0-2.5m Hw₁: 0.0-2.0m

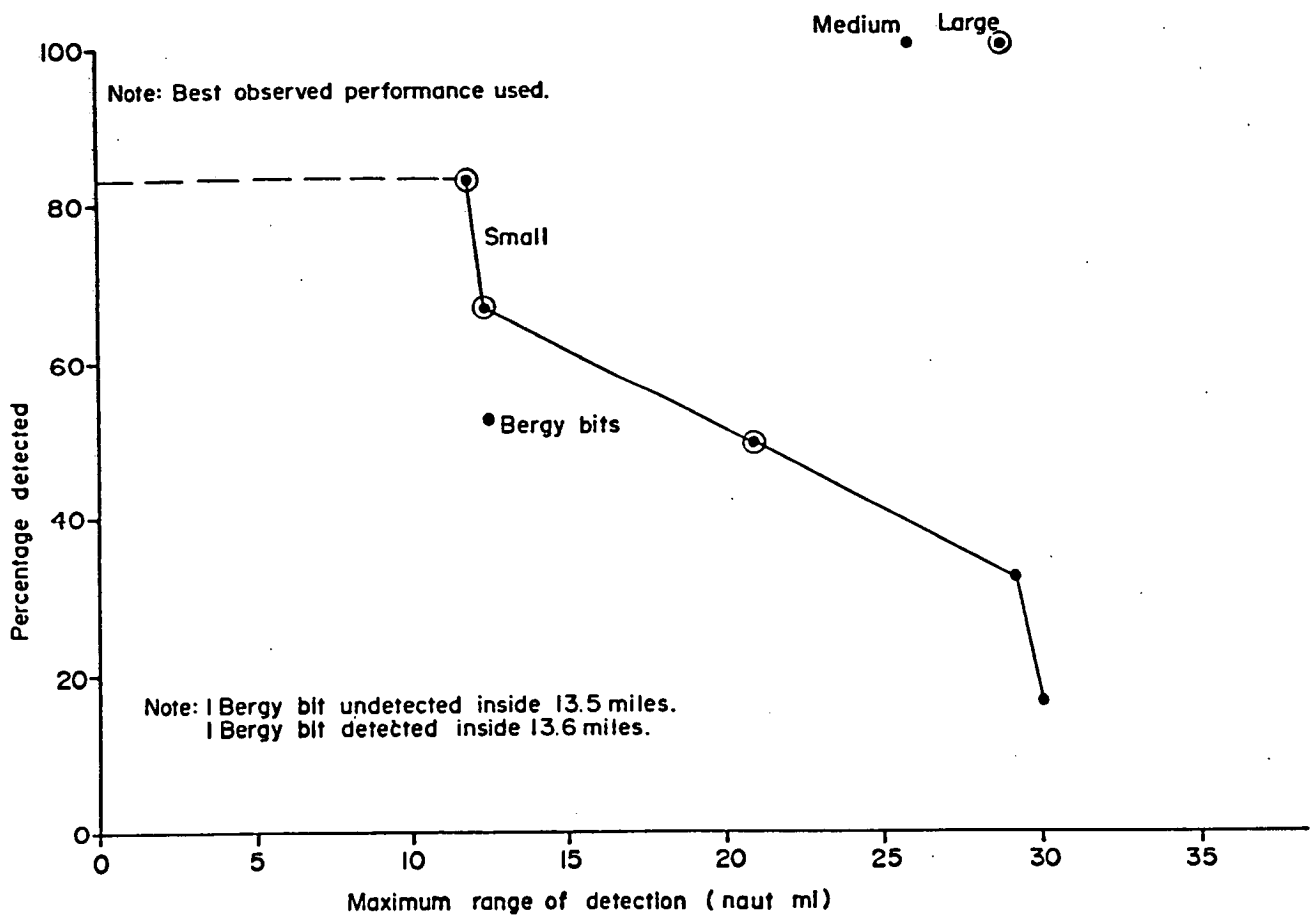


Figure 59. Best observed radar performance for iceberg detection using pulse width A at >500 ft altitude (14 May, 15 May, and 22 June). Down clutter region only.
 Populations = Large(2), Medium(6), Small(6), Bergy bits(2), Growlers(0).
 Wind: 15-35kt Hw: 1.0-2.5m Hw₁: 0.0-2.0m

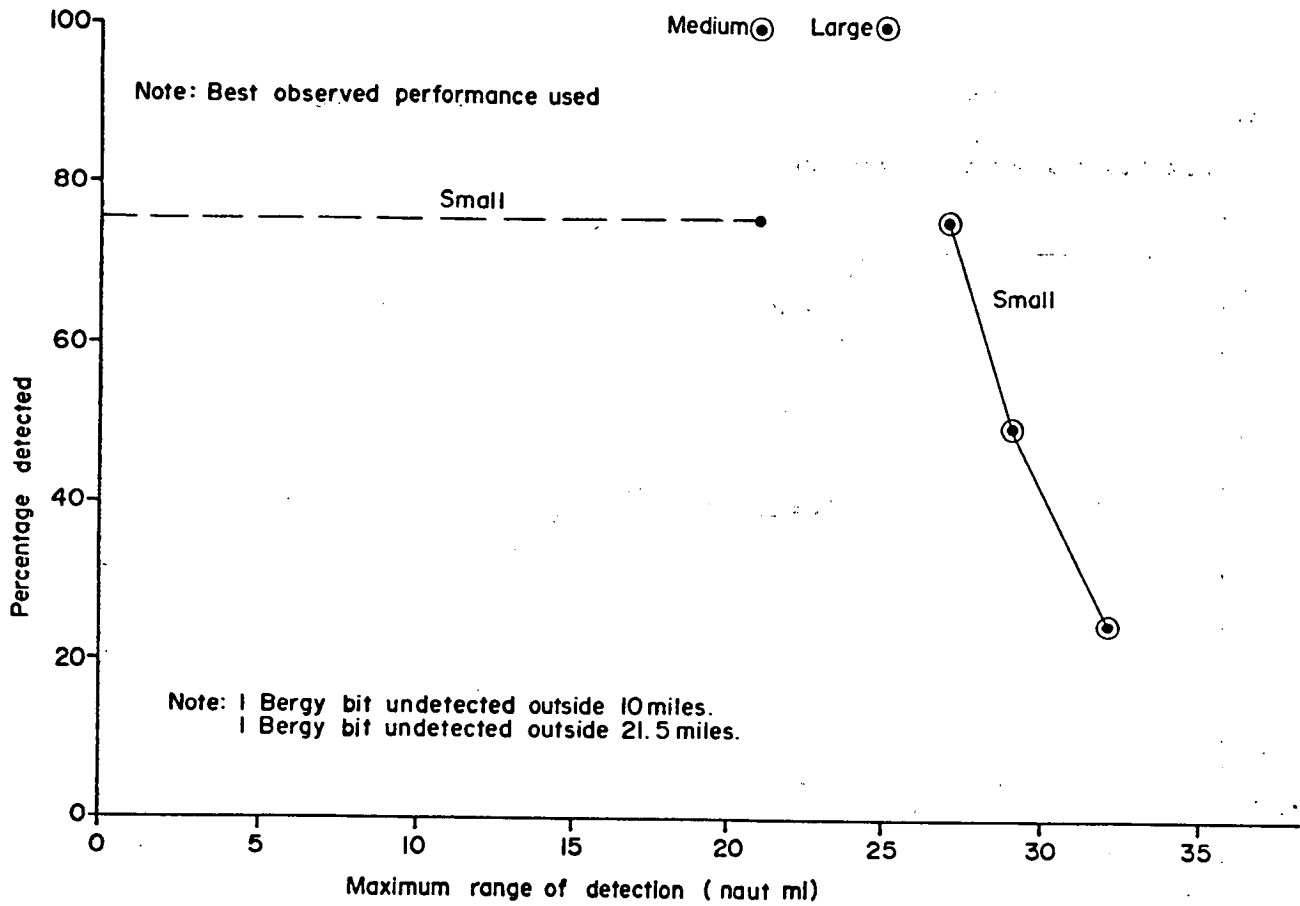


Figure 60. Best observed radar performance for iceberg detection using pulse width B at >500 ft altitude (14 May, 15 May, and 22 June). Down clutter region only. Populations = Large(6), Medium(8), Small(4), Bergy bits(2), Growlers(0). Wind: 15-35kt Hw: 1.0-2.5m Hw₁: 0.0-2.0m

In a limited number of cases two runs were completed, one with and one without the described processing options. Table 31 lists four cases that occurred on 9 June 1987 for which detection was noise-limited. Maximum range of detection is tabulated for pulse width A as a function of fixed frequency transmission (F-8), with no scan integration versus agile frequency transmission (AG1) and scan integration (SS, slow rise, slow decay).

No distinguishable trend suggests that if scan integration and frequency agility affect noise-limited detection, the effect is smaller than other factors at work.

TABLE 31
Range of detection comparison

Iceberg type	Ref. no.	Mode	Maximum range (naut mi)	Mode	Maximum range (naut mi)
Bergy bit	4A	AG1-:SS	=17.5	F-8-:-	=15.7, =17.4
Bergy bit	7	AG1-:SS	=13.0	F-8-:-	=12.1, =15.9
Small	4	AG1-:SS	>22.7	F-8-:-	=17.8, >21.0
Small	5	AG1-:SS	>23.5	F-8-:-	>19.0, =21.0

CONCLUSIONS

From results for conditions when sea clutter is not a problem ($H_w = 0.0 - 0.5$ m, $H_{w1} = 1.5$ m, wind speed = 5-15 knots), the radar with pulse width A at an altitude of 500 ft gave the best combined detection of bergy bits and small icebergs. Using pulse width B at 1,500 ft, the radar gave the best detection of small icebergs, and lack of data prevents making an

assessment of its capability for bergy bit detection. Growler detection was observed to be poor for both pulse widths at 500 ft. For clutter-limited detection, the down-clutter region is the best side of the radar screen, whereas the up-clutter region is the worst. The following remarks refer to the down-clutter region.

At the transition to where sea clutter starts to limit detection, ($H_w = 0.5 - 1.0$ m, $H_{w1} = 1.0 - 2.0$ m, wind speed = 10 to 25 kt), the radar performed poorly at altitudes above 500 ft compared with 500 ft. Using pulse A at this altitude demonstrated the best combined bergy bit and small iceberg detection capability of the radar whereas pulse B at the same altitude had a longer range detection of small icebergs, but a slightly poorer percentage of detection. Insufficient data prevent making an assessment of the bergy bit detection capability of the radar on pulse B. Growler detection is expected to be poor at 500 ft. For the strongest sea clutter conditions observed, ($H_w = 1.0 - 2.5$ m, $H_{w1} = 0 - 2.0$ m, wind speed = 15 to 35 knots) no obvious improvement in detection was observed using altitudes above 500 ft. At 500 ft, pulse width A gave the best observed combined detection of bergy bits and small icebergs. Pulse width B gave better observed detection of small icebergs. Detection of growlers by the radar was not observed with either pulse width at 500 ft.

RADAR SIGNAL ANALYSIS

The digitally recorded radar signal data collected during the program has been analysed to provide reference points for the observed performance analysis and scientific data on the radar cross-sections of icebergs and ocean. The following subsections present the results of the radar calibration and radar cross-section statistics of selected icebergs and ocean targets. The present program provided only for the analysis of a portion of the collected data. All digital data recordings are presently stored at Sigma Engineering Limited. Data were analysed to investigate the effects of pulse length, altitude, and frequency agility on iceberg radar cross-sections. In addition, ocean sea clutter data are presented for a selected event. A discussion is provided on the effects of pulse length and grazing angle. The last subsection provides a discussion on the effects of multi-path propagation and frequency agility and how they may alter the effective radar cross-section seen by the radar.

RADAR SYSTEM CALIBRATION

The radar system, including the recording system, was calibrated using the procedure described earlier in Part II (Radar Signal Data Acquisition). Table 32 summarizes the radar parameters used for the analysis. Appendix II-B contains the results of the injected power versus output digital voltage measurements as well as the set of STC curves. As examples, Figure 61 provides the calibration curve for the 30.0- μ s pulse and Figure 62 provides the STC curve for an intermediate setting.

TABLE 32

Radar parameters used for analysis

Frequency	8.9-9.4 GHz		
Transmitter power	8 kW		
Uncompressed pulse length	0.20 μ s	30 μ s	10 μ s
Compressed pulse length	0.20 μ s	0.20 μ s	0.03 μ s
Processing gain ^a	0 dB	17.5 dB	23.8 dB
Pulse Compression Gain ^b	0 dB	21.7 dB	25.2 dB
Receiver noise figure	5 dB		
Polarization	horizontal		
Peak antenna gain	32 dB		
Antenna horizontal beamwidth	2.3°		
Antenna vertical beamwidth	7.0°		
System losses	1.6 dB		

^a Processing gain was calculated from measurements made of calibrated radar targets and must be used with calibration curves for each pulse to calculate received power.

^b Calculated as the ratio of uncompressed pulse length to compressed pulse length.

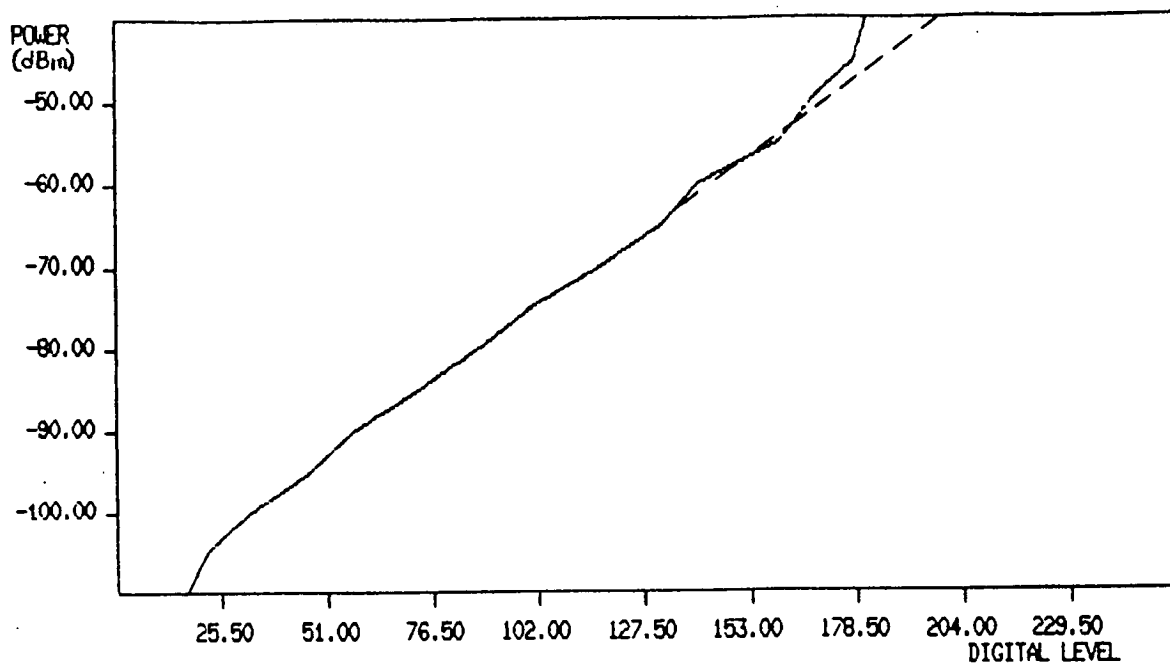


Figure 61. Receiver calibration curve for the 30- μ s compressed pulse.

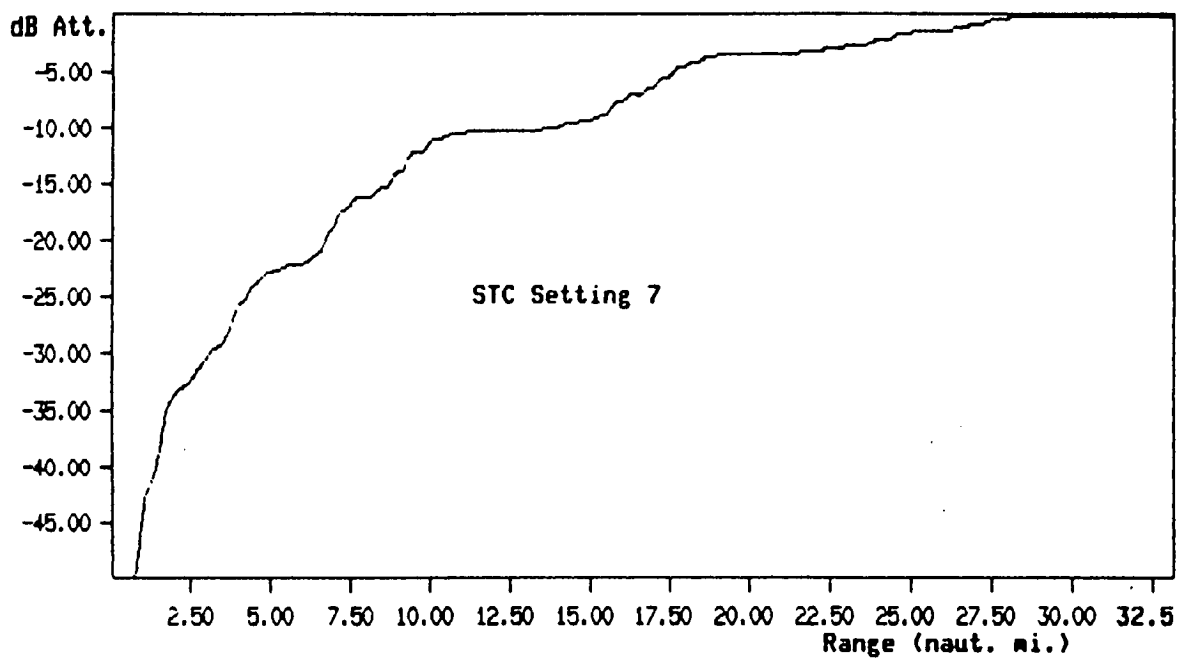


Figure 62. Sensitivity time control (STC) curve for an intermediate setting.

The free-space radar cross-sections for the 10 m^2 reference target were extracted from the radar signal data using the $0.2\text{-}\mu\text{s}$ uncompressed pulse data. A cross-section was calculated from the maximum received power on each scan. These cross-sections are presented as a cumulative radar cross-section (RCS) probability distribution in Figure 63. The average cross-section was calculated to be 7.3 m^2 with a maximum of 64.1 m^2 . The 7.3 m^2 average was used with data recorded on the reference target using the two compressed pulses to derive processing gains (not equivalent to pulse compression gain) for each of the compressed pulses. The processing gain is defined here as the ratio of the calculated average radar cross-section of the reference target using the compressed pulse to the calculated radar cross-section using the $0.2\text{-}\mu\text{s}$ uncompressed pulse. This method assumes the average radar cross-section of the reference target will be the same for all three radar pulses. The processing gains were calculated to be 17.5 dB for the $30.0\text{-}\mu\text{s}$ pulse and 23.8 dB for the $10.0\text{-}\mu\text{s}$ pulse. These processing gains must be used with the calibration curves for each pulse to calculate received power.

Figures 64 and 65 present the RCS probability distribution for the reference target using the 10- and $30\text{-}\mu\text{s}$ pulse data with the processing gain removed. These figures are useful for comparing the probability distributions. It may be seen from Figure 63 that the $0.2\text{-}\mu\text{s}$ pulse data on the target tends to follow the negative exponential (Swerling Case 1) distribution plotted on the same figure whereas Figures 64 and 65 for the compressed pulses demonstrate some deviation from these statistics, with distributions having much longer tails typical of log-normal statistics. The negative exponential distribution was generated using the mean of the data.

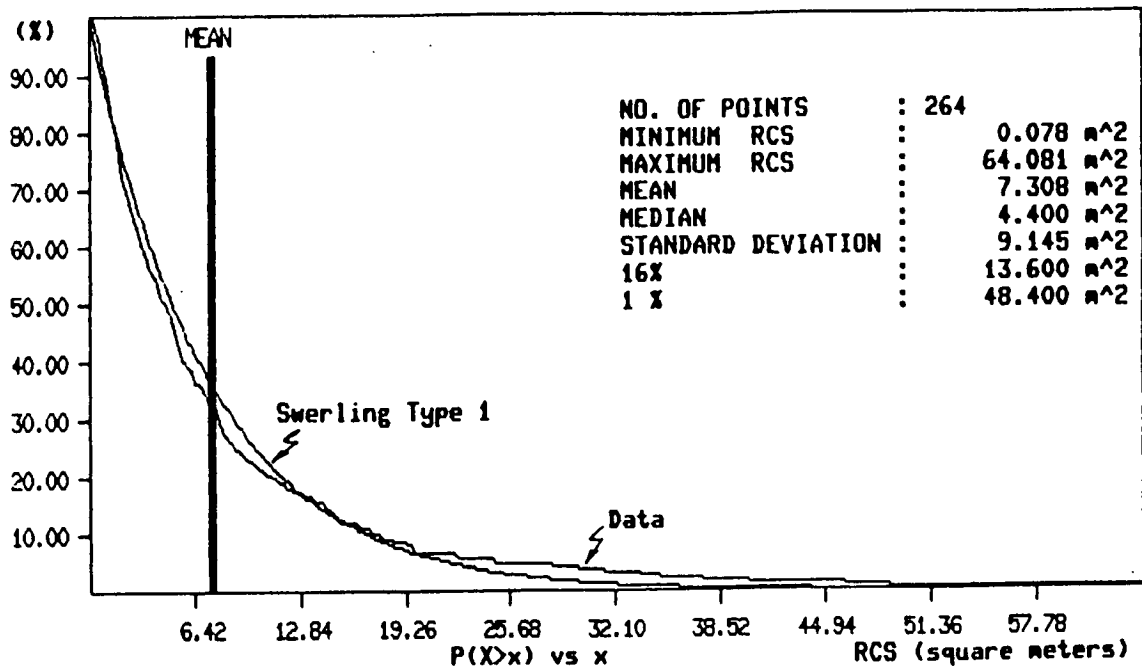


Figure 63. Cumulative radar cross-section probability distribution for a reference target using the 0.20- μ s pulse and fixed frequency operation.

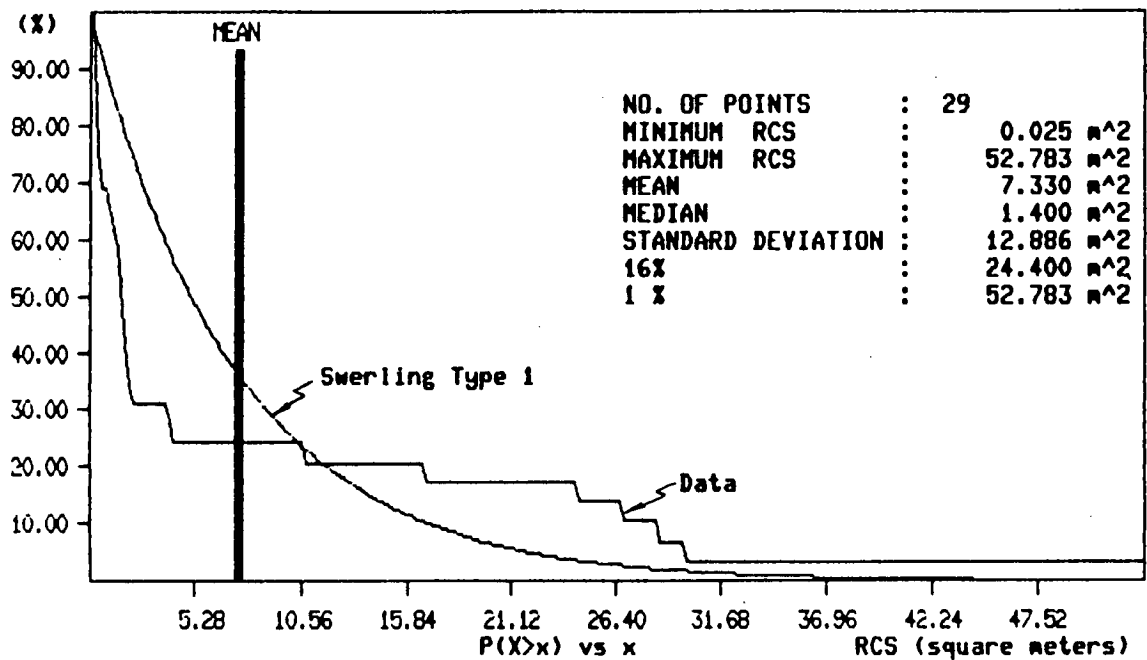


Figure 64. Cumulative radar cross-section probability distribution for a reference target using the 10.0- μ s pulse and fixed frequency operation.

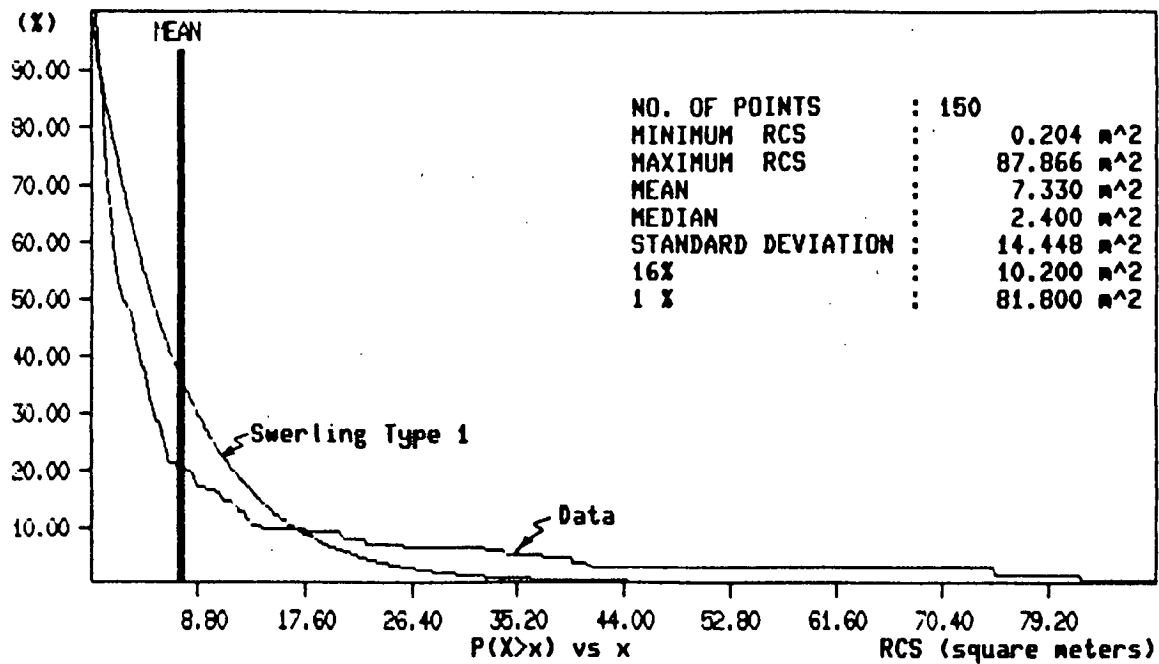


Figure 65. Cumulative radar cross-section probability distribution for a reference target using the 30.0- μ s pulse and fixed frequency operation

In these figures calculated points on the probability distribution of the data are provided. The 16% and 1% points on the distribution correspond to the points above which the probability of a radar cross-section occurring is 16% and 1%.

ICEBERG RADAR CROSS-SECTIONS

Data for seven iceberg targets, mostly bergy bits, have been analysed. The data were selected for analysis to investigate the effect of pulse length, altitude (grazing angle), and frequency agility on iceberg radar cross-section and its distribution. During data collection only one variable was purposely changed, however, as the data collection sequence takes time to complete it is possible that although the flight path was the same for two passes by an iceberg, a different aspect of the iceberg may be seen by the radar if the iceberg is rotating. To increase the confidence in the comparisons among the parameters, at least two icebergs were considered for each parameter combination. Table 33 summarizes the results of the analysis providing the significant radar cross-section statistics obtained for each target and parameter combination.

Data from a small iceberg and two bergy bits were used for the pulse length comparison (see targets 1,2, and 3 in Table 33). In all cases the 30.0- μ s pulse (15-m range resolution) gave an average radar cross-section two to three times larger than the 10.0- μ s pulse (4.5- m range resolution). This advantage for the 30.0- μ s pulse could be caused by the radar range resolution. Target 2 in Table 33 has a range dimension of 15 m, one-half the 30- m resolution size of the 30.0- μ s pulse.

TABLE 33

Summary of iceberg radar cross-section statistics, APS-504(V)5

Target No.	Iceberg class	Size(m) (LxWxH)	Parameters ^a	Min. (m ²)	Max. (m ²)	Mean (m ²)	50% (m ²)	S.D. (m ²)	16% (m ²)	1% (m ²)
1	Small	35x28x10	10/F-8/500	0.110	159.1	12.7	3.5	24.6	18.0	159.1
			30/F-8/500	0.500	177.9	26.6	17.0	28.5	43.5	129.5
			30/AG1/500	1.600	179.5	28.8	21.0	29.4	48.0	178.5
2	Bergy Bit	15x15x5	10/F-8/500	0.002	34.7	3.2	0.6	6.8	4.4	34.7
			30/F-8/500	0.040	218.6	11.5	5.0	22.4	20.0	73.5
			30/AG1/500	2.500	190.3	28.4	18.5	33.5	42.5	188.0
3	Bergy Bit	-	10/F-8/500	0.010	1.9	0.3	0.03	0.5	0.9	1.9
			30/F-8/500	0.020	9.7	0.9	0.40	1.5	1.6	9.7
4	Bergy Bit	-	30/F-8/500	0.010	58.5	4.7	1.25	10.2	6.8	58.5
5	Bergy Bit	-	30/F-8/500	0.030	9.9	1.3	0.4	2.1	2.4	9.9
6	Bergy Bit	19x16x5	30/AG1/1500	0.310	68.0	12.1	8.8	11.5	20.8	68.0
			30/AG1/500	0.040	170.4	9.3	3.0	23.0	13.0	170.4
7	Bergy Bit	-	30/AG1/1500	0.080	12.7	1.0	0.5	1.9	1.7	12.7
			30/AG1/500	0.040	7.0	0.6	0.2	1.6	0.6	7.0

a. Pulse(μ s)/Frequency agility(F-8/AG1)/Altitude(ft).

However, the 10.0 μ s pulse covers, at most, one third of the iceberg's range dimension at a time. If the peak radar cross-section of the iceberg is proportional to the area illuminated, then the radar cross-section of the target could change significantly when changing pulse length. This effect would be reduced if a significant portion of the energy is reflected from the iceberg's front face, as may be the case for blocky icebergs. However, a wedge- or dry dock-shaped iceberg, with multiple reflectors viewed by the radar at different ranges within the resolution cell, could exhibit a peak cross-section dependent on pulse length. Figures 66 and 67 present the cumulative RCS probability distribution for target 2 of Table 33 for 10.0- μ s and 30.0- μ s pulses respectively. Both show deviations from negative exponential statistics, with the 10.0- μ s pulse showing the greatest deviation.

It should be noted that for the small iceberg (Target 1), having a range dimension greater than 30 m, the difference in cross-section between pulse lengths is only a factor of 2 for fixed frequency operation while the range resolution differs by a factor of 7. This would seem to indicate that the dominant scattering from this iceberg is not from the whole range resolution but from a smaller portion probably the face of the iceberg. In addition, as the azimuth dimension of the resolution cell varies from about 400 m at 5 naut mi to 1,200 m at 15 naut mi it is not appropriate to use the extended target form of the radar equation for this analysis as the target data was collected over this range.

The effect of frequency agility is also illustrated in Table 33 for targets 1 and 2. The average radar cross-section of the small iceberg, target 1, changed very little when frequency agility was applied, whereas

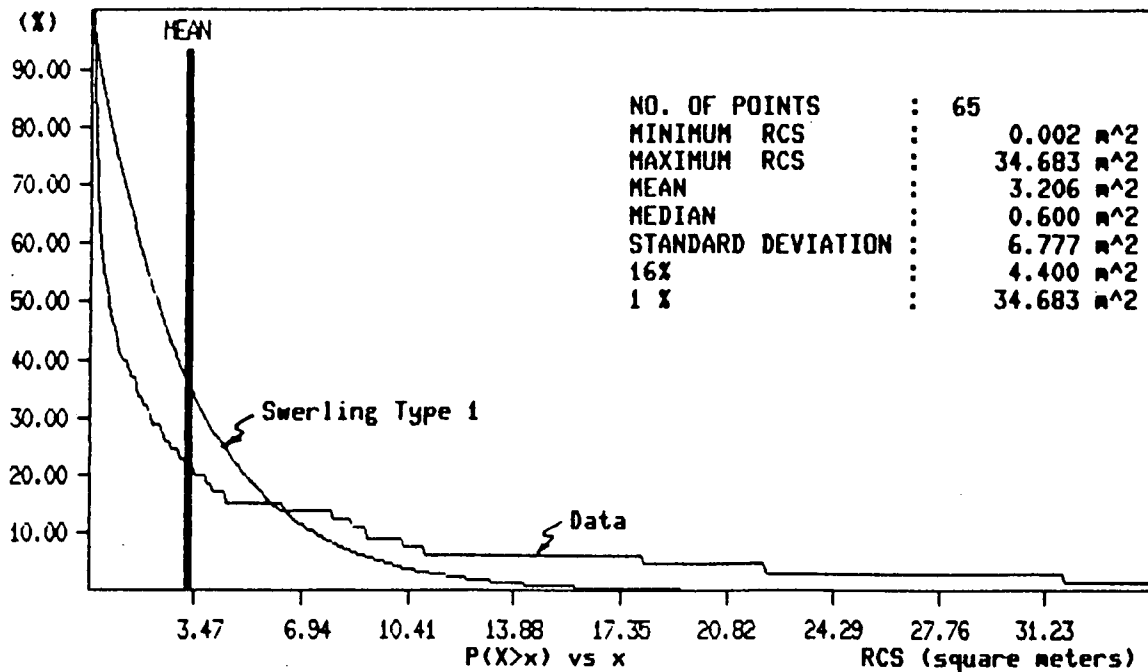


Figure 66. Cumulative radar cross-section probability distribution for a bergy bit using the 10.0- μ s pulse and fixed frequency operation (altitude of 500 ft.)

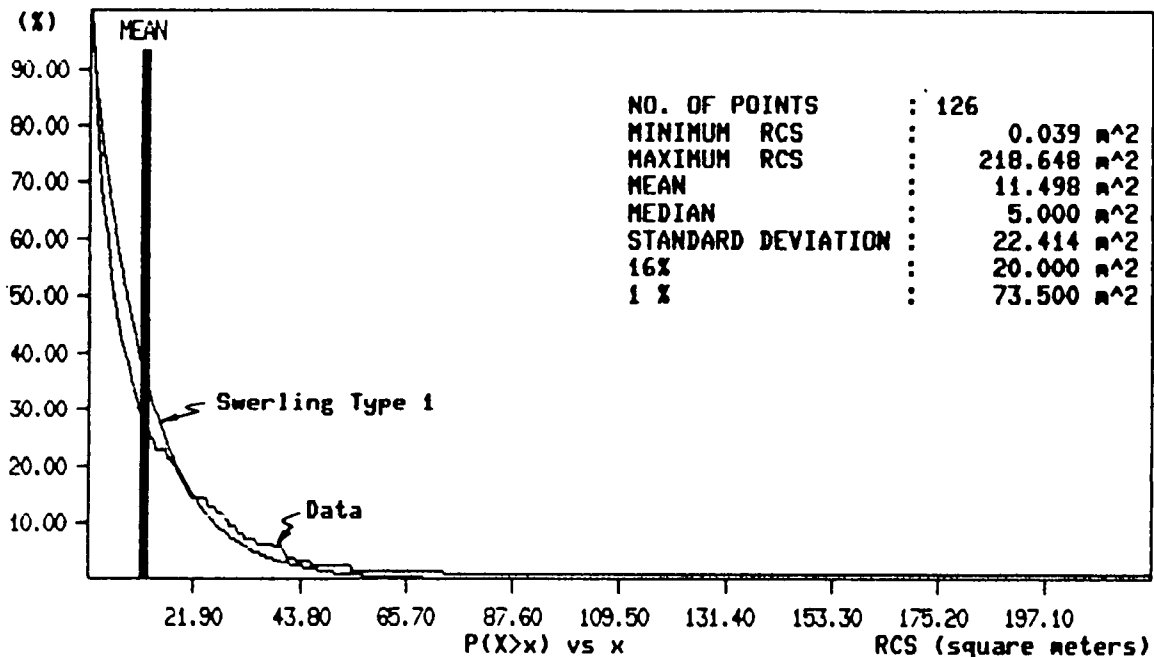


Figure 67. Cumulative radar cross-section probability distribution for a bergy bit using the 30.0- μ s pulse and fixed frequency operation (altitude of 500 ft.)

the bergy bit, target 2, showed a significant increase in average cross-section. The cumulative RCS probability distribution of Figure 68 compared to that of Figure 67 illustrates a significant change in target statistics for target 2 with frequency agility applied. The effects of frequency agility on radar cross-section are discussed further later.

The effect of altitude on radar cross-section was investigated using targets 6 and 7 of Table 33. A small advantage was seen for detection from the higher altitude in both cases, indicating a possible grazing angle effect.

In summary, the information on bergy bits presented in Table 33 shows average cross-sections over the range from 0.27 m^2 to 28.4 m^2 for a factor of 100 between the smallest and the largest. Using all the radar cross-sections calculated for this group the median cross section of this population is about 2 m^2 . This number may be biased on the high side considering that targets 2 and 6 were close to the small iceberg size classification. Radar pulse length does appear to effect the average radar cross-section seen by the radar and, furthermore, it appears to alter the cumulative RCS probability distribution. Higher radar cross-sections were seen in all the cases analysed when using the $30.0\text{-}\mu\text{s}$ pulse. While the radar cross-sections for the $30.0\text{-}\mu\text{s}$ pulse were observed to be larger than those obtained using the shorter $10.0\text{-}\mu\text{s}$ pulse, the difference is not significant enough to be wholly attributed to the difference in range resolution. A more in depth comparison between pulse lengths may be carried out by normalizing the radar cross-section to the area of the iceberg illuminated by the radar for each pulse. Frequency agility also appeared to have some effect on radar cross-section, with the

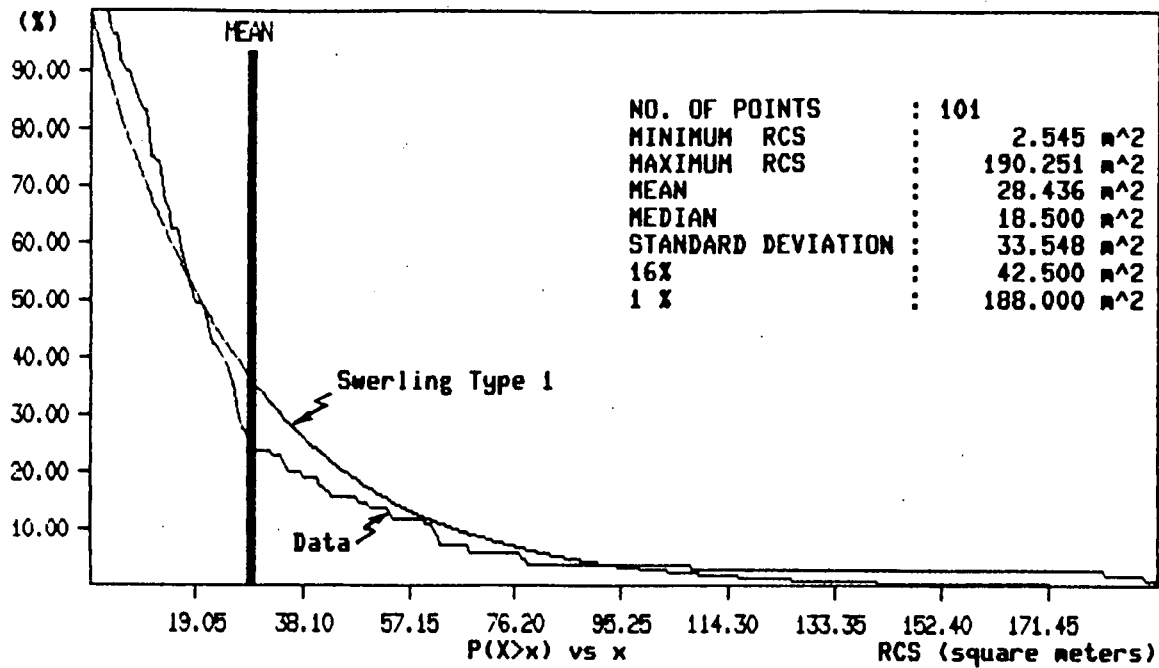


Figure 68. Cumulative radar cross-section probability distribution for a bergy bit using the 30.0- μ s pulse and frequency agility (altitude of 500 ft.)

analysis indicating that the cumulative RCS probability distribution changes significantly for the bergy bits considered. Comparison of the data collected at two altitudes gives a slight advantage to 1,500 ft over 500 ft.

Although these data illustrate some of the effects of the main radar operating parameters on iceberg radar cross-sections, analysis of more targets will be required before definitive statements can be made as to a preference for a particular operating mode. The results of the observed performance analysis should demonstrate any statistical significance in these parameters.

SEA CLUTTER STATISTICS

The APS-504 (V)5 was designed to detect small targets in sea clutter. To achieve this the clutter signal competing with the target signal is reduced by reducing the radar resolution cell. The received clutter power is proportional to the resolution cell size and the reflectivity of the ocean per unit area. The size of the resolution cell is governed by the radar pulse length and antenna beam width. The (V)5 provides resolution cell reduction over the (V)3 by reducing the pulse length. The alternative to reducing the pulse length is to reduce the horizontal beamwidth of the antenna by increasing its length, however, this change is usually not feasible because of the physical size constraints of an aircraft. It is assumed that the average backscatter from the ocean per unit area does not change as the area is changed, so that a decrease in the resolution cell area will cause a decrease in the sea clutter power received by the radar per resolution cell. As the target signal is

competing with adjacent clutter a decrease in this background clutter level will aid target detection. Unfortunately, as the resolution cell is decreased the sea clutter statistics change significantly, going typically from a Rayleigh type distribution (exponential cdf) to a long tailed distribution indicative of a log-normal distribution (Croney et al. 1975). As a result, the received signal from clutter may exhibit target-like spikes that may be difficult for the radar operator to handle. The design of the (V)5 incorporates various stages of signal processing to control these target-like false alarms. Scan-to-scan integration of the data is used to suppress or integrate out the spikiness of the sea clutter. The order of processing may influence the effectiveness of each stage and overall performance will be dependent upon the statistics of the sea clutter and the target.

During the study sea clutter data were collected on 11 different days using the two modes described earlier. The data may be used to derive ocean-normalized radar cross-section (NRCS) statistics that may aid in the development and optimization of radar signal-processing functions. Sea clutter data were analysed to investigate the effect of pulse length, grazing angle, and look-direction on NRCS statistics. Data were chosen for one of the higher sea states (sea state 5) encountered and were analysed to produce Table 34, in which data have been rounded to the nearest dB.

Comparison of the average (Mean) NRCS for the 0.2-, 30.0-, and 10.0- μ s pulses at a 2 degree grazing angle show a spread of no more than 2 dB for upwind and crosswind.

TABLE 34

Ocean normalized radar cross-section statistics for sea state 5

Pulse Orientation ^b length ^a (μ s)		Backscatter coefficient (dB below 1 m ² /m ²)																	
		2.0° grazing angle				1.0° grazing angle				0.3° grazing angle									
		Mean	50	10	1 .1 Max ^c	Mean	50	10	1 .1 Max ^c	Mean	50	10	1 .1 Max ^c						
0.20	up	31	31	29	28	27	26												
	cross	34	36	30	29	28	26												
	down	34	35	30	29	28	27												
30.0 (0.20)	up	31	33	28	25	22	22	32	32	29	28	26	25	41	42	38	33	28	28
	cross	36	36	33	29	27	24	37	38	34	29	28	27	45	47	42	39	34	28
	down	36	36	34	30	26	26	36	37	34	30	28	28	44	46	41	37	32	29
10.0 (0.03)	up	30	35	26	22	16	13	32	35	29	22	17	15	39	42	36	32	27	20
	cross	36	40	33	24	19	15	37	39	35	30	26	18	40	42	37	34	29	19
	down	37	41	34	26	22	15	39	40	36	32	28	23	40	42	37	33	30	26

a. Pulse length is given in microseconds(μ s) with the quantity in brackets indicating the compressed pulse length for pulse compression modes.

b. Orientation is with respect to maximum sea clutter return.

c. Table values are mean and cumulative probability distribution points of 50% (median), 10%, 1%, and 0.1%, and maximum.

Comparing the distributions for the 0.2- μ s real pulse to the 0.2- μ s compressed pulse (30.0- μ s pulse), a change to a slightly more spiky distribution is apparent on the compressed pulse as the 1.0%, 0.1%, and maximum values were higher in the upwind direction. Plots of the cumulative NRCS probability distribution provided in Figures 69 and 70 for these pulses for the upwind case demonstrate this.

Comparing the distributions of the 10.0- and 30.0- μ s pulses illustrate a dramatic change in clutter distribution with the 10.0- μ s pulse having peaks about 10 dB higher than the 30.0- μ s pulse for all look directions at the 2.0° grazing angle. Figure 71 presents the cumulative NRCS probability distribution for the 10.0- μ s pulse, upwind, for comparison with Figure 70 for the 30.0- μ s pulse. At the 0.30° grazing angle the 10 μ s pulse was still showing peaks 3 to 9 dB higher than the 30.0- μ s pulse.

The effect of grazing angle on the upwind average NRCS on both the 30.0- and 10.0- μ s pulses is almost identical, falling about 10 dB from 2.0 to 0.30°. These data also agree quite closely with the values provided by Nathanson (1969). The maximums dropped only by 6 dB upwind and 3 dB downwind on the 30.0- μ s pulse and 7 dB upwind and 9 dB downwind on the 10.0- μ s pulse. Figures 72 and 73 present the cumulative NRCS probability distribution plots for the 10.0- μ s pulse, upwind, for 1.0° and 0.30° grazing angles. Comparing the difference between maximum NRCS and mean NRCS in Table 34 it would appear from this data set that the statistics of the 30.0- μ s pulse data become more long-tailed with decreasing grazing angle whereas the statistics of the 10.0 μ s pulse data do not change significantly over this same grazing angle range.

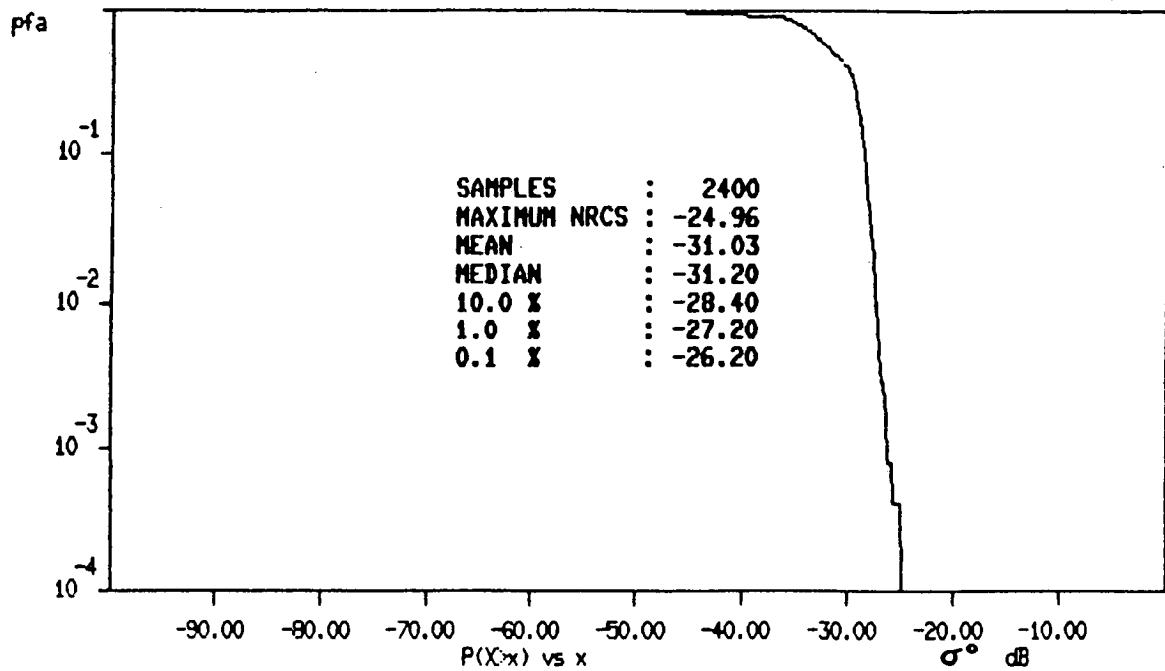


Figure 69. Cumulative normalized radar cross-section probability distribution of sea clutter expressed as probability of false alarm (pfa) for sea state 5, upwind at a 2.0° grazing angle, using the 0.2- μ s pulse and fixed frequency operation.

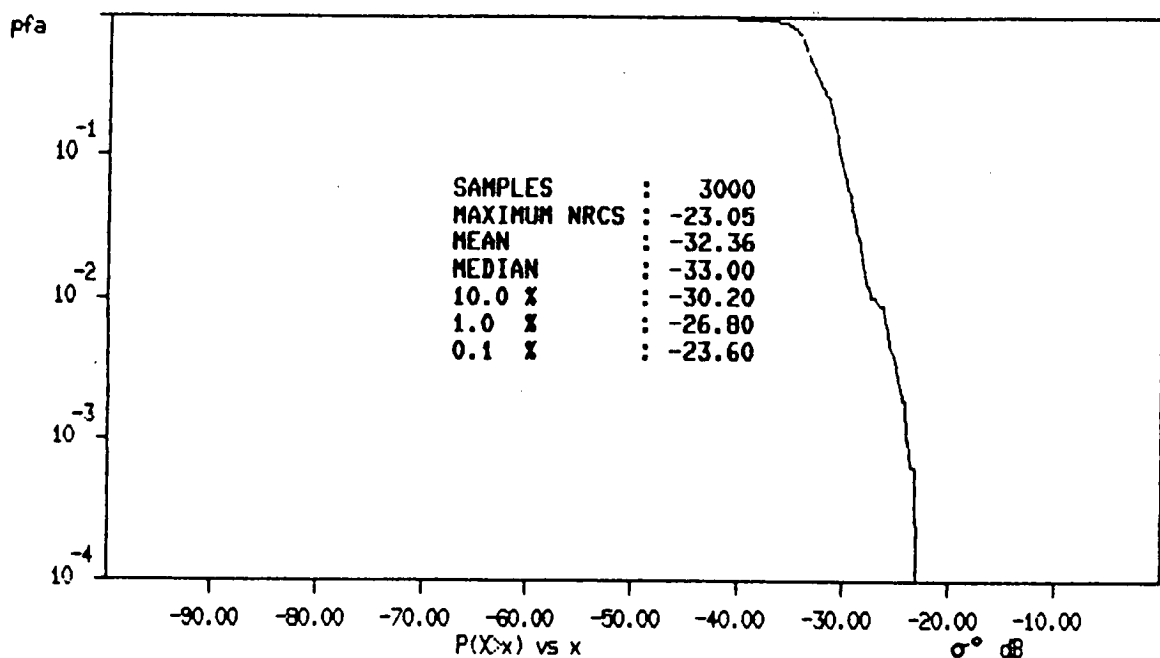


Figure 70. Cumulative normalized radar cross-section probability distribution of sea clutter expressed as probability of false alarm (pfa) for sea state 5, upwind at a 2.0° grazing angle, using the 30.0- μ s pulse and fixed frequency operation.

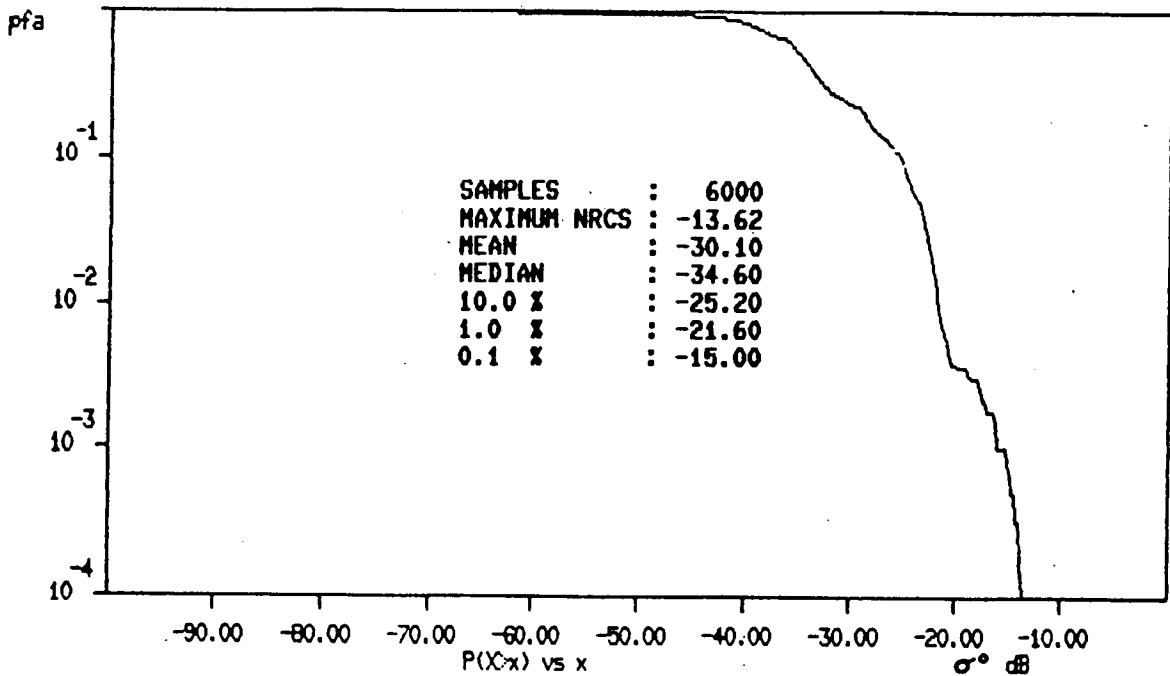


Figure 71. Cumulative normalized radar cross-section probability distribution of sea clutter expressed as probability of false alarm (pfa) for sea state 5, upwind at a 2.0° grazing angle, using the 10.0- μ s pulse and fixed frequency operation.

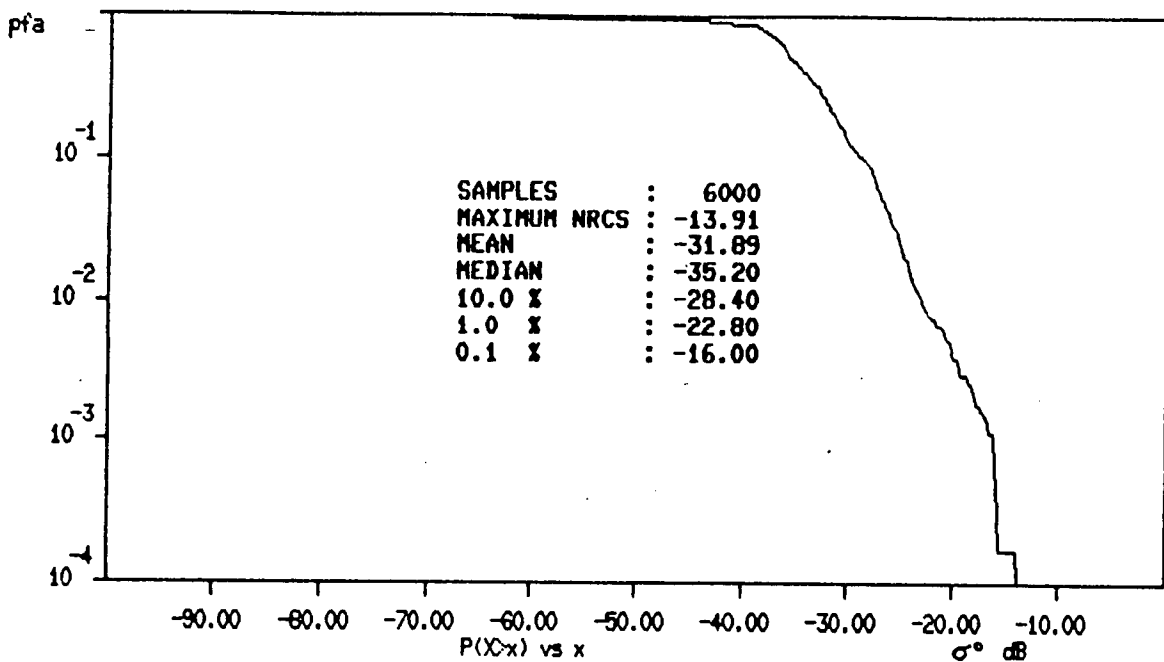


Figure 72. Cumulative normalized radar cross-section probability distribution of sea clutter expressed as probability of false alarm (pfa) for sea state 5, upwind at a 1.0° grazing angle, using the 10.0- μ s pulse and fixed frequency operation.

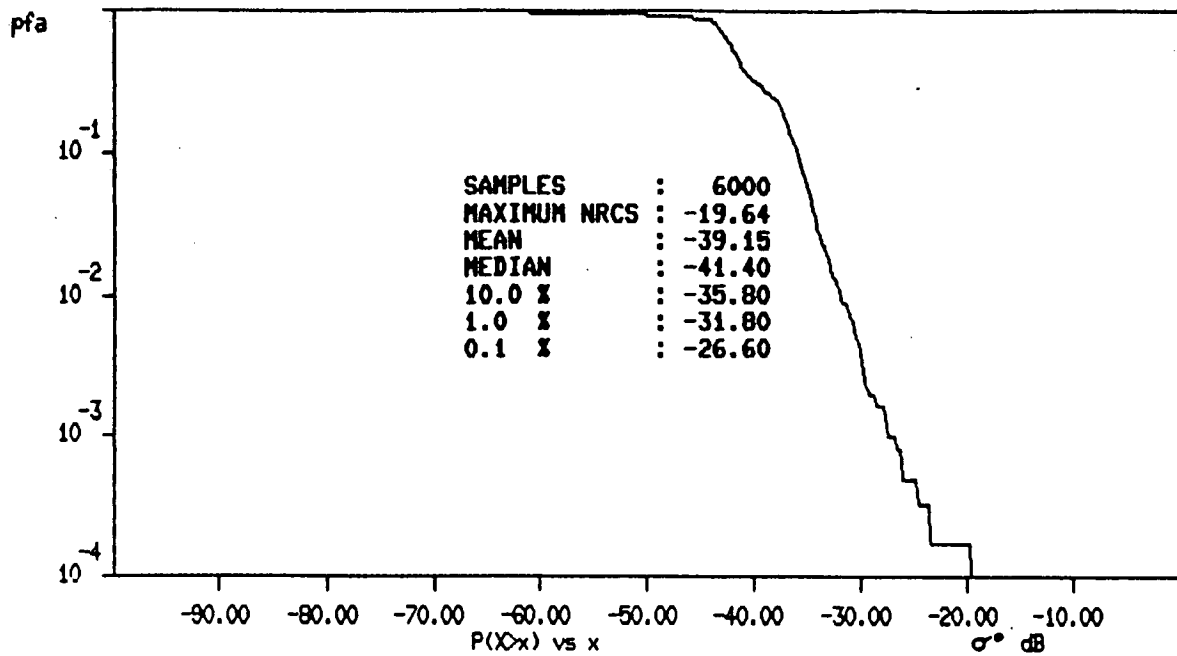


Figure 73. Cumulative normalized radar cross-section probability distribution of sea clutter expressed as probability of false alarm (pfa) for sea state 5, upwind at a 0.3° grazing angle, using the $10.0\text{-}\mu\text{s}$ pulse and fixed frequency operation.

Table 34 represents the type of data that is available within the collected data base. There are sufficient independent clutter samples such that probability levels as low as 10^{-5} may be calculated. These data will prove useful for radar detection performance modelling and radar signal processing design.

A DETECTION EXAMPLE

This section presents the case of observed and measured detection of a bergy bit; target 2 in Table 33. The example serves to illustrate the type of data available within the data set. Unfortunately, a more in-depth analysis of this and other targets was not possible due to budgetary restrictions.

The data for the bergy bit considered here was collected using both fixed frequency and frequency agile operation. The particular two passes considered here were for the 30.0- μ s pulse at a 500 ft altitude with and without frequency agility. The maximum observed range using a fixed frequency (F-8) was 19.1 naut mi whereas the maximum for frequency agility (AG1) was 16.8 naut mi. This target was continuously detected right out to its maximum range on both passes. Figures 74 and 75 present the measured average signal-to-noise ratio (upper data points) and median signal-to-noise ratio (lower data points) calculated using a 9-point moving range window. Figure 74 is for fixed frequency and Figure 75 is using frequency agility. The average free-space radar cross-section for the fixed frequency pass was 11.5 m^2 which increased to 28.8 m^2 when frequency agility was applied. The substantial signal-to-noise ratios indicated in Figures 74 and 75 would suggest that detection should be

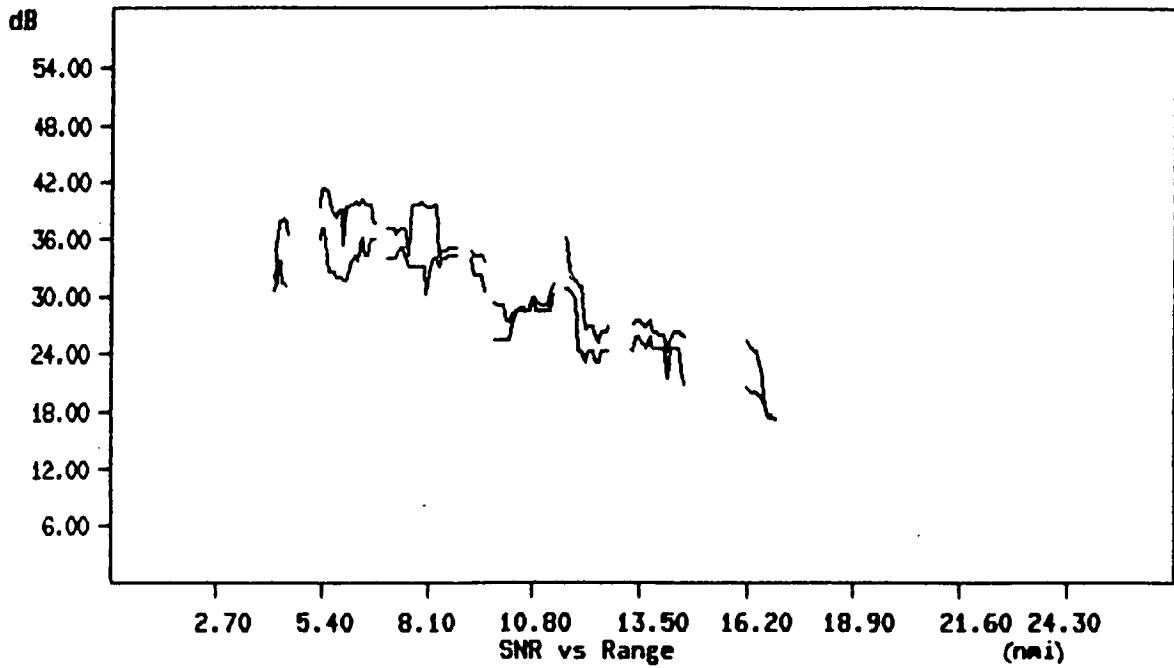


Figure 74. Measured mean and median signal-to-noise ratio as a function of range for a bergy bit using a 30.0- μ s pulse and fixed frequency operation.

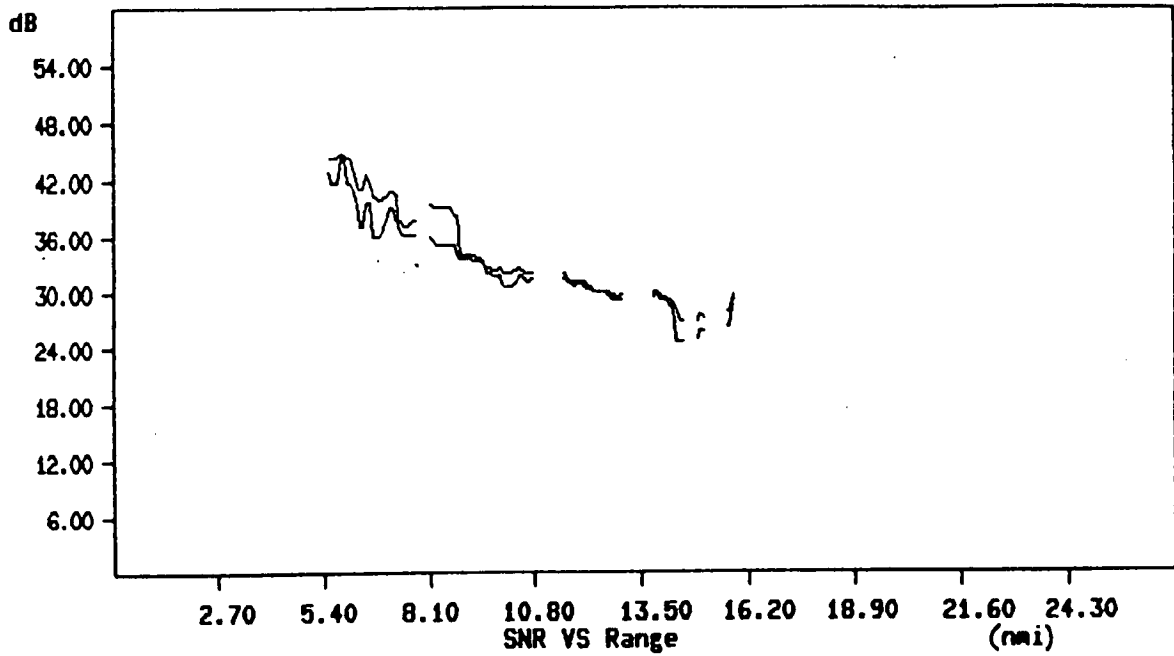


Figure 75. Measured mean and median signal-to-noise ratio as a function of range for a bergy bit using a 30.0- μ s pulse and frequency agile operation.

carried further out than the observed ranges. The data of Figure 74 indicates a signal-to-noise ratio of 20 dB at 17 naut mi yet this target was lost both in the recorded data and from the radar screen at 19 naut mi. Similarly, the data of Figure 75 indicates a signal-to-noise ratio of 28 dB at 16 naut mi and the target was lost at 16.8 naut mi. The high signal-to-noise ratios indicated in Figures 74 and 75 would suggest that some mechanism, such as multi-path enhancement, may contribute significantly to the observed target radar cross-section and when this enhancement is lost the signal-to-noise ratio falls rapidly. It should be noted that the data was analyzed by taking the maximum received power from the target for each scan.

Aside from an obvious increase in radar cross section for this one case, frequency agility appears to alter the radar cross section statistical distribution (Figures 67 and 68) and smooth out the scan to scan target fluctuation. This smoothing effect may be seen by comparing Figures 74 and 75.

A clearer picture of the different phenomena and their interaction could be obtained with further analysis of this and other iceberg targets. It would be especially informative to investigate the effect of frequency agility on the variation of radar cross section within each scan (every third radar pulse is available for analysis with approximately 21 pulses per beamwidth). This investigation might shed some light on the differences in radar cross sections measured for the bergy bit considered here.

OPERATIONAL CONSIDERATIONS

The conclusions drawn earlier and the observed performance figures are used to determine flight line spacing and resulting detection performance for operational iceberg surveillance.

LINE SPACING AND OBSERVED PERFORMANCE

The spacing between flight lines is determined by the smallest iceberg size class of interest for which practical detection performance is desired, and the environmental conditions present. There was no observed performance to suggest that detection of growlers is practical. Medium and large icebergs were not observed to present a detection problem to the combinations of altitude and pulse width that gave the best performance for bergy bits and small icebergs.

Therefore, each group of environmental conditions will be examined for two cases, when the region of coverage is close enough to the area of operations to demand bergy bit detection and when the region of coverage is sufficiently far removed that small icebergs are the smallest size class of interest.

It should be noted that the subsequent calculation of flight line spacing was based on obtaining the highest percentage of detection for the smallest size class of interest. If the user is prepared to reduce the percentage detection requirements line spacing will usually increase. The trade off is percentage detection versus area of coverage.

NOISE-LIMITED DETECTION

On days when the wind-wave was less than 0.5 m, wind speed was 5 to 15 kt, and swell was typically 1.5 m, sea clutter did not limit detection and the best detection performance was observed. Pulse width A at an altitude of 500 ft gave the best observed combined detection of bergy bits and small icebergs (see Figure 47).

The maximum observed bergy bit detection was 70% at ranges inside 9.0 naut mi. The radar will have this detection capability on both left and right hand sides of the flight track (no sea clutter). Therefore, an aircraft track spacing of 2 x 9.0 naut mi, or a 18.0 naut mi spacing, will allow at least one opportunity to detect a bergy bit within 9.0 naut mi with a detection rate of about 70% (based on observed performance). At this line spacing, small bergs will have a detection rate of about 90%. Reducing the required percentage detection of bergy bits to about 60% would allow the line spacing to increase to approximately 24 naut mi.

Pulse width B at 1,500 ft gave the best observed detection of small icebergs (but not bergy bits), 100% inside 19.0 naut mi (see Figure 50). Applying the same considerations as before, an aircraft track spacing of 38.0 naut mi will allow the operator a minimum of one opportunity to detect a small iceberg inside 19.0 naut mi, at a high detection rate near 100% based on observed performance.

TRANSITION TO CLUTTER LIMITED DETECTION

When the wind-wave was 0.5 to 1.0 m, wind speed was 10 to 25 kt and swell was 1.0 to 2.0 m, sea clutter began to limit detection. Detection was found to decrease over about half of the radar screen in the up-

clutter region. Therefore, two parallel flight lines in opposite directions will provide only one opportunity to detect a target between the lines in the down-clutter region.

The combination of pulse A at an altitude of 500 ft gave the best observed combined detection of bergy bits and small icebergs (see Figure 51). Bergy bits were observed to be 56% detected out to 10.0 naut mi, in the down-clutter region only. For the operator to have one opportunity to detect a bergy bit inside 10.0 naut mi in the down-clutter region, a line spacing of 10.0 naut mi is required. The detection rate would be about 56% based on observed performance. Detection of small icebergs would be high, near 100%, based on observed performance. Reducing the required percentage detection of bergy bits to 40%, and small icebergs to 90% would allow line spacing to increase to about 15 miles. Pulse width B at 500 ft gave the best long-range, small iceberg detection capability with an observed detection of 86% inside 25.0 naut mi. When small icebergs are the smallest class of interest, this combination with a line spacing of 25.0 naut mi will give the radar operator one opportunity to detect a small iceberg inside 25.0 naut mi, in the down-clutter region. Detection would be about 86%, based on observed performance.

CLUTTER LIMITED DETECTION

When the wind-wave was 1.0 to 2.5 m, wind speed was 15 to 35 kt, and swell was 0 to 2.0 m, the strongest sea clutter conditions were observed. As described in the previous subsection, the best region of detection is confined to the down-clutter region, or about half of the radar display.

The combination of pulse A and 500 ft altitude gave the best

combined bergy bit and small iceberg detection (see Figure 57). Because the population is small, the range for maximum detection (50% at 15.0 naut mi) is probably optimistic, because in the previous case 50% detection was achieved at 11.0 naut mi. Realistically then, the same line spacing is probably more correct, 10.0 naut mi. Observed performance suggests that about 50% detection is likely for bergy bits, and that about 80% is probable for small icebergs.

Pulse B at 500 ft gave the best detection (100% at 20.0 naut mi or more) for small icebergs, excluding bergy bits. A line spacing of 25.0 naut mi should provide a high detection rate, near 100%, for small icebergs, when detection of bergy bits is not required.

DISCUSSION

The radar display: During both programs, it was found that detection could be reduced by factors that ultimately were related to the radar display. The threshold control of the (V)3 could be set too low. This would allow the background from noise and clutter to become excessively bright. As a result, target contrast and therefore detection was apparently reduced.

The test pattern used in the (V)5 to set display contrast and intensity was apparently not matched to the video signal range from the radar. The use of threshold and STC to unknowingly compensate for this mismatch again resulted in a situation similar to that of the (V)3, with target contrast being reduced impacting on detection.

For (V)3, proper use of the threshold control was required to avoid losing target contrast.

For (V)5, comparison with a secondary black and white radar display in flight, allowed the radar display contrast and intensity to be adjusted independent of the test pattern, removing the source of the problem.

Altitude: It was initially expected that higher altitudes, corresponding to larger grazing angles would increase sea clutter and reduce detection capability. Indeed the modelled results from (V)3 supported this, assuming iceberg radar cross-sections did not also increase appreciably with grazing angle. Independent measurements during the (V)5 program on two bergy bits indicated their average radar cross-section did increase somewhat with altitude, but observed performance found overall detection

to decrease substantially with increasing altitude. This suggests that at higher altitudes the increase in sea clutter outweighs any increase in iceberg radar cross-section, thus reducing overall detection capability for both radars.

Clutter limited detection: Clutter limited detection was not expected to be uniform over 360° of azimuth and this was observed for both (V)3 and (V)5. This is just a consequence of non-uniform clutter, being more severe on one half of the radar screen compared to the other half. Although clutter was weaker in the general downwind direction there was variability between downwind direction and the weakest clutter region. For this reason, the region of best detection was later referred to as down clutter as opposed to down wind. The radar operator is in the best position to identify this region from the clutter on the radar display, but a change in control settings away from those used for optimum detection will be required.

Both modelled (V)3 and observed (V)5 performance showed a substantial difference in percentage detection between the down clutter region (best) and any other region on the radar display. As a result only the greater detection capability of the down clutter region was considered when calculating operational flight line spacing for surveillance in order to achieve the highest percentage of detection.

Noise limited detection: During calm environmental conditions, sea clutter may be almost entirely absent from the radar display in which case system noise tends to limit detection. When this is the case, the term

"best" region for detection on the radar display becomes vague as detection becomes uniform with azimuth.

The (V)3 model: The model calculated radar cross-sections of icebergs by emulating the signal processing of the radar with samples of received power from sea clutter collected in flight, and solving for the target radar cross-section that would give the same detectability actually observed.

Two basic approximations were made in the model. Multipath propagation effects were neglected. The radar cross-section of a target was assumed to fluctuate about a characteristic average value, with an exponential probability distribution (Swerling statistics). From comparison with a limited number of cases where the radar cross-section was independently measured, the model appeared to be able to calculate a cross-section within an accuracy of ± 3 dB, but a larger number of test cases would have been desirable for assessing the model's limitations.

It was intended that the observed detection of the calibrated radar buoys in different clutter conditions would be used to test the capability of the model to predict detection. However, as sea state increased the buoys could not be relied on to remain sufficiently vertical to keep the radar reflector beam patterns near horizontal. Hence their value as a reference target diminished as seastate increased and made assessment of the model's prediction capability difficult.

An error estimate assuming the buoys remained upright suggested the model underestimated radar cross-sections necessary for detection by about 4 dB. This introduced some spread in the predicted percentage of

icebergs detectable in each class by the (V)3 as a function of environmental conditions. Since video tape records of the buoys indicate they can list to one side, the error estimate may be somewhat pessimistic.

Independent radar cross-section measurements (V)3: Analysis of independent measurements on both icebergs and the calibrated radar buoys indicated that the radar cross-sections of all but the larger icebergs seemed to follow the assumed Swerling probability distribution for ranges up to about 12.5 naut mi after which the probability distribution appeared more normally distributed to a maximum range of 16.7 miles. However, examination of the data for the effects of multipath propagation proved inconclusive, due to the large statistical variations present.

The radar cross-sections for different iceberg classes were observed to span a wide range of values. Large fluctuations in cross-section were observed to occur on individual icebergs.

Independent radar cross-section measurements (V)5: Unlike the (V)3 where all measurements were made using one fixed frequency transmitted pulse width, these measurements were collected using two pulse widths with the addition of pulse compression.

The observed statistical distributions of radar cross-section for both icebergs and the radar reflectors deviated noticeably from the Swerling type distributions observed with (V)3 appearing more log-normal. Different average values of radar cross-section for the same target were observed depending on the pulse width, attributed to the difference in

range resolution with the longer pulse yielding the larger values.

A broad range of average radar cross-section values for bergy bits was observed, with the highest 100 times that of the smallest.

Inferring detection performance from seastate number:

It was anticipated that a sea state number calculated from wind speed and total significant wave height would be a good indication of the detection performance to expect. Increasing seastate would indicate increased sea clutter and consequently reduced detection. But seastate number and modelled (V)3 performance did not always correlate well. Increasing seastate number was not always accompanied by predictions of poorer detection performance. Since modelled performance was ultimately governed by the samples of sea clutter recorded in flight, it was concluded that either detection was not well related to a seastate number based on wind speed and significant wave height or some seastate numbers had been over estimated. In the latter case the probable cause was thought to be under developed seas. Although seastate number would not be expected to indicate irregular clutter conditions it should be noted that the contours defining lines of uniform detection could on occasion, have substantial variation in their characteristic shape. This was attributed to changes in the spatial distribution of sea clutter, from one flight to the next.

Relating environmental conditions to detection performance: Since (V)3 detection performance could not be well related to seastate number, the range of environmental conditions were noted for flights which had similar modelled detection performance. Three such classes of environmental

conditions were defined for the (V)3 in terms of wind speed, wind wave (Hw) significant wave height, and swell wave (Hw₁) significant wave height. They indicated radar detection performance will be most sensitive to the wind driven wave component, somewhat affected by wind speed, and fairly insensitive to swell.

The same approach was adopted during the (V)5 program. The observed detection performance was broken down according to the same environmental parameters. Severity of sea clutter was indicated from the extent visible on the radar display, and helped distinguish the detection conditions present. Detection conditions were again divided into 3 groups.

From (V)3 the classes of conditions were identified as:

Class 1:

Wind ≤ 20 knots
Hw = 0
Hw₁ ≤ 0 to 4m

Class 2:

Wind ~ 10 to 30 knots
Hw ~ 1 to 2.5m
Hw₁ ~ 1 to 2.5m
(Hw + Hw₁) ~ 2 to 4m

Class 3:

Wind ~ 20 to 30 knots
Hw ~ 2.5m
Hw₁ ~ 3 to 4.5m
(Hw + Hw₁) ~ 6 to 7m

In (V)5 detection was broken down to reflect class 1 conditions, the transition between class 1 and class 2 conditions, and class 2 conditions. Based on the environmental hindcasts, none of the flights used to document detection occurred during class 3 conditions.

PERFORMANCE SUMMARY (V)3

The detection capability of the (V)3 for bergy bits is poor at best, and non-existent for growlers. The (V)3 provides moderate detection capability for small icebergs, and good detection capability for medium icebergs.

If it is necessary to search for bergy bits, which are only detectable in class 1 conditions, then flight lines would appear to be limited to about 10 naut mi apart to achieve 28-41% detection. For small icebergs, 26 naut mi spacing seems appropriate for class 1 conditions to achieve 66-84% detection, 12 naut mi for class 2 (53-68%) conditions, and 10 naut mi spacing for class 3 (49-64%). For medium icebergs, 26 naut mi spacing is expected to provide reasonable detection capabilities (near 100%) during all three classes of conditions.

At 10 naut mi flight line spacing the percentage of targets detectable, calculated from the model are:

	Bergy bits	Small	Medium
Class 1	28-41%	87-95%	100%
Class 2	0%	53-68%	100%
Class 3	0%	49-64%	100%

The line spacing was calculated on the basis that the best region for detection on the radar screen is only obvious under class 1 conditions.

The choice of line spacing is limited by the detection required of the lowest size class of iceberg and the class of conditions present.

It is assumed that the aircraft is confined to 500 ft altitude and that a threshold setting can be found to limit background display intensity without removing regions of the display entirely. If altitude has to be increased, it will be at the expense of detection, possibly not too severely for class 1 conditions, but it would appear to impose a serious lowering of detection for class 2 and 3 conditions.

The overall modelled detection capabilities of the (V)3 are given in Table 18 and Figures 34 to 36.

PERFORMANCE SUMMARY (V)5

The overall detection capability of the (V)5 was observed to be excellent for large and medium icebergs, good for small icebergs, moderate for bergy bits and poor for growlers. Large and medium icebergs were not observed to pose a detection problem under the conditions encountered.

When it is necessary to search for bergy bits and larger size icebergs under class 1 conditions (minimal sea clutter) flight line spacing appears limited to about 18.0 naut mi to achieve about 70% detection of bergy bits and about 90% detection of small icebergs. Under class 2 conditions, flight line spacing appears to be limited to about 10 naut mi to achieve about 50-56% detection of bergy bits and about 80% for small icebergs. These detection percentages were observed with the radar set on pulse A and operating at an altitude of 500 ft, which gave the best combined detection of bergy bits and small icebergs.

When the region of surveillance is sufficiently removed from the area of operations and it is only necessary to search for small icebergs and larger size classes under class 1 conditions flight line spacing appears limited to approximately 38 naut mi to achieve a high detection of small icebergs approaching 100%. This detection was observed with the radar set on pulse B and operating at an altitude of 1500 ft. Under class 2 conditions flight line spacing appears limited to about 25 naut mi to achieve about 85% detection of small icebergs. This detection was observed with the radar set on pulse B and operating at an altitude of 500 ft.

In all the above cases the observed detection percentages were only achieved with the indicated combinations of pulse width and altitude. Other combinations may yield poorer results. Line spacings were calculated to obtain the highest percentage of detection of the smallest iceberg size class of interest at the expense of area of coverage. The overall observed capabilities of the (V)5 are given in greater detail in tables 28 to 30, and figures 47 to 54, 57 and 58 (Matrix of Results and Analysis).

COMPARISON OF APS 504 (V)3 VS APS 504 (V)5

Both systems were operated from the same aircraft and used the same radar antenna and radome. In Table 35, the projected performance of the (V)3 for iceberg detection is summarized for the same type of environmental conditions as observed with (V)5, for an altitude of 500 ft. The performance for the (V)5 for equivalent ranges and environmental conditions is tabulated for pulse A at an altitude of 500 ft.

TABLE 35

Comparison of performance of (V)3 and (V)5

Conditions	Bergy bit detection inside 10 naut mi (%)	Small iceberg detection inside 15 naut mi (%)
(V)3:		
Noise-limited detection	28 - 41	59 - 72
Clutter-limited detection (down-clutter)	0	37 - 59
(V)5:		
Noise-limited detection	68	87
Clutter-limited detection (down-clutter)	50 - 56	80 - 90

CONCLUSIONS

1. The APS (V)5 evaluated in 1987 substantially outperformed the modelled performance of APS 504 (V)3 evaluated in 1986. For the same range the (V)5 had substantially higher percentage of detection of bergy bits and small icebergs.
2. Large and medium icebergs were not observed to present a detection problem to the (V)5. Provided the appropriate combination of line spacing, altitude, and pulse width are used, observed performance indicates detection of small icebergs in the vicinity of 90% whereas detection of bergy bits is between 50% and 70%, for the suite of environmental conditions observed. Although growlers were occasionally detected, the detectability was poor for modes that gave the best detection of bergy bits and small icebergs.
3. The combination of pulse width A and 500 ft altitude gave the best detection of bergy bits and small icebergs.
4. When the area of coverage does not require bergy bit detection, observed performance indicates that pulse width B will give both a high percentage of detection and allow line spacing to increase substantially, giving broader coverage.
5. Signal processing, such as sensitivity time control (STC), CFAR, and scan integration, were all judged to be necessary components of the (V)5, rather than options. Frequency agility was observed to be useful, but no conclusion was reached on its necessity.

6. The (V)5 has more controls to operate than the (V)3 and was not considered by the radar operator, to be user friendly, which may be because the (V)5 is of very recent design.
7. Analysis of the radar signal data has demonstrated that the radar achieves effective reduction of the average sea clutter levels when used with pulse compression modes. However, for the highest resolution pulse (4.5 m range resolution) the clutter statistics change significantly, becoming more spiky, thereby placing more demands on the signal processing stages of the radar.
8. An investigation into the effects of pulse length, frequency agility, and altitude on the radar cross-section of a small iceberg and a number of bergy bits indicates that these parameters can alter the cross-section seen by the radar. The larger of the available pulse lengths provided higher radar cross-sections for the iceberg targets analyzed. Frequency agility gave radar cross-sections that were at least as high, and sometimes higher, than fixed frequency operation. Comparison of altitude demonstrated a slight increase in cross-section at 1,500 ft over 500 ft.

RECOMMENDATIONS

1. The internally generated display test pattern of the (V)5 appeared to misalign the display and radar video signal ranges to the point at which detection was suffering, which is counter-productive. Display calibration signals should come from farther inside the radar system.
2. The environmental conditions observed were limited in severity. A test of the radar in more severe sea clutter conditions is required if its performance under those conditions is to be quantified.
3. The ASW (anti-submarine watch) mode was apparently not fully optimized to its intended configuration by the manufacturer and was not evaluated. Data should be collected in this mode once the situation changes.
4. It is recommended that further analysis of the radar signal data collected during the program be carried out to:
 - a. Extract radar cross-section information on icebergs and ocean. These data are required for performance prediction modelling and radar signal processing design.
 - b. The analysis should include an investigation into the effect of multi-path propagation on radar cross-section estimation and should consider the influence of frequency agility.

- c. Sea clutter data should be analysed to investigate the decorrelation achievable when using frequency agile operation.

Note: The manufacturer has indicated that the APS 504 (V)5 is currently being modified (Appendix II-C).

APPENDICES FOR APS 504-(V)3

Appendix I-A	- Description of (V)3 model.	I- 1
Appendix I-B	- Clutter cross-sections transferred to tape	I-22
Appendix I-C	- Partial specifications	I-25
Appendix I-D	- Sea State and Iceberg Classification	I-26

APPENDIX I-A

Description of (V)3 Model

Appendix I-A

Description of (V)3 Model

A brief overview of the model is presented, followed by a step by step description. See figure 17 for a block diagram. (All calculations are in MKS units.)

Summary: After a pulse transmission by the (V)3, received power collected by the radar antenna is converted to voltage. As this voltage is produced various signal processing steps are applied culminating in an azimuthal filter voltage output, followed by a transfer of this information to the radar display.

The model emulates the internal signal processing of the (V)3 to arrive at the voltage output from the azimuthal filter. This voltage output is calculated at a large number of points over a complete radar scan. These voltages in turn were generated by emulating the signal processing using complete radar scans of power received, collected in flight over open ocean (no targets), and represent sea clutter and noise.

The presence of a target is simulated by calculating the additional increase in received power over that of just sea clutter and noise, and then calculating the net increase in voltage at the azimuthal filter output.

The detection of a simulated target at a particular range and bearing is modelled as the required voltage increase, if any, from the azimuthal filter to compete with the local voltages in the same area (i.e. Simulate a radar blip from a target as bright as the local returns from sea clutter or noise).

The voltage increase calculated is then transformed into the minimum S/C (signal-to-clutter ratio) for detection. S/C is then used to calculate the minimum required radar cross-section for detection at that location.

The model makes use of power received collected over 360 degrees in azimuth within the range interval defined by the antenna vertical beam width, aircraft altitude, and the ocean surface. The recording system sampled every sixth radial, producing 1024 samples in range from 0 to approximately 16.7 nautical miles slant range, and 512 radials per radar scan (Figure I-A1).

Description:

Step 1 converts the digitally represented power to numerical received power in watts and then calculates a clutter cross-section.

This is accomplished using the calibration curve supplied by Viatic and interpolating between points where appropriate (Figure I-A2).

As an example if the digital number N representing P_r is 18, the $P_r = -100\text{dBm}; 10^{-10} \text{ mW}; 10^{-13} \text{ Watts}$.

For $N = 10$ interpolation is used.

$$P_r = -105\text{dBm} + \frac{(10-8)}{(18-8)} \times 5\text{dBm} = -104\text{dBm}; 3.9811 \times 10^{-11} \text{ mW}; 3.9811 \times 10^{-14} \text{ Watts}.$$

This power (represents sea clutter plus noise) is then converted to σ° , unit cross section for sea clutter.

The calculation of σ° (from equation A1) assumes flat earth geometry,

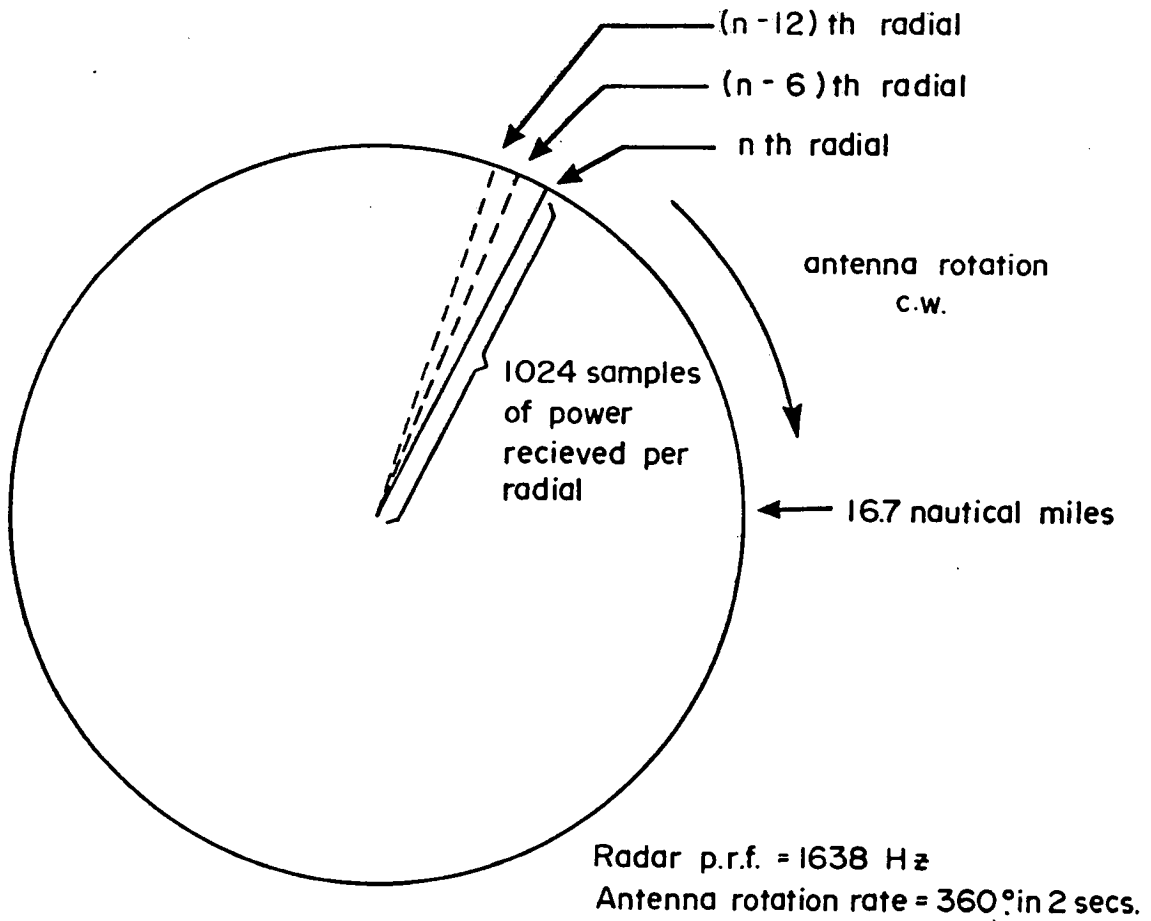


Figure I-A1. Format of digital power received collected by Viatec.

Calibration results for 5.0-MHz sampling
and 0.5- μ s pulse

<u>POWER (DBM)</u>	<u>VOLTAGE (V)</u>	<u>DIGITAL LEVEL</u>
-110.0	1.50	5
-105.0	1.52	8
-100.0	1.58	18
-95.0	1.74	37
-90.0	1.90	58
-85.0	2.10	82
-80.0	2.28	101
-75.0	2.50	119
-70.0	2.72	140
-65.0	2.92	161
-60.0	3.14	181
-55.0	3.32	197
-50.0	3.52	218
-45.0	3.68	233
-40.0	3.76	245

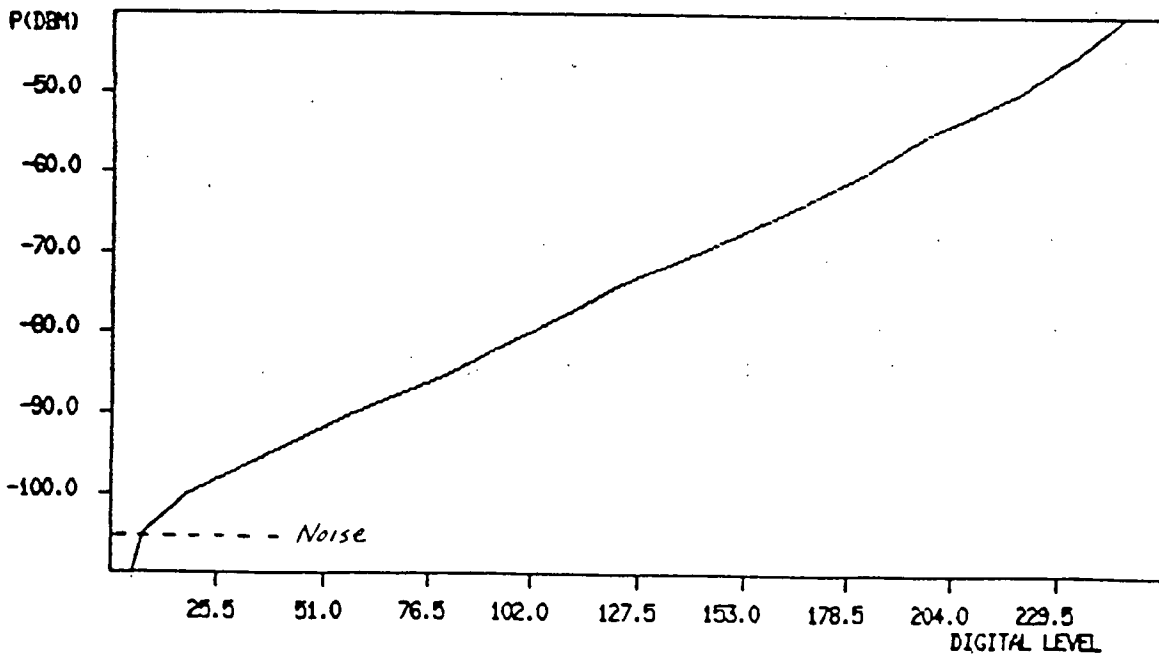
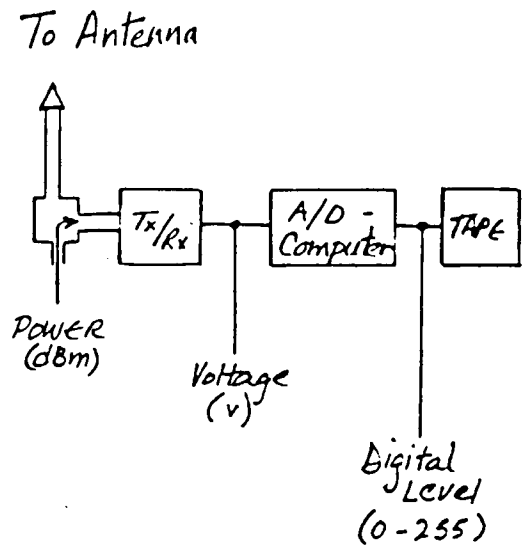


Figure I-A2: Plot of overall system calibration for 0.5- μ s pulse at 5.0-MHz sampling.

and incorporates the $(\sin x)/x$ pattern of the antenna in the vertical plane, allowing for antenna dip.

$$\sigma^\circ(n, \phi) = \frac{2 (4\pi)^3 R^3 P_r}{P_t G^2 \lambda^2 C \Delta t \theta_B \sec \phi L} \quad (\text{I-A1})$$

where:

- n = digital sample number (1 to 1024)
- P_r = power received at range R,
(sample n)
- G = antenna gain = $G_0(1-134.16 \sin^2 \alpha)$
- λ = wavelength
- G_0 = 1584.9 (Antenna gain at beam centre)
- α = angle away from beam centre (vertical plane)
- R = slant range = $nc/(2f)$
- C = 3×10^8 m/sec
- f = sample frequency
- θ_B = antenna horizontal beamwidth
- Δt = pulse length
- ϕ = grazing angle, $\sin^{-1}(h/R)$
- h = altitude
- $\sec(\phi) = R/(R^2-h^2)^{1/2}$
- L = system loss = 0.69

The software checks that only data within the main lobe of the antenna intersecting the ocean surface is used for this calculation.

Typically, processing of recorded power received produces 6 to 12 scans of 512 radials each, with a maximum of 1024 σ° 's per radial.

These data form the input to the model. From this point on, the model reconstructs signal voltage in the signal processing unit by emulating the processing techniques in the same order as they occur.

Step 2 is the reconstruction of received power. In the more general case the flight being modeled may have different altitude and antenna tilt than the flight that collected received power. Software first checks the incidence angle ranges for the sea clutter flight and the modeled flight. A range of incidence angles common to both flights is established. In practice altitudes are usually identical and received power is reconstructed as it was originally received. However constructing received power for higher altitudes is limited to using received power distributions well above the radar noise level over the grazing angle region of interest. Otherwise radar system noise will be treated as clutter. Moving clockwise the power received for n samples on each radial is calculated using σ° 's from the same radial of the clutter distribution, with the appropriate incidence angle. Because voltage will eventually pass through an azimuthal filter, the first radial processed is 45 radials counter clockwise from the radial of interest which gives the azimuthal filter time to stabilize.

Step 3 is the conversion of received power to signal voltage. Each power sample along the radial is converted to voltage using the same calibration curve of power as in Step 1 and the corresponding voltages. Again linear interpolation is used for powers between calibration points.

The finite number of bits used in the radar to represent voltage is emulated by calculating the integer number of voltage increments (represented by the least significant bit) that will represent each analog voltage, and then calculating the digital voltage equivalent. The equation used is of the form,

$$V \text{ digital} = V_{\text{BIT}} \times J_{\text{INT}} \text{ (VOLTS/V}_{\text{BIT}}) \quad (\text{I-A2})$$

where: V_{BIT} = the voltage increment represented by the least significant bit

VOLTS = the voltage representing received power

JINT = the integer function which truncates the decimal part of a real number

Vdigital = the desired digital voltage.

Summarizing to this point, the digital voltage at each sample, along each radial, is calculated, radial by radial, in a clockwise sense, using σ 's with correct incidence angle, limited to the common region within the 3dB vertical beamwidth of the radar antenna.

Step 4 is the application of CFAR and azimuthal filtering. The CFAR voltage to be subtracted from each digital voltage is calculated immediately after completion of each radial. The model emulates Litton's CFAR with a sliding window before and after each sample of interest, taking into account the CFAR digitization rate, and the number of bits used in Litton's A/D and D/A process.

The appropriate CFAR voltage is then subtracted from the relevant digital voltage sample producing a second radial of voltages.

The result is two radials of digital voltage representing CFAR OFF and CFAR ON.

Each radial of CFAR OFF/ON is then filtered azimuthally using a recursive digital 1 pole filter similar to that of Litton's. Because only 512 radials of clutter are available per scan out of 3276 (Viatec digitizes 1 in 6), the azimuthal filter time constant is reduced appropriately, (by about 6).

The form of the digital filter is,

$$V_{out}(n,m) = \frac{V_{in}(n,m)}{G} + e^{-1/k} V_{out}(n-1,m) \quad (I-A3)$$

where: $V_{in}(n,m)$ = digital voltage from radial n, range sample m

$V_{out}(n,m)$ = azimuthal filter output from radial n ,
range sample m

G = filter gain for time constant K

K = time constant in terms of # of digital samples.

Step 5 models the effects of range collapsing, peak detection, and calculates a voltage difference. With a horizontal antenna beam width of 2.3 degrees, rotation rate of 30 r.p.m., and a p.r.f. of 1638 Hz, a stationary target's position is scanned with about 21 radials. With one radial in six available, three radials of digital clutter are used to represent the sweep across a target (see Figure I-A3).

Dependent on range scale, the radar collapses more than one sample into a range cell and then applies peak detection. On 25 naut mi range this collapsing ratio is closest to an integer value of 4. The digital sample at the target location has been grouped with three other samples on the same radial. Similarly, the range cells on the same radial before and after the target's range cell contain four digital samples.

The threshold control has set a minimum voltage for detection, V_{thresh} . The peak detection process selects the maximum voltage from each range cell. Detection is modelled as the capability of distinguishing a target from adjacent background on the display. Distinguishing a target on the radar display requires the target's pixel to be at least as bright as the adjacent pixels in range, and if the adjacent pixels are not illuminated, only requires the digital target voltage to reach V_{thresh} .

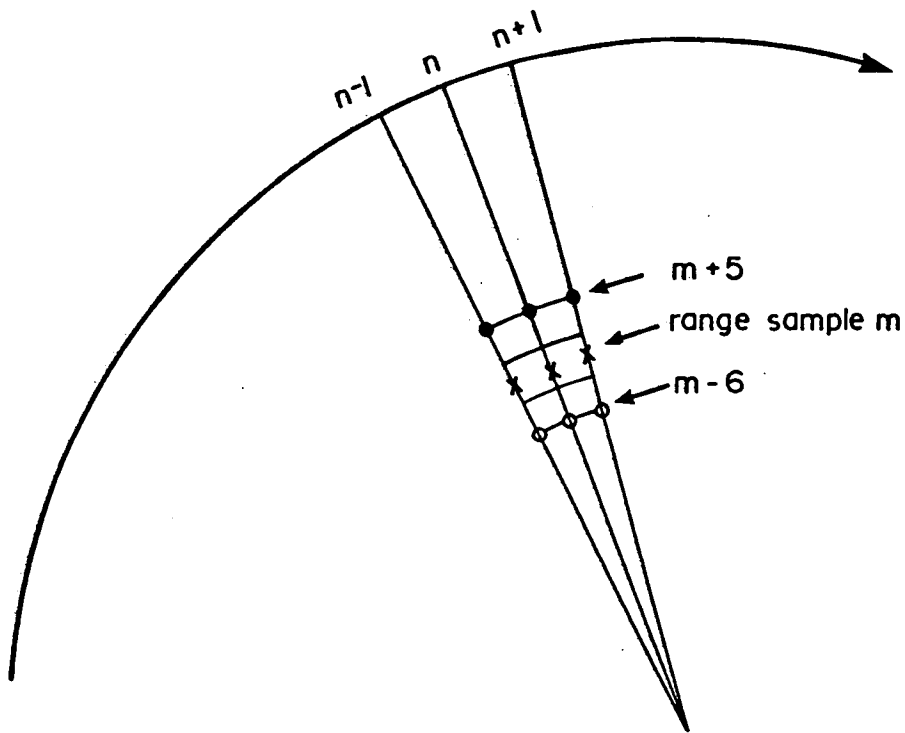


Figure I-A3. Characterization for 25 mile range scale.

After each radial's voltages ($V_{out}(n,m)$) are calculated, the voltages are then grouped about the range sample of interest. The number of samples used to model detection probability is determined by the radar range scale used, the number of digital samples in one radial, and the number of pixels used for radar display (800 x 800).

For example, the target is located such that it is swept by radials $n-1$, n , $n+1$, and lies at range sample m .

The model on 25 naut mi range scale calculates $V_{avg}(n,m)$,

$$V_{avg}(n,m) = 1/3 (V_{out}(n-1,m) + V_{out}(n,m) + V_{out}(n+1,m)) \quad (I-A4)$$

taken to be the average voltage produced by clutter (and noise) at target location.

The voltage jump required for detection at range sample m is taken to be $V_{req'd}$,

$$V_{req'd} = V_{avg}(n,m) - AMAX1(V_{thresh}, V_{max}) \quad (I-A5)$$

where: $V_{max} =$ maximum voltage $V_{out}(j,k)$
 $j = n-1, n, n+1$
 $k = m-6, \dots, m-1, m+1, \dots, m+5$

$AMAX1(V_1, V_2)$ takes the maximum of V_1, V_2 .

Thus, surrounding clutter and the threshold setting determine the voltage level for detection. The model calculates the voltage difference between the effective voltage level modelled for detection and the average voltage calculated at target location from clutter.

Step 6 uses $V_{req'd}$, the average clutter power at range sample m , (radials $(n-1), n, (n+1)$), and a calculated lookup table to determine the signal to clutter ratio required for detection. (This lookup table will be subsequently described in more detail, and is not to be confused with Litton's internal look-up table). With the required S/C established, and the average clutter power at range sample m calculated, the required power for detection is then given in dB by,

$$P_{req'd} = P_{avg} + S/C \quad (I-A6)$$

where: $P_{avg} =$ average clutter power in dB
 $S/C =$ signal to clutter ratio in dB,

The flat earth radar range equation is then rearranged to calculate

$\sigma_{req'd}$, the required free space target cross-section for detection.

$$P_{req'd} \text{ (WATTS)} = 10 (P_{req'd} / 10)$$

$$\sigma_{req'd} = \frac{(4 \pi)^3 R^4 P_{req'd} \text{ (WATTS)}}{P_t G^2 \lambda^2 L} \quad \text{(I-A7)}$$

where: $P_t = 10^5$ WATTS

$R =$ slant range in metres

$\lambda = 0.032$ metres

$G =$ antenna gain at α , the angle from beam center

$L = 0.69$ (system loss)

Probability of detection for a target with exponential cross-sectional (free-space) distribution $P(\sigma)$,

$$P(\sigma) = \frac{1}{\sigma_{AV}} e^{-\sigma/\sigma_{AV}} \quad \text{(I-A8)}$$

is then calculated using,

$$Pd = e^{-\sigma_{req'd}/\sigma_{AV}} \quad \text{(I-A9)}$$

where: $P(\sigma) =$ Probability density of cross-section σ

$\sigma_{AV} =$ average target cross-section

$Pd =$ probability of detection.

These are the six basic steps in the model to arrive at a Pd for a specific point on the radar screen given a particular σ_{AV} .

When the B/S (blip-to-scan ratio) observed from a flight is used to calculate a target's average cross-section, based on exponential distribution, then Pd is calculated at each available point along the observed path of the target, for a given σ_{AV} . B/S is then matched to the σ_{AV} for which,

$$B/S = 1/N \sum_{i=1}^N Pd_i \quad (I-A10)$$

where: N = # of points at which Pd was calculated

Pd_i = Pd at the i th point.

Look-up table: The look-up table referred to in the model's description, is actually a family of calculated curves of required S/C versus average azimuthal filter voltage increase.

These curves represent S/C required for a desired increase in azimuthal filter output voltage as a target of fixed cross-section is swept by the antenna pattern.

The azimuthal filter described in Step 4 is modelled as a linear process. Its response to the superposition of two signals was separated into the response to one signal plus the response to the second. The model calculates the azimuthal filter output voltage from clutter plus noise, and then the voltage increase required to reach an effective voltage threshold set by adjacent clutter and/or the threshold control, (i.e., the condition modelled for detection). The look-up table supplies a calculated S/C for detection given the required voltage increase and average clutter plus noise power received.

These look-up table curves were calculated using the calibration curve supplied by Viatec (Voltage versus Power), the azimuthal filter, and a horizontal beam width of 2.3° with $\sin x/x$ pattern. Because the calibration curve of voltage versus power is non-linear with very little voltage increase/unit power at the low end of the log amp, it was necessary to calculate a family of curves at intervals of 5dB increasing average received power, along the calibration curve.

To illustrate, the azimuthal filter is of the form,

$$V_{out}(n) = \frac{V_{in}(n)}{G} + e^{-1/k} V_{out}(n-1)$$

$$\text{Let } V_{in}(j) = V_1(j) + V_2(j)$$

$$\begin{aligned} V_{out}(n) &= \frac{(V_1(n) + V_2(n))}{G} + e^{-1/k}(V_1(n-1) + V_2(n-1)) \\ &= \frac{V_1(n)}{G} + e^{-1/k} V_1(n-1) + \frac{V_2(n)}{G} + e^{-1/k} V_2(n-1) \end{aligned}$$

The azimuthal filter's response was separable into two components; $V_1(n)$ from clutter plus noise; and $V_2(n)$, from a target.

Let $V_2(n) = 0$ $n \leq j$ (before target enters beam pattern).

$V_2(n)$, $n = j + 1, j + 21$ must then be calculated (as a target is scanned over 21 radials). The average voltage response of the azimuthal filter over 21 radials is calculated for a given clutter/noise power and S/C.

Let P_c = clutter power in dB

S/C = K (some integer) in dB

ϕ = horizontal angle in radians from antenna beam center

G = antenna gain at ϕ relative to beam center

For a 2.3 degree beam width, sin x/x pattern,

$$G = (1 - 1241.3 \sin^2 \phi) \text{ (horizontal plane)}$$

$$P_r = P_c + 10 \text{ Log } (G^2) + K$$

where P_r is the power received in dB.

P_r is calculated at each of 21 radials, the 11th of which is beam center. As each P_r is calculated, it is converted to voltage using the calibration curve, and then becomes the next input to the azimuthal filter. The average voltage of the azimuthal filter over 21 radials is then calculated, yielding one point on the curve, at clutter power

$P_c, S/C = K.$

These calculations also account for the number of bits used for digitization. The curves are illustrated in two graphs, because some overlap occurs, (Figures I-A4 & I-A5). The S/C for a given azimuthal filter output voltage increase is largest on the -140 dB curve where the log amp is least sensitive to increasing power.

The non-linear shape of the calibration curve of the log amp appears to explain the location of the curves relative to each other. When power received + S/C lies on the linear portion of the log amp voltage versus power curve and the region 6 dB below this is also linear, the input voltage to the azimuthal filter will climb quickly as a target is swept by 21 radials yielding a higher azimuthal filter response. But when the 6 dB region (antenna pattern effect) overlaps the low or high non-linear end of the log amp calibration curve, the input voltage to the azimuthal filter will not climb as quickly, decreasing the azimuthal filter output. For large fixed voltage increases, more S/C is required at lesser received powers between -140 dB and -110 dB, most noticeably between -140 and -130 dB at the low end of the log amp curve. Above -110 dB the trend reverses, and increasing received power requires higher S/C as the top of the log amp curve is reached. Above -100 dB the curves stop where the S/C ratio plus received power reach the top of the log amp calibration curve. The wobble in the individual curves is likely from the finite number of bits used and the linear interpolation.

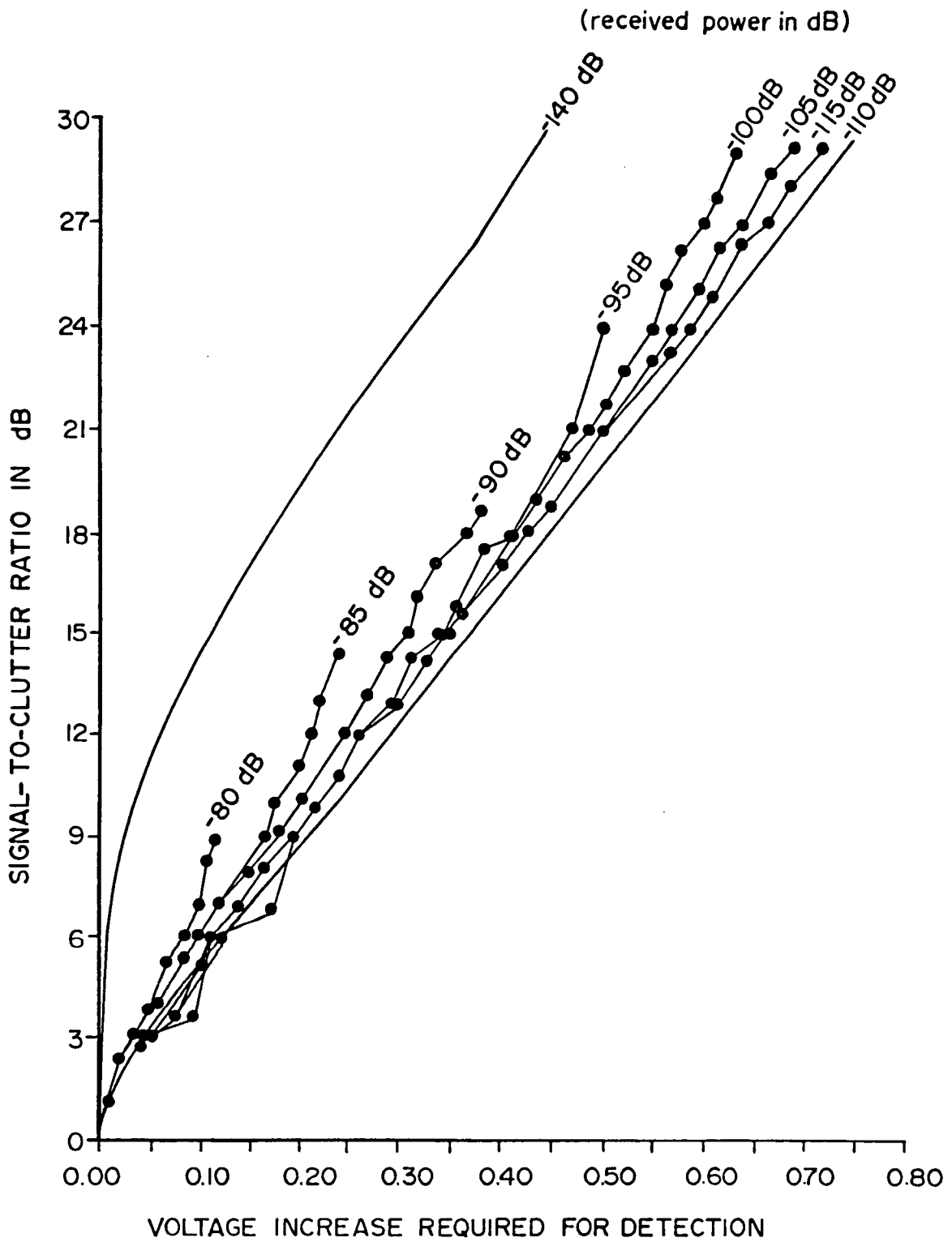


Figure I-A4. Calculated signal-to-clutter ratio required for detection as a function of the voltage increase required and received power.

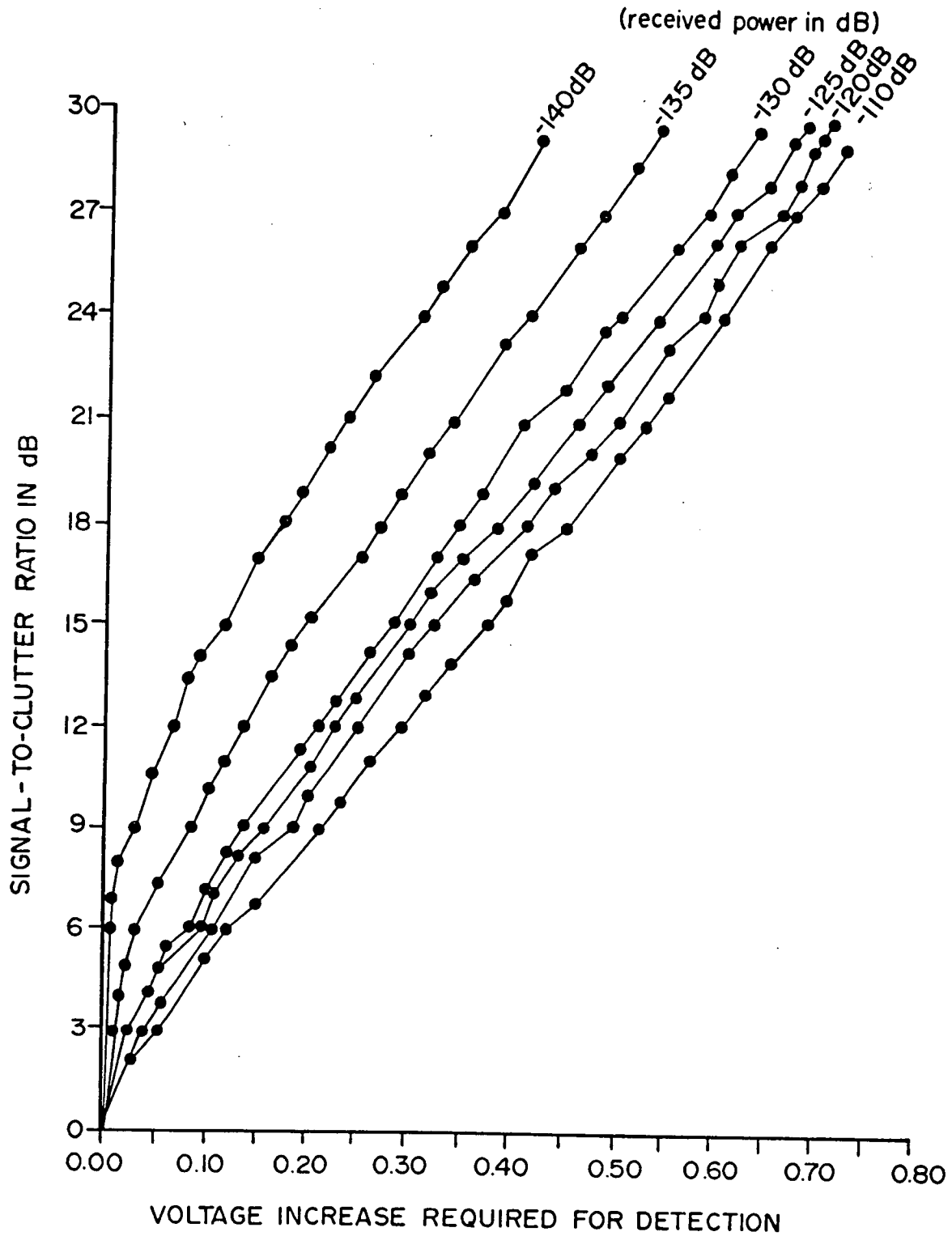


Figure I-A5. Calculated signal-to-clutter ratio required for detection as a function of the voltage increase required and received power.

Threshold control: The relation of the threshold control to input power (and then voltage) was modelled from measurements made before and after the data collection program, within the capabilities of the calibration equipment available. The results were used by the model to emulate the effect of the threshold control.

Using the same setup that Viatec used for calibration, power was injected, then the threshold reduced until a faint segmented ring was observed on the radar display. The threshold value was found to be independent of range scale and range, out to 25 naut mi. CFAR ON/OFF did however, make a difference, in the second set of measurements but not the first, (or the accuracy of measurement was better the second time around). The threshold settings for a faint ring (no segments) was measured once.

Figure I-A6 illustrate the results of those measurements. The threshold setting which just permitted a signal to be observed on the display is plotted against the injected power.

A point worth noting is the precision of these measurements. An unknown power input was set which would then be identified by the method described. On average, the power input could be identified within 2 dB.

The threshold relation to power was non-linear for a 'faint segmented ring' whereas for a 'faint full ring' it was linear. This points to noise limiting from the background. Two straight line fits were made to the linear portions of each data set as shown. The threshold was modeled to lie between the two curves for CFAR ON where almost all data collection measurements were made. Figure I-A7

L1: Linear Regression fit to points of curve Y1
(-104 to -95 dBm)

Y1: CFAR ON 6, 12, 25 naut mi Radar Range August 26/86
Faint circular trace with gaps at 4 naut mi

Y4: CFAR ON 25 naut mi Radar Range May 16/86
Faint circular trace with gaps at 21.6 naut mi

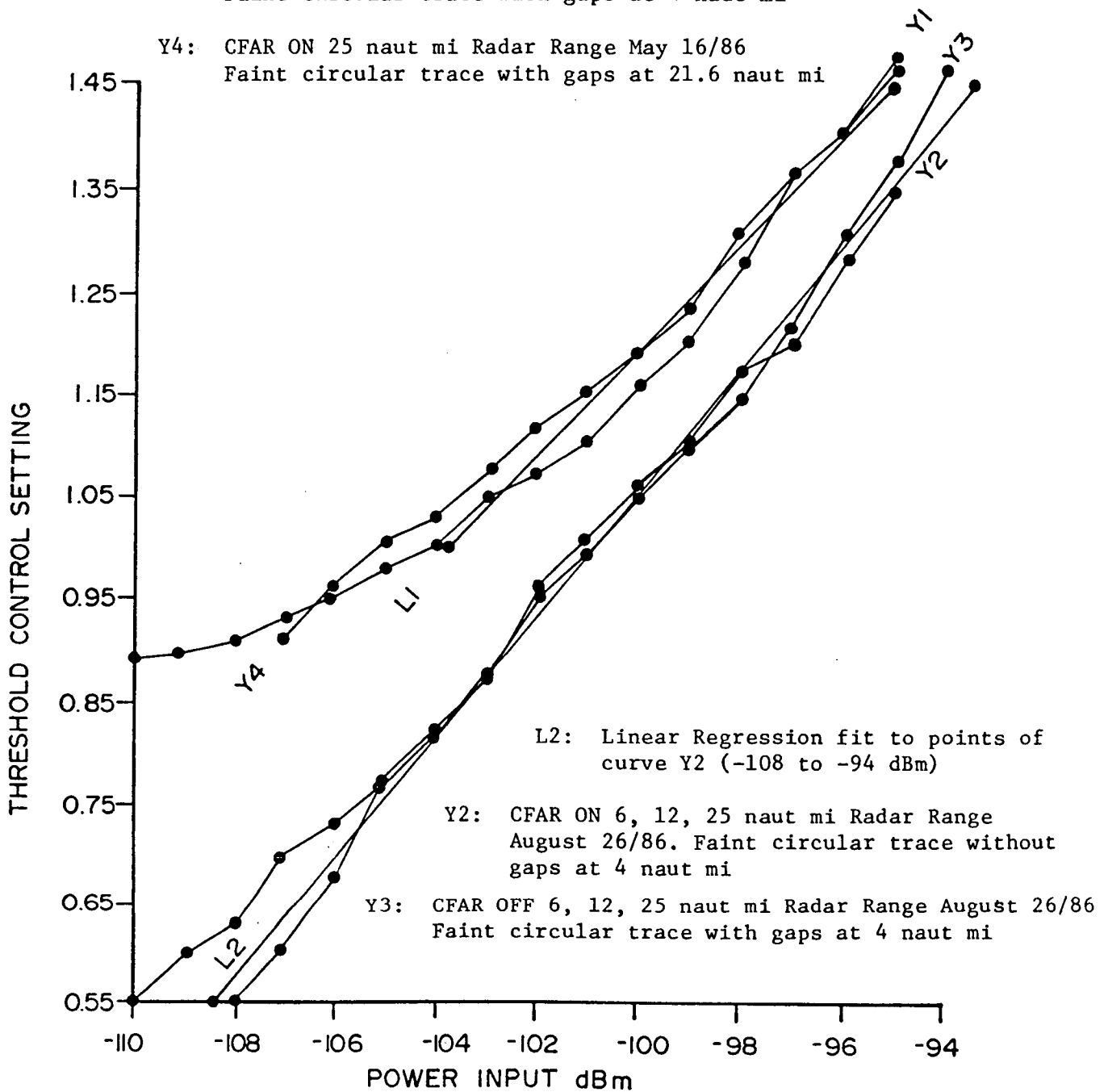


Figure I-A6. Observed threshold setting as a function of injected power for signal to be just visible on radar display.

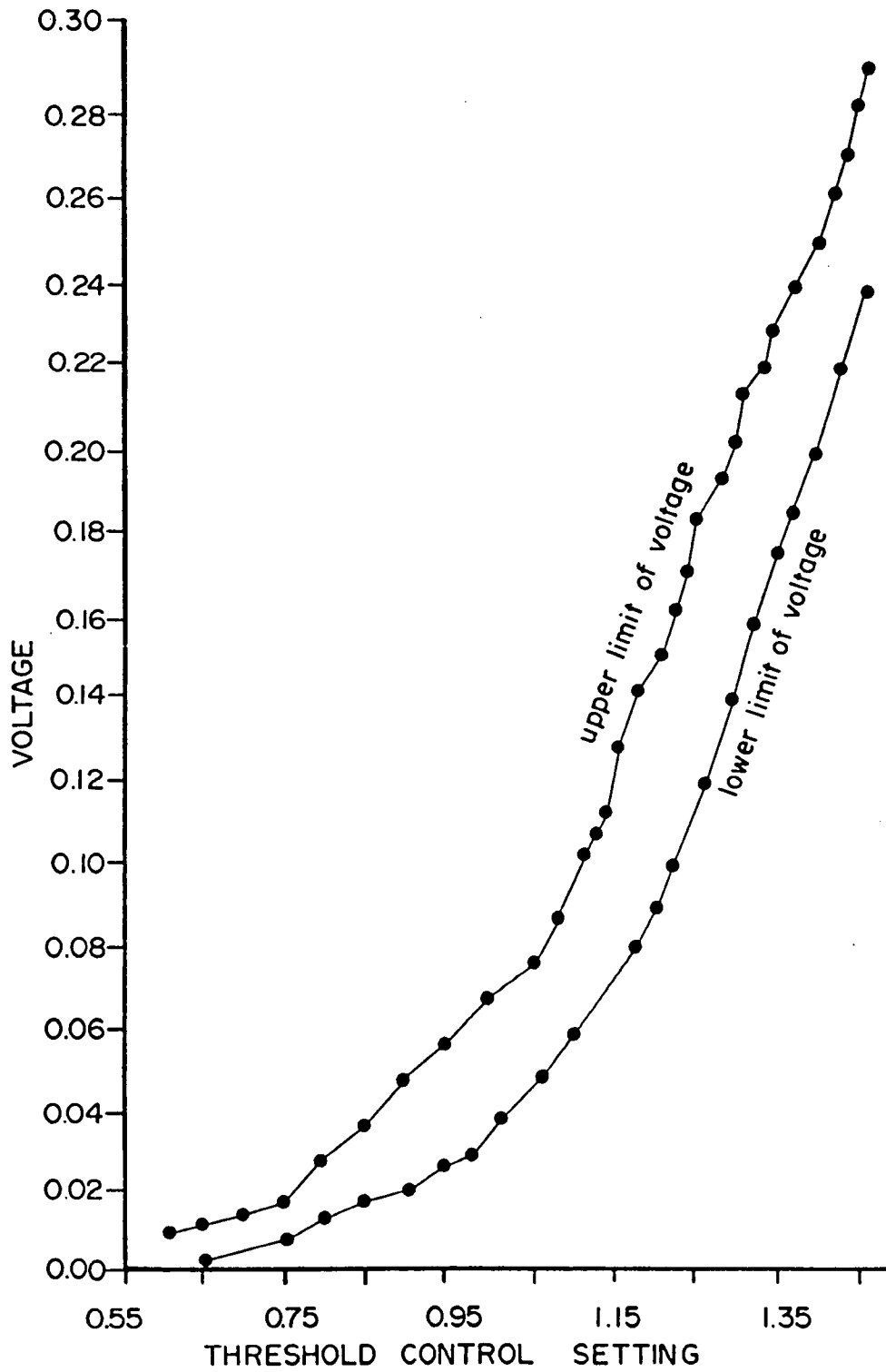


Figure I-A7. Calculated video voltage threshold as a function of threshold control setting.

illustrates conversion of the threshold limits to voltage using the calibration curve of power and voltage.

Consequently, all target cross-sections were calculated from B/S using both upper and lower threshold limits and then taking the average value of the two cross-sections calculated.

Modelling Limitations

The moored radar reflector buoys used as standard reference targets have been observed from recorded video to exhibit 10 degree deviations from the vertical under relatively calm seastates. As the vertical beam pattern of the calibrated target is ± 18 degrees, it is likely that under heavy sea states the motions of the buoy may exceed the beam pattern limits.

This motion would reduce the apparent cross-section of the calibrated targets significantly and cannot be accounted for in the model.

Information from Litton on their look-up table is not available. This component has been left out of the model. Consequently, the model does not take into account any loss associated with the look-up table. When high thresholds are used and the background does not paint on the radar display, calculated required cross-section will be more accurately determined. When low thresholds are used, the background enters the display region of the look-up table. Under this condition, the model only calculates the required cross-section for a target as bright as its local surroundings. For true detection, the target should be one intensity level above its surroundings. Therefore, the model under estimates required cross section for detection at lesser thresholds.

APPENDIX I-B

Clutter Cross-sections Transferred to Tape

Appendix I-B

Clutter Cross-sections Transferred to Tape

On 13 separate flights the aircraft was flown at constant altitude and heading while the power received by the radar was digitized. In many cases this was repeated at a second altitude.

This unit cross-section of sea clutter was calculated from power received producing an approximately equal size distribution to that originally recorded. The size of these distributions is of the order of 25 Megabytes each and were stored on a 9-track tape.

Table I-B1 lists the date of flight, the tape name containing the clutter distribution, the file for that distribution, the number of radar scans contained, and the altitude and antenna dip during original recording.

TABLE I - B1

Clutter cross-sections transferred to tape

Flight date	Tape	File	# Scans	Alt (ft)	Tilt
May 8/86	SIG 1	1	6	4000	-5.0
		2	6	500	-3.5
May 26/86	SIG 2	1	12	500	-3.5
		2	6	4000	-5.0
May 31/86	SIG 3	1	6	500	-3.5
		2	6	4000	-5.0
June 4/86 (Trip #1)	SIG 4	1	6	500	-3.5*
		2	6	4000	-5.0
		3	6	500	-0.5
June 4/86 (Trip #2)	SIG 5	1	6	500	0.0
		2	6	4000	-5.0
June 13/86 (Trip #2)		3	6	500	-3.0
June 8/86	SIG 6	1	12	500	-3.5
June 13/86 (Trip #1)	SIG 7	1	12	500	-0.5
June 19/86	SIG 9	1	6	4000	-5.0
		2	6	500	-3.0
June 27/86	SIG 10	1	12	500	-0.5
July 3/86	SIG 11	1	6	4000	-5.0
		2	6	500	-3.0
July 4/86	SIG 12	1	12	330	-1.0
		2	8	500	-1.0
July 14/86	SIG 13	1	12	500	-3.0
		2	6	4000	-5.0

* NOTE: Tilt as documented probably incorrect. Reprocessed with 0.5 (file 3).

APPENDIX I-C
Partial Specifications

Appendix I-C

Partial Specifications

The partial specifications of the APS 504 (V)3 (as used) are listed below and are accurate to the best of our knowledge. Litton Systems Canada Limited should be contacted for any clarification or adjustments to this description.

The following is only for the (V)3 in log and sea mode, 25 naut mi range scale, unstabilized display. Pulse width and antenna rotation rate may change for other modes.

Transmit Frequency: 9.375 GHz

Pulse Width: 0.5 μ sec

Transmit Power: 100 kW

prf: 1638 Hz

Antenna:	Type	Parabolic (Horn Fed)
	Horizontal	Beamwidth 2.3 degrees
	Vertical	Beamwidth 7.0 degrees
	Gain	32 dB
	Rotation Rate	30 RPM

Video Signal Processing: CFAR

Peak Detection

Azimuth Filtering

Memory and Display: Digital Scan Converter

16 grey scale

875 lines (800 active)

APPENDIX I-D

Sea State and Iceberg Classification

Appendix I-D

Sea state as a function of wind speed and wave height (Source: Long 1975)

Douglas Sea State	1	2	3	4	5	6
Wind speed (kts)	≤7	7-12	12-16	16-19	19-23	23-30
Wave height (m) ^a	0.3	0.3-0.9	0.9-1.5	1.5-2.5	2.5-3.7	3.7-6.1

^a Height of waves is given as the crest to trough height of the highest 1/3 of the waves present and applies only for local wind driven waves and not swell arriving from other areas.

Iceberg Classification

The size classifications of icebergs in Sea Ice Nomenclature (WMO 1970) and the Handbook of Drillship Stationkeeping in Iceberg Areas (Marex, 1972) were merged to classify iceberg sizes according to the following:

Type	Height (m)	Length (m)	Area (m ²)
Growler	<1	-	~20
Bergy Bit	1-5	-	100-300
Small iceberg	5-15	<60	
Medium iceberg	15-46	60-120	

In cases of conflict, more importance was placed on height.

APPENDICES FOR APS 504 (V)5

	<u>Page</u>
Appendix II-A - Iceberg population documented in the flying program	1
Appendix II-B - Radar calibration curves	10
Appendix II-C - Telex comment on APS 504 (V)5 by Litton Systems Canada Limited	20

Appendix II-A

Iceberg Population Documented in the Flying Program

Appendix A

Legend

Size Class: GG = growler
BB = bergy bit
Small = small iceberg
Med = medium iceberg
Lrg = large iceberg

Shape: Pin = pinnacle
DDK = drydock
Dome = rounded
Tab = tabular
Blk = blocky
Wedge = wedge shaped

Dimensions: L = length (m)
W = width (m)
H = height (m)

Iceberg Population Documented in the Flying Program

Flight Date: 5 May 1987

<u>Ref#</u>	<u>Type</u>	<u>Lat</u>	<u>Long</u>	<u>L</u>	<u>W</u>	<u>H</u>	
1	Small Dome	48 39.1'N	52 49.2W	71	41	12	m
2	GG	~ 49 08.7'N	52 52.1W	6	3	-	m
3	GG	~ 49 07.8'N	52 49.8'W	6	4	-	m
4	GG	~ 49 07.7'N	52 51.3'W	5	5	-	m
5	GG	~ 49 10.7'N	52 52.8'W	4	3	-	m
6	GG	~ 49 10.7'N	52 52.8'W	4	3	-	m
7	BB	49 25.6'N	52 46.2'W	10	8	-	m
8	GG (2)	49 25.0N	52 44.7'W	6	5	-	m
9	BB	49 41.7'N	52 59.8'W	12	11	-	m
10	Small DDK	49 43.0'N	52 59.5'W	59	54	-	m
11	BB	49 44.7'N	52 58.1'W	18	18	-	m
12	Small Dome	49 44.7N	52 53.6'W	-	-	-	m
13	Med Pin	49 39.2N	52 51.6'W	-	-	-	m
14	GG	49 08.1N	52 50.2'W	6	4	-	m
15	Small DDK	49 02.7'N	52 42.7'W	63	57	-	m

Flight Date: 14 May 1987

<u>Ref#</u>	<u>Type</u>	<u>Lat</u>	<u>Long</u>	<u>L</u>	<u>W</u>	<u>H</u>	
1	Bergy Bit	48 59.6'N	52 20.7'W	9	5	3	m
2	Med Pinnical	48 59.5N	52 22.5W	145	119	40	m
3	Growler	49 01.2N	52 16.7W	5	3	-	m
4	Growler	49 00.7N	52 16.7W	5	5	-	m
5	Med Dome	48 49.2N	52 08.1W	-	-	-	m
6	Small Dome	49 07.0N	52 41.7W	60	31	-	m
7	Lrg Pinnical	47 26.8N	52 35.7W	212	153	51	m
8	Bergy Bit	49 04.2N	51 28.7W	12	9	3	m
9	Large Wedge	49 4.2N	51 49.7W	244	152	-	m
10	Small Tabular	48 57.2N	51 23.7W	-	-	-	m
11	Small Dome	49 22.3N	51 41.2W	64	39	-	m
12	Med Drydock	49 25.7N	52 00.7W	92	84	-	m
13	Med Wedge	49 28.7N	52 21.0W	134	77	-	m

Flight Date: 15 May 1987

<u>Ref#</u>	<u>Type</u>	<u>Lat</u>	<u>Long</u>	<u>L</u>	<u>W</u>	<u>H</u>
1	Med Pinnical	48 49.8N	52 05.7W	-	-	-
2	Lrg Pinnical	48 53.3	52 02.3	-	-	-
3	Lrg Pinnical	49 00.7	52 06.0	-	-	-
4	Small Berg	49 05.0	52 04.2	15	10	6 m
5	Lrg Pinnical	49 21.2	52 26.0	-	-	-
6	Med Tabular	49 25.5	52 15.5	-	-	-
7	Small Dome	49 05.3	52 37.7	87	41	7 m
8	Small Tabular	49 00.2	53 07.2	-	-	-
9	Med Pinnical	49 21.2	53 00.5	76	47	21 m
10	Med Pinnical	49 40.2	53 18.7	80	50	17 m
11	Small Dome	49 54.8	53 19.8	42	26	- m
12	Bergy Bit	49 56.2	53 18.2	15	9	- m
13	Large Tabular	49 55.0	53 11.6			
14	Med Tabular	49 58.3	53 27.1			
15	Lrg Drydock	49 33.7	53 27.2	212	125	- m
16	Med Pinnical	49 29.2	53 26.1	77	64	- m
17	Small Dome	49 07.2	53 17.6	81	39	- m

Flight Date: 21 May 1987

<u>Ref #</u>	<u>Type</u>	<u>Lat</u>	<u>Long</u>	<u>L</u>	<u>W</u>	<u>H</u>
1	Lrg Pin	46° 18.2 N	51° 54.1 W	-	-	-
2	Small DDK	48° 42.8	52° 13.6	78	75	13
3	Small DDK	48° 45.6	52° 14.2	33	33	5.5
4	Lrg Tab	49° 13.8	52° 21.3	189	151	15
5	Med Pin DDK	49° 06.0	52° 18.7	92	41	18
6	Small Dome	48° 56.2	52° 08.7	-	-	-
7	Lrg Berg	48° 59.6	51° 44.3	-	-	-
8	Lrg Pin	48° 51.2	52° 14.6	-	-	-
9	Med Berg	49° 11.1	51° 56.5	-	-	-
10	Med Tab	49° 24.2	52° 52.1	-	-	-
11	Small Pin	49° 21.2	53° 00.8	-	-	-
12	Med Berg	49° 30.7	52° 50.8	-	-	-
13	BB	48° 53.6	53° 18.2	-	-	-
14	BB	48° 53.0	53° 24.3	16	22	-
15	Med DDK	48° 43.7	53° 18.3	-	-	-

Flight Date: 6 June 1987

<u>Ref#</u>	<u>Type</u>	<u>Lat</u>	<u>Long</u>	<u>L</u>	<u>W</u>	<u>H</u>
1	Med Pin DDK	47° 28.3 N	52° 14.7 W	94	89	26
2	Med Pin DDK	47° 46.1 N	52° 19.3 W	58	40	17
3	BB Small	47° 46.6 N	52° 16.8 W	7 23	5 19	2 6
4	Med Pin	47° 25.7 N	51° 48.6 W	-	-	-
5	Med Pin	47° 42.1 N	51° 18.3 W	-	-	-
6	Small DDK	47° 22.5 N	52° 35.7 W	52	34	13
7	Med Tab	48° 15.0 N	52° 01.2 W	-	-	-
8	Small Blk	48° 06.1 N	52° 24.0 W	-	-	-
9	Small DDK GG	47° 29.3 N	52° 16.5 W	26 5	15 3	6 -
10	Lrg Pin	47° 16.2 N	52° 23.6 W	-	-	-
11	GG	47° 26.3 N	52° 19.3 W	4	3	1
12	GG	47° 28.2 N	52° 17.7	3	2	1
13	GG	47° 28.3 N	52° 16.7	4	1	1

Flight Date: 9 June 1987

<u>Ref#</u>	<u>Type</u>	<u>Lat</u>	<u>Long</u>	<u>L</u>	<u>W</u>	<u>H</u>
1	Med Pin	47° 27.5' N	52° 13.2' W	-	-	-
2	Lrg Pin DDK	47° 50.2'	51° 43.6'	150	135	53
3	Med Pin DDK & GG's	47° 36.1'	51° 17.2'	108	104	43
4	Small BB	47° 50.5'	51° 33.6'	35 15	28 15	- -
5	Small Dome	47° 50.8'	51° 36.8'	60	44	8
6	Small Small Small	47° 51.1	51° 38.2'	40 29 -	34 24 -	14 10 -
7	BB	47° 51.5'	51° 35.5'	8	7	2
8	Med DDK	48° 07.7	51° 45.7'	-	-	-
9	Lrg Pin	48° 03.2	52° 29.2'	-	-	-
10	Small DDK	47° 18.3	52° 13.2'	28	26	6
11	Small DDK	47° 19.0	52° 13.7'	21	14	5
12	GG	47° 18.5	52° 10.1'	5	3	-
13	BB	47° 19.8'	52° 11.5'	5	3	2

Flight Date: 17 June 1987

<u>Ref #</u>	<u>Type</u>	<u>Lat</u>	<u>Long</u>	<u>L</u>	<u>W</u>	<u>H</u>
1	Small DDK	48° 42.1	51° 42.0	34	24	5
2	Med Tab	48° 35.8	51° 50.2	-	-	-
3	Med Pin	48° 32.8	51° 24.7	-	-	-
4	Med Pin	48° 56.2	51° 38.6	-	-	-
5	Lrg Pin DDK	48° 39.1	52° 07.6	220	135	45
	(15-20) GG & BB & Small			19	16	5
			Sample dimensions	6	6	2
				3	3	1

Flight Date: 19 June 1987

<u>Ref#</u>	<u>Type</u>	<u>Lat</u>	<u>Long</u>	<u>L</u>	<u>W</u>	<u>H</u>
1	BB	50° 04.5'N	53° 03.5'W	8	8	-
2	Small Pin	50° 10.7'N	53° 03.6 W	53	48	-
3	Small Wedge	50° 17.5'N	53° 09.2 W	30	28	9
4	BB	50° 19.3'N	53° 06.1 W	13	3	3
5	GG	50° 18.6'N	53° 07.2 W	9	4	-
6	Lrg Pin	49° 42.5'N	62° 42.8'W	200	133	-

Flight Date: 22 June 1987

<u>Ref#</u>	<u>Type</u>	<u>Lat</u>	<u>Long</u>	<u>L</u>	<u>W</u>	<u>H</u>
1	Lrg Pin DDK	49 20.0'N	52° 21.8'W	157	92	-
3	Med Pin BB	49° 55.8'N	52° 32.7'W	83 16	90 11	- -
4	Med DDK BB	50° 16.7'N	53° 30.8'W	55 16	46 13	17 3
5	Med Berg	49° 56.7'N	54° 13.1'W	-	-	-
6	Lrg Berg	50° 02.3'N	54° 13.3 W	-	-	-
7	Lrg Berg	50° 19.2'N	53° 17.8 W	-	-	-
8	Med Berg	Pos'n in Error (Ignore)		-	-	-
9	BB	50° 34.3'N	53° 51.7 W	4	4	2
10	Med Pin	50° 37.8'N	53° 51.7 W	-	-	-
11	GG	50° 51.8'N	54° 29.2 W	2	2	1
12	GG	50° 52.1'N	54° 29.7 W	2	1	-
13	BB	50° 52.5'N	54° 31.0 W	20	18	3
14	BB	50° 52.0'N	55° 02.7 W	8	4	2
15	BB	50° 50.6'N	55° 06.1 W	21	11	3
16	Small Pin	49° 55.2'N	52° 52.2 W	33	28	-

APPENDIX II-B

Radar Calibration Curves

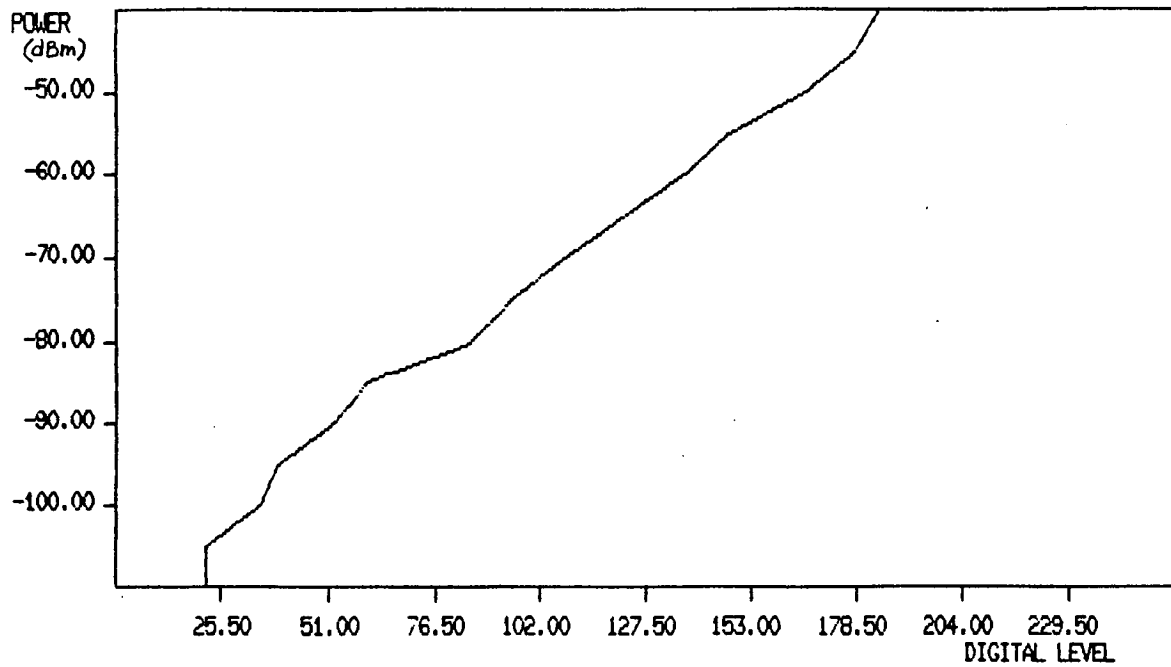


Figure II-B1 Receiver calibration curve for 0.20-μs pulse.

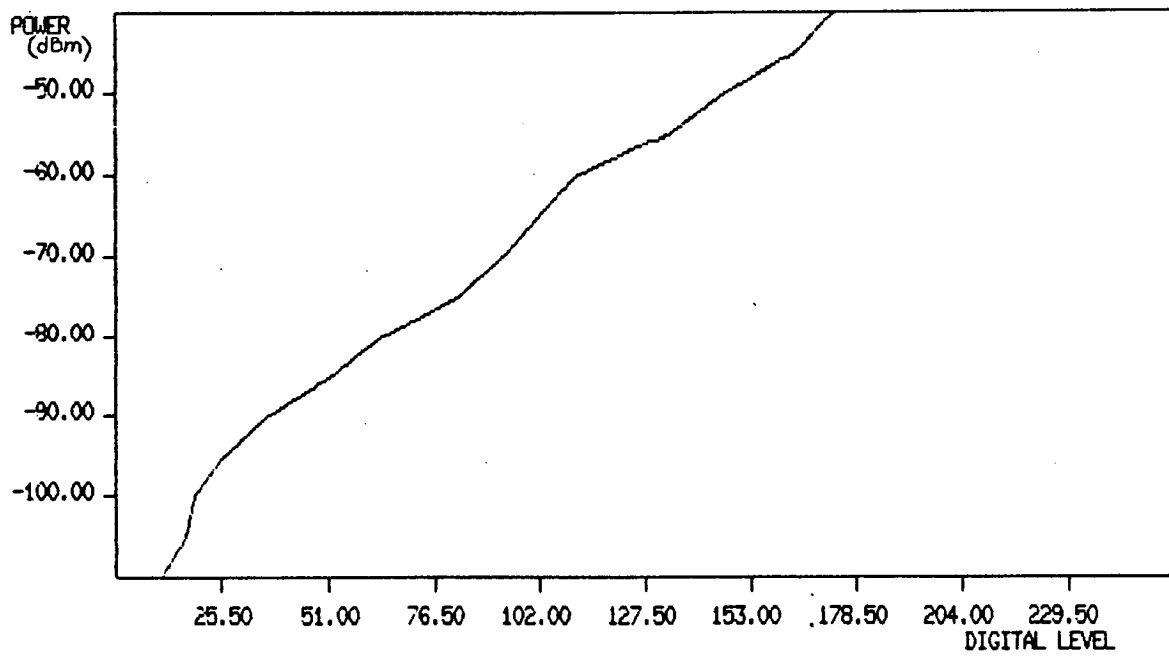


Figure II-B2 Receiver calibration curve for 10.0-μs pulse.

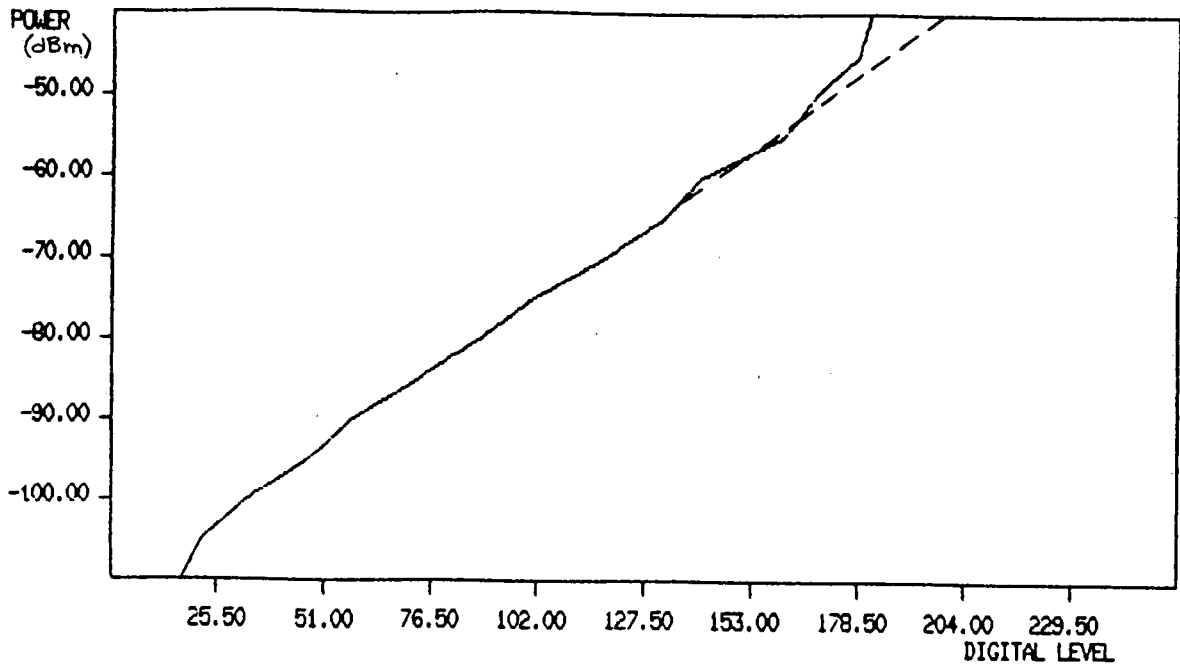


Figure II-B3 Receiver calibration curve for 30.0- μ s pulse.

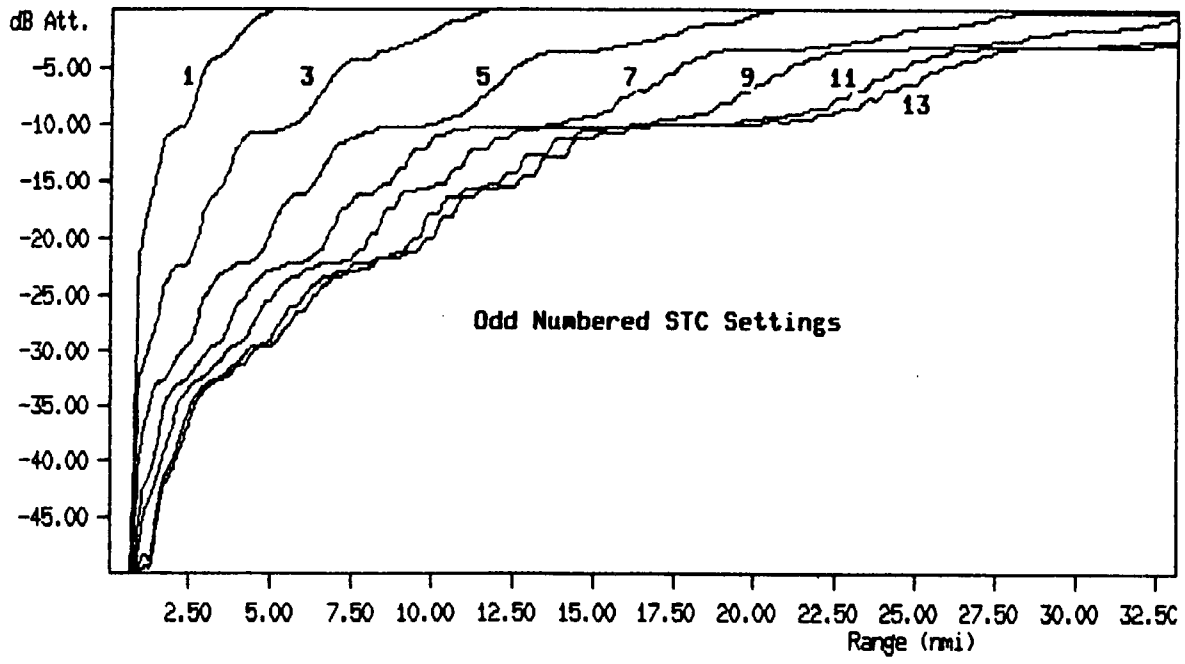


Figure II-B4 Sensitivity Time Control (STC) attenuation as a function of range for odd numbered settings.

APPENDIX II-C

Telex Comment on APS 504-(V)5 by Litton Systems Canada Limited

TELEX

C:\TLXDOC\TLX0012.IN

16:41:09

02 OCT 87

⊥
MEMORIAL SNF

LITTON TOR

NR 00025 871002 1510

SEACOR
ST. JOHN'S NFLD

ATTN: KEN KLEIN

SUBJECT: LITTON COMMENT

THE VERSION OF THE VS RADAR CURRENTLY IN USE WITH ATLANTIC AIRWAYS AND THE SUBJECT OF THIS STUDY IS THE FIRST DELIVERABLE VERSION OF THE NEW RADAR. AS SUCH, IT INCORPORATES DESIGN FEATURES THAT WERE CONSIDERED APPROPRIATE BEFORE THE BENEFIT OF ACTUAL FLYING EXPERIENCE WAS AVAILABLE. IN THE LIGHT OF ACTUAL FLIGHT PERFORMANCE AND SUBSEQUENT EVALUATION, SIMULATION AND ANALYSIS, A NUMBER OF DESIGN CHANGES HAVE NOW BEEN IMPLEMENTED THAT SIGNIFICANTLY IMPROVE THE GREY SCALE MAPPING AND DISPLAY QUALITY OF THE RADAR.

THESE MODIFICATIONS ARE CURRENTLY BEING APPLIED INTO THE ATLANTIC AIRWAYS RADAR.

THIS IS A MODIFICATION TO A PREVIOUS TELEX. THE CHANGE WAS MADE TO CLARIFY THE STATUS OF THE SYSTEM IN QUESTION.

D. BAIRD
LITTON SYSTEMS CANADA LTD
LITCAN/LM

⊥
MEMORIAL SNF

LITTON TOR

GLOSSARY OF RADAR TERMINOLOGY

backscatter: the energy reflected (scattered) back to the radar by a target or surface area.

blip-to-scan ratio (B/S): ratio of detectable returns (blips visible on radar display from a target) to the number of scans on target.

clutter: signal returns from a distributed target which may mask a point target return. (e.g. sea clutter is backscatter from the ocean's surface, a distributed target. An iceberg would be a point target).

constant false alarm rate (CFAR): a process of removing the mean background from the radar signal to provide a constant probability of false alarm over the entire radar display. Adaptive video technique to remove average local intensity leaving only the variations about the local average.

decibel (dB): 10 times the logarithm to the base 10 of the natural unit quantity, e.g., 100 watts in dB is 20 dBW, 100 m² is 20 dBm². The decibel has context when used, to describe power transmitted or received compared to 1 Watt, to describe the effective reflecting capability of an object per square metre compared to a perfect reflector of 1 square metre, etc. It is useful when numbers must be compared that differ by orders of magnitude.

free space: the space illuminated by the transmitted radar signal is considered void except for the radar and the target. Other surfaces between the radar and target do not provide an alternate path between the two.

frequency agility: capability of changing radar frequency from one pulse transmission to the next.

frequency modulation (FM): technique used to broaden the transmission spectrum of a radar. Frequency modulation can be used to increase the range resolution of the radar. The transmission frequency is varied (coded) as transmission occurs, and received target signals are processed (decoded) according to frequency. This in turn can be related to target range. See pulse compression.

grazing angle: the vertical angle measured at the target location between the radar and the local horizon (complement of incidence angle).

minimum detectable signal (MDS): the smallest signal that can be detected by the radar.

multipath propagation: result of radar energy propagating to the target by a direct path and reflected path(s). Over the ocean the sea provides a reflecting surface between radar and target.

normalized radar cross-section (NRCS): radar cross-section of an object normalized to the physical area of the object. This indicates the overall quality of an object to reflect radar transmissions independent of its physical size.

plan position indicator (PPI): conventional radar display, with rotating sweep of the received signal. Signals are displayed in polar format as a function of range and azimuth.

probability of detection (Pd): probability the signal received from a target will exceed a predetermined threshold and background signals from noise and clutter.

pulse compression: process of transmitting a long frequency modulated pulse and processing the received signal in a matched filter. This process permits the transmission of the large radiated power of the long pulse while providing the range resolution of a much shorter pulse.

pulse repetition frequency (PRF): rate at which the radar pulses are emitted (or transmitted) by the system.

pulse width (PW): duration of each radar pulse, measured with time.

radar cross-section (RCS): strength (reflection capability) of a radar target expressed in terms of an ideal reflector. Has units of area.

radar equation: an equation that relates the power received from a target to the radar's transmitter power, wavelength, antenna gain, target radar cross-section and target range. For free space the power received is inversely proportional to the fourth power of range ($1/R^4$). See eqn (1) for one form of this equation and a discussion of propagation effects.

radar frequency (RF): frequency range over which the radar operates (transmit/receive).

received power: strength of signal returned to the radar from a target or surface area.

resolution cell: instantaneous area illuminated by the radar.

scan-to-scan integration: integration of returns from successive scans to provide substantial improvement in the signal-to-clutter ratio. A technique which averages several scans together and displays the result.

search radar: airborne system, pencil beam radar, low aspect ratio (small grazing angles), 360° or restricted to more forward-looking sweep, high performance transceivers, various post-processing options.

sensitivity time control (STC): control that attenuates a received radar signal as a function of signal range. Used to suppress the range dependent signals from sea clutter.

signal-to-clutter ratio (S/C): ratio of signal power to clutter power.

signal-to-noise ratio (S/N): ratio of signal power to noise power.

side-looking airborne radar (SLAR): imaging airborne radar system, with single-look, real aperture, and usually slant range projection of a wide swath (25 to 100 km) imaged on both sides of the system.

Swerling statistics: probability model for four different fluctuations of radar cross section (Cases 1 to 4). The radar cross section of a target varies about some average value. Swerling statistics gives the distribution of how the radar cross section varies about the average. See figure 5 for an example of case 1.

threshold level: sets the lower limit of the minimum detectable signal.

REFERENCES

- Blake, L.V. 1980. Radar range-performance analysis. D.C. Heath and Company, Lexington, Massachusetts. 443 p.
- Croney, J., A. Woroncow, and B.R. Gladman. 1975. Further observations on the detection of small targets in sea clutter. The Radio and Electronic Engineer 45(3): 105-115.
- Currie, B.W., and S. Haykin. 1985. Experimental evaluation of Eaton airborne radar for iceberg detection. Part I: Summary report. Communications Research Laboratory, McMaster University, Hamilton. Report No.142.
- Dawe, B. 1985. A radar cross-section model for icebergs, International Radar Conference, Arlington, VA, May 6-9.
- Harvey, M., and J.P. Ryan. 1986. Further studies on the assessment of marine radars for the detection of icebergs. Environmental Studies Revolving Funds Report No.035, Ottawa. 82 p.
- Long, M.W. 1975. Radar reflectivity of land and sea. D.C. Heath and Co.
- Marex, 1972. Handbook of drillship stationkeeping in iceberg areas. Marine Exploration Ltd. report to Eastcan Exploration Ltd.
- Nathanson, F.E. 1969. Radar design principles - signal processing and the environment. McGraw-Hill, New York, NY. 626 p.
- Rossiter, J.R., L.D. Arsenault, E.V. Guy, D.J. Lapp, E. Wedler, B. Mercer, E. McLaren, and J. Dempsey. 1985. Assessment of airborne imaging radars for the detection of icebergs. Environmental Studies Revolving Funds Report No. 016. Ottawa. 321 p.
- Ryan, Joseph P. 1985. Enhancement of the radar detectability of icebergs. Environmental Studies Revolving Funds Report No. 022. Ottawa. 93 p.
- Ryan, J.P., M. Harvey, and A. Kent. 1985. Assessment of marine radar for the detection of ice and icebergs. Environmental Studies Revolving Funds Report No.008. Ottawa. 127 p.
- Skolnik, M.I., 1980. Introduction to radar systems. McGraw-Hill, New York, NY. 581 p.
- World Meteorological Organization. 1970. WMO sea-ice nomenclature. World Meteorological Organization, Geneva, Switzerland.